

ISSN 1316-7081

ISSN Electrónico 2244-8780

CIENCIA e INGENIERÍA



Vicerrectorado Administrativo y
Académico
Mérida, Venezuela

**UNIVERSIDAD DE LOS ANDES
(ULA)**

**Facultad de Ingeniería
Núcleo Universitario
«Pedro Rincón Gutiérrez»
Mérida - Venezuela**

Comportamiento electroquímico de la amlodipina

Electrochemical behavior of amlodipine

Calderon, Viery¹; Martínez, Yris^{1*}; Ayala, Carlos²; Hernandez, Ricardo¹; Laguna, Alexander¹; Méndez, Fernando²

¹Laboratorio de Electroquímica, Universidad de Los Andes Mérida, Venezuela.

²Laboratorio de Espectroscopia Analítica, Universidad de Los Andes Mérida, Venezuela.

* ymartin@ula.ve

Resumen

Se estudió el comportamiento electroquímico de la amlodipina por voltametría cíclica utilizando un electrodo de carbón vítreo sumergido en una solución de amlodipina a 0,4 mg/mL en buffer fosfato. Se determinó que el proceso de oxidación de la amlodipina está controlado por difusión, con una adsorción significativa del producto oxidado sobre la superficie del electrodo. Los resultados muestran una clara dependencia del potencial de pico anódico con respecto al pH, identificándose tres regiones lineales que reflejan distintos mecanismos de oxidación. En el intervalo de pH 2,14–4,00, el proceso está dominado por una transferencia electrónica inicial sin desprotonación. En el intervalo 5,5–8,2, se muestra una transferencia acoplada de un electrón y un protón. Mientras que en el intervalo de pH 9,00–12,40, la desprotonación previa facilita la oxidación.

El estudio cinético revela un comportamiento irreversible con un único pico anódico, atribuible a la formación de un anillo aromático estable. El coeficiente de transferencia de carga $\alpha = 0,70 \pm 0,04$, indica una asimetría energética favorable que facilita la oxidación de la amlodipina. La amlodipina es un excelente candidato para aplicaciones electroanalíticas, especialmente en el desarrollo de sensores voltamétricos sensibles y selectivos.

Palabra clave: Amlodipina, Bloqueadores de canales de calcio, Aromatización oxidativa, Enfermedades del corazón.

Abstract

The electrochemical behavior of amlodipine was studied using cyclic voltammetry with a glassy carbon electrode immersed in a 0.4 mg/mL amlodipine solution in phosphate buffer. It was determined that the oxidation process of amlodipine is diffusion-controlled, with significant adsorption of the oxidized product onto the electrode surface. The results show a clear dependence of the anodic peak potential on pH, identifying three linear regions that reflect distinct oxidation mechanisms. In the pH range of 2.14–4.00, the process is dominated by an initial electron transfer without deprotonation. In the range of 5.5–8.2, a coupled transfer of one electron and one proton is observed. In the basic range of pH 9.00–12.40, prior deprotonation facilitates oxidation.

The kinetic study reveals an irreversible behavior with a single anodic peak, attributed to the formation of a stable aromatic ring. The charge transfer coefficient $\alpha = 0.70 \pm 0.04$ indicates a favorable energetic asymmetry that enhances the oxidation of amlodipine. These findings position amlodipine as an excellent candidate for electroanalytical applications, particularly in the development of sensitive and selective voltammetric sensors.

Keywords: Amlodipine, Calcium channel blockers, Oxidative aromatization, Heart diseases.

1 Introducción

Las enfermedades no transmisibles (ENT) o crónicas son afecciones que no se contagian entre personas y generalmente tienen un desarrollo gradual. Según la Organización Mundial de la Salud (OMS), las cuatro principales enfermedades no transmisibles son el cáncer, las enfermedades respiratorias crónicas, la diabetes, y las enfermedades cardiovasculares. La hipertensión arterial es una enfermedad cardiovascular que se caracteriza por un incremento constante de la presión arterial por encima de los niveles considerados normales, los cuales oscilan entre 80 y 120 mmHg. Se considera que hay presión alta cuando los valores se encuentran entre 120 y 129 mmHg, y se diagnostica hipertensión cuando estos superan los 130 mmHg. Si no se trata adecuadamente la hipertensión, puede incrementar el riesgo de sufrir ataques cardíacos, accidentes cerebrovasculares y angina de pecho (Muntner y col. 2019).

Una vez diagnosticada la enfermedad, es necesario tratarla eficazmente con medicamentos antihipertensivos (Buford. 2016). En este caso en particular, nuestro interés está centrado en la amlodipina en la cual está enmarcado entre los medicamentos antihipertensivos denominados bloqueadores de los canales de calcio. Estos medicamentos que inhiben la entrada del ion Ca^{2+} a través de los canales de calcio en las células del músculo cardíaco, lo que resulta en una disminución de la concentración interna de este ion y una reducción en la capacidad de contracción del corazón. Disminuyendo el dolor anginoso, provocado por los espasmos de las arterias coronarias. Con la consecuente relajación en las arterias, vasodilatación y aumento del flujo sanguíneo coronario, lo que conduce a la reducción de la presión sanguínea (Lozano-Jimenez y Sanchez. 2021, Story y col 2003, Barnes y Bui 1991, Tang y colaboradores 2019).

La amlodipina (Figura 1) pertenece al grupo de los bloqueadores de calcio de 1,4-dihidropiridinas. Tiene propiedades antioxidantes y la habilidad de mejorar la producción de óxido nítrico (NO), el cual juega un papel importante en la regulación de la presión arterial por ser un vasodilatador (National Center for Biotechnology Information 2025).

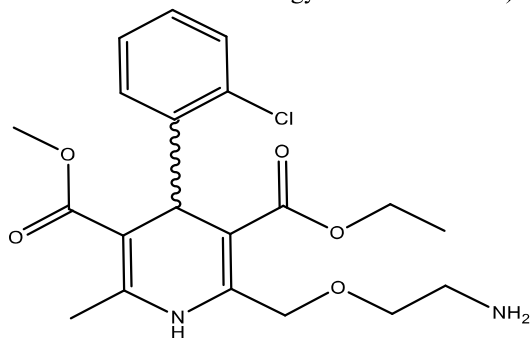


Fig.2. Estructura de la amlodipina (AML)

Su reactividad está determinada principalmente por el anillo de dihidropiridina y el grupo amino. La aromatización oxidativa del fragmento dihidropiridina es el camino de

degradación principal de esta molécula (Figura 2), se puede presentar tanto en solución como en estado sólido. Al oxidarse, pierde electrones y se transforma en un anillo de piridina, que tiene tres dobles enlaces alternados y es mucho más estable. (Shafitabar-Samakosh y col. 2024, Ananchenko y col. 2012)

El anillo de dihidropiridina es el núcleo funcional de la amlodipina cuya. Su función está directamente relacionada con la farmacodinámica, es decir, cómo actúa el medicamento en el cuerpo. Es responsable de la capacidad del fármaco de bloquear los canales de calcio. Al estar parcialmente saturado, es más reactivo. Cuando el anillo pierde electrones gana estabilidad química. Lo que hace pierda su actividad farmacológica, porque no puede interactuar con los canales de calcio como lo hacía antes.

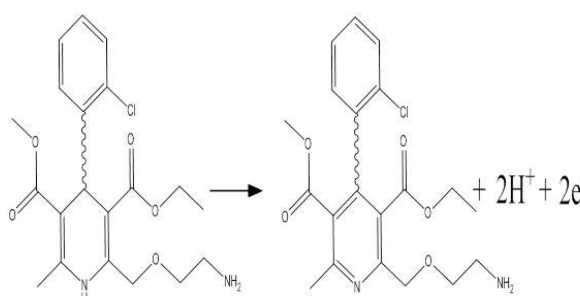


Fig. 3. Aromatización oxidativa de la amlodipina

Por otro lado, la función principal del grupo amino de la amlodipina está relacionada con la farmacocinética es decir de cómo se absorbe, distribuye y elimina del cuerpo, y puede participar en reacciones químicas formando enlaces o interactuando con otras moléculas. (Darrell 1989)

Es este trabajo nos enfocarnos en el estudio de la oxidación electroquímica de la amlodipina a diferentes pH.

2 Metodología

2.1- Celda electroquímica y electrodos

Para este trabajo se utilizó una celda electroquímica tipo H con tres electrodos: un electrodo de referencia de Ag/AgCl saturado, un contraelectrodo de alambre de platino (Pt), y un electrodo de trabajo de carbón vítreo (ECV) en la cual fue pulido a espejo antes de cada experiencia. Todo el material de vidrio fue sometido a un riguroso proceso de limpieza para eliminar residuos orgánicos e inorgánicos remanentes. Los reactivos utilizados en las distintas experiencias son de grado analítico. Como electrolito soporte se utilizó un buffer fosfato 0,50 M, ajustando el pH de las diferentes soluciones estudiadas, con HCl y NaOH 0,10 M. Para mantener la fuerza iónica se utilizó KCl 0,30M. Debido a que la amlodipina es poco soluble en agua, la misma fue disuelta en una mezcla agua-metanol en una relación 75:25. Para los estudios electroquímicos se utilizó un potenciostato-galvanostato, Autolab 20 ecochemie.

La técnica electroquímica empleada fue la voltametría cíclica, esta técnica se caracteriza por medir la corriente en

función del potencial aplicado, es decir, a una celda electroquímica se le aplica un potencial variable (señal de excitación), y se mide la intensidad de corriente que se desarrolla en la celda en función del tiempo. La respuesta en corriente va a depender del proceso electroquímico que se desarrolle en la superficie del electrodo de trabajo, de las condiciones hidrodinámicas y del potencial aplicado.

3 Resultados y Discusiones

3.1 Estudios del pH

El efecto del pH en la oxidación electroquímica de la amlodipina fue realizado por voltametría cíclica estudiando soluciones de amlodipina a una concentración de 0,4 mg/mL en diferentes buffers de fosfato en un intervalo de pH de 2,14 a 12,4 a una velocidad de barrido de 25 mV/s.

La respuesta voltamétrica para el proceso redox de la amlodipina en estas condiciones de trabajo, está bien definida para cada pH en estudio (Figura 3). A pH 2,14 se observa un pico atribuido a la oxidación de la amlodipina a 896 mV. El cual se va desplazando hacia potenciales menos positivos a medida que se incrementa el pH de la solución,

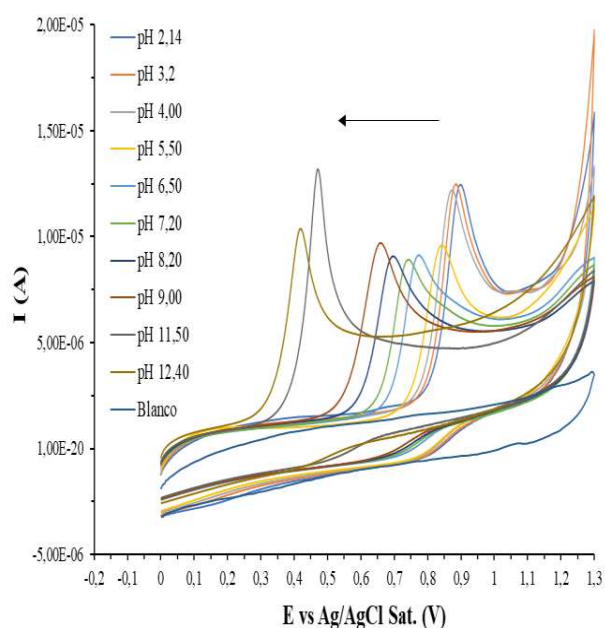


Fig. 3. Respuesta electroquímica de un ECV sumergido en una solución de AML 0,4 mg/mL a diferentes pH. $v = 25$ mV/s

Esta dependencia del potencial de pico anódico (E_{pa}) de la amlodipina frente al pH, se analizó haciendo uso de la ecuación de Nernst (ecuación 1) (Bard y Faulkner 2001):

$$E_{pa} = E^{\circ} - 0,059 \left(\frac{m}{n} \right) pH \quad Ec 1$$

Donde:

E_{pa} es el potencial de pico anódico (V)

E° es el potencial formal o estándar (V)
 m es el número de protones transferidos
 n es el número de electrones transferidos
 0,059 V corresponde al factor RT/F a 25 °C

En la gráfica de E_{pa} vs. pH (Figura 4) se identifican tres intervalos lineales bien definidos: el primer intervalo entre 2,14 – 4,00, el segundo entre 5,5 y 8,2 y el último entre 9,00 – 12,40, los parámetros de cada una de las rectas de regresión lineal se muestran en la Tabla 1.

Tabla 1: Regiones lineales de E_{pa} vs pH

Región	Rango de pH	Ecuación de la recta	R^2
1	2,14 – 4,00	$E_{pa} = -0,0139 \text{ pH} + 0,9261$	0,9987
2	5,5 – 8,2	$E_{pa} = -0,0589 \text{ pH} + 1,1603$	0,9877
3	9,00 – 12,40	$E_{pa} = -0,0679 \text{ pH} + 1,2574$	0,9968

Este comportamiento concuerda un estudio realizado por Álvarez-Lueje y col.1994, ellos reportan el comportamiento electroquímico de cinco compuestos derivados de 1,4-dihidropiridinas (nifedipina, nitrendipina, nimodipina, nicardipina y furaldipina), en ese estudio, los autores reportan tres regiones lineales al relacionar potencial de pico con respecto al pH, tal como se representa en el caso de la amlodipina.

En la primera región (intervalo de pH 2,14 – 4,00) la pendiente muestra un valor de $-0,0139$ V/pH, lo que indica la existencia de una leve dependencia del potencial de pico anódico con respecto al pH. Recordemos que la pendiente teórica esperada para la relación potencial vs pH es igual a $-0,059 \times m/n$ V/pH (ecuación 1). Esto sugiere que la transferencia del primer electrón es el paso determinante de la reacción con la formación de un catión radical en el anillo dihidropiridina, por lo tanto, la desprotonación no ocurre antes ni durante el paso limitante, ya que el medio ácido impide este proceso. De manera que, el mecanismo inicia con un paso electroquímico

En la segunda región (intervalo 5,5 – 8,2) la pendiente es $-0,0589$ V/pH compatible con una transferencia acoplada de 1 electrón + 1 protón. Por lo tanto, se propone un mecanismo electroquímico – químico (EQ)

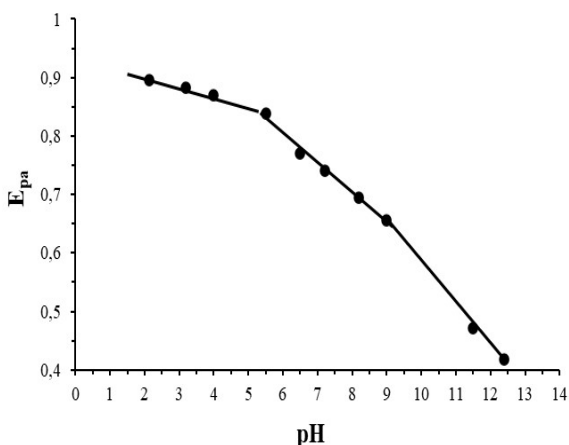


Fig. 4. Dependencia del potencial de pico anódico respecto al pH

En la tercera región (intervalo 9,00 – 12,40) la pendiente de -0,067 indica que estamos en presencia de un mecanismo químico – electroquímico (QE), debido a que el medio básico facilita la desprotonación de la amlodipina previo a la oxidación.

La relación entre la corriente de pico anódica (I_{pa}) y el pH (Figura 5) muestra una dependencia compleja y no lineal, con intervalos donde la corriente no se ve afectada por el pH de la solución, esto también concuerda con lo reportado por Álvarez-Lueje y col. 1994. Se observa que la I_{pa} mantiene una corriente relativamente estable entre pH 2,14 y 4,00.

A medida que el pH aumenta, la I_{pa} disminuye gradualmente, manteniendo otra región estable entre pH, 5,5 y 8,2. Lo que sugiere que el proceso está controlado por la difusión de la amlodipina hacia la superficie del electrodo. Sin embargo, en el intervalo básico, la I_{pa} experimenta un incremento, llegando a un máximo a pH 11,5 atribuida a la desprotonación de la amlodipina permitida por el medio básico.

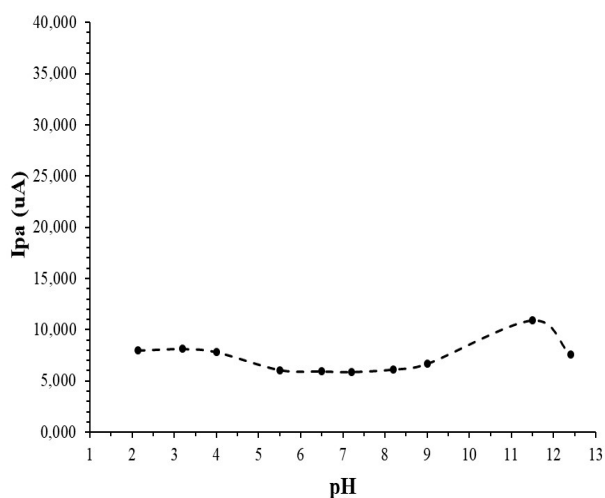


Fig. 5. Dependencia de la corriente pico anódica con respecto al pH

3.2- Efecto de la velocidad de barrido

Una vez realizado el estudio a diferentes pH se seleccionó para estudios posteriores una solución de amlodipina 0,4 mg/mL disuelta en metanol al 10%, KCl 0,2 M y un buffer de fosfato a pH 2,14 ya que a este pH el buffer de fosfato alcanza su máxima capacidad amortiguadora, lo que proporciona una mayor estabilidad al sistema y minimiza fluctuaciones en el pH de la doble capa que podrían afectar los resultados experimentales.

Otro factor importante para la elección de este pH fue realizado porque en un estudio posterior donde se va a cuantificar la cantidad de amlodipina en fármacos, al electrodo de carbón vítreo se le va a realizar una modificación utilizando que la poli-(2,5-dimetoxianilina, y esta película es más estable en medios ácidos, en medios alcalinos, ha sido reportado que la película se descompone comprometiendo así, la integridad de la película depositada sobre la superficie del electrodo de carbón vítreo (Alzate y col. 20026).

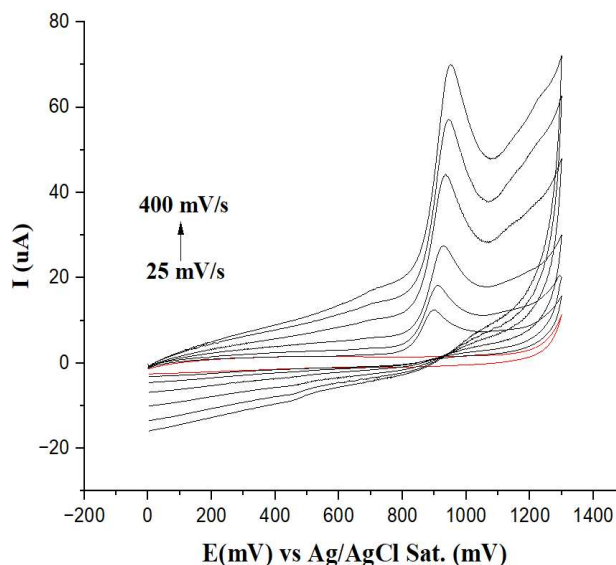


Fig. 6. Respuesta electroquímica de amlodipina 0,4 mg/mL a pH 2,14 sobre un electrodo de carbón vítreo a diferentes velocidades de barrido

La influencia de la velocidad de barrido en la respuesta electroquímica se estudió en una solución de amlodipina 0,40 mg/mL, en el buffer de fosfato de pH 2,14, el cual fue establecido como pH óptimo en el estudio anterior. El intervalos de de velocidades en estudio fueron de 25, 50, 100, 200, 300, y 400 mV/s. La Figura 6 muestra la respuesta obtenida para este sistema. En esta figura se observa claramente un aumento en la corriente de pico atribuida a la oxidación de la amlodipina.

El estudio del efecto de la velocidad de barrido reveló que la oxidación electroquímica de la amlodipina presenta un comportamiento irreversible, el cual está caracterizado por un único pico anódico tal como se muestra en la figura 6, el cual es atribuible a la estabilidad del anillo aromático del producto de la oxidación.

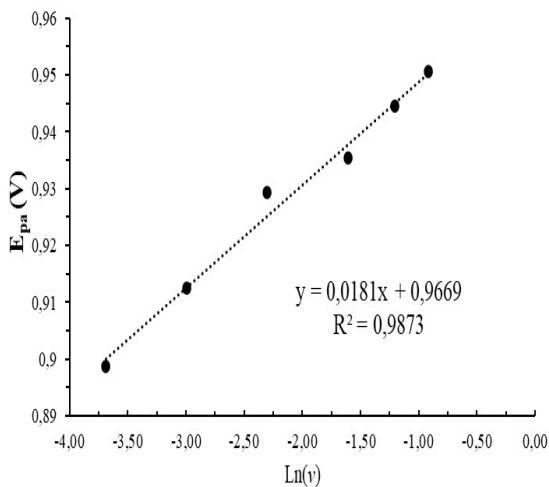


Fig. 7. Relación potencial con la velocidad de barrido (E_{pa} vs. $\ln(v)$)

A partir de los voltamogramas obtenidos, se aplicó la ecuación de Laviron (Ecuación 2) con el fin de establecer la relación entre el potencial de pico (E_{pa}) y la velocidad de barrido (v), para calcular parámetros cinéticos como el coeficiente de transferencia de carga (α). La Figura 7 muestra la gráfica de E_{pa} vs. $\ln(v)$, cuyo coeficiente de correlación $R^2 = 0,9873$. El valor de α fue calculado a partir de la pendiente de la recta de regresión dando un valor de $0,70 \pm 0,04$.

Este resultado indica una asimetría energética que favorece la oxidación de la amlodipina. Según la literatura (González-Velasco 2012) valores de α superiores a 0,5 reflejan que el estado de transición está más próximo al oxidado, facilitando la transferencia electrónica desde el analito al electrodo. Esta característica contribuye a una oxidación más eficiente, aspecto clave en el diseño de sensores voltamétricos sensibles y selectivos.

$$E_{pa} = E^\circ + \left(\frac{RT}{\alpha nF}\right) * \ln\left(\frac{RTk_s}{\alpha nF}\right) + \left(\frac{RT}{\alpha nF}\right) * \ln(v) \quad \text{Ec. 2}$$

Donde:

E_{pa} : Potencial de pico anódico (en voltios).

E° : Potencial estándar formal (en voltios).

R : Constante de los gases ideales (8,314 J/mol).

T : Temperatura (en Kelvin).

α : Coeficiente de transferencia de carga.

n : Número de electrones transferidos en la reacción.

F : Constante de Faraday (96485 C/mol).

k_s : Const. velocidad de transferencia de e^- (en cm/s).

v : Velocidad de barrido (en V/s).

Dos gráficas adicionales fueron construidas para completar el estudio cinético. La intención es identificar el mecanismo que controla la transferencia de carga. La gráfica 8 relaciona la corriente de pico anódico con la velocidad de barrido y da información sobre los procesos controlados por adsorción (ecuación 3)

$$I_p = \frac{n^2 F^2 A \Gamma}{4RT} v \quad \text{Ec. 3}$$

Donde,

I_p Corriente pico en amperios (A).

n Número de electrones.

R Constante de gases ideales

T Temperatura en K

F Constante de Faraday

A Área superficial del electrodo

Γ Cantidad de sustancia adsorbida por unidad de área

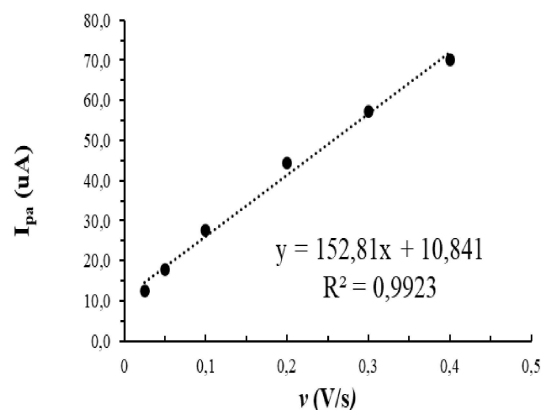


Fig. 8. Aplicación de la ecuación para procesos controlados por adsorción superficial.

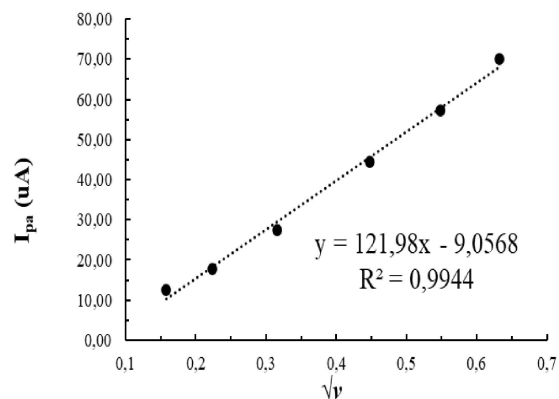


Fig. 9. Aplicación de la ecuación para procesos controlados por difusión (Randles – Sevcik)

Por otro lado, haciendo uso de la ecuación de Randles – Sevcik para procesos irreversibles. Se graficó I_{pa} vs $v^{1/2}$ (Figura 9). Esto permite identificar si la transferencia de carga, esta controlada por difusión o por adsorción (Pletcher 2002).

Los resultados mostraron una correlación lineal en ambos casos, con coeficiente $R^2 = 0,9923$ para I_{pa} vs v $R^2 = 0,9944$ y para la gráfica correspondiente a I_{pa} vs $v^{1/2}$. Este

último valor más alto sugiere que el proceso de oxidación de la amlodipina está mayoritariamente controlado por difusión, de acuerdo con el modelo de Randles-Sevcik. Este comportamiento es típico de sistemas donde la corriente depende del transporte de las especies electroactivas desde el seno de la solución hacia la superficie del electrodo.

Sin embargo, además de que el proceso está controlado por difusión, se observó que existe una adsorción significativa del producto oxidado sobre la superficie del electrodo, generando efectos de pasivación con su consecuente disminución progresiva de la respuesta analítica (figura 10).

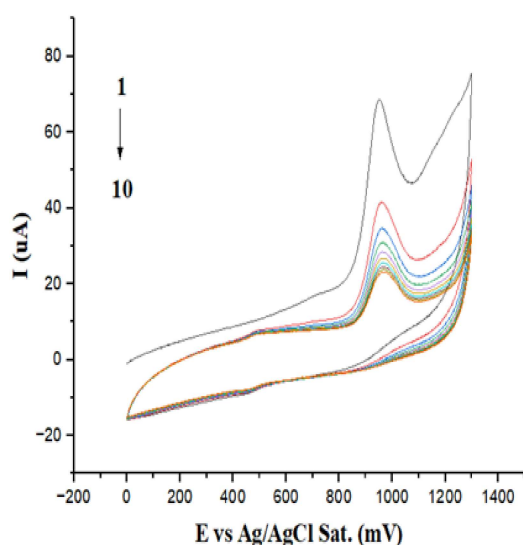


Fig. 10. Adsorción del producto de oxidación de amlodipina.

Esto puede ser observado en I con mayor calidez en Figura 7B, donde se observa una disminución sistemática de la corriente de pico con cada nuevo barrido, lo que confirma el efecto inhibitor del producto formado sobre la superficie activa del electrodo.

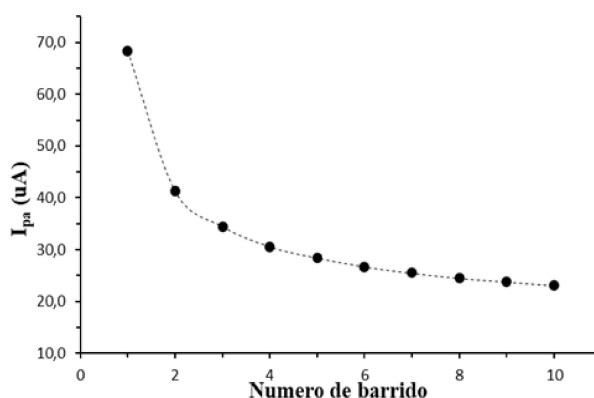


Fig. 11. Disminución de la corriente en función del número de barridos

En consecuencia, aunque el sistema muestra un perfil

cinético favorable para la oxidación ($\alpha = 0,70$), la adsorción del producto formado pasiva la superficie del electrodo lo que es desfavorable para realizar estudios de cuantificación. Para preservar la reproducibilidad en las medidas es necesaria la reactivación de la superficie a través de la limpieza mecánica del electrodo entre mediciones.

4 Conclusiones

El estudio del comportamiento voltamétrico de la amlodipina en función del pH reveló una clara dependencia del potencial de pico anódico con respecto al medio ácido. Tres regiones lineales bien definidas. Estas regiones reflejan distintos mecanismos de oxidación: En medio ácido (pH 2,14–4,00), la pendiente de la recta (-0.0139V/pH) nos indica que el proceso está dominado por una transferencia electrónica inicial sin desprotonación. A pH intermedio (5,5–8,2), la pendiente (-0.0589V/pH) cercana al valor teórico sugiere una transferencia acoplada de 1 electrón y 1 protón. Mientras que en un medio fuertemente básico (9,00–12,40), la pendiente (-0.0679V/pH) nos indica que la desprotonación previa facilita la oxidación.

El proceso de oxidación de la amlodipina está controlado por difusión, aunque se observó adsorción producto sobre el electrodo, generando pasivación de la superficie.

El valor de α de $0,70 \pm 0,04$, obtenido a partir del estudio del E_{pa} vs. $\ln(v)$, revela que la oxidación de la amlodipina ocurre con una marcada asimetría energética, lo que confirma la reactividad del anillo dihidropiridina de la amlodipina. Contribuyendo de esta manera en una oxidación más eficiente, aspecto clave en el desarrollo de sensores voltamétricos sensibles y selectivos. Este resultado que posiciona a la amlodipina como un excelente candidato para aplicaciones electroanalíticas

Referencias

- Alvarez-Lueje A., Núñez-Vergara L. & Squella J., Voltammetric behavior of 1,4-dihydropyridine calcium antagonists, *Electroanalysis*, 6(1994)259
- Agarwal, A. K., Raja, A., & Brown, B. D. (2023, August 7). Chronic obstructive pulmonary disease. In *StatPearls* [Internet]. StatPearls Publishing. <https://www.ncbi.nlm.nih.gov/books/NBK559281/>
- Alzate V., Vasco D. & González J (2006) The effect of pH on morphology and electrical properties of polyaniline. *Revista Facultad de Ingeniería* 38 (2006)88. DOI: <https://doi.org/10.17533/udea.redin.343237>
- Ananchenko G, Novakovic J, & Lewis J. (2012). Besilato de amlodipino, Perfiles de sustancias farmacológicas, excipientes y metodología relacionada 37(2012)31. DOI: <https://doi.org/10.1016/B978-0-12-397220-0.00002-7>

- Appu S., Anusha B., Thilak S. & Prashantha K. (2025) Electrochemical sensing of Amlodipine besylate using ZnIn₂S₄/ZnO composite Electrodes: A High-Performance Approach. *Microchem J.* 214 (2025) 113925.
DOI: <https://doi.org/10.1016/j.microc.2025.113925>
- Appu S., Anusha B., Thilak S. & Prashantha K. (2025) Electrochemical sensing of Amlodipine besylate using ZnIn₂S₄/ZnO composite Electrodes: A High-Performance Approach. *Microchem J.* 214 (2025) 113925.
DOI: <https://doi.org/10.1016/j.microc.2025.113925>
- Bard A. & Faulkner L. (2001), *Electrochemical Methods: Fundamentals and Applications*, Nueva York: Wiley, 2001.
- Cen Y., Fang Y. & Li X. (2025). NiCo₂O₄@g-C₃N₄ heterojunction for the construction of electrochemical sensor for the detection of amlodipine besylate. *Microchem J.* 216(2025) 114712.
DOI: <https://doi.org/10.1016/j.microc.2025.114712>
- Darrell R., & Abernethy M. (1989) The pharmacokinetic profile of amlodipine. *American Heart Journal.* 118(1989)1100 DOI: [doi.org/10.1016/0002-8703\(89\)90834-X](https://doi.org/10.1016/0002-8703(89)90834-X)
- Elkady E., Moffid M., Mostafa E., M.Sayed R. (2025) Enhancing the practicality along with greenness sustainability of a high throughput HPLC-MS/MS bio-analytical method for the simultaneous determination of amlodipine, perindopril, and its active metabolite perindoprilat in human plasma: Application to a pharmacokinetic study. *J. Chromatogr A* 1740 (2025) 465559.
DOI: <https://doi.org/10.1016/j.chroma.2024.465559>
- Gong H., Ouyang X., Chen C. & Cai C. (2025) Biomimetic molecularly imprinted hollow fiber membranes for continuous Enantioseparation of amlodipine. *Microchem J.* 216(2025)114574,
DOI: <https://doi.org/10.1016/j.microc.2025.114574>
- González-Velasco J. (2012) Aspectos teóricos de las reacciones de transferencia de carga. Madrid, Universidad Autónoma de Madrid, 2012
- Hajilo S. & Reza M. (2025) Spectrophotometric method based on Continuous wavelet transform and ratio subtraction methods for the rapid simultaneous quantification of Valsartan, Amlodipine, and hydrochlorothiazide in cardiovascular tablet formulation. *Spectrochim Acta A Mol. Biomol. Spectrosc* 330 (2025) 125715.
DOI: <https://doi.org/10.1016/j.saa.2025.125715>
- Jadon N., Jain R. & Pandey A. (2017) Electrochemical analysis of amlodipine in some pharmaceutical formulations and biological fluid using disposable pencil graphite electrode *J. Electroanal. Chem* 788,(2017) 7-13.
DOI: <https://doi.org/10.1016/j.jelechem.2017.01.055>
- Neda Z. & Ghoreishi S. (2025) Electrochemical detection of hydrochlorothiazide in the presence of amlodipine and valsartan using FeMOF/g-C₃N₅-Modified Carbon Paste Electrode. *Electrochim. Acta* 536(2025) 1466652025.
DOI: <https://doi.org/10.1016/j.electacta.2025.146665>
- Pletcher D., Greff R., Peter L. & Robinson J. (2002) *Instrumental methods in electrochemistry*, Woodhead Publishing Limited (2002) 178.


Recibido: 7 de julio 2025

Aceptado: 20 de octubre 2025

Martínez, Yris: *Dr Química Aplicada, mención: Electroquímica. Profesora Titular del Departamento de Química. Miembro del personal de Investigación del Laboratorio de Electroquímica, Facultad de Ciencias Universidad de los Andes. Merida-Venezuela. Líneas de Investigación: Electrosíntesis Orgánica, Electroanálisis y Celdas de Combustibles.*


 <https://orcid.org/0000-0003-4479-0318>

Hernandez, Ricardo: *Licenciado en Química, Universidad de Los Andes, 1989. Magister Scientiae (MSc). Electroquímica. Universidad de Los Andes, 1994. Philosophy Doctor (PhD). Physical-Chemistry. University of Wales, United Kingdom. 1998. Profesor Titular a dedicación exclusiva del Departamento de Química de la Facultad de Ciencias en la Universidad de Los Andes. Coordinador del Grupo de Electroquímica. Miembro del Postgrado de Electroquímica Fundamental y Aplicada. Líneas de investigación: Electrocatalisis, Electroanalítica, Energía Electroquímica. Correo electrónico: rmhr@ula.ve*

 <https://orcid.org/0000-0002-3295-914X>


Ayala, Carlos: *Licenciado en Química, MSc. y Dr. en Química Analítica. Miembro del Laboratorio de Espectroscopia Molecular (Coordinador del Postgrado en Química Analítica, PQA). Profesor Titular de la planta profesoral del Departamento de Química, Facultad de Ciencias, Universidad de los Andes. Líneas de Investigación: Desarrollo de metodologías analíticas mediante el uso de Técnicas Espectroscópicas, Cromatográficas, Análisis en flujo, Quimiometría*

Correo electrónico: carlosayala@ula.ve

 <https://orcid.org/0000-0002-7246-5208>

Laguna, Alexander: *Lic. en Química 2004. MSc. en Electroquímica Fundamental y Aplicada 2015. Investigador en Ciencias Básicas Naturales y Aplicadas, Laboratorio de Electroquímica Departamento de Química, Facultad de Ciencias. Universidad de los Andes. Merida-Venezuela Líneas de Investigación: Electrosíntesis Orgánica, Electroanálisis.*

Correo electrónico: alexanderlaguna@gmail.com

 <https://orcid.org/0009-0007-0484-9713>


Calderon, Viery: *Licenciado en Química 2025. Laboratorio de Electroquímica. Departamento de Química, Facultad de Ciencias, Universidad de Los Andes, Mérida-Venezuela. Líneas de Investigación: Electroanálisis.*

Correo electrónico: viery.calderon2@gmail.com

 <https://orcid.org/0009-0006-1990-0043>

Méndez, Fernando: *Licenciado en Química y Doctor en Química Analítica, Profesor del Departamento de Química, Facultad de Ciencias. Universidad de los Andes. Mérida-Venezuela. Líneas de Investigación: Desarrollo de metodologías analíticas.*

Correo electrónico: mendezpj@gmail.com

 <https://orcid.org/0009-0004-5427-6384>.

The Jacobsen catalyst in asymmetric synthesis: Structure, mechanism, and applications

El catalizador de Jacobsen en síntesis asimétrica: estructura, mecanismo y aplicaciones

Contreras, Ricardo R.^{1*}

¹Laboratorio de Organometálicos, Departamento de Química, Facultad de Ciencias,
Universidad de los Andes, Mérida 5101, Venezuela.

*ricardo@ula.ve ; ricardo.r.contreras@gmail.com

Abstract

The Jacobsen catalyst has become a benchmark in asymmetric synthesis over the past three decades, particularly in the enantioselective epoxidation of unfunctionalized alkenes. This work provides a critical overview of the structural features, mechanistic insights, and synthetic applications of the (R,R)-Jacobsen catalyst and its analogues. Particular emphasis is placed on its ability to achieve high enantiomeric excess, its commercial availability, and its broad substrate scope. Recent advancements, including metal substitution, heterogeneous immobilization, and the integration of computational approaches, have further expanded the catalyst's utility and improved its sustainability profile. Representative examples from the total synthesis of natural products and pharmacologically active compounds underscore the continued relevance of Jacobsen-type systems in contemporary chemistry. Overall, the catalyst stands as a paradigmatic model of selectivity, efficiency, and adaptability in modern stereoselective catalysis, in accordance with the principles of green chemistry.

Keywords: Catalysis, Jacobsen catalyst, manganese, olefins, epoxidation, asymmetric synthesis.

Resumen

El catalizador de Jacobsen se ha convertido en un referente en la síntesis asimétrica durante las últimas tres décadas, en particular en la epoxidación enantioselectiva de alquenos no funcionalizados. Este trabajo ofrece una revisión crítica de las características estructurales, los aspectos mecanísticos y las aplicaciones sintéticas del catalizador (R,R)-Jacobsen y sus análogos. Se hace especial énfasis en su capacidad para lograr altos excesos enantioméricos, su disponibilidad comercial y su amplio espectro de sustratos. Los avances recientes, como la sustitución metálica, la inmovilización heterogénea y la integración de enfoques computacionales, han ampliado aún más la utilidad del catalizador y mejorado su perfil de sostenibilidad. Ejemplos representativos de síntesis total de productos naturales y compuestos con actividad farmacológica destacan la vigencia de los sistemas tipo Jacobsen en la química contemporánea. En conjunto, el catalizador se erige como un modelo paradigmático de selectividad, eficiencia y adaptabilidad en la catálisis estereoselectiva moderna, de acuerdo con los principios de la química verde.

Palabras clave: Catálisis, catalizador de Jacobsen, manganeso, olefinas, epoxidación, síntesis asimétrica.

1 Introduction

A significant advance in modern chemistry has been the development of enantioselective (or asymmetric) synthesis (Brown et al., 1989). This progress is particularly relevant considering that most naturally occurring compounds are chiral, possessing one or more stereogenic carbon centres and exhibiting optical activity. The impact of this field has been so profound that it was acknowledged with the

2001 Nobel Prize in Chemistry, awarded to K. Barry Sharpless, William S. Knowles, and Ryoji Noyori for their pioneering contributions to asymmetric catalysis (Periasamy, 2002; Noyori, 2002). Two decades later, the 2021 Nobel Prize in Chemistry was awarded to Benjamin List and David W. C. MacMillan, whose contributions to chiral organocatalysis further expanded the scope of asymmetric synthesis (Hargittai, 2022).

Asymmetric synthesis can be defined as the field of chemistry focused on the development of molecules con-

taining chiral centres, employing strategies that enable stereoselective control to generate specific enantiomers or diastereomers. This process typically involves the selective formation of one or more stereogenic centres, most commonly achieved through the use of asymmetric catalysts (Behera et al., 2023), chiral reagents (Wang et al., 2018), or kinetic resolution techniques (Imayoshi et al., 2021). A central objective is to maximize the enantiomeric excess (e.e.) of the resulting products, a key parameter in the design and synthesis of bioactive molecules and pharmaceutical agents.

In this context, one of the most successful catalysts in asymmetric synthesis emerged: the Jacobsen catalyst, named after the American chemist Eric N. Jacobsen, whose pioneering contributions to the asymmetric epoxidation of alkenes are widely recognized. In this system, the active centre consists of a Mn(III) ion coordinated by a *salen*-type ligand that provides the chiral environment required for enantioselectivity (Contreras et al., 2018). The Jacobsen catalyst, formally designated as *N,N'*-bis(3,5-di-*tert*-butylsalicylidene)-1,2-cyclohexanediaminomanganese(III) chloride (see Fig. 1), was first reported in 1991 as an effective enantioselective system for the epoxidation of a representative range of unfunctionalized alkenes (Jacobsen et al., 1991). This seminal publication was preceded by earlier studies on related analogues (Zhang et al., 1990; Zhang et al., 1991), conducted as part of a broader research program at the Roger Adams Laboratory, Department of Chemistry, University of Illinois (USA).

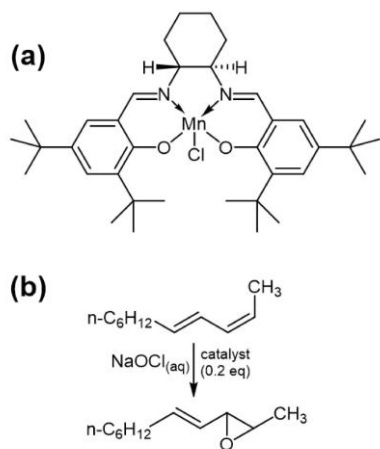


Fig. 1. (a) Structure of the (R,R)-Jacobsen catalyst. (b) Example of a reaction involving a pharmaceutically relevant substrate catalyzed by Jacobsen's catalyst (Chang et al., 1993).

Since the publication of Jacobsen's initial results (Lee et al., 1991; Deng et al., 1992; Palucki et al., 1992; Jacobsen et al., 1994), the catalyst rapidly gained widespread recognition as a powerful tool in asymmetric synthesis (Chang et al., 1994). In recognition of its remarkable efficiency in producing highly enantiomerically enriched epoxides from unfunctionalized olefins, the (R,R)-Jacobsen catalyst was designated "Reagent of the Year" by *Fluka* in 1994 (Hanson, 2001). Furthermore, Eric N. Jacobsen received two

prestigious honors for his pioneering contributions: the 2016 Arthur C. Cope Award (Wang, 2016), "for his contributions, both fundamental and practical, to the fields of asymmetric catalysis and organic synthesis," and the 2024 Willard Gibbs Medal (Cottle, 2024).

In this regard, it is important to emphasize the strategic relevance of transition metal catalysis (Contreras, 2021a), both in homogeneous and heterogeneous phases, in advancing research and development, particularly due to its broad applicability in organic synthesis (Wang, 2015). Along these lines, a wide range of homogeneous catalysts have been developed, many of which, like the Jacobsen catalyst, have become indispensable tools for the chemical transformation of structurally diverse substrates. Notable examples that have received considerable recognition in recent decades include Wilkinson's catalyst (Contreras et al., 2017a), Vaska's complex (Contreras et al., 2020a), Grubbs' catalyst (Contreras et al., 2020b), Crabtree's catalyst (Contreras et al., 2020c), Stryker's reagent (Contreras, 2021b), Schwartz's reagent (Contreras et al., 2021c), and the Lindlar catalyst (Contreras, 2023), among others.

Given the significance of asymmetric epoxidation reactions and in commemoration of nearly thirty-five years since Eric N. Jacobsen's seminal publication introducing the catalytic activity of his Mn(III)-based system, this article presents a concise review of the Jacobsen catalyst and its most relevant applications, highlighting the fundamental role of catalysis within the framework of the twelve principles of green chemistry (Contreras, 2017b).

2 Methodology

The methodology employed consisted of a systematic review of the specialized scientific literature aimed at examining the Jacobsen catalyst in the context of its relevance to asymmetric synthesis. For this purpose, the following databases were consulted: ACS Publications, ScienceDirect, Scopus, Google Scholar, and the digital catalogs of Strem Chemicals and Sigma-Aldrich (Merck KGaA®). The search strategy utilized the keywords "Jacobsen catalyst," "epoxidation," and "catalysis," in combination with terms such as "manganese catalyst," "asymmetric catalysis," and "enantioselective epoxidation." The review covered the period from 1991 to 2024, taking as its starting point the seminal article by Eric N. Jacobsen published in the *Journal of the American Chemical Society* in 1991 (Jacobsen et al., 1991). Additionally, a keyword co-occurrence analysis was performed using the VOSviewer software (version 1.6.20) (Van Eck et al., 2010) based on a Scopus® database search with "Jacobsen catalyst" as the primary keyword. The dataset was filtered by relevance, and the records were clustered using the program's algorithm. The resulting bibliometric map revealed color-coded thematic clusters, highlighting the main research areas associated with Jacobsen-type catalysts.

3 Results and Discussion

3.1 Synthesis of (*R,R*)-Jacobsen Catalyst

The synthetic route to the (*R,R*)-Jacobsen catalyst, as originally described by Eric N. Jacobsen, involves at least four steps (Larow et al., 2003), beginning with the preparation of the ligand (1*R*,2*R*)-(-)-1,2-cyclohexane-*N,N'*-bis(3,5-di-*tert*-butylsalicylidene), which is obtained through the condensation of (*R,R*)-1,2-diaminocyclohexane mono-(+)-tartrate with 3,5-di-*tert*-butylsalicylaldehyde. Both the (*R,R*)-Jacobsen ligand (CAS 135616-40-9; Sigma-Aldrich: 40,441-1; Strem Chemicals: 07-0316) and the catalyst itself (CAS 138124-32-0; Sigma-Aldrich: 40,444-6; Strem Chemicals: 25-0300) are now commercially available. For illustrative purposes, the final two steps of the synthesis were selected and are shown in Fig. 2.

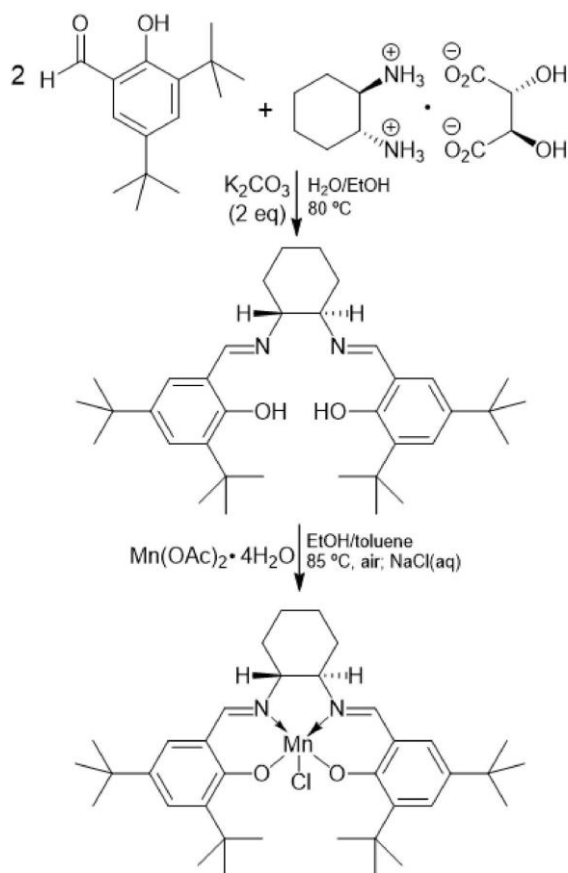


Fig. 2. Synthesis of Jacobsen's catalyst, adapted from the Organic Syntheses database (Larow et al., 2003).

3.2 (*R,R*)-Jacobsen Catalyst structure and molecular architecture

Structurally, the Jacobsen catalyst exemplifies the application of molecular architecture in the design of catalysts capable of directing chemical transformations and, in this case, facilitating enantioselective reactions. The proposed mechanistic model considers the presence of a *salen*-type

ligand containing highly sterically demanding groups, such as *tert*-butyl substituents, which promote a lateral or "side-on" approach for the stereoselective transfer of oxygen to the substrate (Fig. 3a). This model was originally introduced in the context of asymmetric epoxidation catalyzed by metal-porphyrin complexes (Groves et al., 1983). According to this interpretation, the alkene is sterically constrained by the bulky ligand environment, forcing a lateral approach to the metal-oxo intermediate, an interaction that accounts for the high levels of enantioselectivity observed. Although the exact sequence of bond formation remains a matter of debate, there is clear consensus that steric effects play a critical role in the reaction. This mechanistic model has become a widely accepted paradigm for the epoxidation of olefins using tetradentate metal complexes, particularly those featuring *salen*-based ligands. Moreover, it has been proposed that the same *salen*-type ligands responsible for enantioselectivity in epoxidation also create a chiral environment favourable for the nucleophilic ring-opening of epoxides through Lewis acid-base activation (Jacobsen, 2000) (Fig. 3b).

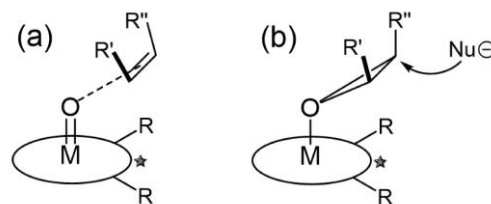


Fig. 3. (a) Schematic representation of the side-on approach model for the epoxidation of alkenes by chiral metal-*salen* complexes. (b) Possible mode of Lewis acid-base activation of epoxides.

3.3 El (*R,R*)-Jacobsen Catalyst en la literatura especializada

The number of publications related to the Jacobsen catalyst has shown an upward trend over time, as illustrated in Fig. 5. The graph, based on data from Google Scholar, ScienceDirect, ACS Publications, and Scopus, reflects a steady increase in research activity beginning in 1991 and peaking between 2005 and 2015. This surge in publications coincides with the widespread recognition of the Jacobsen catalyst in the field of enantioselective epoxidation. Google Scholar reports the highest number of entries due to its broader coverage, which includes journal articles, books, theses, patents, and preprints. ScienceDirect and Scopus display a similar trend, although with comparatively fewer publications, while ACS Publications shows a more limited representation but follows the same general pattern of growth. The decline in the number of studies published after 2015 suggests that the topic has reached a stage of maturity, with ongoing research increasingly focused on specific applications. These findings highlight the Jacobsen catalyst as a topic of sustained scientific interest, particularly in the development of asymmetric epoxidation methodologies. The

overall trend, together with the continued presence of references in databases such as Google Scholar, underscores the catalyst's enduring relevance in contemporary scientific literature.

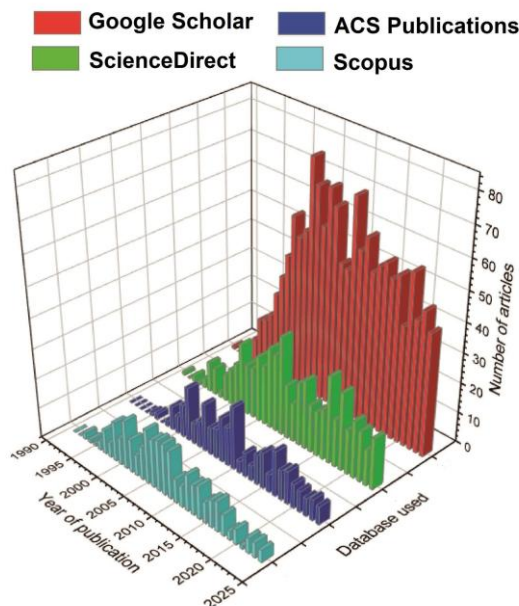


Fig. 4. Annual distribution of published articles on the Jacobsen catalyst during the period 1991–2024. The search was refined to exclude duplicate results, yielding 1232 entries in Google Scholar, 458 in ScienceDirect, 275 in Scopus, and 263 in ACS Publications. Keyword used: “Jacobsen catalyst”.

In addition, based on data retrieved from Scopus using “Jacobsen catalyst” as the search keyword and processed with the VOSviewer software (Van Eck et al., 2010), a network visualisation was generated (Fig. 5). The resulting map illustrates the interconnections among key concepts emerging from the literature on the Jacobsen catalyst, particularly those related to the catalytic epoxidation of alkenes and their association with enantioselective synthesis, highlighting the central role of this catalytic system. The structure displayed in the network reveals three main clusters: (1) a red cluster, where terms such as *catalysis*, *epoxidation*, *enantioselectivity*, and *manganese compounds* emphasise the relevance of manganese complexes in alkene epoxidation; (2) a green cluster, which reflects the connection to enantioselective synthesis and pharmaceutical applications, represented by terms such as *stereochemistry*, *drug synthesis*, and *epoxide*; and (3) a blue cluster, which associates epoxidation with the use of prochiral ligands and oxidising agents, reinforcing the role of metal complexes in modulating catalytic activity. The strong interconnection between the Jacobsen catalyst and enantioselective epoxidation processes highlights its ongoing relevance in the field and reaffirms its status as a foundational system for asymmetric transformations with broad impact across modern chemistry.

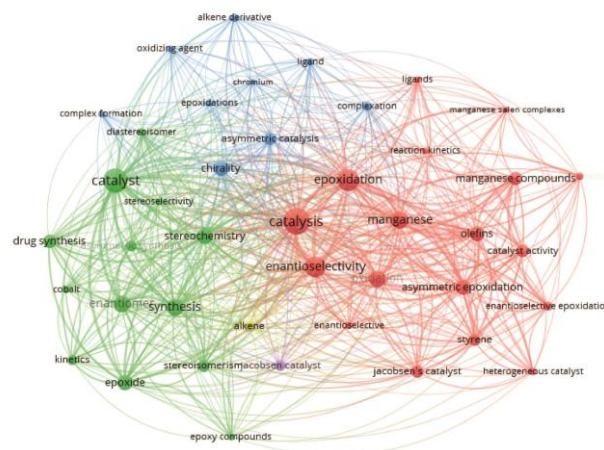


Fig. 5. Network visualization generated with VOSviewer (version 1.6.20) using data retrieved from Scopus with “Jacobsen catalyst” as the search keyword. The resulting map reveals three main thematic clusters: (1) manganese complexes and enantioselective epoxidation (red), (2) enantioselective synthesis and pharmaceutical chemistry (green), and (3) prochiral ligands and oxidising agents (blue). Jacobsen’s catalyst appears as a central node in the network.

Considering its relevance, the review of the primary literature reveals a substantial number of studies devoted to specific applications of the Jacobsen catalyst, together with numerous investigations employing Mn(III) complexes bearing various *salen*-type ligands (Sasaki et al., 1994; Hosoya et al., 1994) for the epoxidation of alkenes with a wide range of molecular substituents. These substrates include heterocyclic rings such as chromones (Yang et al., 2019; Adam et al., 1996), isoflavones (McGarrigle et al., 2005; Adam et al., 1998), indene and styrene derivatives, as well as long-chain saturated and polyunsaturated alkenes, among other functionalised groups. Notably, from around 1995, these complexes began to be referred to in the literature as “Jacobsen-type” *salen* complexes (Pietikäinen, 1995) or as Jacobsen’s Mn(III) *salen* catalysts (Adam et al., 1995).

In this context, the Jacobsen catalyst has been applied in a variety of emerging areas, including the structural modification of carbohydrates (Wang et al., 2018) and the development of novel methodologies such as its immobilisation on organic and inorganic supports, for example ZnPS–PVPA (Huang et al., 2019). Although such immobilisation strategies had already been reported (Silva et al., 2004), recent innovations have focused on the incorporation of new types of support materials. Moreover, several recent studies have highlighted its role in the total synthesis of pharmacologically relevant compounds, including centrolobine and other molecules exhibiting antitubercular activity (Kumar et al., 2021).

In recent years, research has increasingly centred on modifying the Jacobsen catalyst to develop a new generation of catalytic systems (Martines et al., 2005; Fig. 6), thereby opening a promising and rapidly evolving area of investigation.

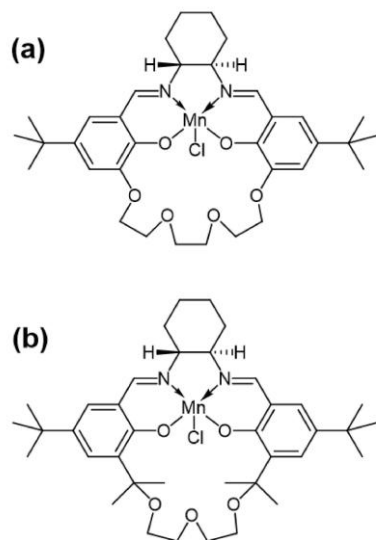


Fig. 6. Jacobsen catalysts of the first (a) and second (b) generations.

3.4 The Jacobsen catalyst in the total synthesis of complex molecules and natural products

A review of the Jacobsen catalyst's role in the total synthesis of natural products demonstrates its relevance as a key tool in organic chemistry, particularly for enabling direct asymmetric epoxidation of alkene functionalities and for performing kinetic resolution strategies such as hydrolytic kinetic resolution (HKR), in which the catalyst selectively differentiates between enantiomers in racemic mixtures. These transformations often represent crucial steps in synthetic strategies designed to achieve products with the desired enantioselectivity. In this regard, the Jacobsen catalyst has been employed in the synthesis of numerous pharmacologically relevant compounds, including S-atenolol, a β -adrenergic receptor antagonist used to treat cardiovascular conditions (Subhas et al., 2005); 7(S),17(S)-resolvin D5, a potent anti-inflammatory agent (Rodríguez et al., 2005); divergolides E and H, compounds investigated for anti-inflammatory, antioxidant, and antineoplastic properties (Caplan et al., 2018); (–)-galanticic acid, with therapeutic potential for cognitive and neurological disorders (Rahman et al., 2020); dendrodolide L, a medium-sized cyclic compound with antibacterial and anticancer potential (Regalla et al., 2017); relgro and 10'-oxorelgro, macrolides of interest due to their antibiotic, immunomodulatory, anti-inflammatory, and antitumour properties (Mohapatra et al., 2019); (2E)-macrolactin 3, known for its broad-spectrum biological activity, including antibacterial, antifungal, antiviral, anticancer, and anti-inflammatory effects (Reddy et al., 2023); chromanol 293B, studied for its pharmacological applications in arrhythmia, hypertension, and other cardiovascular conditions (Ma et al., 2020); and bistramide A, which interacts with actin and contributes to antitumour effects (Hanna et al., 2018).

Other noteworthy applications include (+)-desmethylestospongins B, an IP3R inhibitor relevant to cancer therapy development (Borum et al., 2024); diphosphatidyltrehalose, a component of the *Mycobacterium tuberculosis* cell wall targeted for diagnostic and therapeutic purposes (Mishra et al., 2019); pyrenophorol, exhibiting antifungal and antimicrobial activity against a variety of organisms (Anusha et al., 2024); (+)-muconin, showing cytotoxicity towards human tumour cells (Srinivas et al., 2018); greensporone F and dechlorogreensporone F, fungal metabolites with antimicrobial and anticancer properties (Gaddam et al., 2020); cryptorigidifoliol K, a diterpenoid from *Cryptocarya rigidifolia* with antimycobacterial, antiparasitic, and antitumour activity (Reddy et al., 2017); berkeleylactone A, a macrolide displaying promising antibiotic potential (Schmidt et al., 2023); crispine A, a pyrroloisoquinoline alkaloid with potential applications in oncology (Mohan et al., 2021); combretastatins D-1, a natural product with anti-inflammatory and anticancer activity (de Lima et al., 2023); methoxylated ether lipids, intermediates in the synthesis of anti-inflammatory and anticancer drugs (Sigurjónsson et al., 2022); and miyakolide, madeirolide A, lasonolide A, polycavernoside A, and clavosolides, marine natural products containing a 4-O-2,3,4,6-tetrasubstituted tetrahydropyran moiety and exhibiting diverse biological activities, particularly anti-inflammatory and anticancer effects (Fariñas-Ramos et al., 2021).

As illustrated by the examples above, the Jacobsen catalyst has found broad application in the total synthesis of natural products and other bioactive compounds. Its use continues to expand, particularly in the design of synthetic strategies for novel pharmaceutical agents and fine chemicals.

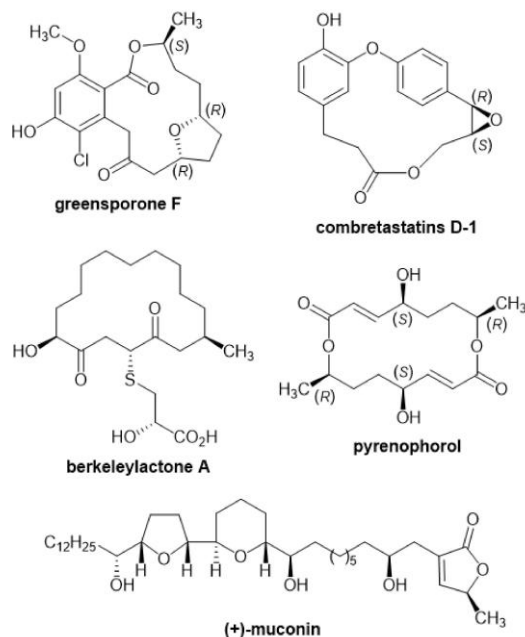


Fig. 7. Structures of selected natural products whose total syntheses involve the use of the Jacobsen catalyst.

3.5 Current trends in the use and application of the Jacobsen catalyst

Over the past three decades, the Jacobsen catalyst has undergone a series of modifications aimed at broadening its applications in asymmetric epoxidation and in the kinetic resolution of racemic mixtures, thereby consolidating its status as a powerful tool in stereoselective chemical synthesis. One of the earliest and most influential developments was the substitution of the Mn(III) ion with other transition metals, significantly expanding the scope and efficiency of asymmetric catalytic transformations. Among these, Cr(III) complexes [Cr(*salen*)] have shown excellent performance in the enantioselective epoxidation of alkenes, offering notable improvements in both catalytic activity and selectivity (Shaw et al., 2019; McGarrigle et al., 2005). In particular, such complexes have been encapsulated within catalytic nanoreactors employing thermoresponsive polymer matrices formed through the folding of amphiphilic random copolymers, namely poly(N-isopropylacrylamide-co-IL/Cr(*salen*)) [poly(NIPAAM-co-IL/Cr(*salen*))], which exhibit superior performance compared to conventional [Cr(*salen*)] systems in aqueous asymmetric epoxidation (Wang et al., 2019). In parallel, Co(III) complexes [Co(*salen*)] have been widely employed in the hydrolytic kinetic resolution of terminal epoxides, affording enantiomerically pure epoxides and diols with excellent yields and minimal environmental impact (Kang et al., 2023; Vyas et al., 2021). Furthermore, the incorporation of alternative transition metals such as aluminium, iron, ruthenium, and vanadium has led to the development of new and valuable catalytic transformations, thereby enhancing the synthetic versatility of these systems (Gualandi et al., 2019; Cozzi, 2004). These advances have not only improved the reactivity of [M(*salen*)] complexes but have also enabled their application under more sustainable catalytic conditions, including aqueous media, ionic liquids, and heterogeneous supports (silica or functionalised polymers), in full accordance with the principles of green chemistry (Guo et al., 2023; Freire et al., 2019; Kaur, 2018; Guedes et al., 2005) (Fig. 8).

Alternatively, the design of more complex molecular architectures, such as dimeric and trimeric systems, has promoted cooperative interactions between metal centres and enabled catalyst reuse over multiple cycles without significant loss of efficiency (Lv et al., 2011).

Finally, the increasing use of computational tools for theoretical calculations has significantly deepened our understanding of this catalytic system and its role in reaction mechanisms, thereby refining strategies aimed at optimizing its performance (Teixeira et al., 2014; Kemper et al., 2009). For instance, computational studies have provided valuable insight into how the Jacobsen catalyst coordinates with nitrogen-doped graphene (Jang et al., 2020), as well as into the mechanism of imine formation from alcohols and amines, accompanied by the release of molecular hydrogen,

in a Jacobsen-type analogue (Samuelsen et al., 2019).

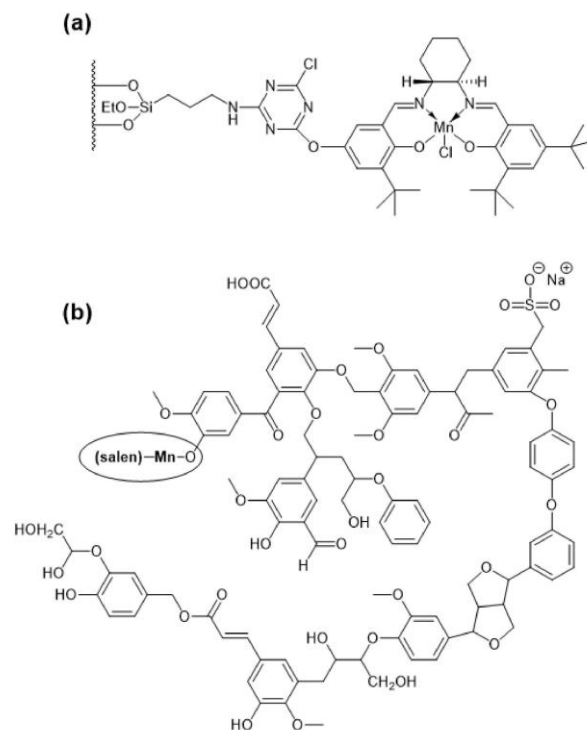


Fig. 8. (a) Representation of the immobilisation of Jacobsen-type complexes onto functionalised mesoporous silica via 3-aminopropyltriethoxysilane (Freire et al., 2019). (b) A Mn(*salen*)@lignin-based catalyst with ultra-low Mn content for the selective epoxidation of olefins under mild conditions (60 °C, 1 bar O₂) (Guo et al., 2023).

These trends position the Jacobsen catalyst as a robust system capable of responding to the demands of modern asymmetric catalysis, with proven relevance in both fundamental research and high-impact industrial applications.

5 Conclusiones

Since its introduction more than thirty years ago, the Jacobsen catalyst has established itself as one of the most versatile and effective systems for asymmetric epoxidation. Its distinctive structural design, centred on a Mn(III) *salen* complex, has enabled the development of highly enantioselective transformations applicable to a wide variety of unfunctionalised alkenes. The catalyst's commercial availability, broad substrate scope, and operational simplicity have all contributed to its widespread adoption in both academic research and industrial applications.

The continuous evolution of the Jacobsen catalyst, including the substitution of manganese with other transition metals and its immobilization on heterogeneous supports, has greatly broadened its synthetic versatility and environmental compatibility. Furthermore, the integration of computational methodologies has deepened mechanistic understanding, facilitating rational design and application in more sustainable catalytic processes.

The extensive number of total syntheses of natural products and pharmacologically active molecules that rely on Jacobsen-type systems attests to their enduring scientific relevance. Asymmetric catalysis remains a cornerstone of modern synthesis, and the Jacobsen catalyst continues to stand as a paradigmatic model of selectivity and adaptability in the field.

Acknowledgment

This work was supported by the Consejo de Desarrollo Científico, Humanístico, Tecnológico y de las Artes (CDCHTA-ULA) under Grant No. C-2010-25-08-B.

References

- Adam, W., Fell, R. T., Lévai, A., Patonay, T., Peters, K., Simon, A., Tóth, G. (1998). Enantioselective epoxidation of isoflavones by Jacobsen's Mn(III)salen catalysts and dimethyldioxirane oxygen-atom source. *Tetrahedron: Asymmetry*, 9(7), 1121–1124. [https://doi.org/10.1016/s0957-4166\(98\)00102-5](https://doi.org/10.1016/s0957-4166(98)00102-5)
- Adam, W., Jekő, J., Lévai, A., Majer, Z., Nemes, C., Patonay, T., Párkányi, L., Sebők, P. (1996). Determination of the absolute configuration of optically active 2,2-dimethyl-3,4-epoxychromans prepared by the catalytic enantioselective epoxidation with the dimethyldioxirane/Jacobsen Mn(III)salen system. *Tetrahedron: Asymmetry*, 7(8), 2437–2446. [https://doi.org/10.1016/0957-4166\(96\)00302-3](https://doi.org/10.1016/0957-4166(96)00302-3)
- Adam, W., Jekő, J., Lévai, A., Nemes, C., Patonay, T., Sebők, P. (1995). Enantioselective epoxidation of 2,2-dimethyl-2H-chromenes by dimethyldioxirane and Jacobsen's Mn(III)salen catalysts. *Tetrahedron Letters*, 36(21), 3669–3672. [https://doi.org/10.1016/0040-4039\(95\)00599-8](https://doi.org/10.1016/0040-4039(95)00599-8)
- Anusha, B., Kothapalli, R. B., Victor Prem Sagar, M., Surendra, B., Subba Reddy, U. V. (2024). Concise review on isolation, biological activity, structure elucidation, and total synthetic approaches of 16-membered C2-symmetric macrolide pyrenophorol. *Synthetic Communications*, 54(5), 323–347. <https://doi.org/10.1080/00397911.2023.2297966>
- Behera, P., Ramakrishna, D. S., Chandrasekhar, M. M., Kothakapu, S. R. (2023). A concise review on recent advances in catalytic asymmetric hydrogenation. *Chirality*, 35(8), 477–497. <https://doi.org/10.1002/chir.23559>
- Borum, A. K., Chen, K. Y., Zakarian, A. (2024). Scalable Total Synthesis of (+)-Desmethyloxestospingin B. *The Journal of Organic Chemistry*, 89(11), 8120–8130. <https://doi.org/10.1021/acs.joc.4c00779>
- Brown, J. M., Davies, S. G. (1989). Chemical asymmetric synthesis. *Nature*, 342(6250), 631–636. doi:10.1038/342631a0
- Chang, S., Lee, N. H., Jacobsen, E. N. (1993). Regio- and enantioselective catalytic epoxidation of conjugated polyenes. Formal synthesis of LTA4 methyl ester. *The Journal of Organic Chemistry*, 58(25), 6939–6941. <https://doi.org/10.1021/jo00077a001>
- Chang, S., Galvin, J. M., Jacobsen, E. N. (1994). Effect of Chiral Quaternary Ammonium Salts on (salen)Mn-Catalyzed Epoxidation of cis-Olefins. A Highly Enantioselective, Catalytic Route to Trans-Epoxides. *Journal of the American Chemical Society*, 116(15), 6937–6938. <https://doi.org/10.1021/ja00094a059>
- Contreras, R.R., Cardozo, E., García-Molina, L.O.J. (2017a). Transformando la catálisis homogénea: cincuenta años del catalizador de Wilkinson. *Avances en Química*, 12(2-3), 61–67. <https://doi.org/10.53766/AVANQUIM/2017.12.02.01>
- Contreras, R.R. (2017b), *Química Verde*. Caracas: Fondo Editorial OPSU.
- Contreras, R.R., y Rojas-Pérez, Y. (2018). Ligandos tipo salen en química de coordinación. Una breve revisión. *Revista Ciencia e Ingeniería*, 39(3), 307–314. <http://erevistas.saber.ula.ve/index.php/cienciaeingenieria/article/view/12994>
- Contreras, R.R., Cardozo-Villalba, E., y Fontal, B. (2020a). El complejo de Vaska y la química organometálica. *NOVASINERGÍA*, 3(1), 96–110. <https://doi.org/10.37135/ns.01.05.10>
- Contreras, R.R., Cardozo-Villalba, E., Lacruz-Vielma, E., y Paparoni-Bruzual, G. (2020b). El catalizador de Grubbs. Una breve revisión. *Revista Ciencia e Ingeniería*, 41(3), 323–336. <http://erevistas.saber.ula.ve/index.php/cienciaeingenieria/article/view/16419>
- Contreras, R.R., Urbina-Gutiérrez, J.A., y Rodríguez-Sulbarán, P.J. (2020c). El catalizador de Crabtree. Una breve revisión. *Revista Ciencia e Ingeniería*, 41(1), 3–14. <http://erevistas.saber.ula.ve/index.php/cienciaeingenieria/article/view/15867>
- Contreras, R.R. (2021a). Catálisis homogénea con metales de transición: transformando el mundo de la química. Parte 1. Mérida: Publicaciones CDCHTA-ULA. <https://doi.org/10.53766/BA/LIBULA/CatalisisI.2021>
- Contreras, R.R. (2021b). Polihidruros de cobre: una poderosa herramienta en síntesis química. El reactivo de Stryker en perspectiva, *Avances en Química*, 16(2), 39–48. <https://doi.org/10.53766/AVANQUIM/2021.16.02.01>
- Contreras, R.R., Bellandi, F., y Sánchez-Velasco, O. (2021c). Química organometálica aplicada. El reactivo de Schwartz. *Revista Ciencia e Ingeniería*, 42(2), 205–214. <http://erevistas.saber.ula.ve/index.php/cienciaeingenieria/article/view/17011>
- Contreras, R.R., Fonseca, Y. (2023). El catalizador de Lindlar. Una breve revisión. *Revista Ciencia e Ingeniería*, 44(1), 85–94. <http://erevistas.saber.ula.ve/index.php/cienciaeingenieria>

- [ja/article/view/18589](#)
- Cozzi, P. G. (2004). Metal–Salen Schiff base complexes in catalysis: practical aspects. *Chemical Society Reviews*, 33(7), 410–421. <https://doi.org/10.1039/b307853c>
- Cottle, S. (2024). Jacobsen receives 2024 Willard Gibbs Medal. *Chemical & Engineering News*, 102, 13, 36–37. <https://cen.acs.org/acs-news/Jacobsen-receives-2024-Willard-Gibbs/102/i13>
- de Lima Neto, J., Menezes, P. H. (2023). Combretastatins D series and analogues: from isolation, synthetic challenges and biological activities. *Beilstein Journal of Organic Chemistry*, 19(1), 399–427. <https://doi.org/10.3762/bjoc.19.31>
- Caplan, S. M., Floreancig, P. E. (2018). Total Synthesis of Divergolides E and H. *Angewandte Chemie*, 130(48), 16092–16096. <https://doi.org/10.1002/ange.201810336>
- Deng, L., Jacobsen, E. N. (1992). A practical, highly enantioselective synthesis of the taxol side chain via asymmetric catalysis. *The Journal of Organic Chemistry*, 57(15), 4320–4323. <https://doi.org/10.1021/jo00041a054>
- Fariña-Ramos, M., García, C., Martín, V. S., Álvarez-Méndez, S. J. (2021). Synthetic efforts on the road to marine natural products bearing 4-O-2, 3, 4, 6-tetrasubstituted THPs: an update. *RSC Advances*, 11(10), 5832–5858. <https://doi.org/10.1039/d0ra10755g>
- Gaddam, J., Reddy, A. V. V., Sarma, A. V., Yadav, J. S., Mohapatra, D. K. (2020). Total synthesis and structural revision of greensporone F and dechlorogreensporone F. *The Journal of Organic Chemistry*, 85(19), 12418–12429. <https://doi.org/10.1021/acs.joc.0c01644>
- Gualandi, A., Calogero, F., Potenti, S., Cozzi, P.G. (2019). Al(Salen) Metal Complexes in Stereoselective Catalysis. *Molecules*, 24(9), 1716. <https://doi.org/10.3390/molecules24091716>
- Guedes, D. F. C., Leod, T. C. O. M., Gotardo, M. C. A. F., Schiavon, M. A., Yoshida, I. V. P., Ciuffi, K. J., Assis, M. D. (2005). Investigation of a new oxidative catalytic system involving Jacobsen's catalyst in the absence of organic solvents. *Applied Catalysis A: General*, 296(1), 120–127. <https://doi.org/10.1016/j.apcata.2005.08.045>
- Guo, L., Yan, T., Zhang, R., Yi, L., Wang, Z., He, G., Chen, J., Wu, X. (2023). Ultra-low Mn (salen) supported on lignin and selective epoxidation of olefins. *ChemistrySelect*, 8(48), e202303634. <https://doi.org/10.1002/slct.202303634>
- Hanna, R. D., Naro, Y., Deiters, A., Floreancig, P. E. (2018). Potent and readily accessible bistramide analogues through diverted total synthesis. *Chemistry—A European Journal*, 24(61), 16271–16275. <https://doi.org/10.1002/chem.201804417>
- Hanson, J. (2001). Synthesis and use of Jacobsen's catalyst: Enantioselective epoxidation in the introductory organic laboratory. *Journal of Chemical Education*, 78(9), 1266–1268. <https://doi.org/10.1021/ed078p1266>
- Hargittai, I. (2022). The 2021 chemistry Nobel laureates and asymmetric organocatalysis. *Structural Chemistry*, 33(1), 303–305. <https://doi.org/10.1007/s11224-021-01857-0>
- Hosoya, N., Hatayama, A., Irie, R., Sasaki, H., Katsuki, T. (1994). Rational design of Mn–Salen epoxidation catalysts: Preliminary results. *Tetrahedron*, 50(15), 4311–4322. [https://doi.org/10.1016/s0040-4020\(01\)89368-6](https://doi.org/10.1016/s0040-4020(01)89368-6)
- Huang, J., Liu, S., Ma, Y., Cai, J. (2019). Chiral salen Mn (III) immobilized on ZnPS-PVPA through alkoxyl-triazole for superior performance catalyst in asymmetric epoxidation of unfunctionalized olefins. *Journal of Organometallic Chemistry*, 886, 27–33. <https://doi.org/10.1016/j.jorgchem.2019.02.008>
- Imayoshi, A., Lakshmi, B. V., Ueda, Y., Yoshimura, T., Matayoshi, A., Furuta, T., Kawabata, T. (2021). Enantioselective preparation of mechanically planar chiral rotaxanes by kinetic resolution strategy. *Nature Communications*, 12(1), 404. <https://doi.org/10.1038/s41467-020-20372-0>
- Jacobsen, E. N., Zhang, W., Muci, A. R., Ecker, J. R., Deng, L. (1991). Highly enantioselective epoxidation catalysts derived from 1,2-diaminocyclohexane. *Journal of the American Chemical Society*, 113(18), 7063–7064. <https://doi.org/10.1021/ja00018a068>
- Jacobsen, E. N., Deng, L., Furukawa, Y., Martínez, L. E. (1994). Enantioselective catalytic epoxidation of cinnamate esters. *Tetrahedron*, 50(15), 4323–4334. [https://doi.org/10.1016/s0040-4020\(01\)89369-8](https://doi.org/10.1016/s0040-4020(01)89369-8)
- Jacobsen, E. N. (2000). Asymmetric catalysis of epoxide ring-opening reactions. *Accounts of Chemical Research*, 33(6), 421–431. <https://doi.org/10.1021/ar960061v>
- Jang, D., Lee, Y., Shin, Y., Park, S., Jo, C., Kim, Y. H., Park, S. (2020). Coordination structure of Jacobsen catalyst with N-modified graphene and their electrocatalytic properties for reducing oxygen molecules. *Applied Catalysis B: Environmental*, 263, 118337. <https://doi.org/10.1016/j.apcatb.2019.118337>
- Kang, S. M., Song, X., Zhang, T. T., Xu, L., Zhu, Y. Y., Wu, Z. Q. (2023). Cobalt (III)–salen decorated stereoregular optically active helical polyisocyanides enable highly effective cooperative asymmetric catalysis toward the kinetic resolution of epoxides. *Inorganic Chemistry Frontiers*, 10(11), 3345–3358. <https://doi.org/10.1039/D3QI00384A>
- Kaur, N. (2018). Green synthesis of three- to five-membered O-heterocycles using ionic liquids. *Synthetic Communications*, 48(13), 1588–1613. <https://doi.org/10.1080/00397911.2018.1458243>
- Kemper, S., Hrobárik, P., Kaupp, M., Schlörer, N. E. (2009). Jacobsen's catalyst for hydrolytic kinetic resolution: structure elucidation of paramagnetic Co(III) salen complexes in solution via combined NMR and


- quantum chemical studies. *Journal of the American Chemical Society*, 131(12), 4172–4173. <https://doi.org/10.1021/ja806151g>
- Kumar, P., Fernandes, R. A., Ahmad, M. N., Chopra, S. (2021). Catalytic δ -hydroxyalkynone rearrangement in the stereoselective total synthesis of centrolobine, engelheptanoxides A and C and analogues. *Tetrahedron*, 96, 132375. <https://doi.org/10.1021/ja806151g10.1016/j.tet.2021.132375>
- Larrow, J. F., Jacobsen, E. N. (2003). (R,R)-N,N'-Bis(3,5-di-tert-butylsalicylidene)-1,2-Cyclohexanediamino Manganese(III) Chloride, A Highly Enantioselective Epoxidation Catalyst. *Organic Syntheses*, 75, 1. <https://doi.org/10.1002/0471264180.os075.01>
- Lee, N. H., Muci, A. R., Jacobsen, E. N. (1991). Enantio-merically Pure Epoxychromans via Asymmetric Catalysis. *Tetrahedron Letters*, 32(38), 5055–5058. [https://doi.org/10.1016/s0040-4039\(00\)93426-9](https://doi.org/10.1016/s0040-4039(00)93426-9)
- Lv, C., Xu, D., Wang, S., Miao, C.-X., Xia, C., Sun, W. (2011). A practical Ti-salen catalyst based on dimeric salen ligand for asymmetric addition of trimethylsilyl cyanide to aldehydes. *Catalysis Communications*, 12(13), 1242–1245. <https://doi.org/10.1016/j.catcom.2011.04.022>
- Martinez, A., Hemmert, C., Meunier, B. (2005). A macro-cyclic chiral manganese(III) Schiff base complex as an efficient catalyst for the asymmetric epoxidation of olefins. *Journal of Catalysis*, 234(2), 250–255. <https://doi.org/10.1016/j.jcat.2005.06.021>
- Ma, S.-H., Su Kim, Y., Min Jung, J., Reddy Boggu, P., Chan Kim, S., Su Kim, I., Hoon Jung, Y. (2019). Total Synthesis of Chromanol 293B and Cromakalim via Stereoselective Amination of Chiral Benzylic Ethers. *Tetrahedron Letters*, 151431. <https://doi.org/10.1016/j.tetlet.2019.151431>
- McGarrrigle, E. M., Gilheany, D. G. (2005). Chromium- and Manganese-salen Promoted Epoxidation of Alkenes. *Chemical Reviews*, 105(5), 1563–1602. <https://doi.org/10.1021/cr0306945>
- Mishra, V. K., Buter, J., Blevins, M. S., Witte, M. D., Van Rhijn, I., Moody, D. B., Brodbelt, J. S., Minnaard, A. J. (2019). Total Synthesis of an Immunogenic Trehalose Phospholipid from Salmonella Typhi and Elucidation of Its sn-Regiochemistry by Mass Spectrometry. *Organic Letters*, 21(13), 5126–5131. <https://doi.org/10.1021/acs.orglett.9b01725>
- Mohan, C., Krishna, R. B., Sivanandan, S. T., Ibnusaud, I. (2021). Synthesis of Pyrrolo [2, 1-a] isoquinoline Class of Natural Product Crispine A. *European Journal of Organic Chemistry*, 2021(35), 4911–4926. <https://doi.org/10.1002/ejoc.202100738>
- Mohapatra, D. K., Gaddam, J., Reddy, G. S., Kanakaraju, M., Kunwar, A. C., Yadav, J. S. (2019). Total synthesis and stereochemical revision of Relgro and 10'-Oxorelgro. *Organic & Biomolecular Chemistry*, 17(22), 5601–5614. <https://doi.org/10.1039/c9ob00838a>
- Noyori, R. (2002). Asymmetric catalysis: science and opportunities (Nobel lecture). *Angewandte Chemie International Edition*, 41(12), 2008–2022. [https://doi.org/10.1002/1521-3773\(20020617\)41:12<2008::AID-ANIE2008>3.0.CO;2-4](https://doi.org/10.1002/1521-3773(20020617)41:12<2008::AID-ANIE2008>3.0.CO;2-4)
- Palucki, M., Hanson, P., Jacobsen, E. N. (1992). Asymmetric oxidation of sulfides with H₂O₂ catalyzed by (salen)Mn(III) complexes. *Tetrahedron Letters*, 33(47), 7111–7114. [https://doi.org/10.1016/s0040-4039\(00\)60849-3](https://doi.org/10.1016/s0040-4039(00)60849-3)
- Pierasamy, M. (2002). 2001 chemistry nobel prize. *Resonance*, 7(2), 55–65. <https://doi.org/10.1007/bf02867269>
- Pietikäinen, P. (1995). Asymmetric epoxidation of unfunctionalized alkenes with periodates catalyzed by chiral (salen)Mn(III) complexes. *Tetrahedron Letters*, 36(2), 319–322. [https://doi.org/10.1016/0040-4039\(94\)02240-c](https://doi.org/10.1016/0040-4039(94)02240-c)
- Rahman, M. A., Haque, A., Yadav, J. S. (2020). Stereoselective total synthesis of (–)-galantinic acid and 1-deoxy-5-hydroxysphingolipids via prins cyclization. *Tetrahedron Letters*, 61(30), 152149. <https://doi.org/10.1016/j.tetlet.2020.152149>
- Reddy, A. V. V., Choudhury, U. M., Sarma, A. V., Mohapatra, D. K. (2023). Asymmetric Total Synthesis of (2E)-Macrolactin 3. *Synlett*, 34(01), 67–72. <https://doi.org/10.1055/a-1957-3966>
- Reddy, G. S., Padhi, B., Bharath, Y., Mohapatra, D. K. (2017). Total Synthesis of Four Isomers of the Proposed Structures of Cryptorigidifoliol K. *Organic Letters*, 19(24), 6506–6509. <https://doi.org/10.1021/acs.orglett.7b03174>
- Regalla, V. R., Addada, R. R., Puli, V. S., Saxena, A. S., Chatterjee, A. (2017). A short and concise route to total synthesis of Dendrodolide L. *Tetrahedron Letters*, 58(24), 2344–2346. <https://doi.org/10.1016/j.tetlet.2017.04.097>
- Rodríguez, A. R., Spur, B. W. (2005). First total synthesis of 7(S),17(S)-Resolvin D5, a potent anti-inflammatory docosanoid. *Tetrahedron Letters*, 46(21), 3623–3627. <https://doi.org/10.1016/j.tetlet.2005.03.175>
- Sasaki, H., Irie, R., Hamada, T., Suzuki, K., Katsuki, T. (1994). Rational design of Mn-salen catalyst (2): Highly enantioselective epoxidation of conjugated cis olefins. *Tetrahedron*, 50(41), 11827–11838. [https://doi.org/10.1016/s0040-4020\(01\)89298-x](https://doi.org/10.1016/s0040-4020(01)89298-x)
- Samuelson, S. V., Santilli, C., Ahlquist, M. S., Madsen, R. (2019). Development and mechanistic investigation of the manganese(III) salen-catalyzed dehydrogenation of alcohols. *Chemical Science*, 10(4), 1150–1157. <https://doi.org/10.1039/c8sc03969k>
- Schmidt, F., Viswanathan Ammanath, A., Götz, F., Maier, M. E. (2023). Synthesis of berkeleylactone A by

- ring-closing alkyne metathesis. *European Journal of Organic Chemistry*, 26(36), e202300615. <https://doi.org/10.1002/ejoc.202300615>
- Sigurjónsson, S., Lúthersson, E., Gudmundsson, H. G., Haraldsdóttir, H., Kristinsdóttir, L., Haraldsson, G. G. (2022). Asymmetric Synthesis of Methoxylated Ether Lipids: A Glyceryl Glycidyl Ether Key Building Block Design, Preparation, and Synthetic Application. *The Journal of Organic Chemistry*, 87(18), 12306–12314. <https://doi.org/10.1021/acs.joc.2c01515>
- Silva, A. R., Freire, C., de Castro, B. (2004). Jacobsen catalyst anchored onto an activated carbon as an enantioselective heterogeneous catalyst for the epoxidation of alkenes. *Carbon*, 42(14), 3027–3030. <https://doi.org/10.1016/j.carbon.2004.06.037>
- Shaw, S., White, J. D. (2019). Asymmetric Catalysis Using Chiral Salen–Metal Complexes: Recent Advances. *Chemical Reviews*, 119(16), 9381–9426. <https://doi.org/10.1021/acs.chemrev.9b00074>
- Srinivas, B., Reddy, D. S., Mallampudi, N. A., Mohapatra, D. K. (2018). A General Diastereoselective Strategy for Both cis- and trans-2, 6-Disubstituted Tetrahydropyrans: Formal Total Synthesis of (+)-Muconin. *Organic Letters*, 20(21), 6910–6914. <https://doi.org/10.1021/acs.orglett.8b03053>
- Subhas Bose, D., Venkat Narsaiah, A. (2005). An efficient asymmetric synthesis of (S)-atenolol: using hydrolytic kinetic resolution. *Bioorganic & Medicinal Chemistry*, 13(3), 627–630. <https://doi.org/10.1016/j.bmc.2004.10.057>
- Teixeira, F., Mosquera, R. A., Melo, A., Freire, C., Cordeiro, M. N. D. (2014). Effects of axial coordination on immobilized Mn (salen) catalysts. *The Journal of Physical Chemistry A*, 118(45), 10788–10796. <https://doi.org/10.1021/jp506206b>
- Van Eck, N. J., Waltman, L. (2010). Software survey: VOSviewer, a computer program for bibliometric mapping. *Scientometrics*, 84(2), 523–538. <https://doi.org/10.1007/s11192-009-0146-3>
- Wang, H. Y., Blaszczyk, S. A., Xiao, G., Tang, W. (2018). Chiral reagents in glycosylation and modification of carbohydrates. *Chemical Society Reviews*, 47(3), 681–701. <https://doi.org/10.1039/C7CS00432J>
- Wang, L. (2016). Arthur C. Cope Award: Eric N. Jacobsen. *Chemical & Engineering News*, 94(2), 33–35. <https://cen.acs.org/articles/94/i2/Arthur-C-Cope-Award-Eric.html>
- Wang, W., Li, C., Pi, Y., Wang, J., Tan, R., Yin, D. (2019). Chiral salen Cr(III) complexes encapsulated in thermo-responsive polymer nanoreactors for asymmetric epoxidation of alkenes in water. *Catalysis Science & Technology*, 9(20), 5626–5635. <https://doi.org/10.1039/C9CY01398A>
- Yang, Q., Guo, R., Wang, J. (2019). Catalytic Asymmetric Synthesis of 2-Aryl Chromenes. *Asian Journal of Organic Chemistry*, 8(10), 1742–1765. <https://doi.org/10.1002/ajoc.201900360>
- Zhang, W., Jacobsen, E. N. (1991). Asymmetric olefin epoxidation with sodium hypochlorite catalyzed by easily prepared chiral manganese(III) salen complexes. *The Journal of Organic Chemistry*, 56(7), 2296–2298. <https://doi.org/10.1021/jo00007a012>
- Zhang, W., Loebach, J. L., Wilson, S. R., Jacobsen, E. N. (1990). Enantioselective epoxidation of unfunctionalized olefins catalyzed by salen manganese complexes. *Journal of the American Chemical Society*, 112(7), 2801–2803. <https://doi.org/10.1021/ja00163a052>

Received: 16 de octubre de 2025

Accepted: 17 de noviembre de 2025

Contreras, Ricardo R.: Doctor of Chemistry with a major field in Inorganic and Organometallic Chemistry. Full Professor of Inorganic Chemistry in the Department of Chemistry, Faculty of Science, University of Los Andes. Coordinator of the Organometallic Laboratory and Chair of the Inorganic Chemistry Teaching Division. He is also a Fellow of the Academy of Mérida.

 <https://orcid.org/0000-0002-8168-5093>

Decidability between recognizable K-subsets

Decidibilidad entre K-subconjuntos reconocibles

Mantilla Morales, Gisella^{1*}; Bastidas Chalán, Rodrigo²; Rentería Torres, Aníbal²; Bustos Ganchozo, Oscar²; Ferrer-Guillén, María³; Mata-Díaz, Guelvis⁴

¹ Technical University of Manabí, Ecuador

² University of the Armed Forces-ESPE, Ecuador.

³ Faculty of Engineering, Department of Calculating, University of Los Andes, Mérida, Venezuela.

⁴ Faculty of Sciences, Department of Mathematics, University of Los Andes, Mérida, Venezuela.

*gbmantilla@espe.edu.ec

Abstract

This research deals with the problem of extending the conventional finite automata theory to the study of the equality theorem. For this purpose, an algebraic approach centered on the concepts of semi-rings, recognizable K-subsets and K- Σ -automata is proposed. The decidability of any pair of recognizable K-subsets is proved in this context. This means that the semiring K must be known well enough to permit such decisions.

Keywords: algebra, systems, automata, languages, equations, the equality theorem.

Resumen

Esta investigación aborda la extensión de la teoría convencional de autómatas finitos al estudio del teorema de igualdad. Para ello, se propone un enfoque algebraico centrado en los conceptos de semianillos, K-subconjuntos reconocibles y K- Σ -autómatas. En este contexto, se demuestra la decidibilidad de cualquier par de K-subconjuntos reconocibles. Esto significa que el semianillo K debe conocerse con suficiente precisión para permitir tales decisiones.

Palabras clave: álgebra, sistemas, autómatas, lenguajes, ecuaciones, el teorema de igualdad.

1 Introduction

In systems theory, a class called Systems of Discrete Events (SED) is well known (see Branicky, 1995). It includes Manufacturing Systems, Chemical Systems, Economic Systems, Legal Systems, Air Traffic Systems, Telecommunications Systems; in short, any system whose states change in discrete time due to the occurrence of actions or events (see Caspi, 1991).

In this manuscript the Automata are presented by means of an algebraic approach as it is exposed in (Eilenberg, 1974), where the arguments and demonstrations are constructive; in this way it breaks with the conventional form imposed in the current literature on Automata.

It is of utmost importance to mention that the basic notions on which the theory of Automata is built are those of

actions: events; and states: configurations of the system in time. Although these notions seem to be related to time, they are independent structurally speaking (see Mata, 2017). Indeed, at a logical level of abstraction, one is always interested, in the representation of a SED, only in the possible orders in which the actions of the system can occur (see Mata et al., 2018). This situation reasonably leads to verbally describe an SED as the set of all trajectories of a directed graph. Therefore, if Σ and Q are two sets representing actions and states respectively, and E is a proper subset of $Q \times \Sigma \times Q$, representing changes states by the occurrence of actions, then a SED is modeled by a quintuple $A = (Q, \Sigma, E, I, T)$, where I and T are subsets of Q representing the states in which the system can start and the goals respectively. Finally, A is an automaton.

Now, from practice, we consider automata whose sets of actions and states are finite. Thus, the trajectories of an SED can be viewed as finite sequences of the form $(q_0, \alpha_1, q_1), (q_1, \alpha_2, q_2),$

..., (q_{n-1}, α_n, q_n) , where each of these triples are elements of E . More precisely, the interest is focused on trajectories such that $q_0 \in I$ and $q_n \in T$. This set of trajectories corresponds to a set of labels of the form $\alpha_1\alpha_2 \dots \alpha_n$, which constitute the so-called behavior of the automaton A (or system dynamics), denoted by $|A|$. This work consists of the study of mathematical structures (sets, functions, and relations) that can be described (or recognized) by finite state divides without auxiliary memory or storage capacity, and join it we see that the equality theorem silently assumes that a number of other facts are decidable.

2 Preliminaries

The main purpose of this work is to include the most relevant notions of automata theory: regular languages, operations with automata, among others, which allow to fix the terminology and notations that later lead to an extension problem.

Let Σ be a set. The free monoid Σ^* with basis Σ is defined as follows: the elements of Σ^* are n -tuples $s=(\alpha_1, \alpha_2, \dots, \alpha_n)$, $n>0$, of elements of Σ . The integer n is called the length of s , which is denoted by $|s|$. If $w=(w_1, w_2, \dots, w_m)$ is another element of Σ^* , then the product is defined by concatenation; that is, $sw=(\alpha_1, \alpha_2, \dots, \alpha_n, w_1, w_2, \dots, w_m)$. Then, one obtains the monoid Σ^* with unit $\theta = ()$, the 0-tuple. Clearly, $|sw|=|s|+|w|$ and $|\theta|=0$. Putting $\alpha=(\alpha)$, $\alpha \in \Sigma$, one can write $s=\alpha_1\alpha_2 \dots \alpha_n$, if $n>1$.

Any subset L of Σ^* is called a language over Σ . On the other hand, $s \in \Sigma^*$ is called a prefix of $w \in \Sigma^*$, denoted $s \leq w$, if there exists a word $\sigma \in \Sigma^*$ such that $w=s\sigma$. Let $L \subset \Sigma^*$ be a language over Σ , the subset of all word prefixes of L is called the closure of L , denoted \bar{L} ; i.e., $\bar{L}=\{s \in \Sigma^*/\exists w \in L, sw \in L\}$. Finally, L is closed if $L=\bar{L}$.

For its part, automata theory is an approach that contains a state transition structure, which allows directing the analysis and synthesis by making use of the transition mechanism. Formally, let Σ be a finite alphabet. A Finite Automaton A (AF) over Σ or simply a deterministic Σ -automaton is a quin-tuple (Q, Σ, E, I, T) , where Q is a finite set whose elements are called states, I and T are subsets of Q called initial and final state sets respectively, and E is a subset of $Q \times \Sigma \times Q$, whose elements are called events. Additionally, if A has at most one initial state, and for all $q \in Q$ and $\alpha \in \Sigma$, there exists at most one event $(q, \alpha, p) \in E$, then A is called deterministic.

An event (q, σ, p) is denoted $q \xrightarrow{\sigma} p$, and this is said to begin at q and end at p with label σ .

A path c in A is a finite succession $c=(q_0, \alpha_1, q_1)(q_1, \alpha_2, q_2) \dots (q_{k-1}, \alpha_k, q_k)$ of consecutive arcs, where q_0 and

q_k are called the beginning and end of the path c respectively, and the integer $k \geq 1$ is called the length of the path. The following notations are used for a path c : $q_0 \xrightarrow{\sigma_1} q_1 \xrightarrow{\sigma_2} \dots \xrightarrow{\sigma_k} q_k$, $q_0 \xrightarrow{c} q_k$ or $c: q_0 \rightarrow q_k$. The element $=\alpha_1\alpha_2 \dots \alpha_k \in \Sigma^*$ is called the label of c and is denoted by $|c|$. The length of s is denoted by $|s|$ and that of the path by $\|c\|$. Thus, it follows that $|s|=\|c\|=k$.

For each state q , we include the null path (trivial path) 1_q , which starts and ends at q . By definition, the null path has label θ and length 0; that is, $|1_q|=0$ and $\|1_q\|=0$. Moreover, given two paths $c: p \rightarrow q$ and $c': q \rightarrow r$, the path $cc': p \rightarrow r$ (path composition) is defined by concatenation. then, $\|cc'\|=|c|+|c'|$ y $\|cc'\|=\|c\|+\|c'\|$.

Let $c: i \rightarrow t$ be a path in A , c is said to be a successful path if $i \in I$ and $t \in T$. The label of this path is called a successful label. The set of all successful labels in A is called the behavior or dynamics of A , and is denoted by $|A|$; i.e., $|A|=\{s \in \Sigma^*/\exists c: i \rightarrow t \text{ in } A, \text{ with } i \in I, t \in T, |c|=s\}$.

A language B of Σ^* is called regular if there exists a Σ -automaton A such that $B=|A|$.

In what follows we write $\alpha^*=\{\alpha\}^*$, for all $\alpha \in \Sigma$, in order to simplify the writing. Also, we treat $\alpha \in \Sigma$ and $s \in \Sigma^*$ as unitary sets.

Next, some basic automata operations are studied and their behaviors are analyzed. Let two AF be, $A=(Q_A, \Sigma, E_A, I_A, T_A)$ and $B=(Q_B, \Sigma, E_B, I_B, T_B)$, where $Q_A \cap Q_B=\emptyset$. The Σ -automaton union is given by $C=A \cup B=(Q_C, \Sigma, E_C, I_C, T_C)$, where $Q_C=Q_A \cup Q_B$, $I_C=I_A \cup I_B$, $T_C=T_A \cup T_B$. Moreover, an event is in E_C , if and only if, it is in E_A or it is in E_B . Therefore, a path is in C , if and only if, it is in A or it is in B .

The Σ -automaton product (or intersection) of A and B is given by $C=A \times B=(Q_C, \Sigma, E_C, I_C, T_C)$ where $Q_C=Q_A \times Q_B$, $I_C=I_A \times I_B$, $T_C=T_A \times T_B$. Consequently, an event $(p', p'') \xrightarrow{\alpha} (q', q'')$ is in E_C , if and only if, $p' \xrightarrow{\alpha} q'$ is an event in E_A and $p'' \xrightarrow{\alpha} q''$ is an event in E_B .

On the other hand, we call the inverse automaton of A the Σ -automaton given by $A^\circ=(Q, \Sigma, E^\circ, I, T)$, where E° is the subset whose elements are the inverse events of E ; that is, if $p \xrightarrow{\alpha} q$ is an event in E , then $q \xrightarrow{\alpha} p$ is an event in E° .

Note that, if c is a path in A with label $|c|=\alpha_1 \dots \alpha_k$, then c° is a path in A° with label $|c^\circ|=\varphi(\alpha_1 \dots \alpha_k)=\alpha_k \dots \alpha_1$, where $\varphi: \Sigma^* \rightarrow \Sigma^*$ is the inverse function defined by $\varphi(\theta)=\theta$, $\varphi(\alpha)=\alpha$, $\varphi(st)=\varphi(t)\varphi(s)=ts$.

It can be shown that the class of regular subsets is

closed under union, intersection and inverse.

Now, some constructions on automata are given, relating them by a monoid homomorphism $f: \Gamma^* \rightarrow \Sigma^*$, where Γ and Σ are two alphabets. Also, f is assumed to be a fine homomorphism: $f(\alpha) \in \Sigma \cup \theta$, $\forall \alpha \in \Gamma$. The identities θ_1 and θ_2 of Γ^* and Σ^* respectively are referred to as θ .

Indeed, let $f: \Gamma^* \rightarrow \Sigma^*$ be a fine homomorphism. We call the inverse image of A the Γ -automaton $f^{-1}(A)$, where Q, I, T are unperturbed, and the events are given by $\mathbf{p} \xrightarrow{\gamma} \mathbf{q}$, if $f(\gamma) = \alpha$ and $\mathbf{p} \xrightarrow{\alpha} \mathbf{q}$ is an event in A , and $\mathbf{q} \xrightarrow{\gamma} \mathbf{p}$, if $f(\gamma) = \theta$.

A path $c': \mathbf{p} \rightarrow \mathbf{q}$ in $f^{-1}(A)$ can be viewed as a pair (c, g) , where $c: \mathbf{p} \rightarrow \mathbf{q}$ is a path in A and $g \in \Gamma^*$ is such that $|c'|=g$ and $f(g)=|c|$; whence, it can be shown that if $f: \Gamma^* \rightarrow \Sigma^*$ is a fine homomorphism and $A \subset \Sigma^*$ is regular, then $f^{-1}(A) \subset \Gamma^*$ is regular.

Finally, let $f: \Gamma^* \rightarrow \Sigma^*$ be a homomorphism such that $f(\gamma) \neq \theta$, for all $\gamma \in \Gamma$ (or equivalently that $f^{-1}(\theta) = \emptyset$ or still equivalently that $|g| \leq |f(g)|$, for all $g \in \Gamma^*$). Let $\mathbf{A} = (Q, \Gamma, E, I, T)$ be a Γ -automaton. We call the direct image of \mathbf{A} the Σ -automaton $f(\mathbf{A}) = (Q', \Sigma, E', I, T)$ where $Q' \supset Q$ and the events are determined as follows: let $\mathbf{p} \xrightarrow{\gamma} \mathbf{q}$ be an event in A and $f(\gamma) = \alpha_1 \dots \alpha_n$, $n \geq 1$; if $n=1$, then the arc $\mathbf{p} \xrightarrow{\alpha_1} \mathbf{q}$ is in $f(A)$; if $n > 1$, then the arcs $\mathbf{p} \xrightarrow{\alpha_1} \mathbf{q}_1 \xrightarrow{\alpha_2} \mathbf{q}_2 \rightarrow \dots \rightarrow \mathbf{q}_{n-1} \xrightarrow{\alpha_n} \mathbf{q}$ are in $f(A)$, where the $n-1$ intermediate states are new distinct states added to Q' . Repeating this, for every arc in A , $f(A)$ is obtained.

As before, if $f: \Gamma^* \rightarrow \Sigma^*$ is a homomorphism such that $f^{-1}(\theta) = \emptyset$, and $A \subset \Gamma^*$ is regular, then $f(A) \subset \Sigma^*$ is regular.

3 K- Σ -Automatas

As a methodological support to formalize the technique describing the dynamics of an AF, the concept of multiplicity is included. This allows an extension grounded on mathematical objects (sets, functions, relations, among others) in the field of system dynamics.

To make it a little more precise, consider an AF $\mathbf{A} = (Q, \Sigma, E, I, T)$ with dynamics $|\mathbf{A}|$. If $c: i \rightarrow t$, $i \in I$, $t \in T$, $|c|=s$ is in \mathbf{A} and n determines the number of these paths, then one can define an application $\mu: \Sigma^* \rightarrow \mathbb{N}$ that specifies the multiplicity of the elements of Σ^* . This is referred to for $s \in \Sigma^*$, with multiplicity n . With abuse of language it is written $\mu = |\mathbf{A}|$ and $|\mathbf{A}|(s) = n$; whence, $|\mathbf{A}|(s) = 0$ expresses that $s \notin |\mathbf{A}|$. Finally, Σ^* is identified in what follows with $|\mathbf{A}|: \Sigma^* \rightarrow \mathbb{N}$. It is also emphasized that any subset A of Σ^* is equivalent to a function $A: \Sigma^* \rightarrow \beta$, with $\beta = \{0, 1\}$, in the sense that $s \in A \Leftrightarrow A(s) = 1$.

A fundamental structure for the development of this article is included. In fact, the notion of semiring is a weak structure of the conventional concept of ring.

Definition 1. A semiring K is a subset endowed with two operations: addition (+) and multiplication (.); such that $(K, +)$ is a commutative monoid with neutral element 0 and (K, \cdot) is a monoid with identity element 1. Moreover, for all $x, y, z \in K$ one has that $x(y + z) = xy + xz$; $(y + z)x = yx + zx$; $x0 = 0 = 0x$. A semiring K is called commutative if (K, \cdot) is commutative. Clearly, every ring with unity is a semiring.

Consider $\{x_i\}_{i \in I}$ an arbitrary collection of elements of a semiring K , with I a given set of indices.

$$\text{Assuming finiteness of } I, \sum_{i \in I} x_i \in K \quad (1)$$

The following properties with respect to the sum are true:

$$I = \{i\} \Rightarrow \sum_{i \in I} x_i = x_i \quad (2)$$

$$\text{Let } I = \bigcup_{j \in J} I_j \text{ be a partition of } I, z \in K \Rightarrow \sum_{i \in I} x_i = \sum_{j \in J} \left(\sum_{i \in I_j} x_i \right); z \left(\sum_{i \in I} x_i \right) = \sum_{i \in I} zx_i; \left(\sum_{i \in I} x_i \right) z = \sum_{i \in I} x_i z; I = \emptyset \Rightarrow \sum_{i \in I} x_i = 0. \quad (3)$$

Considering (1) as the sum $x+y$ and taking (2), (3), (K, \cdot) , as axioms, we define $x_1 + x_2 := \sum_{i \in I} x_i$ with $I = \{1, 2\}$; and $0 := \sum_{i \in I} x_i$ if $I = \emptyset$.

If I is finite, then clearly (1) is well defined. On the other hand, if I is an arbitrary index set, then (1) must be well-defined, and is an element of K . Thus, one has the concept of a complete semiring under the new definition. Consequently, every complete semiring is a semiring.

Definition 2. Given two semirings K and K' , a homomorphism $\varphi: K \rightarrow K'$ is any function such that $\varphi(x_1 + x_2) = \varphi(x_1) + \varphi(x_2)$, $\varphi(0) = 0'$; and $\varphi(x_1 \cdot x_2) = \varphi(x_1) \varphi(x_2)$, $\varphi(1) = 1'$.

Definition 3. A semiring K is called positive if it satisfies: $0 \neq 1$; if $x + y = 0$, then $x = y = 0$; if $xy = 0$, then $x = 0$ or $y = 0$.

K -subconjuncts, with K a semiring, are objects that allow identifying functions with their domains, and this constitutes a technical approach to notational handling and proof construction. In the following it is assumed that K is a nontrivial ($0 \neq 1$) and commutative semiring.

Definition 4. Let X be a set. A K -subset A of X is any function $A: X \rightarrow K$. For each $x \in X$, the element $A(x)$ is

called the multiplicity with which x belongs to A . If the values taken by A are 0 and 1, the K -subset A of X is said to be unambiguous.

Example 1. The subsets X, \emptyset and x , for all $x \in X$, defined by $X(x) = 1$, for all $x \in X$; $\emptyset(x) = 0$, for all $x \in X$; $x(y) = \begin{cases} 1, & \text{if } x = y \\ 0, & \text{in another case} \end{cases}$, respectively, are unambiguous.

The unambiguous subsets of x given in Example 1 are referred to as simplexes. If A is an unambiguous subset of X , then $x \in A$ and $A(x) = 1$ indicate the same thing.

We define the sum or union operation as follows: for each family $\{A_i\}_{i \in I}$ of K -subsets of X , with I an arbitrary family of indices $\left(\bigcup_{i \in I} A_i\right)(x) = \left(\sum_{i \in I} A_i\right)(x) = \sum_{i \in I} A_i(x)$. (4)

Now, consider the operation product (or multiplication) of $k \in K$ by a K -subset A as follows $(kA)(x) = kA(x)$ (5)

i.e., the result is a K -subset kA .

We have the following properties: $1A = A$, $0A = \emptyset$, $(k_1 k_2)A = k_1(k_2 A)$, $\left(\sum_{i \in I} k_i\right)A = \sum_{i \in I} k_i A$; and furthermore, $k\left(\sum_{i \in I} A_i\right) = \sum_{i \in I} k A_i$.

We define the intersection $A \cap B$ of two K -subsets as $(A \cap B)(x) = A(x)B(x)$.

The sum $\sum_{x \in X} A(x)x$ is called the expansion of A . This expression is useful for manipulating K -subsets.

Example 2. $kA = \sum_{x \in X} kA(x)x$; and further, $A \cap B = \sum_{x \in X} A(x)B(x)x$.

The study of the multiplication or product of K -subsets of S is included, being (S, \cdot) a semigroup. Indeed, a category of objects with the above-mentioned operations of addition and multiplication is included to formalize matrix notions and structures.

Definition 5. Let (S, \cdot) be a semigroup, A and B K -subsets of S , where K is a complete semiring. The K -subset product AB is given by $(AB)(z) = \sum_{xy=z} A(x)B(y)$.

It is clear that the operation AB is associative. Therefore, K^M is a semiring with identity θ , provided M is a monoid, where θ is the identity of M .

Consider P, Q two finite sets. A K -subset of $P \times Q$ is any matrix whose rows and columns are indexed using the elements of P and Q respectively, and whose entries are in K . Then, $A \in K^{P \times Q}$ is written A_{pq} instead of $A(p, q)$; thus, the matrix is written $A = [A_{pq}]$.

The matrix sum operation is established by the sum of K -subsets. That is, $(A+B)_{pq} = A_{pq} + B_{pq}$, provided that $B \in K^{P \times Q}$.

The matrix multiplication operation is given as follows: let $A \in K^{P \times Q}$ and $B \in K^{Q \times R}$ be, then $(AB)_{pr} = \sum_{q \in Q} A_{pq} B_{qr}$.

Some properties of multiplication: if $P = Q$, then $K^{P \times P}$ is a semiring with unit I_P , where $(1_P)_q' = \begin{cases} 1, & \text{if } q = q' \\ 0, & \text{if } q \neq q' \end{cases}$. A is called a row vector, provided that $A \in K^{P \times Q}$ and P is unitary. Also, A is called a column vector, provided that Q is unitary.

Definition 6. Let Σ be a finite alphabet and K a commutative semiring. A K - Σ -automaton A (or a deterministic K - Σ -automaton) is a quintuple, $A = (Q, \Sigma, E, I, T)$ where Q is a finite set, I and T are K -subsets of Q and E is K -subsets of $Q \times \Sigma \times Q$.

Given $A = (Q, \Sigma, E, I, T)$ a K - Σ -automaton, if $E(p, \alpha, q) = k \neq 0$, then there is said to be an arc from p to q denoted $p \xrightarrow{k\alpha} q$, labeled $k\alpha$. Also, $p \xrightarrow{k\alpha} q$ is said to be in A .

Thus, analogous to Σ -automata, one can consider paths $c: p \rightarrow q$. Then, if c is a path $p \xrightarrow{k_1 \alpha_1} q_1 \xrightarrow{k_2 \alpha_2} \dots \xrightarrow{k_n \alpha_n} q$, then $|c| = k\alpha$ is its label, with $k = k_1 \cdot \dots \cdot k_n$ and $s = \alpha_1 \cdot \dots \cdot \alpha_n$, and length $\|c\| = n = |s|$.

Definition 7. Let $A = (Q, \Sigma, E, I, T)$ be a K - Σ -automaton. The behavior or dynamics of A is a K -subset of Σ^* , denoted $|A|$, and is given by $|A| = \sum_{p, q \in Q} \sum_c I(p) |c| T(q)$, with c varying over all paths $c: p \rightarrow q$; i.e., $|A|(s) = \sum_{p, q \in Q} \sum_{k \in C} I(p) k T(q)$, where $C = \{k \in K: \exists c: p \rightarrow q, |c| = ks\}$.

Note that the K -subset E of $Q \times \Sigma \times Q$ can be viewed as a function $E: Q \times \Sigma \times Q \rightarrow K$. In what follows we write $E(p, \alpha, q) = E_{pq}(\alpha)$. Then, for all $p, q \in Q$, one has that E_{pq} is a K -subset of Σ . Then, E can be identified with a matrix $E: Q \times Q \rightarrow K^\Sigma$ called the transition matrix.

Any K -subset of Σ can be extended to a K -subset of Σ^* as follows: for $p, q \in Q$, $E_{pq}: \Sigma^* \rightarrow K$, $E_{pq}(s) =$

$\begin{cases} E_{pq}(s), & \text{si } s \in \Sigma \\ 0, & \text{si } s \notin \Sigma \end{cases}$. Thus, E can be viewed as a K^{Σ^*} -sub-

set of $Q \times Q$; that is, a $Q \times Q$ matrix with entries in K^{Σ^*} .

Consequently, since K^{Σ^*} is a semiring, the corresponding operations are used.

Now, for each $n \in \mathbb{N}$, we consider the matrices $E^n: Q \times Q \rightarrow K^{\Sigma^*}$ by $E^0 = 1_Q$, $E^1 = E$ and $E^n = EE^{n-1}$, $n \geq 2$, with $E^n_{pr} = \sum_{q \in Q} E_{pq} E^{n-1}_{rq}$, where $p, q \in Q$. It is clear that if $s \in \Sigma^*$ and $|s| \neq n$, one has that $E^n_{pq}(s) = 0$, with $p, q \in Q$; whereupon, $\{E^n_{pq}\}_{n \in \mathbb{N}}$ is locally finite. Then, one can define $E^*_{pq} = \sum_{n=0}^{\infty} E^n_{pq}$, and hence, it results in the matrix $E^*: Q \times Q \rightarrow K^{\Sigma^*}$, $E^* = 1_Q + E + E^2 + \dots + E^n + \dots$ called the extended transition matrix.

For each $s \in \Sigma^*$, let $E^*(s) = E^*_{pq}(s) \in K^{Q \times Q}$ be, if $s = \alpha_1 \dots \alpha_n$, it follows that $E^*(s) = E^n(s) = E(\alpha_1) \dots E(\alpha_n) = E^*(\alpha_1) \dots E^*(\alpha_n)$.

Theorem 1. For any $p, q \in Q$, the K -subset E^*_{pq} is the sum of all labels of $c: p \rightarrow q$ in A .

Proof: Let $p, q \in Q$ be, as $E^*_{pq} = \sum_{n=0}^{\infty} E^n_{pq}$, it suffices to show that E^n_{pq} is the sum of all path labels of length n . If $n = 0$, then $E^0_{pq} = \begin{cases} \theta, & \text{si } p = q \\ 0, & \text{si } p \neq q \end{cases}$, where θ is the identity of K^{Σ^*} . If $n = 1$, then $E^1_{pq} = \sum_{r \in Q} E_{pq}(1_Q)_{rp} = \sum_{r \in Q} E_{pr} E^0_{rq}$. Assume that the result is true for $n-1$, $n \geq 2$; i.e., $E^{n-1}_{pq} = \sum_{r_1, r_2, \dots, r_{n-1} \in Q} E_{pr_1} E_{r_1 r_2} \dots E_{r_{n-1} q}$. Then $E^n_{pq} = \sum_{r \in Q} E_{pr} E^{n-1}_{rq} = \sum_{r \in Q} E_{pr} E^{n-1}_{rq} = \sum_{r_1 \in Q} E_{pr_1} \left(\sum_{r_2, \dots, r_n \in Q} E_{r_1 r_2} E_{r_2 r_3} \dots E_{r_{n-1} r_n} \right) = \sum_{r_1, r_2, \dots, r_n \in Q} E_{pr_1} E_{r_1 r_2} \dots E_{r_{n-1} r_n} = \sum_{r \in Q} E_{pr} E^{n-1}_{rq}$. Consequently, E^n_{pq} is the sum of the labels of paths with length n . Therefore, E^*_{pq} is the sum of the labels of $c: p \rightarrow q$ in A .

Corollary 1. The behavior of A is $|A| = IE^*T$ with I

viewed as a row vector and T as a column vector.

$$\text{Proof: } |A| = \sum_{p, q \in Q} \sum_c I(p) |c| T(q) = \sum_{p, q \in Q} I(p) E^*_{pq} T.$$

Definition 8. Let K be a commutative semiring, and Σ be a finite alphabet. A K -subset A of Σ^* is called regular, if there exists a K - Σ -automaton A such that $|A| = A$.

In what follows, it is always assumed that given two K - Σ -automata $A = (Q_A, \Sigma, E_A, I_A, T_A)$ and $B = (Q_B, \Sigma, E_B, I_B, T_B)$, $Q_A \cap Q_B = \emptyset$.

Definition 9. Let A, B be two K - Σ -automata, the K - Σ -automata union of A and B is given by $A \cup B = (Q_{A \cup B}, \Sigma, E_{A \cup B}, I_{A \cup B}, T_{A \cup B})$, where, $Q_{A \cup B} = Q_A \cup Q_B$,

$$I_{A \cup B}(p) = \begin{cases} I_A(p), & \text{si } p \in Q_A \\ I_B(p), & \text{si } p \in Q_B \end{cases}, \quad T_{A \cup B}(p) = \begin{cases} T_A(p), & \text{si } p \in Q_A \\ T_B(p), & \text{si } p \in Q_B \end{cases},$$

$$E_{A \cup B}(p, \alpha, q) = \begin{cases} E_A(p, \alpha, q), & \text{si } p, q \in Q_A \\ E_B(p, \alpha, q), & \text{si } p, q \in Q_B \\ 0, & \text{en otro caso} \end{cases}$$

Proposition 1. The union of two regular K -subsets of Σ^* is a regular K -subset of Σ^* .

Proof: Consider A and B two regular K -subsets of Σ^* , and A, B two K - Σ -automata such that $|A| = A$ and $|B| = B$. Let $A \cup B$ be a K - Σ -automaton. Then, for all $s \in \Sigma^*$,

$$|A \cup B| = \left(\sum_{p, q \in Q_{A \cup B}} \sum_c I_{A \cup B}(p) |c| T_{A \cup B}(q) \right) (s)$$

$$= \sum_{p, q \in Q_A \cup Q_B} \sum_k I_{A \cup B}(p) k T_{A \cup B}(q),$$

where $k \in K$ is such that there exists $c: p \rightarrow q$ in $A \cup B$ with $|c| = k$; thus,

$$\begin{aligned} & \sum_{p, q \in Q_A \cup Q_B} \sum_k I_{A \cup B}(p) k T_{A \cup B}(q) = \\ & \sum_{p, q \in Q_A} \sum_k I_A(p) k T_A(q) + \sum_{p, q \in Q_B} \sum_k I_B(p) k T_B(q) = |A|(s) + |B|(s) \\ & = A(s) + B(s) \\ & = (A \cup B)(s). \text{ Asi, } |A \cup B| = A \cup B. \end{aligned}$$

Definition 10. Let A, B be two K - Σ -automata. The K - Σ -automaton product (or intersection) of A and B is given by $A \times B = (Q_{A \times B}, \Sigma, E_{A \times B}, I_{A \times B}, T_{A \times B})$, with $Q_{A \times B} = Q_A \times Q_B$, $I_{A \times B}((p, q)) = I_A(p) I_B(q)$, $T_{A \times B}((p, q)) = T_A(p) T_B(q)$,

$$E_{A \times B}((p, q), \alpha, (p', q')) = E_A(p, \alpha, p') E_B(q, \alpha, q').$$

Proposition 2. The intersection of two K-regular subsets of Σ^* is a K-regular subset of Σ^* .

Proof: Let A and B be two regular K-subsets of Σ^* and A, B be two K- Σ -automata such that $|A|=A$ and $|B|=B$. Let $A \times B$ be the K- Σ -automaton. Then, for all $s \in \Sigma^*$,

$$\begin{aligned} |A \times B|(s) &= \left(\sum_{(p, q), (p', q') \in Q_A \times Q_B} \sum_c I_{A \times B}(p, q) |c| T_{A \times B}(p', q') \right) (s) \\ &= \left(\sum_{p, p' \in Q_A; q, q' \in Q_B} \sum_{c=(c', c'')} I_A(p) I_B(q) |c'| T_A(p') T_B(q') \right) (s) \\ &= \sum_{p, p' \in Q_A; q, q' \in Q_B} \sum_{k_1, k_2} I_A(p) k_1 T_A(p') I_B(q) k_2 T_B(q') \\ &= \sum_{p, p' \in Q_A} \sum_{k_1} I_A(p) k_1 T_A(p') \sum_{q, q' \in Q_B} \sum_{k_2} I_B(q) k_2 T_B(q') \\ &= \left(\sum_{p, p' \in Q_A} \sum_{c'} I_A(p) |c'| T_A(p') \right) (s) \left(\sum_{q, q' \in Q_B} \sum_{c''} I_B(q) |c''| T_B(q') \right) (s) \\ &= |A|(s) |B|(s) = (|A| \cap |B|)(s) = (A \cap B)(s). \end{aligned}$$

Where $c': p \rightarrow p'$ is a path in A, $c'': q \rightarrow q'$ is a path in B, $|c'|=k_1s$, $|c''|=k_2s$ and $k_1k_2=k$ with $ks=|c|$.

Definition 11. Let $A=(Q, \Sigma, E, I, T)$ be a K- Σ -automaton. We call K- Σ -automaton inverse K- Σ -automaton $A^\varphi=(Q, \Sigma, E_\varphi, I_\varphi, T_\varphi)$, where $I_\varphi(q)=T(q)$, $T_\varphi(q)=I(q)$, and $E_\varphi(p, \alpha, q)=E(p, \alpha, q)$.

Remark 1. A path $c^\varphi: p \rightarrow q$ in A^φ , with label $|c^\varphi|=ks$, is given by a path $c: q \rightarrow p$ in A with label $|c|=k\varphi(s)$, where $\varphi: \Sigma^* \rightarrow \Sigma^*$ is the inverse function defined by $\varphi(\theta)=\theta$, $\varphi(\alpha)=\alpha$, $\varphi(st)=\varphi(t)\varphi(s)$, where $t, s \in \Sigma^*$.

Proposition 3. If A is a regular K-subset of Σ^* and $\varphi: \Sigma^* \rightarrow \Sigma^*$ is the inverse function given in Remark 1, then $A \circ \varphi$ is a regular K-subset of Σ^* ; that is, the class of regular K-subsets of Σ^* is stable under inverse function.

Proof: Let A be a K-regular subset of Σ^* and A be a K- Σ -automaton such that $|A|=A$. Consider A^φ the inverse K- Σ -automaton of A, then for all $s \in \Sigma^*$,

$$\begin{aligned} |A^\varphi|(s) &= \left(\sum_{p, q \in Q} \sum_{c^\varphi} I_\varphi(p) |c^\varphi| T_\varphi(q) \right) (s) \\ &= \sum_{p, q \in Q} \sum_k T(p) k I(q), \end{aligned}$$

with $|c^\varphi|=ks$, where $k \in K$ and

$$\begin{aligned} |c| &= k\varphi(s) = \left(\sum_{p, q \in Q} \sum_c I(q) |c| T(p) \right) (\varphi(s)) \\ &= (|A|)(\varphi(s)) = (A \circ \varphi)(s). \end{aligned}$$

Thus, $|A^\varphi| = A \circ \varphi$.

Definition 12. Let $A=(Q, \Sigma, E, I, T)$ be a K- Σ -automaton and $f: \Gamma^* \rightarrow \Sigma^*$ is a fine homomorphism. We call the inverse image of A the K- Γ -automaton $f^{-1}(A)=(Q, \Gamma, E', I, T)$, where E' is given by

$$E'(p, \gamma, q) = \begin{cases} E(p, \alpha, q), & \text{si } f(\gamma) = \alpha \text{ y } E(p, \alpha, q) \neq 0 \\ 1, & \text{si } f(\gamma) = \theta \text{ y } p = q \\ 0, & \text{otherwise.} \end{cases}$$

Remark 2. A path $c: p \rightarrow q$ in $f^{-1}(A)$, with label $|c|=kg$, is given as $c=(c', g)$ where $c': p \rightarrow q$ is a path in A and $g \in \Gamma^*$ is such that $|c'|=kf(g)$; that is, a path $c: p \rightarrow q$ in $f^{-1}(A)$, which associates some $g \in \Gamma^*$ in its label, is given by a path c' in A which associates $f(g)$ in its label.

Proposition 4. If $f: \Gamma^* \rightarrow \Sigma^*$ is a fine homomorphism and A is K-regular subset of Σ^* , then $A \circ f$ is a K-regular subset of Γ^* .

Proof: Let A be a K- Σ -automaton such that $|A|=A$. Consider the K- Γ -automaton $f^{-1}(A)$, the inverse image of A, and let $g \in \Gamma^*$ be, then

$$\begin{aligned} |f^{-1}(A)|(g) &= \left(\sum_{p, q \in Q} \sum_c I(p) |c| T(q) \right) (g) \\ &= \left(\sum_{p, q \in Q} \sum_{c'} I(p) |c'| T(q) \right) (f(g)) = |A|(f(g)) \\ &= (A \circ f)(g). \end{aligned}$$

Thus, $|f^{-1}(A)| = A \circ f$.

Definition 13. Let $f: \Gamma^* \rightarrow \Sigma^*$ be a homomorphism, such that $f(\gamma) \neq \theta$, $\forall \gamma \in \Gamma$, and let $A=(Q, \Gamma, E, I, T)$ be a K- Γ -automaton. We call the direct image of A the K- Σ -automaton $f(A)=(Q', \Sigma, E', I', T')$, where $Q' \supset Q$ and E' are given as follows: Let $E(p, \gamma, q) = k \neq 0$ in A, and let $f(\gamma) = \alpha_1 \alpha_2 \dots \alpha_n$, with $n \geq 1$. If $n=1$, then $E'(p, \alpha_1, q) = E(p, \gamma, q) = k$, is an arc in $f(A)$. If $n > 1$, consecutive arcs $p \xrightarrow{k_1 \alpha_1} q_1 \xrightarrow{k_2 \alpha_2} \dots \xrightarrow{k_n \alpha_n} q_n \xrightarrow{k_{n+1} \alpha_{n+1}} q$ with $k_1 \dots k_n = k$, are in $f(A)$, where q_1, \dots, q_n are new states added to Q. These determine states of Q'. Finally, repeating this process for every arc in A, we obtain $f(A)$, with

$$\begin{aligned} T(p') &= \begin{cases} I(p'), & \text{si } p' \in Q \\ 0, & \text{si } p' \in Q' \setminus Q \end{cases} \\ T'(p') &= \begin{cases} T(p'), & \text{si } p' \in Q \\ 0, & \text{si } p' \in Q' \setminus Q \end{cases} \end{aligned}$$

Remark 3. To say that $f: \Gamma^* \rightarrow \Sigma^*$ is a homomorphism such that $f(\gamma) \neq \emptyset$, $\forall \gamma \in \Gamma^*$ is equivalent to saying that $f^{-1}(\emptyset) = \emptyset$, or it is also equivalent to saying that $f^{-1}(s)$ is finite, for all $s \in \Sigma^*$.

Proposition 5. Let $f: \Gamma^* \rightarrow \Sigma^*$ be a homomorphism such that $f^{-1}(s)$ is finite, for all $s \in \Sigma^*$. If A is K -regular subset of Γ^* , then $f(A): \Sigma^* \rightarrow K$, given by

$$f(A)(s) = \sum_{g \in f^{-1}(s)} A(g)$$

is a K -regular subset of Σ^* .

Proof: Consider A a K - Γ -automaton such that $|A| = A$. Let $f(A)$ be the K - Σ -automaton direct image of A , then, for all $s \in \Sigma^*$, it follows that

$$\begin{aligned} |f(A)| &= \sum_{p', q' \in Q'} \sum_{c'} I'(p') |c'| T'(q') \\ &= \left(\sum_{p, q \in Q} \sum_{c'} I(p) |c'| T(q) \right) \end{aligned}$$

Then,

$$|f(A)| = \sum_{p, q \in Q} \sum_k I(p) k T(q),$$

with k varying over $c': p \rightarrow q$, with $|c'| = ks$, $s = f(g)$, $kg = |c|$, $c: p \rightarrow q$ in A . Thus,

$$|f(A)| = \sum_{p, q \in Q} \sum_k I(p) k T(q),$$

with k varying over all paths $c: p \rightarrow q$, such that $|c'| = kf(g)$, $g \in f^{-1}(s)$, $kg = |c|$, $c: p \rightarrow q$ in A . Therefore,

$$|f(A)|(s) = \sum_{g \in f^{-1}(s)} \left(\sum_{p, q \in Q} \sum_k I(p) k T(q) \right)$$

with k varying over all paths $c: p \rightarrow q$ in A , $kg = |c|$; that is,

$$|f(A)|(s) = \sum_{g \in f^{-1}(s)} |A|(g) = \sum_{g \in f^{-1}(s)} A(g)$$

Finally, $f(A)$ is a K -regular subset of Σ^* .

Definition 14. A K - Σ -automaton $A = (Q, \Sigma, E, I, T)$ is called normalized if $I = i$ and $T = t$ are two distinct simple K -subsets, and there exist no arcs $p \xrightarrow{k\alpha} i, t \xrightarrow{k\alpha} q$ with $k \neq 0$; that is, $E(q, \alpha, i) = E(t, \alpha, q) = 0$, for all $q \in Q$ and $\alpha \in \Sigma$.

Remark 4. If A is normalized, then $|A|(\emptyset) = 0$. Then, if one observes Σ^+ as a B -subset of Σ^* , one obtains $|A| \subset \Sigma^+$.

Proposition 6. For every K - Σ -automaton A there exists a normalized K - Σ -automaton A' such that $|A'| = |A| \cap \Sigma^+$.

Proof: Let $A = (Q, \Sigma, E, I, T)$ be a K - Σ -automaton, and let $Q' = Q \cup i \cup t$, where i and t are two different new states. Consider the new matrix E' as follows: $E'_{pq} = E_{pq}$,

$$\begin{aligned} E'_{iq} &= \sum_{p \in Q} I_p E_{pq}, E'_{pt} = \sum_{q \in Q} E_{pq} T_q, E'_{it} = \\ &\sum_{p, q \in Q} I_p E_{pq} T_q, \\ E'_{pi} &= E_{ti} = E_{tq} = \emptyset, \text{ where } I_p = I(p) \text{ and } T_q = \\ &T(q). \text{ A calculation determines that } E'^*_{it} = IE^+T, \text{ where } \\ &E^+ = E + E^2 + \dots + E^n + \dots = EE^+. \end{aligned}$$

The K - Σ -automaton $A' = (Q', \Sigma, E', i, t)$ is normalized, and using **Corollary 1** one has $|A'| = E'^*_{it} = IE^+T = IE^+T \cap \Sigma^+ = |A| \cap \Sigma^+$.

Remark 5. The construction of A' from A , as in Proposition 6, is always interpreted as the normalization design.

Proposition 7. Let A be a K -regular subset of Σ^* , and let $k \in K$, then kA is a K -regular subset of Σ^+ .

Proof: Let A be a K - Σ -automaton such that $|A| = A$, and let $k \in K$ be, consider the K - Σ -automaton $kA = (Q, \Sigma, E, kI, T)$, where $(kI)_q = kI_q$, then

$$\begin{aligned} |kA| &= \sum_{p, q \in Q} kI_p E^*_{pq} T_q = k \sum_{p, q \in Q} I_p E^*_{pq} T_q \\ &= k|A| = kA \end{aligned}$$

Proposition 8. A K -subset A of Σ^* is regular, if and only if, the K -subset $A' = A \cap \Sigma^+$ is also regular.

Proof: Let A be a K - Σ -automaton such that $|A| = A$. Then, there exists a normalized K - Σ -automaton A' such that $|A'| = |A| \cap \Sigma^+ = A \cap \Sigma^+ = A'$. Reciprocally, suppose that $A \cap \Sigma^+ = A'$ is a K -regular subset of Σ^* . Since $A'(\emptyset) = 0$ ($\Sigma^+(\emptyset) = 0$), it follows that $A = k\emptyset + A'$, where $k = A(\emptyset)$. Then, since \emptyset is a K -regular subset of Σ^* , then from Proposition 1 and Proposition 7 one has that A is regular.

Proposition 9. If A and B are two K -regular subsets of Σ^* , then AB is a K -regular subset.

Proof: Let $A = k\emptyset + A'$, $B = l\emptyset + B'$, with $A' = A \cap \Sigma^+$, $B' = B \cap \Sigma^+$, $k = A(\emptyset)$ and $l = B(\emptyset)$. Then, $AB = kl(\emptyset) + kB' + lA' + A'B'$. It suffices to show that $A'B'$ is regular, for this, let $A = (Q_1, \Sigma, E_1, i_1, t_1)$ and $B = (Q_2, \Sigma, E_2, i_2, t_2)$ be two K - Σ -normalized automata recognizing A' and B' respectively. Consider the normalized K - Σ -automaton $C = (Q, \Sigma, E, i_1, t_2)$, where Q is a partition of Q_1 and Q_2 , except when $t_1 = i_2$. Then, an arc in C is either an arc in A or is an arc in B . Thus, $|C| = E^*_{i_1 t_2} = E^*_{i_1 i_1 t_2} = E^*_{i_2 i_2 t_2} = |A| |B| = A'B'$.

Proposition 10. Let A be a K -regular subset of Σ^+ . Then, the K -subsets $A^+ = A + A^2 + \dots + A^n + \dots$ and

$A^* = \emptyset + A + A^2 + \dots + A^n + \dots$ are regular.

Proof: Since $A \subset \Sigma^+$, it follows that $A^n(s) = 0$, when $|s| < n$. Then, $\{A^n\}_{n \in \mathbb{N}}$ is locally finite; thus, A^+ and A^* are well defined. Let $A = (Q, \Sigma, E, i, t)$ be a K - Σ -normalized automaton recognizing A . Then, considering i and t as a single state, which is initial and final, we obtain a K - Σ -normalized automaton A^* , where $|A^*| = A^*$. Thus, A^* is regular. Then, since $A^+ = A^* \cap \Sigma^+$, it follows that A^+ is regular.

Theorem 2. A K -subset A of Σ^+ is regular, if and only if, there exists an integer $n > 1$ and a matrix E $n \times n$ whose entries are K -subsets of Σ such that $A = E^+$.

Proof: Let A be a K -regular subset of Σ^+ , and $A = (Q, \Sigma, E, i, t)$ be a K - Σ -normalized automaton that recognizes A . There is no loss of generality in assuming $Q = \{1, \dots, n\}$, with $i = 1$ and $t = n$. Since $i \neq t$ has to $n > 1$. Then, from Corollary 1 it follows that $|A| = E^+_{in} = E^+_{in} = A$. Reciprocally, if, $A = E^+_{1n}$, where E is a matrix $n \times n$ of K -subsets of Σ and $n > 1$, then, with $Q = \{1, \dots, n\}$, $I = 1$ and $T = n$, one obtains a K - Σ -automaton $A = (Q, \Sigma, E, 1, n)$ such that $|A| = E^+ = A$.

Corollary 2. If E is a matrix $n \times n$ of K -subsets of Σ , then for any $1 \leq i, j \leq n$, the K -subsets E^*_{ij} and E^+_{ij} are regular.

Proof: It follows from Theorem 2.

Proposition 11. Let $\varphi: K \rightarrow K'$ be a homomorphism of semirings. If A is a regular K -subsubset of Σ^* , then $\varphi \circ A$ is a regular K' -subset of Σ^* .

Proof: Let $A = (Q, \Sigma, E, I, T)$ be a K - Σ -automaton such that $|A| = A$, then the K' - Σ -automaton $\varphi(A) = (Q, \Sigma, \varphi(E), \varphi(I), \varphi(T))$ satisfies $|\varphi(A)| = \varphi(|A|) = \varphi(A)$. Since K is a positive semiring, then $T: K \rightarrow B$, given by $T(0) = 0$ and $T(x) = 1$, for all $x \neq 0$, is a homomorphism.

Corollary 3. If K is a positive semiring, and A is a regular K -subset of Σ^* , then $T(A)$ is a regular B -subset of Σ^* .

Proof: It follows from the composition of the image automaton and from Proposition 11.

Proposition 12. Let A be a regular B -subsubset of Σ^* . Then, A viewed as an unambiguous K -subsubset of Σ^* is regular.

Proof: Let A be a deterministic Σ -automaton with dynamics A . If A is viewed as a K - Σ -automaton, then its dynamics is viewed as a K -subset of Σ^* .

Remark 6. Corollary 3 and Proposition 12 simultaneously show that for any unambiguous subsets of Σ^* , regularity is independent of the choice of K .

4 The Equality Theorem

In this section it will be assumed that K is a subsemiring of a commutative semiring.

Theorem 3. (The Equality Theorem). Let A_1 and A_2 be recognizable K -subsets of Σ^* and let $A_i = (Q_i, \Sigma_i, E_i, I_i, T_i)$ be K - Σ -automata such that $|A_i| = A_i$, $i = 1, 2$. If $n_i = \text{Card } Q_i$ and if $A_1(s) = A_2(s)$, $\forall s \in \Sigma^*$ such that $|s| < n_1 + n_2$, then $A_1 = A_2$.

Proof: Consider the automaton $A_1 \cup A_2 = (Q_1 \cup Q_2, \Sigma_1 \cup \Sigma_2, E_1 \cup E_2, I_1 \cup I_2, T_1 \cup T_2)$, where Q_1 and Q_2 are assumed disjoint and the transition matrix is From $A_1 \cup A_2$ we derive the automata $B_i = (Q_i \cup Q_2, E_i \cup E_2, I_i, T_i \cup T_2)$, $i = 1, 2$ and observe that $|B_i| = |A_i| = A_i$, $i = 1, 2$. Thus the conclusion of Theorem 3 follows from:

Theorem 4. Let $A_i = (Q_i, \Sigma_i, E_i, I_i, T_i)$, $i = 1, 2$ be K - Σ -automata differing only in their initial subsets. Then $|A_1| = |A_2|$ if and only if $|A_1|(s) = |A_2|(s)$, $\forall s \in \Sigma^*$ such that $|s| < \text{Card } Q$.

Proof: By assumption K is a subsemiring of a semiring (field F). Thus, we may regard A_i as F - Σ -automata. If $|A_1|$ and $|A_2|$ are equal as F -subsets of Σ^* , then they are also equal as K -subsets. Thus, we may replace K by F , or equivalently assume that K is a field. Thus K^Q is a vector space over K of dimension $n = \text{Card } Q$. Consider the K - Σ -automaton $A = (Q, \Sigma, E, I, T)$ with $I = I_1 \setminus I_2$. Since $|A|(s) = |A_1|(s) \setminus |A_2|(s)$ we have $|A|(s) = 0$ if $|s| < n$, and we wish to prove that $|A|(s) = 0$, $\forall s \in \Sigma^*$. Equivalently, in view of Corollary 1, we are given that $(I(s))T = 0$, if $|s| < n$ and we wish to prove that $(I(s))T = 0$, $\forall s \in \Sigma^*$. Define $W = \{X \mid X \in K^Q, XT = 0\}$, $V_j = \text{subspace of } K^Q \text{ generated by vectors } I(s), \text{ with } |s| \leq j$. Assuming that $n > 0$, we have $V_0 \subset V_1 \subset \dots \subset V_{n-1} \subset W$. The cases $I = 0$ or $T = 0$ may be ruled out since then obviously $(I(s))T = 0$. Therefore, $\dim V_0 = 1$, $\dim W = n - 1$. It follows that for some $0 \leq j < n - 1$, $V_j = V_{j+1}$. Since V_{j+2} is generated by all the vectors X and $X\tau$, with $X \in V_{j+1}$, it follows that $V_{j+1} = V_{j+2}$ and thus by induction $V_j = V_{j+p}$, $\forall p \geq 0$. This implies $V_j \subset W$, $\forall j \in \mathbb{N}$. Thus, for any $\forall s \in \Sigma^*$ we have $I(s) \in W$; i.e., $(I(s))T = 0$.

Corolario 4. If $A = (Q, \Sigma, E, I, T)$ is a K - Σ -automaton, then $|A| = 0$, if and only if, $|A|(s) = 0$, $\forall s \in \Sigma^*$ such that $|s| < \text{Card } Q$.

The following example shows that the numerical bound in **Theorem 3** is the best possible.

Example 3. Let $0 < n_1 \leq n_2$ be integers. Consider the alphabet Σ consisting of a single letter τ . Let A_1 be the deterministic automaton, with n_1 states represented symbolically

by the path $\rightarrow \mathbf{i} \xrightarrow{\tau^{n1-1}} \mathbf{t} \rightarrow$. Thus $A_1 = \tau^{n1-1}$. Let A_2 be the deterministic complete automaton, with n_2 states represented symbolically by the loop $\rightarrow \mathbf{i} \xrightarrow{\tau^{n2}} \mathbf{i}$, with $\mathbf{t} = \mathbf{i} \tau^{n1-1}$ as terminal state. Then $A_2 = \tau^{n1-1}(\tau^{n2})$. Thus $\tau^{n1+n2-1} \in A_2 \setminus A_1$. However, for all lower exponents k we have $\tau^k \in A_2$, if and only if, $\tau^k \in A_1$.

5 Conclusion

An important consequence of Theorem 3 is: given any two recognizable K -subsets A_1 and A_2 of Σ^* , it is decidable whether or not $A_1 = A_2$. This statement requires several caveats. First the word given should be interpreted to mean that K - Σ -automata $A_i = (Q_i, \Sigma_i, E_i, I_i, T_i)$ such that $|A_i| = A_i$, for $i=1,2$ are explicitly provided. Then, all the paths of length less than $n = \text{Card } Q_1 + \text{Card } Q_2$ can be enumerated and thus $|A_1|(s)$ and $|A_2|(s)$ can be computed for $|s| < n$.


References

- Branicky, M. (1995). *Studies in hybrid systems: Modeling, analysis and control* [Doctoral dissertation, Massachusetts Institute of Technology]. DSpace. <https://dspace.mit.edu/handle/1721.1/11398>
- Caspi, P. (1991). *Model of discrete event systems in computer science* [Paper presentation]. European Control Conference, Grenoble, France.
- Eilenberg, S. (1974). *Automata, languages and machines* (Vol. A). Academic Press.
- Mata, G. (2017). Supervisory control application to solving optimal control problems for discrete event systems. *Revista Ingeniería UC*, 24(1), 81–90. <https://www.servicio.bc.uc.edu.ve/ingenieria/revista/v24n1/art10-124.pdf>
- Mata, G., Giraldo, R. E., & Rojas, N. M. (2018). A planning algorithm in a class of discrete event systems. *DYNA*, 85(206), 283–293. <https://dialnet.unirioja.es/descarga/articulo/7664680.pdf>


Recibido: 22 de abril 2025

Aceptado: 01 de julio 2025

Mantilla Morales, Gisella. Engineer in Electronics and Telecommunications, Master's degree in Mathematics; full-time professor at the Technical University of Manabí.

 <https://orcid.org/0000-0002-0826-774>

Bastidas Chalán, Rodrigo. Engineer in Electronics and Control. Active professor at the University of the Armed Forces-ESPE. E-mail: rvbastidas@espe.edu.ec


 <https://orcid.org/0000-0002-2811-1672>

Rentería Torres, Aníbal. Engineer in Electrical. Active professor at the University of the Armed Forces-ESPE. E-mail:


avrenteria@espe.edu.ec

 <https://orcid.org/0009-0002-9057-4536>


Bustos Ganchozo, Oscar. Graduate in Physics. Active professor at the University of the Armed Forces-ESPE. E-mail: ofbustos@espe.edu.ec

 <https://orcid.org/0009-0005-3509-0370>

Ferrer-Guillén, María Dolores. Master's degree in Computing. Active Full Professor. Department of Calculation, Faculty of Engineering, ULA. Research area: analysis and control in dynamic systems. E-mail: mariadfg@gmail.com

 <https://orcid.org/0009-0002-8162-233X>

Mata-Díaz, Guelvis E. Graduate in Mathematics. Master of Science in Mathematics. PhD in Applied Sciences. Active Full Professor. Faculty of Sciences, ULA. Department of Mathematics. Research area: analysis and control in discrete-event dynamic systems. E-mail: gema-tad2017@gmail.com

 <https://orcid.org/0000-0001-7147-1422>

Algebraic design of two-degree-of-freedom PID controllers for FOPTD systems

Diseño algebraico de controladores PID de dos grados de libertad para sistemas FOPTD

Teppa-Garran, Pedro^{1*}; Caraballo, Luis²; Garcia, Germain³

¹Departamento de Gestión de Proyectos y Sistemas, Universidad Metropolitana, Caracas, Venezuela.

²Escuela de Ingeniería Eléctrica, Universidad Metropolitana, Caracas, Venezuela.

³CNRS, LAAS, 7 Avenue du Colonel Roche, Toulouse, France, Université de Toulouse, INSA, Toulouse, France.

*teppa@unimet.edu.ve

Abstract

This work proposes a model-based tuning method for two-degree-of-freedom PID controllers founded on a polynomial approach and fundamental notions of control theory for first-order plus time-delay (FOPTD) systems. The technique achieves rejection of constant disturbance signals through a time response that asymptotically approaches zero with a specified overshoot and settling time. Likewise, tracking with zero steady-state error of persistent reference inputs such as step, ramp, or parabola is also attained. Another contribution of the method is that it allows tuning the four PID controller parameters. Several examples show the ease of implementation of the technique, its effectiveness, and how it can be extended to systems other than FOPTD.

Keywords: PID, Two-degree-of-freedom PID, Time delay systems, FOPTD, Tracking, Disturbance Rejection, Heat flow process, Coupled tank system, United Nations SDG 9.

Resumen

Este trabajo propone un método basado en modelos para la sintonización de controladores PID de dos grados de libertad para sistemas de primer orden con retardo en el tiempo (FOPTD) fundamentado en un enfoque polinómico y nociones básicas de la teoría de control. La técnica logra el rechazo de señales de perturbación constante mediante una respuesta temporal que tiende asintóticamente a cero con un sobrepico y un tiempo de establecimiento especificados. Asimismo, se logra un seguimiento con error de estado estacionario cero de entradas de referencia persistentes, como el escalón, la rampa o la parábola. Otra contribución del método es que permite ajustar los cuatro parámetros del controlador PID. Varios ejemplos muestran la facilidad de implementación de la técnica, su eficacia y su extensión a sistemas distintos de los FOPTD.

Palabras clave: PID, PID de dos grados de libertad, Sistemas con tiempo de retardo, FOPTD, Seguimiento, Rechazo de perturbaciones, Proceso de flujo de calor, Sistema de tanques acoplados, ODS 9 de las Naciones Unidas.

1 Introduction

Two fundamental problems arise in the design of control systems: tracking a reference input and rejecting disturbance signals. A basic notion of control theory is that a physical variable can behave in a prescribed manner by using the difference between a desired reference value and the actual output value until the two are matched. This notion results in the classic feedback control loop, where the control signal is generated using the difference of signals indicated above; this scheme is also called a one-degree-of-freedom

(1-DoF) controller. The degree of freedom of a control system is defined as the number of closed-loop transfer functions that can be independently adjusted (Teppa-Garran et al., 2023).

Time-delay control systems are present in numerous industrial applications, such as chemical engineering, biochemistry, aerospace, and power generation, to name just a few (Gu and Niculescu, 2003; Birs et al., 2019). Even if it is not a natural component of the process, actuators and sensors in a control system introduce time delays in its operation (Richard, 2003; Ai et al., 2016). The main reason

for time delays in industrial processes is transporting materials or energy in long pipelines (Bresch-Pietri et al., 2014) or data traffic in communication networks (Ariba et al., 2009). Time delay is known to degrade process performance. From the frequency domain point of view, delay introduces an additional lag in the process phase. This results in lower phases, gain margins, and the possibility of losing stability. This has led to the study of the stability of time delay systems by the Lyapunov and Krasovskii analysis (Hale and Lunel, 2013) and variants within this general analysis procedure, such as the Wirtinger-based inequality (Seuret and Gouaisbaut, 2013), and the Bessel-Legendre inequalities (Zhang et al., 2019, 2022).

As a special case of time-delay systems, many open-loop industrial processes of practical interest can be effectively modeled by a low-order transfer function cascade with a time delay. First-order plus time-delay (FOPTD) systems are the most commonly employed process model in control design (O'Dwyer, 2009).

The proportional-integral-derivative (PID) controller is the industry's most widely used control strategy nowadays (Åström and Hagglund, 1995; Desborough and Miller, 2002). Its success is attributed to its simple structure, the meaning of its three parameters, its easy understanding by technical personnel, and because it provides stability and fast responses for a wide range of operating conditions.

However, despite its wide use, many poorly tuned PID controllers are found at the industrial level (Lee et al., 2015). In controlling systems with time delay, the performance of PID controllers also has limitations. Several factors can be listed to explain this situation, such as nonlinearities, uncertainties, external disturbances, variable loads, etc. (Liu and Daley, 2001). Still, one essential reason is that a 1-DoF controller must achieve a compromise between tracking a reference input and disturbance attenuation (Vilanova et al., 2011; Teppa-Garran et al., 2023). In a two-degree-of-freedom (2-DoF) controller, the reference input and the controlled output are processed independently to generate the control signal. This additional degree of freedom allows the two fundamental control problems mentioned at the beginning to be solved separately. The need to satisfactorily solve both issues motivated the introduction of two-degree-of-freedom PID controllers (2-DoF PID) (Araki, 1985; Araki and Taguchi, 2003). Since then, many methods for tuning their parameters have been proposed, including the internal model control (Mamat, 2013; Jin and Liu, 2014). The gain-phase margin (Xing et al., 2006). The maximum sensitivity function (Alfaro et al., 2010). The fractional order PID controller (Sharma et al., 2015). The desired dynamic equation (Zhang et al., 2010). Combining the desired dynamic equation with the generalized frequency method (Wang et al., 2018) and fuzzy control (Bi, 2020).

Most of these methods rely on complex mathematical notions that undermine the simplicity of understanding the PID operation by industrial technical personnel. The main contribution of our study is to propose a methodology for

tuning the four parameters (K_p, K_i, K_d, τ_d) of a 2-DoF PID controller for a FOPTD plant using a straightforward algebraic approach based on elementary notions of control theory. To this end, a 2-DoF general control system architecture defined by (Araqui and Taguchi, 2003) is employed, which consists of a feedforward and a serial PID controller. The disturbance attenuation problem is solved using a dominant pole guarantee criterion proposed in (Persson and Åström, 1992) and used in various applications, for instance (Teppa-Garran and Garcia, 2017; Teppa-Garran and Vasquez, 2020). Applying the dominant pole guarantee criterion, the control system's response to any constant disturbance signal tends asymptotically to zero, exhibiting a desired overshoot and settling time. On the other hand, the problem of tracking persistent signals of the step, ramp, or parabola type is solved using a zero assignment criterion for the closed-loop transfer function. Several numerical examples show the proposed methodology's effectiveness and ease of implementation.

The results of this work promote innovation in the control of industrial processes by improving the tuning of PID controllers in a 2-DoF control system architecture and, in this way, contribute to SDG 9 of the United Nations.

2 Problem formulation and basic notions

The control scheme in Fig. 1 shows a general two-degree-of-freedom architecture (Araqui and Taguchi, 2003). The signal $r(t): \mathbb{R}^+ \rightarrow \mathbb{R}$ is the reference input, $d(t): \mathbb{R}^+ \rightarrow \mathbb{R}$ is a disturbance signal, $y(t): \mathbb{R}^+ \rightarrow \mathbb{R}$ corresponds to the controlled output, $u(t): \mathbb{R}^+ \rightarrow \mathbb{R}$ is the control signal, and t represents the independent time variable. The controller consists of two PID compensators represented by the transfer functions $G_1(s)$ and $G_2(s)$. The tracking error is defined by

$$e(t) = r(t) - y(t) \quad (1)$$

There are two closed-loop transfer functions in Fig. 1. One from d to y and the other from r to y ; they are given respectively by the expressions.

$$G_{yd}(s) = \frac{Y(s)}{D(s)} = \frac{G_p(s)}{1 + G_1(s)G_p(s)} \quad (2)$$

$$G_{yr}(s) = \frac{Y(s)}{R(s)} = \frac{[G_1(s) + G_2(s)]G_p(s)}{1 + G_1(s)G_p(s)} \quad (3)$$

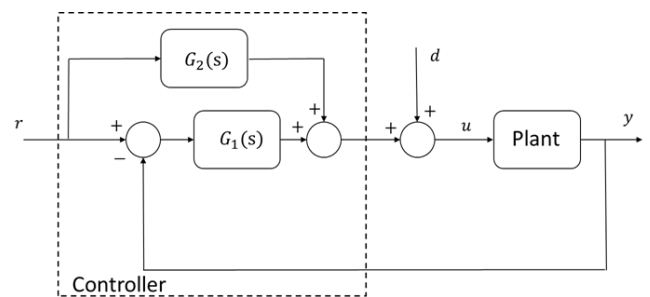


Figure 1. Two-degree-of-freedom (2-DoF) control system.

2.1 Plant model

The plant is modeled by a first-order system with transport delay θ_d (FOPTD) characterized by the transfer function.

$$\frac{Y(s)}{U(s)} = \frac{K}{Ts + 1} e^{-\theta_d s} \quad (4)$$

In this work, the transport delay is approximated in two different ways. (i) Using the denominator Taylor series expansion ($e^{-\theta_d s} \approx 1/(1 + \theta_d s)$) (Hanta and Procháska, 2009). The plant model takes the form

$$G_p(s) = \frac{b_0}{s^2 + a_1 s + a_0} \quad (5)$$

Where

$$b_0 = K/T\theta_d, a_1 = (T + \theta_d)/T\theta_d, a_0 = 1/T\theta_d$$

(ii) Using a first-order Padé model ($e^{-\theta_d s} \approx (2 - \theta_d s)/(2 + \theta_d s)$) (Hanta and Procháska, 2009) allows us to obtain the following transfer function for the plant

$$G_p(s) = \frac{-b_1 s + b_0}{s^2 + a_1 s + a_0} \quad (6)$$

Where

$$b_1 = K/T, b_0 = 2K/T\theta_d, a_1 = (2T + \theta_d)/T\theta_d, a_0 = 2/T\theta_d$$

Equations (5, 6) will be used to design the PID controllers $G_1(s)$ and $G_2(s)$ of Fig. 1.

2.2 PID controller

The mathematical model of a PID controller is given by

$$u(t) = K_p e(t) + K_i \int_0^t e(\tau) d\tau + K_d \frac{d}{dt} e(t) \quad (7)$$

Or, in the Laplace domain, through the equation

$$U(s) = \left(K_p + \frac{K_i}{s} + K_d s \right) E(s) \quad (8)$$

The error signal $e(t)$ is used to generate the proportional, integral, and derivative actions, which are combined to form the control signal $u(t)$. The PID controller parameters are the proportional K_p , the integral K_i , and the derivative K_d constants. These constants must be tuned to meet the design requirements, and several empirical tuning rules have been formulated for this purpose. A non-exhaustive list is given in (Teppa-Garran et al., 2021). These easy-to-implement rules provide tuning methods for PID controller parameters that often do not result in the best constant settings (Lee et al., 2014). For this reason, optimal tuning methods have been proposed: based on genetic algorithms (El-Deen et al., 2015; Gunawan et al., 2018), computer-assisted (Teppa-Garran et al., 2021; Teppa-Garran and El Gharib, 2024), or based on the linear-quadratic regulator (Teppa-Garran et al., 2025a).

In practical applications, the pure derivative action in (7) is never used, due to the derivative kick and the amplification of measurement noise (Atherton and Majhi,

1999; Zhu, 2009). For this reason, the derivative term is cascaded with a first-order low-pass filter, resulting in equation (8) becoming,

$$U(s) = \left(K_p + \frac{K_i}{s} + \frac{K_d s}{\tau_d s + 1} \right) E(s) \quad (9)$$

All the rules (empirical and optimal) mentioned previously consider only the tuning of the three constants K_p , K_i , and K_d , but not the term τ_d . Subsequent simulations based on predefined ranges are usually used to determine the latter. For example, the following interval is proposed in (Goodwin et al., 2001).

$$0.1(K_d/K_p) \leq \tau_d \leq 0.2(K_d/K_p) \quad (10)$$

In this study, the transfer functions of the PID controllers $G_1(s)$ and $G_2(s)$ are modeled by an equation of the form (9). Another significant contribution of this work is the proposal of a method that directly adjusts the four parameters of the PID controller.

2.3 Problem formulation

This work simultaneously aims to solve the two fundamental control problems mentioned in the introduction. To this end, the following problem is formulated.

Problem 1: Given a plant model in the form (5) or (6), determine the four parameters in the controllers $G_1(s)$ and $G_2(s)$ modeled through (9) so that the controlled output $y(t)$ in the control system of Fig. 1 satisfies the following two conditions: (i) It approaches asymptotically to zero exhibiting a desired overshoot (OS) and settling time (T_s) when a constant disturbance signal $d(t)$ is applied. (ii) It tracks with zero steady-state error a reference input $r(t)$ of step, ramp, or parabola type.

3 Problem solution

This section develops the method for synthesizing the controllers $G_1(s)$ and $G_2(s)$ to solve problem 1. The transfer function of $G_1(s)$ is given by

$$G_1(s) = K_{p1} + \frac{K_{i1}}{s} + \frac{K_{d1}s}{\tau_{d1}s + 1} \quad (11)$$

And the transfer function of $G_2(s)$ through

$$G_2(s) = K_{p2} + \frac{K_{i2}}{s} + \frac{K_{d2}s}{\tau_{d2}s + 1} \quad (12)$$

In this work, it is assumed that the following condition is satisfied in (11) and (12)

$$\tau_d = \tau_{d1} = \tau_{d2} \quad (13)$$

Let the controller $G_{12}(s)$ be defined as

$$G_{12}(s) = G_1(s) + G_2(s) = K_p + \frac{K_i}{s} + \frac{K_d s}{\tau_d s + 1} \quad (14)$$

Where $K_p = K_{p1} + K_{p2}$, $K_i = K_{i1} + K_{i2}$ and $K_d = K_{d1} + K_{d2}$. A fundamental result for this study is shown below.

Theorem 1: Any controller of the form

$$G_c(s) = \frac{As^2 + Bs + C}{Ds^2 + Es} \quad (15)$$

It is identical to a PID controller expressed by the equation (9), where

$$\begin{aligned} K_p &= \frac{BE - CD}{E^2} \\ K_i &= \frac{C}{E} \\ K_d &= \frac{AE^2 - BDE + CD^2}{E^2} \\ \tau_d &= \frac{D}{E} \end{aligned} \quad (16)$$

Proof: Equation (9) is rewritten as

$$\frac{(K_{d_1} + K_{p_1}\tau_d)s^2 + (K_{p_1} + K_{i_1}\tau_d)s + K_{i_1}}{\tau_d s^2 + s} \quad (17)$$

And (15) as

$$\frac{\frac{A}{E}s^2 + \frac{B}{E}s + \frac{C}{E}}{\frac{D}{E}s^2 + s} \quad (18)$$

The result is established by equating (17) and (18).

Considering Theorem 1 and the condition (13), the transfer functions of the controllers $G_1(s)$, $G_2(s)$, and $G_{12}(s)$ can be expressed by equations (19), (20), and (21), respectively.

$$G_1(s) = \frac{e_2 s^2 + e_1 s + e_0}{d_2 s^2 + d_1 s} \quad (19)$$

$$G_2(s) = \frac{f_2 s^2 + e f_1 s + f_0}{d_2 s^2 + d_1 s} \quad (20)$$

$$G_{12}(s) = G_1(s) + G_2(s) = \frac{n_2 s^2 + n_1 s + n_0}{d_2 s^2 + d_1 s} \quad (21)$$

Where $n_2 = e_2 + f_2$, $n_1 = e_1 + f_1$, and $n_0 = e_0 + f_0$.

3.1 Synthesis of controller $G_1(s)$

The PID controller in (11) with condition (13) expressed in the form (19) is to be designed such that the time component of the controlled output $y(t)$ in response to a constant disturbance $d(t)$ tends asymptotically to zero with a desired overshoot (OS) and settling time (T_s). This objective is best appreciated in the block diagram of Fig. 2, which results from the simplification of the diagram in Fig. 1 by setting $r(t) = 0$.

A dominant pole guarantee criterion specifies the closed-loop performance requirements of the time response to a constant disturbance signal. This criterion allows the

construction of a desired closed-loop polynomial consisting of a pair of complex conjugate poles that will dominate the time response dynamics, with the remaining poles making a negligible contribution. The dominance of the complex conjugate pole pair $s_{1,2} = -\alpha \pm j\beta$ requires that the ratio of the real parts of the other poles to $-\alpha$ exceeds a factor λ (λ is typically taken as 3 to 10 times). Thus, the other poles are positioned to the left of the vertical line $s = -\lambda\alpha$. In this work, the desired closed-loop polynomial is expressed as

$$(s^2 + 2\zeta\omega_n s + \omega_n^2)(s + \lambda\zeta\omega_n)^2 \quad (22)$$

The damping coefficient ζ and the natural frequency ω_n of the dominant poles are determined in terms of the desired overshoot OS and settling time T_s by making (Dorf and Bishop, 2017).

$$OS = e^{(-\zeta\pi/\sqrt{1-\zeta^2})} \Rightarrow \zeta = \frac{1}{\sqrt{1 + \left(\frac{\pi}{\ln(OS)}\right)^2}} \quad (23)$$

$$T_s = 4/(\zeta\omega_n) \Rightarrow \omega_n = \frac{4}{\zeta T_s}$$

In this way, the desired closed-loop polynomial will meet some design time requirements and will be expressed as

$$t_4 s^4 + t_3 s^3 + t_2 s^2 + t_1 s + t_0 \quad (24)$$

With known parameters $t_i > 0$.

Remark 1: There is no loss in generality if the polynomial (24) is chosen to be monic.

The characteristic equation of the control system in Fig. 2 corresponds to the expression $1 + G_1(s)G_p(s) = 0$. To represent the plant $G_p(s)$, the approximation through the first-order Padé model given by (6) will be used, and for the controller $G_1(s)$, equation (19) will be employed. The characteristic polynomial results in

$$\begin{aligned} &d_2 s^4 + (a_1 d_2 + d_1 - b_1 n_2) s^3 + (a_0 d_2 + \\ &a_1 d_1 + b_0 n_2 - b_1 n_1) s^2 + (a_0 d_1 + b_0 n_1 - \\ &b_1 n_0) s + b_0 n_0 \end{aligned} \quad (25)$$

To consider the approximation of (4) by the Taylor series expansion given by (5), it is enough to set $b_1 = 0$ in equation (25). In the following, a result is presented that allows calculating the constants of the controller $G_1(s)$ in the form (19).

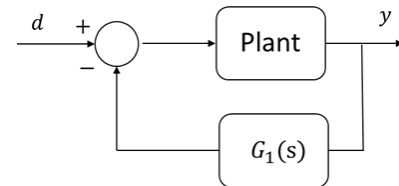


Figure 2. Block diagram for computing the controller $G_1(s)$.

Theorem 2: The constants d_2, d_1, e_2, e_1 , and e_0 of the controller $G_1(s)$ in equation (19) are given by solving the set of simultaneous equations

$$\begin{bmatrix} 1 & 0 & 0 & 0 & 0 \\ a_1 & 1 & -b_1 & 0 & 0 \\ a_0 & a_1 & b_0 & -b_1 & 0 \\ 0 & a_0 & 0 & b_0 & -b_1 \\ 0 & 0 & 0 & 0 & b_0 \end{bmatrix} \begin{bmatrix} d_2 \\ d_1 \\ e_2 \\ e_1 \\ e_0 \end{bmatrix} = \begin{bmatrix} t_4 \\ t_3 \\ t_2 \\ t_1 \\ t_0 \end{bmatrix} \quad (26)$$

Proof: Straightforward, by equating the coefficients of the polynomials (24) and (25).

A legitimate question is why equation (11) of the PID controller is represented in form (19). If equation (11) is used directly to construct the characteristic polynomial in (25), the resulting system of equations is nonlinear and overdetermined instead of the simple form obtained in (26).

Remark 2: The determinant of the coefficient matrix in (26) is equal to $b_0(b_0^2 + a_1b_0b_1 + a_0b_1^2)$. For it to be zero, $b_0 = 0$ must occur. But this is impossible since the gain K in (4) must also be zero. That is, (26) has a unique solution, so one can always find values of the controller parameters K_{p1} , K_{i1} , K_{d1} , and τ_D using (16) from Theorem 1.

The following result shows that the controller $G_1(s)$, with the constants d_2 , d_1 , e_2 , e_1 , and e_0 calculated by solving (26), ensures that the component of the controlled output $y(t)$ in response to a constant disturbance signal $d(t)$ tends asymptotically to zero.

Theorem 3: If in the control system of Fig. 2, the controller parameters in (19) are selected by solving the set of simultaneous equations (26) then the component of the disturbance response at the controlled output $y(t)$ approaches zero asymptotically with a desired overshoot (OS) and settling time (T_s) when a step-type disturbance signal $d(t)$ is applied.

Proof: Given the specifications OS and T_s , and using the dominant pole guarantee criterion, the desired closed-loop polynomial (24) is obtained. For a disturbance signal of constant but unknown amplitude ρ , we have $D(s) = \rho/s$. Using (2), we can compute the steady-state value of the response component of the controlled output as

$$\lim_{s \rightarrow 0} s \frac{G_{yd}(s)D(s)}{Y(s)}$$

Employing (6) and (19) in the expression for G_{yd} , we obtain

$$\lim_{s \rightarrow 0} \frac{s^2(-b_1s + b_0)(d_2s + d_1)}{(t_4s^4 + t_3s^3 + t_2s^2 + t_1s + t_0)s} \frac{\rho}{s}$$

Since the limit is equal to zero, the theorem is established.

Remark 3: It should be noted that if the Taylor approximation (5) is used for the FOPTD plant, Theorem 3 remains valid.

3.2 Synthesis of controller $G_{12}(s)$

To synthesize the $G_{12}(s)$ controller, a criterion for assigning zeros to the closed-loop transfer function (3) will be used. For ease of reference, equation (3) is rewritten as

$$G_{yr}(s) = \frac{Y(s)}{R(s)} = \frac{G_{12}(s)G_p(s)}{1 + G_1(s)G_p(s)} \quad (27)$$

Using in (27), equations (6), (19), and (21) to represent $G_p(s)$, $G_1(s)$, and $G_{12}(s)$, respectively, results in

$$G_{yr}(s) = \frac{-b_1n_2s^3 + (b_0n_2 - b_1n_1)s^2 + (b_0n_1 - b_1n_0)s + b_0n_0}{t_4s^4 + t_3s^3 + t_2s^2 + t_1s + t_0} \quad (28)$$

A zero assignment criterion selects the G_{12} controller constants in (21) by making.

$$\begin{aligned} b_0n_0 &= t_0 \\ b_0n_1 - b_1n_0 &= t_1 \\ b_0n_2 - b_1n_1 &= t_2 \end{aligned}$$

Or equivalent,

$$\begin{aligned} n_0 &= t_0/b_0 \\ n_1 &= \frac{t_1 + b_1n_0}{b_0} \\ n_2 &= \frac{t_2 + b_1n_1}{b_0} \end{aligned} \quad (29)$$

Theorem 4: If the controller parameters in (21) are calculated using (29), then the controlled output $y(t)$ in the control system of Fig. 1 will track with zero steady-state error a reference signal of step, ramp, or parabola type.

Proof: Using (28) and taking the Laplace transform of equation (1) gives

$$E(s) = [1 - G_{yr}(s)]R(s)$$

The steady-state value of the tracking error is obtained by

$$e(\infty) = \lim_{s \rightarrow 0} s[1 - G_{yr}(s)]R(s)$$

Or, equivalently, through the expression

$$e(\infty) = \lim_{s \rightarrow 0} s \left[\frac{N(s)}{t_4s^4 + t_3s^3 + t_2s^2 + t_1s + t_0} \right] R(s)$$

Where

$$N(s) = t_4s^4 + (t_3 + b_1n_2)s^3 + (t_2 - b_0n_2 + b_1n_1)s^2 + (t_1 - b_0n_1 + b_1n_0)s + (t_0 - b_0n_0)$$

Considering $R(s) = \mu/s^k$ with μ a constant value, and $k = 1, 2$, or 3 depending on whether the reference signal is a step, a ramp, or a parabola, respectively. Using (29), the above limit tends to zero; thus, the theorem is established.

3.3 Synthesis of controller $G_2(s)$

The synthesis of this controller is immediate. Using (21) gives $G_2 = G_{12} - G_1$, and the PID controller constants in (20) are computed by

$$\begin{aligned} f_0 &= n_0 - e_0 \\ f_1 &= n_1 - e_1 \\ f_2 &= n_2 - e_2 \end{aligned} \quad (30)$$

It is recalled again that the constants of the PID controllers in the form of equations (11), (12) and (14) can be obtained from the constants computed in the form of equations (19), (20) and (21), respectively, using equation (16) of Theorem 1.

3.4 Synthesis procedure for the 2-DoF PID controller

For ease of reference, Table 1 summarizes the design procedure for controllers $G_1(s)$, $G_{12}(s)$, and $G_2(s)$.

Table 1. Design procedure for the 2-DoF PID controller.

Input	Constants b_1, b_0, a_1 , and a_0 in equations (5) or (6), depending on the time-delay θ_d approximation for the FOPTD model of the plant. Constants t_0, t_1, t_2, t_3 , and t_4 of the desired closed-loop polynomial in (24) from the OS and T_s design specifications.
Step 1	Solve (26) to compute constants d_2, d_1, e_2, e_1 , and e_0 for controller $G_1(s)$ in (19).
Step 2	Apply (16) to find controller constants K_{p1}, K_{i1}, K_{d1} , and τ_d in (11) ($\tau_d = \tau_{d1} = \tau_{d2}$).
Step 3	Use (29) to determine the constants n_2, n_1 , and n_0 for controller $G_{12}(s)$ in (21).
Step 4	Use (30) to determine the constants f_2, f_1 , and f_0 for controller $G_2(s)$ in (20).
Step 5	Apply (16) to find constants K_{p2}, K_{i2}, K_{d2} , and τ_d in (12).
Output	Controllers $G_1(s)$ and $G_2(s)$ in (11) and (12), respectively.

4 Results

In this section, several examples highlight different aspects of the design method for FOPTD systems (examples 1 - 3) and how the technique can be applied to other types of systems (examples 4 and 5).

4.1 Example 1

A heat flow process (Teppa-Garran et al., 2025a) is considered, which consists of a fiberglass duct with a heater and a blower located at one end and three temperature sensors along the duct. The controlled output corresponds to the temperature, and the control signal is the voltage applied to the heating element (the blower voltage is kept constant). The transfer function gives the temperature model at the third (furthest) sensor.

$$\frac{Y(s)}{U(s)} = \frac{6.1}{28s + 1} e^{-0.85s} \quad (31)$$

Using equations (5) and (6) to approximate the time delay in (31) results in the following design plant models, respectively.

$$G_p(s) = \frac{0.256}{s^2 + 1.212s + 0.042} \quad (32)$$

$$G_p(s) = \frac{-0.218s + 0.513}{s^2 + 2.389s + 0.084} \quad (33)$$

To compute the desired closed-loop polynomial in (24), the design specifications were $OS = 10\%$ and $T_s = 40$ s. The two fast poles are repeated and fixed ten times, the real part of the dominant poles. Applying the design procedure specified in Table 1, the controllers (11) and (12) parameters are computed, and their values are given in Table 2. It can be seen that controller G_2 is PD. To generate the following figures, the FOPTD model (31) represents the plant in the control system of Fig. 1. For controllers G_1 and G_2 , the values of Table 2 are employed depending on the time-delay approximation method. Fig. 3 shows the response to a step-type disturbance. Figures 4, 5, and 6 display the tracking of a step, ramp, and parabola input reference, respectively. It can be seen that the disturbance rejection is achieved in the desired settling time, but not with the desired overshoot. The fact that an irrational model, very different from the linear one used in the design of the controllers, is employed to represent the plant in the simulation produces differences. Tracking is attained for all the reference inputs, being best for the parabola and slightly deteriorating until the step. Fig. 7 illustrates the tracking of a reference input composed of a combination of ramps and steps, and Fig. 8 presents the evolution of the control signal for this case. The tracking is very satisfactory for both approximations of the delay-time, using a lower control effort for the Padé approximation.

Table 2. Constant values of PID controllers in Equations (11) and (12) for Example 1.

	K_{p1}	K_{i1}	K_{d1}	K_{p2}	K_{i2}	K_{d2}	τ_{d1} τ_{d2}
Padé	1.39	0.14	0.42	0.16	0	0.98	4.84
Taylor	0.68	0.06	0.0005	0.16	0	4.67	1.01

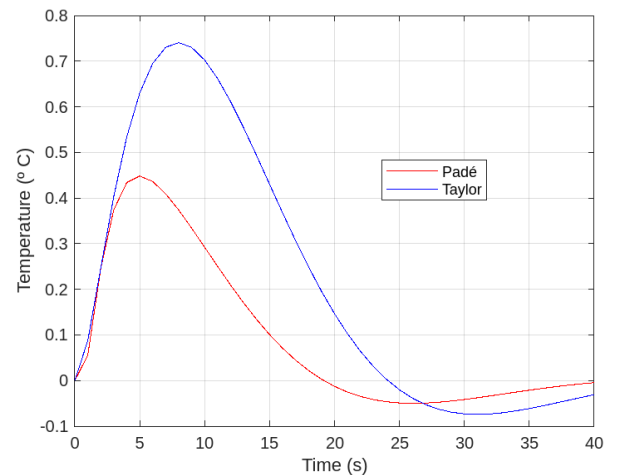


Figure 3. Step disturbance response for Example 1.

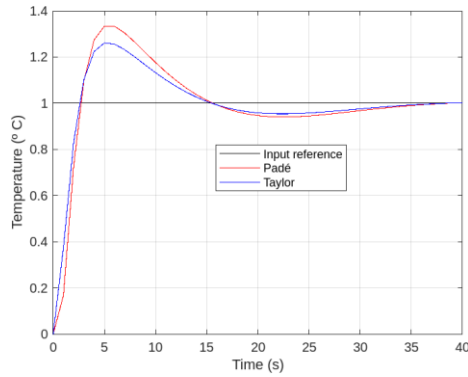


Figure 4. Step tracking response for Example 1.

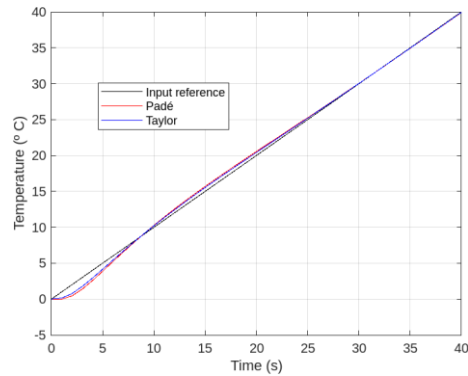


Figure 5. Ramp tracking response for Example 1.

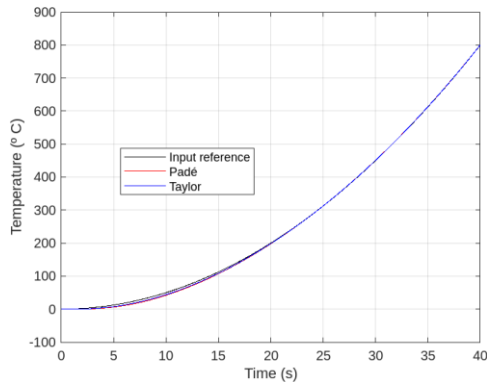


Figure 6. Parabola tracking response for Example 1.

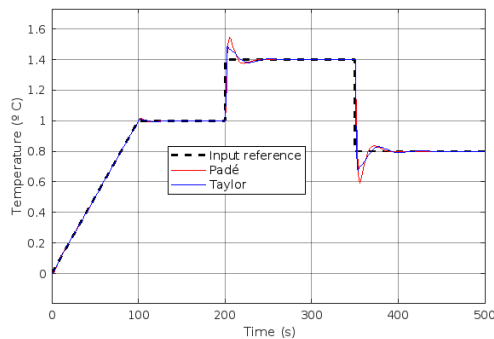


Figure 7. Temperature tracking response for the heat flow process comparing the Padé and Taylor approximations.

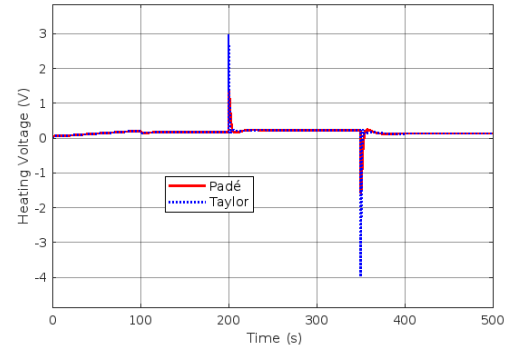


Figure 8. The heating voltage applied for the heat flow process.

4.2 Example 2

In the previous example, the relationship $\theta_d/T < 1$ was fulfilled in (4). In this example, we will deal with the more demanding situation where $\theta_d/T > 1$. For this purpose, it is considered a high-order process described as

$$\frac{Y(s)}{U(s)} = \frac{1}{(s+1)^{10}} \quad (34)$$

Employing the least-squares fitting between process and model frequency responses (Hang and Bi, 1997), the following FOPTD model is obtained.

$$\frac{Y(s)}{U(s)} = \frac{1}{2.72s+1} e^{-7.69s} \quad (35)$$

By applying the design procedure of Table 1, the parameters of the controllers (11) and (12) are given in Table 3. To compute the desired closed-loop polynomial in (24), the design specifications were $OS = 10\%$ and $T_s = 80$ s. The two fast poles are repeated and fixed five times the real part of the dominant poles.

Figure 9 shows the tracking of a combined reference input and the rejection of a constant disturbance signal applied from time $t = 400$ s. The FOPTD model of the plant (35) was used for the simulation. It can be seen that the performance using the Taylor or Padé approximations for the delay time is similar.

Fig. 10 compares the performance of the 2-DoF controller designed with the proposed method (Table 3, Taylor) with that of a 1-DoF PID tuned by the popular Chien-Hrones-Reswick (CHR) method (Teppa-Garran et al., 2021). It may seem that the latter's performance is superior, but it should be noted that the simulation for this case uses the linear model obtained from (35) by employing equation (5). When the FOPTD model (35) is used directly to represent the plant, the PID-CHR controller fails to stabilize the plant, as illustrated in Fig. 11.

Table 3. Constant values of PID controllers in Equations (11) and (12) for Example 2.

	K_{p1}	K_{i1}	K_{d1}	K_{p2}	K_{i2}	K_{d2}	τ_{d1} τ_{d2}
Padé	0.490	0.096	0.698	1	0	0.508	20.51
Taylor	0.116	0.091	0.322	1	0	1.065	9.77

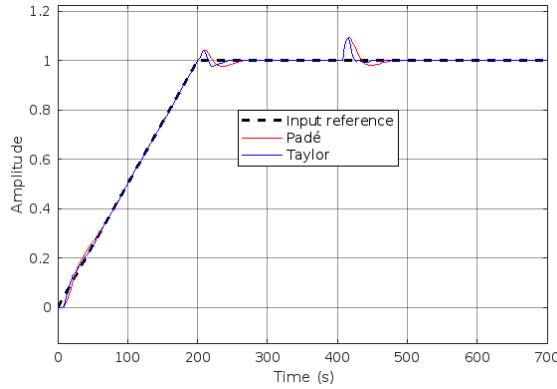


Figure 9. Tracking and disturbance-step rejection for Example 2 by comparing the Padé and the Taylor approximations.

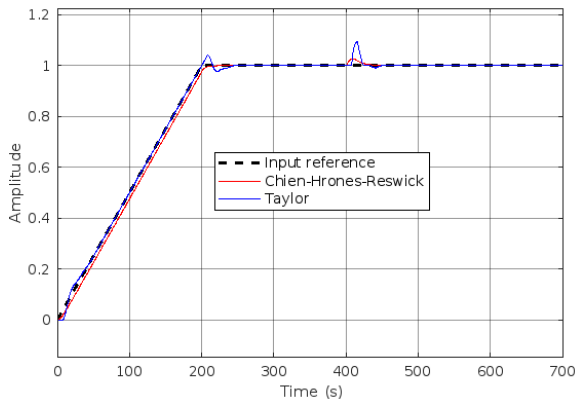


Figure 10. Tracking and disturbance-step rejection for Example 2, comparing the proposed method with a PID tuned by the CHR method.

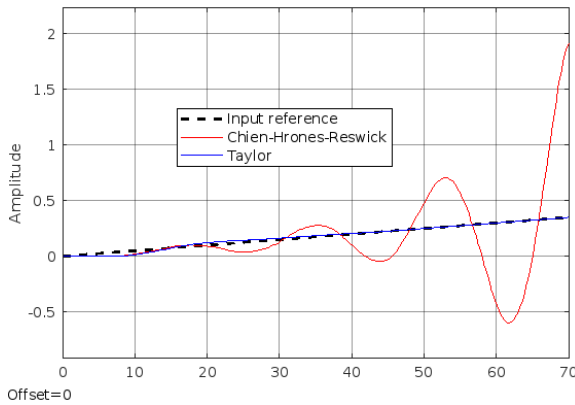


Figure 11. The PID controller tuned by the CHR method fails to stabilize the system in Example 2.

4.3 Example 3

Now we consider an open-loop unstable system described by the following FOPTD model (Yuce, 2023).

$$\frac{Y(s)}{U(s)} = \frac{1}{s-1} e^{-0.4s} \quad (36)$$

The desired closed-loop polynomial is computed for the specifications $OS = 0.05\%$ and $T_s = 20$ s. The two fast poles are repeated and fixed ten times, the real part of the dominant poles. Using the Taylor method (5) to approximate the time delay in (36) and applying the design procedure of Table 1 gives the controllers.

$$G_1(s) = 1.251 + \frac{0.046}{s} + \frac{0.283s}{0.345s + 1} \quad (37)$$

$$G_2(s) = -1 + \frac{1.74s}{0.345s + 1} \quad (38)$$

Using equations (36) – (38), the control system of Fig. 1 gives the response of Fig. 12. It can be appreciated that the correct tracking of the trapezoidal reference input and the rejection of a constant disturbance of negative amplitude applied from time $t = 25$ s.

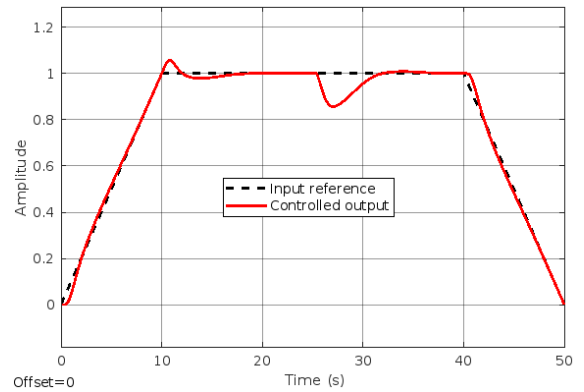


Figure 12. Tracking and disturbance rejection for an open-loop unstable process in Example 3.

4.4 Example 4

This example shows that the proposed method can be adapted to plants other than the FOPTD system. The state equations for a nonlinear model of a coupled tank system (Teppa-Garran et al., 2025b) are

$$\begin{aligned} \dot{x}_1(t) &= -0.904\sqrt{x_1(t)} + 0.258u(t) \\ \dot{x}_2(t) &= 0.904\sqrt{x_1(t)} - 0.508\sqrt{x_2(t)} \\ y(t) &= x_2(t) \end{aligned} \quad (39)$$

The variables x_1 and x_2 are the levels of tanks 1 and 2, respectively. They are restricted to the interval $[0, 30]$ cm. The control signal $u(t)$ is the voltage applied to a pump, limited to the range $[0, 21]$ V, and the controlled output $y(t)$ is the second tank level. To use the design method, the equation (39) is linearized at the point $(15, 15)$ cm, resulting in the transfer function.

$$G_p(s) = \frac{0.0302}{s^2 + 0.183s + 0.0077} \quad (40)$$

Equation (40) has the form (5) (Taylor). Hence, a 2-DoF PID can be designed using the proposed method. To that end, the desired closed-loop polynomial is computed for the

specifications $OS = 0.05\%$ and $T_s = 50$ s. The two fast poles are repeated and fixed ten times, the real part of the dominant poles. The design procedure of Table 1 gives the controllers.

$$G_1(s) = 2.232 + \frac{0.181}{s} + \frac{18.071s}{0.634s + 1} \quad (41)$$

$$G_2(s) = 0.255 + \frac{9.556s}{0.634s + 1} \quad (42)$$

Figure 13 shows the tracking response of the second-level tank to an input reference combining different ramps and steps. From the time instant $t = 325$ s, a constant disturbance signal is applied. The nonlinear model of the tank given in (39) has been used for the simulation. Figure 14 shows the voltage of the pump; it can be seen that it is always within the limits of pump operation.

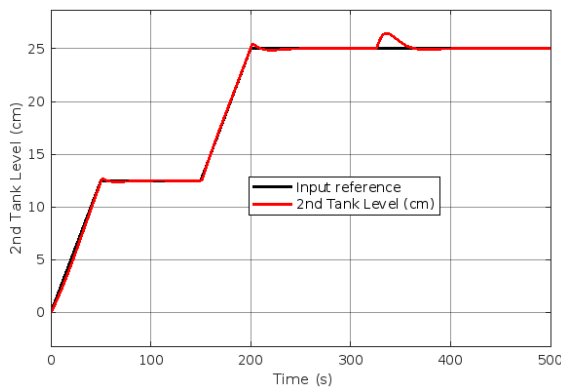


Figure 13. The second tank level response of the coupled tank system is shown in Example 4.

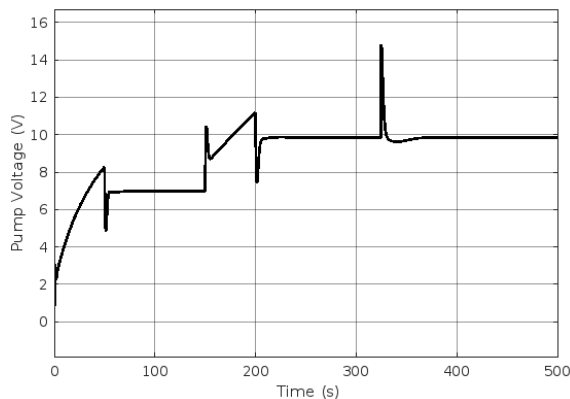


Figure 14. The voltage applied to the pump of the coupled tank system in Example 4.

4.5 Example 5

Consider a large chemical plant with the following transfer function (Tewari, 2003).

$$\frac{Y(s)}{U(s)} = \frac{0.0033}{s^3 + 0.630s^2 + 0.109s + 0.0033} \quad (43)$$

The output is the temperature, and the input is the mass flow rate of the Xylene gas. To obtain the design model in the form (5), the order reduction method (Kuo, 1991) is applied, resulting in

$$G_p(s) = \frac{0.0078}{s^2 + 0.242s + 0.0078} \quad (44)$$

The desired closed-loop polynomial is computed for the specifications $OS = 0.1\%$ and $T_s = 30$ s. The two fast poles are repeated and fixed ten times, the real part of the dominant poles. The design procedure of Table 1 gives the controllers.

$$G_1(s) = 26.445 + \frac{4.308}{s} + \frac{214.66s}{0.372s + 1} \quad (45)$$

$$G_2(s) = 1 + \frac{83.5s}{0.372s + 1} \quad (46)$$

The satisfactory temperature tracking of the large chemical plant can be seen in Fig. 15. The third-order model of the plant (43) is used in the simulation. The complete rejection of a constant disturbance signal applied from time $t = 200$ s can also be observed.

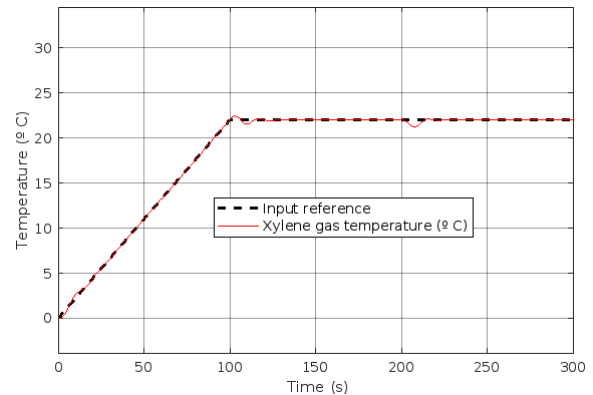


Figure 15. Temperature tracking and disturbance rejection for the large chemical plant of Example 5.

Discussion and Conclusions

A simple model-based method for the design of two-degree-of-freedom PID controllers based on a polynomial approach for FOPTD systems is proposed in this work. The problems of constant disturbance signal rejection and tracking step, ramp, or parabola reference inputs are solved independently. The constant disturbance rejection problem is solved by imposing a dominant pole guarantee criterion that allows choosing a desired overshoot and settling time in the temporal response. The tracking problem is solved by assigning zeros to the closed-loop transfer function.

Three examples of FOPTD system models are considered to cover the main cases that may arise in practical situations. That is, when the ratio of the delay time to the system time constant is greater than or less than one, and when the system is open-loop unstable. No specific advantages were found in using the Taylor or Padé methods to approximate the delay time in the FOPTD system. Other

two examples show that although the method was designed for FOPTD systems, it can be extended to different systems.

A weakness of the method is that the assignment of zeros imposed to solve the tracking problem can deteriorate the overshoot and settling time conditions of the transient component of the response. This is because the zeros cannot be fixed arbitrarily; their values come from solving equations that depend primarily on the characteristic polynomial coefficients, which rely on the overshoot and settling time specifications. What we wish to point out is that specifications could generate dominant zeros (near the imaginary axis of the complex plane), which cause a further increase in overshoot.

Another contribution of this work is that the proposed method allows tuning the four parameters of a PID controller expressed in the parallel form given by equation (9). In one example, it is observed that current tuning procedures, which initially focus on tuning the proportional, integral, and derivative constants using well-known rules and then adjusting the derivation filter parameter through predefined relationships, can result in poor performance.

Acknowledgments

The authors are grateful for the support provided by the Research Program of the Metropolitan University in Caracas, Venezuela, through project number PI-A-01-23-24.


References


- Ai, B., Sentis, L., Paine, N., Han, S., Mok, A., and Fok, C. (2016). Stability and performance analysis of time-delayed actuator control systems, *Journal of Dynamic Systems, Measurement, and Control*, vol. 138, no. 5.
- Alfaro, V., Vilanova, R., and Arrieta, O. (2010). Maximum sensitivity based robust tuning for two-degree-of-freedom proportional–integral controllers, *Industrial & Engineering Chemistry Research*, vol. 49, no. 11, pp. 5415-5423.
- Araki, M. (1985). Two degree of freedom control system: part I, *Systems and Control*, vol. 29, pp. 649-656.
- Araki, M., and Taguchi, H. (2003). Two-degree-of-freedom PID controllers, *International Journal of Control, Automation, and Systems*, vol. 1, no. 4, pp. 401-411.
- Ariba, Y., Gouaisbaut, F., and Labit, Y. (2009). Feedback control for router management and TCP/IP network stability, *IEEE Transactions on Network and Service Management*, vol. 6, no. 4, pp. 255-266.
- Åström, K., and Hagglund, T. (1995). *PID controllers: Theory, design and tuning*, NC: Instrument Society of America, Research Triangle Park.
- Atherton, D. and Majhi, S. (2009). Limitations of PID controllers, *Proc. of the 1999 American Control Conference* (Cat. No. 99CH36251), vol. 6, pp. 3843-3847, IEEE.
- Bi, M. (2020). Control of robot arm motion using trapezoid fuzzy two-degree-of-freedom PID algorithm, *Symmetry*, vol. 12, no. 4, p. 665.
- Birs, I., Muresan, C., Nascu, I., and Ionescu, C. (2019). A survey of recent advances in fractional order control for time delay systems, *IEEE Access*, vol. 7, pp. 30951-30965.
- Bresch-Pietri, D., Chauvin, J., and Petit, N. (2014). Prediction-based stabilization of linear systems subject to input-dependent input delay of integral-type, *IEEE Transactions on Automatic Control*, vol. 59, no. 9, pp. 2385-2399.
- Desborough, L. and Miller, R. (2002). Increasing customer value of industrial control performance monitoring Honeywell's experience, *AICHE symposium*. New York; American Institute of Chemical Engineers, no. 326, pp. 169-189.
- Dorf, R., and Bishop, R. (2017). *Modern control systems*, Pearson Prentice Hall.
- El-Deen, A. Mahmoud, A. and El-Sawi, A. (2015). Optimal PID tuning for DC motor speed controller based on genetic algorithm, *Int. Rev. Autom. Control*, vol. 8, no. 1, pp. 80-85.
- Goodwin, G., Graebe, S., and Salgado, M. (2001). *Control system design*, Upper Saddle River: Prentice Hall.
- Gu, K. and Niculescu, S. I. (2003). Survey on recent results in the stability and control of time-delay systems, *Journal of Dynamic Systems, Measurement, and Control*, vol. 125, no. 2, pp. 158-165.
- Gunawan, S., Yuwono, Y., Pratama, G., Cahyadi, A., and Winduratna, B. (2018). Optimal fractional-order PID for DC motor: Comparison study, *Proc. 4th International Conference on Science and Technology (ICST)*, pp. 1-6, IEEE.
- Hale, J. K., and Lunel, S. M. (2013). *Introduction to functional differential equations*, vol. 99, Springer Science & Business Media.
- Hang, H., and Bi, Q. (1997). A frequency domain controller design method, *Chemical Engineering Research and Design*, vol. 75, no. 1, pp. 64-72.
- Hanta, V. and Procházka, A. (2009). *Rational approximation of time delay*, Institute of Chemical Technology in Prague. Department of computing and control engineering. Technická, vol. 5, no. 166, p. 28.
- Jin, Q., and Liu, Q. (2014). Analytical IMC-PID design in terms of performance/robustness tradeoff for integrating processes: From 2-Dof to 1-Dof, *Journal of Process Control*, vol. 24, no. 3, pp. 22-32.
- Kuo, B. (1991). *Automatic Control Systems*, Sixth Ed. Prentice-Hall, New Jersey, p. 357.
- Lee, J., Cho, W., and Edgar, T. (2014). Simple analytic PID controller tuning rules revisited, *Industrial & Engineering Chemistry Research*, vol. 53, no. 13, pp. 5038-5047.

- Liu, G. and Daley, S. (2001). Optimal-tuning PID control for industrial systems, *Control Engineering Practice*, vol. 9, no. 11, pp. 1185-1194.
- Mamat, R. (2013). A new tuning method for two-degree-of-freedom internal model control under parametric uncertainty, *Chinese Journal of Chemical Engineering*, vol. 21, no. 9, pp. 1030-1037.
- O'Dwyer, A. (2009). *Handbook of PI and PID Controller Tuning Rules*, 3rd ed.; Imperial College Press: London, UK.
- Persson, P., and Åström, K. (1992). Dominant pole design-a unified view of PID controller tuning, *IFAC Proceedings Volumes*, vol. 25, no. 14, pp. 377-382.
- Richard, J. P. (2003). Time-delay systems: an overview of some recent advances and open problems, *Automatica*, vol. 39, no. 10, pp. 1667-1694.
- Seuret, A., and Gouaisbaut, F. (2013). Wirtinger-based integral inequality: Application to time-delay systems, *Automatica*, vol. 49, no. 9, pp. 2860-2866.
- Sharma, R., Gaur, P., and Mittal, A. (2015). Performance analysis of two-degree of freedom fractional order PID controllers for robotic manipulator with payload, *ISA transactions*, vol. 58, pp. 279-291.
- Teppa-Garran, P., and Garcia, G. (2017). Design of an optimal PID controller for a coupled tanks system employing ADRC, *IEEE Latin America Transactions*, vol. 15, no. 2, pp. 189-196.
- Teppa-Garran, P. and Vásquez, W. (2020). Desired Trajectory following by feedforward anticipation, *IEEE Latin America Transactions*, vol. 18, no. 8, pp. 1416-1424.
- Teppa-Garran, P., Arzola, F., and Elyas, E. (2021). Ajuste óptimo de controladores PID mediante Matlab/Simulink, *Anales de Ciencias Básicas, Físicas y Naturales*, vol. 37, no. 15, pp. 15-32.
- Teppa-Garran, P., Faggioni, M. and Garcia, G. (2023). Optimal tracking in two-degree-of-freedom control systems: Coupled tank system, *Journal of Applied Research and Technology*, vol. 21, no. 4, pp. 560-570.
- Teppa-Garran, P., and El Gharib, G. (2024). Sintonización óptima asistida por computadora de controladores PI para sistemas no lineales con restricciones de amplitud en el actuador, *Ciencia e Ingeniería*, vol. 45, no. 1, pp. 1-10.
- Teppa-Garran, P., Bohórquez, G., and Garcia, G. (2025 a). Optimal tuning of PID-type controllers, *Journal of Applied Research and Technology*, vol. 23, no. 2, pp. 145-154.
- Teppa-Garran, P., Muñoz-de Escalona, D., and Zambrano, J. (2025 b). Liquid level tracking for a coupled tank system using quasi-LPV control, *Ingenius*, vol. 33, pp. 15-26.
- Tewari, A. (2003). *Modern control design with Matlab and Simulink*, John Wiley & Sons, USA, p. 100.
- Vilanova, R., Alfaro, V., and Arrieta, O. (2011). Analytical Robust Tuning Approach for Two Degree of Freedom PI/PID Controllers, *Engineering Letters*, vol. 19, no. 3.
- Wang, X., Yan, X., Li, D., and Sun, L. (2018). An approach for setting parameters for two degree of freedom PID controllers, *Algorithms*, vol. 11, no. 4, p. 48.
- Xing, Z., Zhu, Q., and Ding, Y. (2006). Two-degree-of-freedom IMC-PID design of missile servo system based on tuning gain and phase margin, *J. Harbin Eng. Univ*, vol. 27, pp. 404-407.
- Yuce, A. (2023). Analytical design of PI controller for first order transfer function plus time delay: stability triangle approach, *IEEE Access*, vol. 11, pp. 70377-70386.
- Zhang, M., Wang, J., and Li, D. (2010). Simulation analysis of PID control system based on desired dynamic equation, *Proc. 8th World Congress on Intelligent Control and Automation*, IEEE, pp. 3638-3644.
- Zhang, X., Han, Q., Seuret, A., Gouaisbaut, F., and He, Y. (2019). Overview of recent advances in the stability of linear systems with time-varying delays, *IET Control Theory & Applications*, vol. 13, no. 1, pp. 1-16.
- Zhang, X., Han, Q., and Ge, X. (2022). The construction of augmented Lyapunov-Krasovskii functionals and the estimation of their derivatives in stability analysis of time-delay systems: A survey, *International Journal of Systems Science*, vol. 53, no. 12, pp. 2480-2495.
- Zhu, X. (2009). Practical PID controller implementation and the theory behind it, *Proc. Second International Conference on Intelligent Networks and Intelligent Systems* (pp. 58-61). IEEE.

Received: september 5, 2025


Accepted: november 28, 2025

Pedro Teppa-Garrán received the B.S. degree in Electrical Engineering in 1990 at the Universidad Metropolitana (UNIMET) in Caracas, Venezuela, the Master degree in Electronic Engineering in 1994 and the Master degree in Mathematics in 1998; both of them, from the Universidad Simón Bolívar (USB), Caracas, Venezuela. He also received the Ph.D. in Control Systems in 2003 at Université Paul Sabatier in Toulouse, France and completed a Postdoctoral Research in LAAS-CNRS during 2012-2013 in Toulouse, France. He is currently a full professor of UNIMET
 <https://orcid.org/0000-0001-6384-3185>

Luis Caraballo: Electrical Engineer from UNIMET.
 c.luis@correo.unimet.edu.ve
 <https://orcid.org/0009-0004-5507-272X>

Germain Garcia received his diploma in engineering from the Institut National des Sciences Appliquées (INSA), Toulouse, France, in 1984. He also received his Ph.D. degree in Automatic Control from the INSA in 1988 and the Habilitation à Diriger des Recherches (HDR) in 1997 from the same university. He is currently working at the Laboratoire d'Architecture des Systèmes of the Centre National pour la Recherche Scientifique (LAAS-CNRS), Toulouse, France as full professor of INSA.

garcia@laas.fr

 <https://orcid.org/0000-0002-7147-5105>

Evolution of innovation and sustainability research Among the arab world's universities

Evolución de la investigación sobre innovación y sustentabilidad en las universidades del mundo árabe

Román, Jorge^{1*}; Almuaini, Abdelrahman²; Zairi, Adel³; Rivas, Francklin⁴; Villasmil, María Alejandra⁵

1 Environment Agency Abu Dhabi, Dubái UAE.

2 Assistant Undersecretary for Intellectual Property Ministry of Economy.

3 Zairi Institute, Dubai UAE.

4 Department of Computer Science and Engineering, University of Texas at Arlington, USA.

5 Department of Administrative Sciences, University of the Andes, Mérida, Venezuela.

*Jorge.garate@ead.gov.ae

Abstract

Scientific research on innovation and sustainability in Arab world universities has become a topic of increasing importance in recent decades. The objective of this study is to investigate publications focusing on innovation and sustainability using a bibliometric approach. The study uses the Web of Science Core Collection database and VOS viewer software to analyze bibliometric data from 1995 to 2023. Findings reveal significant growth in innovation and sustainability research in Arab countries over the past decade, with notable contributions from Saudi Arabia, United Arab Emirates (UAE), and Egyptian universities. Collaborations in Saudi Arabia and the UAE are mainly with Chinese academics, while Egyptian research extends to the USA, Europe, and Turkey. Scientific production in innovation and sustainability in the Arab region has grown significantly more than the average in other disciplines, undoubtedly due to the influence of global agreements such as the SDGs of United Nations and the Paris Agreement.

Keywords: Bibliometrics, Arab universities, Innovation, Sustainability

Resumen

La investigación científica sobre innovación y sostenibilidad en las universidades del mundo árabe se ha convertido en un tema de creciente importancia en las últimas décadas. El objetivo de este estudio es analizar las publicaciones centradas en innovación y sostenibilidad utilizando un enfoque bibliométrico. El estudio emplea la base de datos Web of Science Core Collection y el software VOSviewer para analizar datos bibliométricos desde 1995 hasta 2023. Los resultados revelan un crecimiento significativo de la investigación en innovación y sostenibilidad en los países árabes durante la última década, con contribuciones destacadas de universidades de Arabia Saudita, Emiratos Árabes Unidos (EAU) y Egipto. Las colaboraciones en Arabia Saudita y los EAU se realizan principalmente con académicos chinos, mientras que la investigación egipcia se extiende a Estados Unidos, Europa y Turquía. La producción científica en innovación y sostenibilidad en la región árabe ha crecido considerablemente más que el promedio de otras disciplinas, sin duda debido a la influencia de acuerdos globales como los ODS de las Naciones Unidas y el Acuerdo de París.

Palabras clave: Bibliometría, universidades árabes, innovación, sostenibilidad.

1 Introduction

In different universities around the world, scientific research on topics of innovation and sustainability has shown continuous growth in recent years (Merigó et al., 2016; Cancino et al., 2017a, 2017b). This trend has also been

observed in Arab world universities, an important region whose countries have actively sought ways to promote sustainable development and innovation in various sectors, including energy, agriculture, technology, and business management.

Some focal areas of scientific research in innovation and sustainability among Arab world universities may encompass subjects such as food waste as a valuable resource to produce chemicals, materials, and fuels (Lin et al., 2013). Also, topics about green innovation and organizational performance aims to analyze the influence of big data with a focus on the moderating role of management commitment and human resources practices (El-Kassar & Singh, 2019). Others explore comprehensive reviews of challenges and potential applications of integrated systems in the realm of renewable energy-driven desalination technologies (Ghaffour et al., 2015). A broader perspective is provided by studies that examine the linkages between natural resources, human capital, globalization, economic growth, financial development, and ecological footprint (Jahanger et al., 2022). In this latter work, the moderating role of technological innovations is particularly analyzed. In addition to these themes, diverse scientific studies are being conducted in Arab world universities to analyze the effects and opportunities of innovation and sustainability in the region, their impact on productive development, and their influence on business performance.

In the Arab world, there is an increasing concern about sustainability and growth, which is evident in the investments made by various economies. For instance, the UAE has invested approximately \$16.8 billion in renewable energy projects across 70 countries (Josefson & Rotar, 2023), with a particular focus on developing nations. This investment is part of an ambitious plan related to the Climate Action Journey in the Energy sector, aiming to achieve net-zero emissions by 2050. Specific actions include the initiation in 2022 of updating the UAE Energy Strategy 2050, the commencement of developing the National Hydrogen Strategy 2050 in the same year, and the declaration of 2023 as the Year of Sustainability by the UAE President, HH Sheikh Mohamed bin Zayed Al Nahyan.

To understand the trends in academic research on innovation and sustainability in Arab world universities, this paper aims to investigate publications with a specific focus on these topics using a bibliometric approach. Bibliometric studies are very common in the scientific community in a wide range of fields including innovation (Podsakoff et al., 2008). To achieve this, the study utilizes the Web of Science Core Collection database and the Visualization Similarities (VOS) viewer software to analyze bibliometric data from January 1995 to September 2023. The focus is exclusively on countries within the Arab world. The keywords employed in the database to select the papers were 'innovation' and 'sustainability,' for the specified time and countries mentioned. Only academic papers were taken into consideration, excluding conference papers or research notes. A total of 1,769 academic papers are analyzed.

The results indicate that over the past decade, research on

innovation and sustainability in Arab countries has experienced significant growth. This exponential growth mirrors trends observed in other global regions, particularly in the United States and Europe. Notably, the findings highlight that it was particularly after the 2015 Paris Agreement and the United Nations declaration of the 17 Sustainable Development Goals (SDGs) in the same year that universities in the Arab region began consistently and significantly developing academic studies in the fields of innovation and sustainability.

Out of the 15 Arab countries analyzed (Saudi Arabia, United Arab Emirates - UAE, Egypt, Tunisia, Morocco, Qatar, Jordan, Lebanon, Iraq, Algeria, Bahrain, Oman, Palestine, Yemen, and Syria), only the first three, Saudi Arabia, UAE, and Egypt, stand out significantly due to the number of papers published by their universities. While Saudi Arabia accounts for just over 30% of the total papers on innovation and sustainability in the region, the UAE and Egypt each contribute approximately 15%. In addition to the results, it is noteworthy to examine the networks Arab world universities have with other international institutions. In their studies on innovation and sustainability, the networks of Saudi Arabia and the UAE primarily involve academics from Chinese universities, while the research collaborations of Egyptian universities extend to academics or researchers from the USA, Europe, and Turkey.

Broadly, keyword analyses of the published papers reveal that the topics studied in Arab universities can be categorized into three major domains concerning innovation and sustainability. Firstly, there is a focus on sustainable innovation management. Secondly, there is an examination of the current effects and impacts of consumption, production, and trade practices. Thirdly, there is an exploration of the performance of companies and economies that promote innovation and sustainability.

The discussion and analysis of the results presented in this paper may be of significant interest to academics in the region who wish to deepen their studies on innovation and sustainability in the Arab world. This is especially relevant at a time when each country is formulating its long-term strategy to address a post-oil world, where new forms of development and competitiveness are crucial to confront emerging global challenges and competitive scenarios.

Following this introduction, Chapter 2 provides a literature review on innovation and sustainability. Chapter 3 outlines the methodology for bibliometric analysis. Chapter 4 presents the paper's results, and Chapter 5 offers a discussion of these findings. The final chapter presents the study's conclusions.

2 Literature review

Academic literature in the Arab Middle East is not only increasing in productivity but also in influence (Jamali et al., 2023), offering an opportunity to drive innovation and entrepreneurship in the region, ultimately leading to potential transformation of its economies and enhancement of its quality of life (Zahra, 2012).

According to Ryan and Daly (2019) the Middle East makes fewer contributions to the creation of new knowledge compared to other regions of the world. Because the Middle East region is characterized by extremely diverse cultures, heavy turmoil, political diversity, differences in the language, economies, and religions, knowledge production in the form of publications and patents has been under expectation (Gul et al., 2015).

Similarly, numerous academic research has been undertaken to comprehend the dynamism in scientific publications across diverse knowledge domains in the Arab world. According to Tamara (2021), the past two decades have witnessed a surge in research efforts directed towards

exploring the behavior, governance, growth, and prosperity of family businesses in the Arab Middle East. This form of family business study is of particular significance in this region as family enterprises constitute 90% of all businesses. In a similar view, Román et al. (2023) also conduct an extensive review of academic literature worldwide about Intellectual Property Rights, with a pronounced emphasis on the Arab world's concerns, particularly from the perspective of the UAE, regarding an issue of significant importance to economic development. Ibrahim (2020) also examines scientific research conducted in the Arab world, specifically in Egypt. Ibrahim paper investigates the role of national awards in the Egyptian scientific research system, aiming to identify the characteristics of State Award laureates in science and technology, determine their international literature, and explore the implications of receiving a national award using bibliometric indicators.

In the following Figure 1, it is possible to observe that the evolution in scientific productivity in the Arab world is significant and steadily increasing over time. In fact, over a decade, the quantity of papers published on scientific topics in the region has multiplied by five or nearly six times.

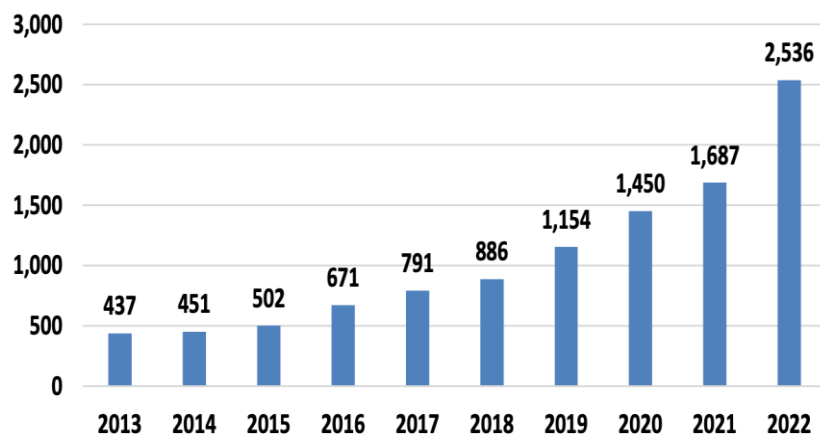


Figure 1. Growth in articles among the 30 accredited Arab business schools. Source: Jamali et al. (2023)

According to Jamali et al. (2023), trends in the two most relevant academic categories for business research, "Business, Management, and Accounting" and "Economics, Econometrics, and Finance" are observed in the Arab region. Research growth in the Arab region is nearly double that of global growth during the same period. In relative terms, the increase in publications in the region has been significant, which can be attributed to the continuous expansion of faculty in Arab business schools and normative pressures on these academics to publish. This indicates the emergence of a research culture and positive trends toward increased productivity among academic institutions in the Arab world. Now, what topics are attracting attention in research? Without a doubt, they are issues related to innovation,

sustainability, and growth, as there is a growing concern in the agendas of Arab countries that aligns with these areas of interest. As mentioned in the Introduction, there are examples of initiatives in all Arab economies, like the ones presented for the UAE below, which then attract researchers' attention to analyze and conduct scientific work on them.

As mentioned in the Introduction, there are examples of initiatives in all Arab economies, like the ones presented for the UAE below, which then attract researchers' attention to analyze and conduct scientific work on them (Table 1).

Table 1. Initiatives in UAE related to innovation, sustainability, and growth.

UAE Vision 2021	UAE Sustainable Development Agenda 2030	UAE Energy Strategy 2050
The Vision aims to make the UAE among the best countries in the world by the Golden Jubilee of the Union. In order to translate the Vision into reality, its pillars have been mapped into six national priorities which represent the key focus sectors of government action in the coming years.	To effectively implement the SDGs, the UAE adopted a whole of government approach that entailed the creation of a National Committee on SDGs. The committee is responsible for promoting sustainable development and creating ownership of the goals.	Building on national policies relevant to green growth and sustainable development, particularly the UAE Green Agenda 2015-2030, and reflecting on valuable inputs received from stakeholders from public, private, and non-governmental sectors, the Climate Plan is envisaged to strengthen the momentum going forward
National Climate Change Plan of the UAE 2017 - 2050	National Policy for Reducing Transport Sector Emissions	UAE Green Agenda – 2015 – 2030
The primary objectives are to manage greenhouse gas (GHG) emissions while sustaining economic growth, minimize risks and improve capacity of adaptation to climate change and enhance the UAE's economic diversification agenda through innovative solutions.	Initiatives focus on leveraging advanced technologies to boost the safety and prepare the infrastructure for autonomous vehicles and high-speed means of transportation, while seeking sustainable and environment-friendly alternatives.	The UAE's Green Agenda - 2030 is a long-term plan to achieve the goals of sustainable development in the UAE and make its economy more environment-friendly. It has strategic objectives and includes various programmes and initiatives to achieve them.

Considering the above, there is an undeniable opportunity to further investigate whether this increased productivity is observed in specific areas of research, such as themes related to innovation and sustainability. As with various studies on publications in the field of innovation within universities worldwide and their diverse regions (Roman et al., 2017; Cancino et al., 2017a, 2017b, 2018, 2023; Farías & Cancino, 2021), it is pertinent to examine the progress that has been made in scientific publications in the Arab world concerning innovation. Today, more than ever, this analysis is crucial, especially in its connection with sustainability, which holds significant relevance for global markets and the world economy (United Nations, 2015).

Based on the previous analysis, and in order to gain a comprehensive understanding of the evolution of innovation and sustainability research within Arab universities, this paper aims to analyze scientific papers with a focus on innovation and sustainability in Arab universities through a bibliometric approach.

3 Methodology

In recent years, in the Arab context bibliometric analysis has gained increasing popularity among scholars as a powerful and adaptable quantitative tool for examining bibliographic data (Román et al., 2023; Jamali et al., 2023). Various

researchers have provided diverse definitions, but for instance, foundational studies by Pritchard (1969) and Broadus (1987) established bibliometrics as a field within library and information sciences that employs quantitative methods to explore bibliographic materials. While this methodology has been in use for nearly half a century, it has seen a growing resurgence of interest among researchers. This revival can be attributed, in part, to the significant advancements in technology over the past few years, which have greatly enhanced the capabilities and applications of bibliometric analysis. These developments, coupled with the increasing recognition of the insights and value that bibliometrics can offer in research contexts, have contributed to its continued relevance and utility in the scholarly community.

In bibliometric studies, the indicators typically analyzed include total publications, total citations, and the h-index. While the first measures productivity and the second measures influence, the h-index represents a metric that combines productivity and influence in a discipline, making it an interesting indicator for the analysis of the growth of a knowledge area (Hirsch, 2005). In this current study, we employ total publications, total citations, and the h-index as bibliometric indicators to present a more comprehensive set of findings.

The database utilized for this study is the Web of Science Core Collection. Our search process commenced with the query: "innovation" AND "sustainability" OR "innovat*" OR "sustain*". The entire search process and analysis were conducted in September 2023. Through this study, we identified a total of 1,769 documents as publications within the analyzed period (from January 1995 to August 2023). Furthermore, in this bibliometric investigation, we incorporate a visual component to aid in the interpretation of bibliometric indicators. VOS viewer provides visual reports that illustrate university collaboration and the co-occurrence

of author keywords. University collaboration visualizes the most frequent co-authorships among different universities in the same papers, while co-occurrence of author keywords reveals the most commonly occurring keywords typically found beneath the abstracts. In the following Table 1, it can be observed the results for total publications (TP), total citations (TC), and the *h*-index across three time periods (1995-2005, 2006-2015, 2016-2023). Additionally, it is feasible to analyze the total number of publications that have received more than 100, 50, 20, 10, and 1 citation.

Table 2. Ranking of countries on innovation and sustainability research in Arab universities.

Period	≥100	≥50	≥20	≥10	≥1	H-Index	TP	TC
1995-2005	0	0	0	4	8	5	9	63
2006 - 2015	7	12	30	44	65	25	65	4,249
2016 - 2023	31	101	290	527	1,294	65	1,695	19,087
Total	38	113	320	575	1,367	68	1,769	26,062
Percentage	2,15%	6,39%	18,09%	32,50%	77,28%			

Note: > 100, > 50, > 20, > 10, > 1 = Number of papers with equal or more than 200, 100, 50, 20, 10 and 1 citations. H = h-index; TP = total number of publications; TC = total number of citations

Source: Own elaboration

Table 2 shows that a total of 1,769 papers were published between 1995 and 2023, with the last decade exhibiting the highest levels of productivity and influence. Only a small number of articles, a total of 38, have garnered more than 100 citations, but approximately one-third of the publications have received at least 10 citations. This phenomenon underscores the increasing influence that academic papers on innovation and sustainability have accumulated over time.

4 Results

This section presents a complete interpretation of the results of the bibliometric analysis. The Figure 2 below depicts the evolution of published articles from 1995 through 2023, which illustrates a significantly greater growth in scientific articles compared to the average growth rate presented in Figure 1, which represented the growth in academic articles across all knowledge areas in the Arab world.

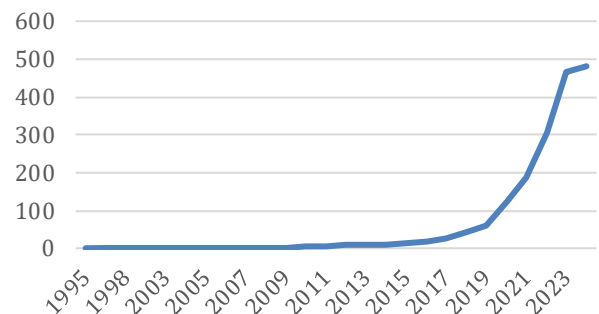


Figure 2. Evolution of innovation and sustainability research in Arab universities.

Source: Own elaboration

Figure 2 displays a conspicuous surge in the publication of papers focused on innovation and sustainability within Arab countries, particularly following two momentous events in 2015. Firstly, in September 2015, the United Nations General Assembly ratified the 2030 Agenda for Sustainable Development. This landmark agreement delineates a transformative vision for economic, social, and environmental sustainability, supported by the 193 Member States who embraced it. Secondly, on December 12, 2015, during the COP21 summit in Paris, the participants in the United Nations Framework Convention on Climate Change (UNFCCC) achieved a historic accord known as the Paris Agreement. The Paris Agreement is designed to combat climate change and expedite the

necessary actions and investments for a sustainable, low-carbon future. It signifies the first-ever collective commitment of all nations to pursue ambitious endeavors aimed at mitigating climate change and adapting to its impacts.

4.1 Publication on innovation and sustainability research by Arab countries

In this section, we present the leading Arab countries with universities actively publishing research on innovation

and sustainability. The ranking is organized by h-index and provides the total number of publications and total citations for each country in the topic under consideration. Additionally, we compare the total publications and citations with the overall population of each country to assess the scientific output adjusted for the size of each economy. While this does not imply a greater or lesser commitment as an economy to the study of a specific topic, it does allow for an initial assessment of the effort made by universities with measurable outcomes in scientific publications.

Table 3. Ranking of countries on innovation and sustainability research in Arab universities.

R	COU	TP	TC	H	TC/TP	POPULATION	TP/POP	TC/POP
1	SAUDI ARABIA	645	10,245	50	15.88	36,947,025	17.46	0,00028
2	UAE	313	4,687	33	14.97	9,537,538	32.82	0,00049
3	EGYPT	297	4,909	30	16.53	113,206,750	2.62	0,00004
4	TUNISIA	130	1,461	20	11.24	12,487,268	10.41	0,00012
5	MOROCCO	122	2,506	26	20.54	37,943,332	3.22	0,00007
6	QATAR	120	2,199	21	18.33	2,722,089	44.08	0,00081
7	JORDAN	102	934	17	9.16	11,350,401	8.99	0,00008
8	LEBANON	94	1,425	16	15.16	5,315,754	17.68	0,00027
9	IRAQ	92	1,026	15	11.15	45,783,454	2.01	0,00002
10	ALGERIA	50	774	10	15.48	45,791,152	1.09	0,00002
11	BAHRAIN	34	343	9	10.09	1,489,146	22.83	0,00023
12	OMAN	30	199	9	6.63	4,663,383	6.43	0,00004
13	PALESTINE	26	260	8	10.00	5,405,416	4.81	0,00005
14	YEMEN	17	75	5	4.41	34,660,561	0.49	0,00000
15	SYRIA	15	194	8	12.93	23,532,985	0.64	0,00000

Note: R = ranking; COU = country; TP = total number of publications; TC = total number of citations.

H = h-index; TC/TP = total number of citations over total number publications; TP/POP = total number publications over population; TC/POP = total number citations over population.

Source: Own elaboration

Table 3 reveals that Saudi Arabia, the UAE, and Egypt stand out as the countries with the highest number of university researchers publishing research on innovation and sustainability. Saudi Arabia stands out with over 30% of the publications and more than 33% of the citations on the subject being analyzed. In the case of the UAE and Egypt, both countries contribute 15% of the research effort in both aspects, respectively. Undoubtedly, these three economies among Arab countries exhibit the most significant scientific research efforts in innovation and sustainability.

Particularly noteworthy is the effort put forth by the UAE in terms of the number of publications and citations it maintains when compared to its population. The research effort as a percentage of the population is remarkably high (32.82), second only to Qatar (44.08), albeit with fewer than half the publications.

4.2 Publications on innovation and sustainability research by Arab universities

In this section, we present the leading Arab universities actively publishing research on innovation and sustainability. Table 3 presents a ranking of Arab universities in the field of innovation and sustainability research.

In addition to the established indicators of h-index, total publications, and total citations, Table 3 also provides information about each university's standing in the ARWU (The Academic Ranking of World Universities, also known as the Shanghai Ranking) and the QS (World University Rankings by Quacquarelli Symonds) rankings.

Table 4. Ranking of Arab universities on innovation and sustainability research.

R	UNIVERSITY	COU	TP	TC	H	TC/T P	ARWU	QS
1	King Saud U.	Saudi Arabia	125	1,529	21	12.23	101-150	-
2	King Abdulaziz U.	Saudi Arabia	78	1,432	20	18.36	151-200	143
3	Qatar U.	Qatar	77	1,199	18	15.57	501-600	173
4	Prince Sattam Bin Abdulaziz U.	Saudi Arabia	61	897	14	14.70	501-600	-
5	U. of Sharjah	UAE	58	1,040	17	17.93	901-1000	364
6	Lebanese American U.	Lebanon	52	1,041	12	20.02	-	661-670
7	U. de Carthage	Tunisia	43	396	10	9.21	-	-
8	Abu Dhabi U.	UAE	39	1,140	14	29.23	-	580
9	Cairo U.	Egypt	37	472	11	12.76	301-400	371
10	King Faisal U.	Saudi Arabia	37	353	8	9.54	801-900	851-900
11	King Fahd U Pet. Minerals	Saudi Arabia	33	275	7	8.33	-	-
12	King Khalid U.	Saudi Arabia	33	454	8	13.76	401-500	761-770
13	Princess Nourah Bint Abdul. U.	Saudi Arabia	33	303	6	9.18	301-400	661-670
14	Khalifa U. Sc. Technology	UAE	32	582	9	18.19	-	-
15	Prince Sultan U.	Saudi Arabia	31	719	13	23.19	-	-

Note: R = ranking; COU = country; TP = total number of publications; TC = total number of citations;

H = h-index; TC/TP = total number of citations over total number publications; ARWU = Shanghai Ranking;

QS = Quacquarelli Symonds ranking.

Source: Own elaboration

Table 4 shows that out of the 15 leading Arab universities in scientific publications on innovation and sustainability, 8 of them are from Saudi Arabia, 3 from the UAE, and one each from Egypt, Qatar, Lebanon, and Tunisia. In the case of the top two universities in the Table 4 ranking, King Saud University and King Abdulaziz University, they also happen to be the best Arab universities according to the ARWU ranking, both ranking within the top 150 and 200 best universities in the world, respectively.

It is intriguing to analyze the case of Abu Dhabi University, which may not rank at the top in terms of the number of publications, but it demonstrates a noteworthy citation-to-publication ratio of 29.23. This indicates that while it may not be the most prolific in terms of output, it is among the universities that wield greater influence in terms of citations whenever a paper is published. In other words, each paper authored by academics from Abu Dhabi University garners significantly more citations on average than those from other universities in the ranking. It underscores the notion that academia is not solely about sheer publication volume but also about exerting influence within the scientific community

through research.

4.3 Most Influential Papers on Innovation and Sustainability Research

In this section, we showcase the leading papers or publications emanating from Arab universities in the field of innovation and sustainability. Table 5 compiles the top 15 most influential papers in the subject of analysis, providing details regarding their total citations and average citations per year. This allows for the comparison of data across papers published in different years.

Table 5. Ranking of most Arab influential paper on innovation and sustainability research

R	TC	Title	Author/s	Year	C/Year
1	1,388	The IPBES Conceptual Framework - connecting nature and people	Díaz, S; Demissew, S; Carabias, J; Joly, C;	2015	173.50
2	736	Food waste as a valuable resource for the production of chemicals, materials and fuels. Current situation and global perspective	Lin, CSK; Pfaltzgraff, LA; Herrero-Davila, L; Mubofu, EB; Abderrahim,	2013	73.60
3	451	Green innovation and organizational performance: The influence of big data and the moderating role of management commitment and HR practices	El-Kassar, AN; Singh, SK	2019	112.75
4	351	Renewable energy-driven desalination technologies: A comprehensive review on challenges and potential applications of integrated systems	Ghaffour, N; Bundschuh, J; Mahmoudi, H; Goosen, MFA	2015	43.88
5	272	The effect of nano-additives in diesel-biodiesel fuel blends: A comprehensive review on stability, engine performance and emission characteristics	Soudagar, MEM; Nik-Ghazali, NN; Kalam, MA; Badruddin, IA;	2018	54.40
6	278	Functional graphene nanosheets: The next generation membranes for water desalination	Mahmoud, KA; Mansoor, B; Mansour, A; Khraisheh, M	2015	34.75
7	244	The linkages between natural resources, human capital, globalization, economic growth, financial development, and ecological footprint: The moderating role of technological innovations	Jahanger, A; Usman, M; Murshed, M; Mahmood, H; Balsalobre-Lorente, D	2022	244.00
8	208	Role of big data analytics in developing sustainable capabilities	Singh, SK; El-Kassar, AN	2019	52.00
9	207	Recent trends in membranes and membrane processes for desalination	Goh, PS; Matsuura, T; Ismail, AF; Hilal, N	2016	29.57
10	198	Offering an innovative composited material for effective lead(II) monitoring and removal from polluted water	Awual, MR; Hasan, MM; Islam, A; Rahman, MM; ...	2019	49.50
11	190	Innovations and technology disruptions in the food sector within the COVID-19 pandemic and post-lockdown era	Galanakis, CM; Rizou, M; Aldawoud, TMS; ...	2021	95.00
12	182	Who Uses Smart City Services and What to Make of It: Toward Interdisciplinary Smart Cities Research	Lytras, MD; Visvizi, A	2018	36.40
13	183	Absorptive capacity and green innovation adoption in SMEs: The mediating effects of sustainable organisational capabilities	Aboelmaged, M; Hashem, G	2019	45.75
14	168	Investigating influence of green innovation on sustainability performance: A case on Malaysian hotel industry	Asadi, S; Pourhashemi, SO; Nilashi, M; Abdullah, R; Samad, S;	2020	56.00
15	160	A Secure Cloud Computing Based Framework for Big Data Information Management of Smart Grid	Baek, J; Vu, QH; Liu, JK; Huang, XY; Xiang, Y	2015	20.00

Note: R = ranking; TC = total number of citations; C/Year = total number of citations by year.

Source: Own elaboration.

One of the most significant characteristics of the papers displayed in Table 5 is their high impact, with all of them surpassing 160 citations, and the leading paper in the ranking exceeding a thousand citations. In terms of their content, the majority of the papers do not specifically address a particular Arab economy but rather explore topics of interest in the Arab region, with the involvement of academics affiliated with Arab universities. Therefore, the most important aspect is to analyze the primary areas of study, which can be investigated through the analysis of keywords within the

analyzed papers.

4.4 Typical keywords used in innovation and sustainability Arab research.

Next, Figure 3 shows the most frequently co-occurring keywords in innovation and sustainability research conducted at Arab universities.

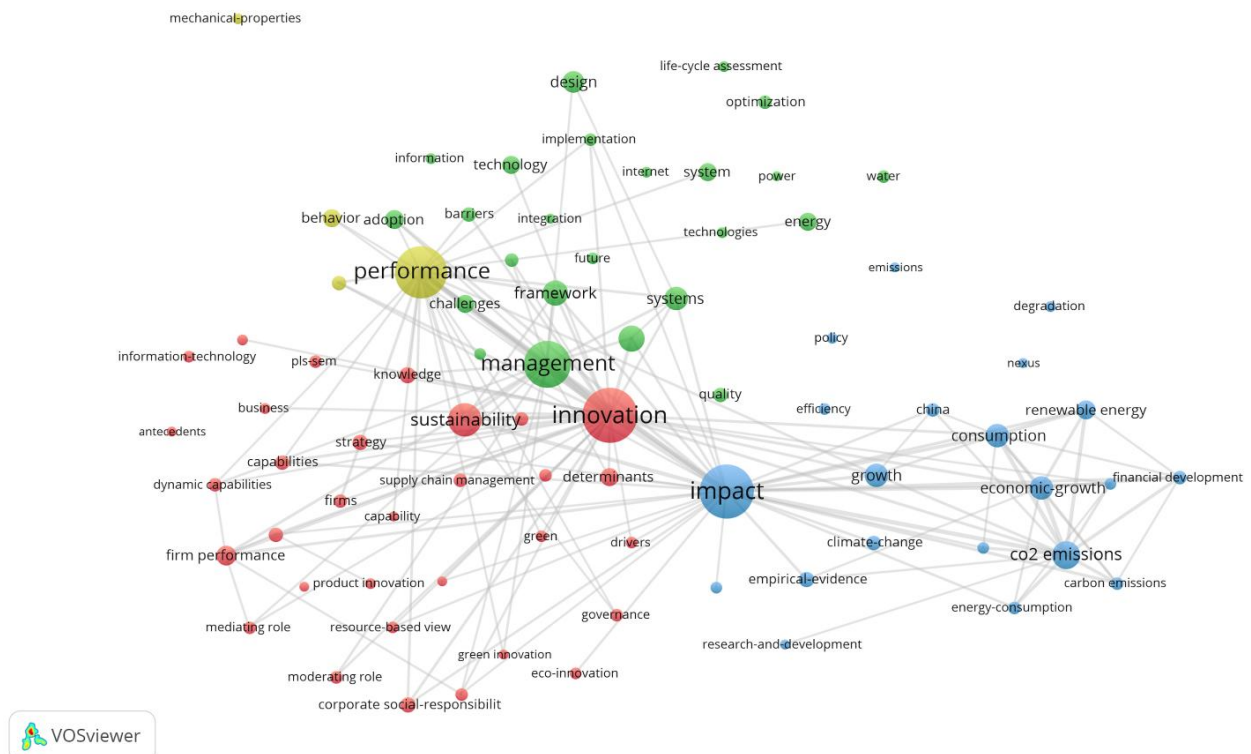


Figure 3. keywords used in innovation and sustainability Arab research.

Source: Own elaboration using VOSviewer program

According to Figure 3, within academic studies on innovation and sustainability in Arab universities, the most frequently co-occurring keywords are innovation, management, impact, and performance. Evidently, in the Arab region, three major clusters of topics of interest to researchers can be observed. These themes are as follows. Firstly, at the center of Figure 3, there is a cluster related to the management of innovation and sustainability, encompassing the analysis of determinants, strategies, and systems, among other factors. Secondly, a second cluster pertains to topics concerning impacts, whether in terms of economic growth, consumption, renewable energy, climate change, and more. Finally, a third cluster focuses on everything related to performance, involving the examination of challenges, barriers, and issues associated with the

implementation of actions that promote innovation and sustainability in various markets.

4.4 Leading universities which Arab universities collaborate.

Now, Figure 4 presents the world universities with which Arab universities collaborate, maintaining joint publication developments.

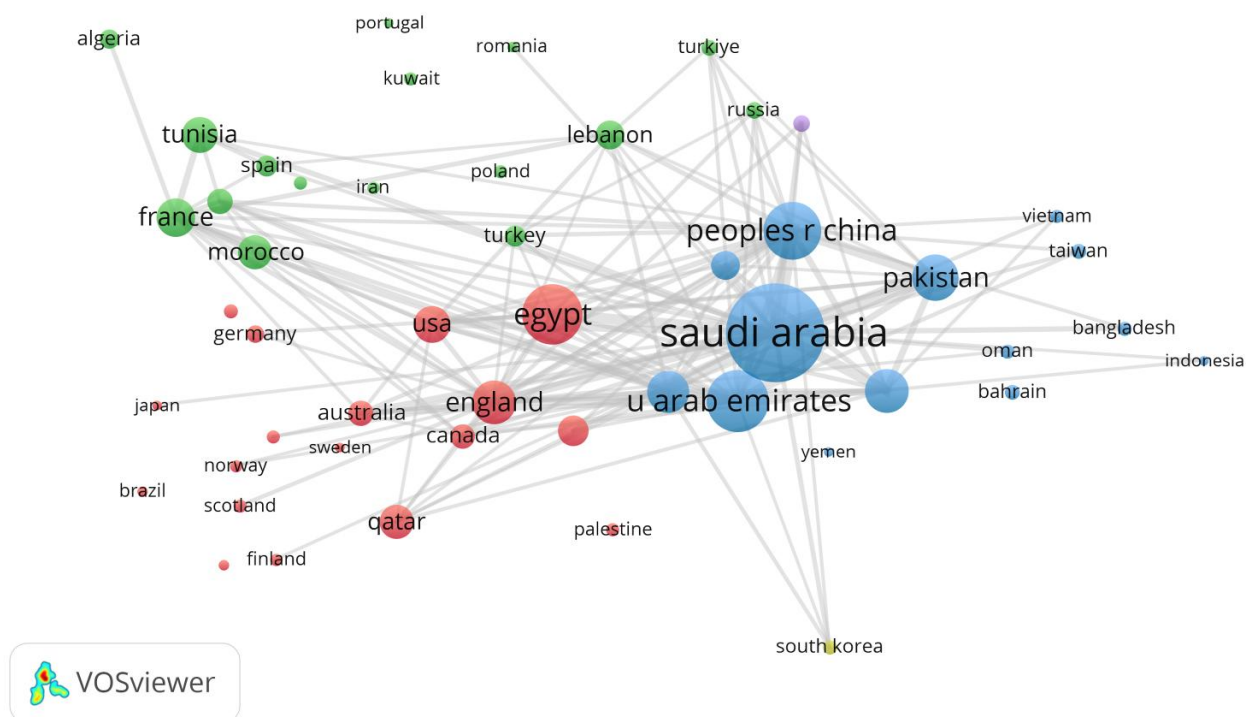


Figure 4. Universities worldwide with which Arab universities collaborate.
Source: Own elaboration using VOSviewer program

Figure 4 reveals two evident clusters characterized by extensive collaboration among countries linked to the Arab region. Particularly, scholars from the UAE and Saudi Arabia predominantly collaborate with peers in China and Pakistan. Conversely, Egyptian academics exhibit stronger affiliations with North American and European counterparts, including the USA, Canada, England, and Australia. The degree of collaboration among nations is particularly remarkable, especially in times of heightened trade tensions, where a competitive struggle for commercial dominance and economic advancement is noticeable, notably between the USA and China.

5 Discussion

In the wake of global agreements, such as the 17 Sustainable Development Goals (SDGs) set by the United Nations and the Paris Agreement with its environmental targets, academic discourse has seen a significant surge in scholarly papers concerning innovation and sustainability within the Arab countries. The year 2015 marked a pivotal point when universities in the Arab world began expressing a heightened interest in exploring the implications of sustainable business

practices, placing innovation at the core of this discourse. This academic trend mirrors the growing concern about global environmental issues and the need for innovative solutions (Jamali et al., 2023).

Arab nations like Saudi Arabia, the UAE, and Egypt have emerged as trailblazers in advancing research on innovation and sustainability in the region. Their commitment is not limited to specific areas but extends to various academic disciplines. These countries have demonstrated leadership not only in the realm of environmental sciences but also in economics, engineering, and social sciences (see Figure 3 and Figure 4). The surge of academic publications from scholars in these regions reflects their proactive efforts to address pressing global challenges through innovative research and multidisciplinary collaboration.

The research output stemming from Saudi Arabia, the UAE, and Egypt manifests their dedication to fostering innovation and sustainability. In fields such as environmental engineering and renewable energy, these nations have emerged as prominent contributors, generating valuable

insights to tackle environmental challenges. Simultaneously, their researchers have made significant strides in areas like economics and management, promoting sustainable business practices and guiding the international community towards a more ecologically conscious future. This academic leadership underscores the commitment of these nations to the global pursuit of innovation and sustainability across diverse academic domains.

Our results are consistent with Jamali et al. (2023), who show that Arab region business schools are actively addressing several significant United Nations SDGs. Among these, SDG 8, focusing on decent work and economic growth, emerges as a critical area of research interest. Furthermore, SDG 17, emphasizing partnerships for the goals, and SDG 9, centering around industry innovation and infrastructure. When analyzing the titles of 15 academic papers (Table 4), common patterns and themes emerge, which can be grouped as follows:

In the first group, papers such as "Green innovation and organizational performance: The influence of big data and the moderating role of management commitment and HR practices" (El-Kassar & Singh, 2019), "Role of big data analytics in developing sustainable capabilities" (Singh & El-Kassar, 2019) and "A Secure Cloud Computing Based Framework for Big Data Information Management of Smart Grid" (Baek et al., 2015) indicate a strong focus on data management and analytics, highlighting the significance of handling and deriving insights from large datasets.

The second cluster revolves around environmental sustainability, with titles like "Renewable energy-driven desalination technologies: A comprehensive review on challenges and potential applications of integrated systems" (Ghaffour et al., 2015), "Functional graphene nanosheets: The next generation membranes for water desalination" (Mahmoud et al., 2015), "Recent trends in membranes and membrane processes for desalination" (Goh et al., 2016) and "Offering an innovative composited material for effective lead (II) monitoring and removal from polluted water" (Awual et al., 2019). These papers underline the importance of sustainable practices, particularly in the context of water treatment, biofuels, and waste management.

The third group explores sustainable energy solutions, as evident from titles such as "Who Uses Smart City Services and What to Make of It: Toward Interdisciplinary Smart Cities Research" (Lytras & Visvizi, 2018), "Innovations and technology disruptions in the food sector within the COVID-19 pandemic and post-lockdown era" (Galanakis et al., 2021), "Absorptive capacity and green innovation adoption in SMEs: The mediating effects of sustainable organizational capabilities" (Aboelmaged & Hashem, 2019) and "Investigating influence of green innovation on sustainability performance: A case on Malaysian hotel industry" (Asadi et al., 2020). This group emphasizes innovative energy technologies and their integration into urban and business systems.

The analysis of these paper titles reveals a coherent thematic

structure. The first group underscores the significance of data and analytics, the second places an emphasis on environmental sustainability, and the third centers on innovative energy solutions. These categorizations shed light on prevailing research trends, showcasing the synergy between data-driven insights, environmental consciousness, and sustainable technological advancements in academic discourse.

In addition to the thematic groupings of academic papers, it is noteworthy that these clusters are to some extent interconnected with a detailed analysis of the most frequently used keywords in academic literature from Arab universities. Figure 3 prominently displays three major keyword clusters that align with the previously identified paper groupings.

- Firstly, at the center of Figure 3, there is a cluster related to the management of innovation and sustainability, encompassing the analysis of determinants, strategies, and systems, among other factors. This aligns closely with the first thematic group of papers, emphasizing data management and analytics, as well as the integration of innovative technologies in the quest for sustainability.
- Secondly, a second cluster pertains to topics concerning impacts, whether in terms of economic growth, consumption, renewable energy, climate change, and more. This resonates with the second thematic cluster highlighting environmental sustainability, reflecting a focus on the consequences and effects of sustainable practices on economic and environmental parameters.
- Finally, a third cluster focuses on everything related to performance, involving the examination of challenges, barriers, and issues associated with the implementation of actions that promote innovation and sustainability in various markets. This mirrors the third thematic group centered on sustainable energy solutions, emphasizing the practical aspects and hurdles related to the deployment of sustainable technologies.

The convergence between these keyword clusters and the thematic groupings in academic literature from Arab universities underscores the comprehensive exploration of innovation, sustainability, and their multifaceted impacts in the academic discourse. This interconnectedness demonstrates a holistic approach to addressing the complex challenges of the contemporary world.

6 Bibliometrics in transit: epilogue of a sowed gaze

From a complementarity perspective, this study's results offer a privileged starting point to undertake a transdisciplinary reading that broadens its scope. The quantitative mapping achieved here not only records the evolution of a field, but also enables a fruitful dialogue between the precision of the data and the interpretative

openness demanded by complex thinking. The metrics, citations, and indicators compiled should be understood not as static figures,

but as dynamic expressions of an expanding scientific framework, whose richness multiplies when integrated with new epistemic perspectives. In this sense, Carías Escoto (2024), in his bibliometric study on artificial intelligence in higher education, emphasizes that this type of analysis not only measures scientific production, but also reveals patterns of collaboration, thematic trends and research gaps that can guide the articulation of academic networks and the connection between regions with different degrees of research development. This approach reinforces the idea that bibliometrics, in addition to quantifying, can serve as a strategic bridge between empirical evidence and the projection of new scientific agendas.

The bibliometrics in transit proposed here is conceived as a bridge between the certainty of data and a broadening of meaning, by articulating the rigor of measurement with the interpretative framework of complex thinking, which

recognizes that knowledge is always under construction. In this sense, to understand the evolution of research on innovation and sustainability is not only to register its growth, but also to investigate how these notions can be re-signified as forms of presence, relating, and ways of being in the contemporary world. Such resignification opens the way to what we call *ontological transitions*: possible shifts from functional understandings to more relational, ethical, and civilizing dimensions.

As an interpretative seed, two tables illustrating these possible transitions in the Asian context are presented below, not as results of the present study, but as prospective input for future research that wishes to explore not only the quantitative evolution of these fields, but also their deepening at the ontological level. As Morin (1999) points out, "*the purpose of the education of the future must be to teach the human condition*" (p. 15), and in this framework, innovating and sustaining cannot be limited to technical labels, but must become principles that guarantee the habitability of the planet and the dignity of the future.

Table 6. Resignification of Innovation

From	To
Isolated technological product	Creative relationship between beings, knowledge, and territories
Speed and disruption	Meaning, coherence, and connection with the collective well-being
Competition between actors	Conscious and ethical collaboration
Innovation as an end	Innovation as a means to human fulfillment
Technology for its own sake	Technology with purpose and soul

Source: Own elaboration

Table 6 induces redefining innovation as a relational and ethical act, not as a goal of technical progress, but as a way

to respond with creativity and care to the challenges of this new era.

Table 7. Resignification of Sustainability

From	To
Technical environmental balance	Existential and cultural balance of ways of life
Development strategy	Civilizational and spiritual commitment to life
Agenda of indicators	Ecosystem of human and non-human ties
Responsible consumption	Re-enchantment of habitat and the reciprocity with Earth
Natural resources	Relational goods with symbolic and vital value
Speed and disruption	Meaning, coherence, and connection with the collective well-being
Competition among actors	Conscious and ethical collaboration
Innovation as an end	Innovation as a means to human fulfillment
Technology for its own sake	Technology with purpose and soul

Source: Own elaboration

This table suggests assuming sustainability not as a strategy of "*less damage to the planet*," but as an integral reconfiguration of life itself, of desire, need, and sense of belonging. Along the same lines, innovation is redefined as a relational and ethical act, and sustainability as a civilizing principle of shared living, beyond its dominant technical-economic interpretations.

From a trialectical perspective, this space is not an endpoint, but a third place where quantitative data and epistemic reflection dialogue to pave the way for new possibilities. Without seeking to broaden the objectives of this study, we do envision future scenarios in which both concepts—innovation and sustainability—cease to be merely analyzed categories and become vectors for transforming the very meaning of knowledge. In this transit, bibliometric observation not only shows evolution, but also poses the challenge of exploring how these notions are integrated in academic life, institutional policies, and in the configuration of a renewed civilizational conscience.

In this horizon, one could ask if they are already operating as curricular foundations. Are they translating into cross-sector practices that respond to the common good? Are they part of the ethical narrative of our digital societies?

Therefore, the "*bibliometrics in transit*" proposed here is understood as a bridge: not only to continue measuring what is growing in production, but also to perceive what is germinating in purpose. Innovating and sustaining, in this sense, imply cultivating ways of being in the world capable of sustaining life, equity, and intergenerational responsibility. This final pause does not pose an immediate research demand, but rather an ethical and metacognitive call to continue thinking of science as a bridge between knowledge, innovation, sustainability, and a shared future. Perhaps, in this transit, knowledge will approach its highest form of shared responsibility: a form of *amānah* (ethical stewardship) that, in dialogue with data and their interpretation, contributes to a more conscious and co-responsible world.

7 Conclusions

The analysis of this paper of academic studies conducted by universities in the Arab world over the past two decades highlights the profound interest and commitment of the region to the pivotal themes of innovation and sustainability. The whole volume of research in these areas is an indicator to the importance attached to addressing global challenges and advancing the principles outlined in international agreements like the Sustainable Development Goals (SDGs) and the Paris Agreement. It is evident that Arab universities have made significant contributions to the global body of knowledge on innovation and sustainability. This is not

merely an academic exercise but reflects a genuine concern for the region's growth, development, and sustainability, as well as its active participation in the global discourse on these critical issues.

Furthermore, the research findings emphasize the symbiotic relationship between scientific development, economic growth, and sustainability. The extensive body of work from Arab universities serves as a valuable resource for policymakers, businesses, and scholars, providing insights into practical strategies and innovative technologies that can foster sustainable development. These insights have the potential to influence decision-making at national and regional levels, ultimately contributing to the broader objectives of a more sustainable and equitable future. This comprehensive analysis underscores the region's intellectual and practical investment in driving innovation, fostering sustainability, and enhancing their position on the global stage. It is a proof to the Arab world's commitment to not only addressing its unique challenges but also to making substantial contributions to the broader global sustainability agenda.

Limitations of this paper and its analysis include a potential language bias towards English publications, a focus on research from the last two decades, and a limited geographic scope. To advance this field, future research should consider interdisciplinary approaches, conduct in-depth case studies of specific Arab countries or universities, engage in comparative analyses with non-Arab regions, include non-English publications, assess the practical impact of academic research, analyze emerging trends such as the implications of emerging technologies, circular economy models, and post-pandemic sustainability, and explore the intersections of innovation and sustainability with other crucial domains like public health, governance, and education, to provide a more comprehensive understanding and ensure broader inclusivity in Arab academic representation.

References

- Aboelmaged, M. & Hashem, G. (2019). Absorptive capacity and green innovation adoption in SMEs: The mediating effects of sustainable organisational capabilities. *Journal of Cleaner Production*, 220, 853-863. <https://doi.org/10.1016/j.jclepro.2019.02.150>
- Asadi, S., Pourhashemi, SO., Nilashi, M., Abdullah, R., Samad, S., Yadegaridehkordi, E., Aljojo, N. & Razali, NS. (2020). Investigating influence of green innovation on sustainability performance: A case on Malaysian hotel industry. *Journal of Cleaner Production*, 258, 120860. <https://doi.org/10.1016/j.jclepro.2020.120860>
- Awual, MR., Hasan, MM., Islam, A., Rahman, MM., Asiri, AM., Khaleque, MA., Chanmiya Sheikh, MC. (2019).

- Offering an innovative composited material for effective lead (II) monitoring and removal from polluted water. *Journal of Cleaner Production*, 231, 214-223. <https://doi.org/10.1016/j.jclepro.2019>.
- Baek, J., Vu, QH., Liu, JK, Huang, XY. & Xiang, Y. (2015). Secure Cloud Computing Based Framework for Big Data Information Management of Smart Grid. *IEEE Transactions on Cloud Computing*, 3,(2), 233-244. <https://doi.org/10.1109/TCC.2014.2359460>
- Broadus, RN. (1987). Early approaches to bibliometrics. *Journal of the American Society for Information Science*, 38(2), 127-129. [https://doi.org/10.1002/\(SICI\)1097-4571\(198703\)38:2%3C127::AID-ASI6%3E3.0.CO;2-K](https://doi.org/10.1002/(SICI)1097-4571(198703)38:2%3C127::AID-ASI6%3E3.0.CO;2-K)
- Cancino, C.A., La Paz, A.I., Ramaprasad, A. & Thant, S. (2018). Technological Innovation for Sustainable Growth: An ontological perspective. *Journal of Cleaner Production*, 179, 31-41. <https://doi.org/10.1016/j.jclepro.2018.01.059>
- Cancino, C.A., Merigó, J.M. & Coronado, F. (2017). A Bibliometric Analysis of Leading Universities in Innovation Research. *Journal of Innovation & Knowledge*, 2, 106-124. <https://www.elsevier.es/en-revista-journal-innovation-knowledge-376-articulo-a-bibliometric-analysis-leading-universities-S2444569X17300288>
- Cancino, C.A., Merigó, J.M., Urbano, D. & Amorós, J.E. (2023). Evolution of the Entrepreneurship and Innovation Research in Ibero-America between 1986 and 2015. *Journal of Small Business Management*, 61(2), 322-352. <https://doi.org/10.1080/00472778.2020.1776578>
- Carías Escoto, R. (2024). Estudio bibliométrico sobre la IA (Inteligencia Artificial) en la educación superior [Bibliometric study on artificial intelligence in higher education]. *Sapienza Organizacional*, 11(23), 23-37. <http://erevistas.saber.ula.ve/index.php/sapienza/article/view/20743>
- Díaz S., Demissew S., Carabias J., Joly C., Lonsdale M., Ash N., Larigauderie A., Adhikari JR., Arico S., Baldi A., Bartuska A., Baste IA., Bilgin A., Brondizio E., Chan KMA., Figueroa VE., Duraiappah A., Fischer M., Hill R., Koetz T., Leadley P., Lyver P., Mace GM., Martin-Lopez B., Okumura M., Pacheco D., Pascual U., Pérez ES., Reyers B., Roth E., Saito O., Scholes RJ., Sharma N., Tallis H., Thaman R., Watson R., Yahara T., Hamid ZA., Akosim C., Al-Hafedh Y., Allahverdiyev R., Amankwah E., Asah ST, Asfaw Z, Bartus G, Brooks LA, Caillaux J, Dalle G, Darnaedi D, Driver A, Erpul G, Escobar-Eyzaguirre P, Failler P, Fouda AMM, Fu B, Gundimeda H, Hashimoto S, Homer F, Lavorel S, Lichtenstein G, Mala WA, Mandivenyi W, Matczak P, Mbizvo C, Mehrdadi M, Metzger JP, Mikissa JB, Moller H, Mooney HA, Mumby P, Nagendra H, Nesshover C, Oteng-Yeboah AA, Pataki G, Roué M, Rubis J, Schultz M, Smith P, Sumaila R, Takeuchi K, Thomas S, Verma M, Yeo-Chang Y & Zlatanova S. (2015). The IPBES Conceptual Framework - connecting nature and people. *Current Opinion in Environmental Sustainability*, 14, 1-16. <https://doi.org/10.1016/j.cosust.2014.11.002>
- El-Kassar, AN. & Singh, SK. (2019). Green innovation and organizational performance: The influence of big data and the moderating role of management commitment and HR practices. *Technological Forecasting and Social Change*, 144, 483-498. <https://doi.org/10.1016/j.techfore.2017.12.016>
- Farías, A. & Cancino, C.A. (2021). Digital Transformation in the Chilean Lodging Sector: Opportunities for Sustainable Businesses. *Sustainability*, 13(14), 8097. <https://doi.org/10.3390/su13148097>
- Galanakis, CM., Rizou, M., Aldawoud, TMS., Ucak, I. & Rowan, NJ. (2021). Innovations and technology disruptions in the food sector within the COVID-19 pandemic and post-lockdown era. *Trends in Food Science & Technology*, 110, 193-200. <https://doi.org/10.1016/j.tifs.2021.02.002>
- Ghaffour, N., Bundschuh, J., Mahmoudi, H. & Goosen, MFA. (2015). Renewable energy-driven desalination technologies: A comprehensive review on challenges and potential applications of integrated systems. *Desalination*, 356, 94-114. <https://doi.org/10.1016/j.desal.2014.10.024>
- Gigand, G. (2010). GIGAND, G. (2010). La trialectica, una herramienta transdisciplinaria (I). *Visión Docente Con-Ciencia*, 9(52), 5-19. [The trialectic: a transdisciplinary tool]. *Revista QUID*, (14), 1-15. Retrieved from.
- Goh, PS., Matsuura, T., Ismail, AF. & Hilal, N. (2016). Recent trends in membranes and membrane processes for desalination. *Desalination*, 391, 43-60. <https://doi.org/10.1016/j.desal.2015.12.016>
- Gul, S., Nisa, N. T., Shah, T. A., Gupta, S., Jan, A., & Ahmad, S. (2015). Middle East: Research productivity and performance across nations. *Scientometrics*, 105, 1157-1166. <https://doi.org/10.1007/s11192-015-1722-3>
- Hirsch, J. E. (2005). An index to quantify an individual's scientific research output. *Proceedings of the National Academy of Sciences of the United States of America*, 102(46), 16569-16572.
- Ibrahim, B. (2020) The role of Egyptian State Awards in changing researchers' performance in the science and technology sector. *Research Evaluation*, Oxford University Press, 29(2), 171-190.
- Jahanger, A., Usman, M., Murshed, M., Mahmood, H. & Balsalobre-Lorente, D. (2022). The linkages between natural resources, human capital, globalization, economic growth, financial development, and ecological footprint:

- The moderating role of technological innovations. *Resources Policy*, 76, 102569. <https://doi.org/10.1016/j.resourpol.2022.102569>
- Jamali, D., Samara, G. & Meho, L. (2023). Determinants of research productivity and efficiency among the Arab world's accredited business schools. *Management Review Quarterly*, <https://doi.org/10.1007/s11301-023-00365-1>
- Josefson, J. & Rotar, A. (2023). Preparing for UAE COP 28: Gulf Countries' Net-Zero and Climate Action Roadmaps. *Morgan Lewis Newsletter*, <https://www.morganlewis.com/pubs/2023/09/preparing-for-uae-cop-28-gulf-countries-net-zero-and-climate-action-roadmaps>
- Lin, CSK; Pfaltzgraff, LA; Herrero-Davila, L; Mubofu, EB; Abderrahim S., Clark JH., Koutinas AA., Kopsahelis N., Stamatelatos K., Dickson F., Thankappan S., Mohamed Z., Brocklesby R. & Luque R. (2013). Food waste as a valuable resource for the production of chemicals, materials and fuels. Current situation and global perspective. *Energy & Environmental Science*, 6, 426-464.
- Mahmoud, KA., Mansoor, B., Mansour, A. & Khraisheh, M. (2015). Functional graphene nanosheets: The next generation membranes for water desalination. *Desalination*, 356, 208-225. <https://doi.org/10.1016/j.desal.2014.10.022>
- Merigó, J.M., Cancino, C.A., Coronado, F. & Urbano, D. (2016). Academic research in innovation: a country analysis. *Scientometrics*, 108(2), 559-593.
- Morin, E. (1999). The seven knowledges necessary for the education of the future. United Nations Educational, Scientific and Cultural Organization (UNESCO).
- Podsakoff, P.M., MacKenzie, S.B., Podsakoff, N.P., & Bachrach, D.G. (2008). Scholarly influence in the field of management: A bibliometric analysis of the determinants of university and author impact in the management literature in the past quarter century. *Journal of Management*, 34, 641-720.
- Pritchard, A. (1969) Statistical Bibliography or Bibliometrics. *Journal of Documentation*, 25, 348-349.
- Román, J., Cancino, C.A. & Gallizo, J.L. (2017). Exploring features and opportunities of rapid-growth wine firms in Chile. *Estudios Gerenciales*, 33, 115-123. <https://doi.org/10.1016/j.estger.2017.02.004>
- Roman, J.J., Alobaidli, A.Q., Almuaini A. & Cancino, C.A. (2023). Evolution and trends of Intellectual Property Crime research between 1991 and 2020. *International Journal of Business Environment*, 14(3), 370-394. <https://doi.org/10.1504/IJBE.2023.131880>
- Samara, G. (2021). Family businesses in the Arab Middle East: what do we know and where should we go? *Journal of Family Business Strategy*, 12(3), 100359. <https://doi.org/10.1016/j.jfbs.2020.100359>
- Singh, SK. & El-Kassar, AN. (2019). Role of big data analytics in developing sustainable capabilities. *Journal of Cleaner Production*, 213, 1264-1273. <https://doi.org/10.1016/j.jclepro.2018.12.199>
- Singh, A. (2019). Challenges in developing university-industry relationship: Quantitative evidence from higher education institutions in the UAE. *Emerald Open Research*, 1, 10. <https://doi.org/10.12688/emeraldopenres.12891.1>
- Soudagar, MEM; Nik-Ghazali, NN; Kalam, MA; Badruddin, IA., Banapurmath, N.R. & Akram, N. (2018). The effect of nano-additives in diesel-biodiesel fuel blends: A comprehensive review on stability, engine performance and emission characteristics. *Energy Conversion and Management*, 178, 146-177. <https://doi.org/10.1016/j.enconman.2018.10.019>
- United Nations (2015). UN General Assembly Transforming our World: The 2030 Agenda for Sustainable Development. United Nations A/RES/70/1.
- Zahra, SA. (2012). Doing research in the (new) middle east: sailing with the wind. *Academy of Management Perspective*, 25(4), 6-21. <https://doi.org/10.5465/amp.2011.0128>

Received: August 28th, 2025

Accepted: October 16th, 2025

Román, Jorge J.: Ph.D. in Strategic Management, Lleida University, Spain; Environment Agency Abu Dhabi, Abu Dhabi, UAE.

<https://orcid.org/0000-0001-9217-1234>

Almuaini, Abdelrahman H.: Ph.D. in Management, University of Aberdeen, UK; Assistant Undersecretary for Intellectual Property, Ministry of Economy, United Arab Emirates. Email: AAlmuaini@economy.ae

<https://orcid.org/0000-0002-7582-4595>


Zairi, Adel: Ph.D. in Quality Management, University of Salford, UK; Hamdan Bin Mohammed Smart University (HBMSU), Dubai, UAE. Email: a.zairi@hbmsu.ac.ae

<https://orcid.org/0000-0002-8851-6743>

Rivas Echeverría, Francklin: Ph.D. in Applied Sciences; Department of Computer Science and Engineering, University of Texas at Arlington, USA. Email: francklin.rivas@uta.edu

<https://orcid.org/0000-0002-5201->

Villasmil Rubio, María Alejandra: Ph.D. in Applied Economics, University of La Laguna, Spain; Organizational Legislation and Management Research Group (GILOG), University of the Andes (ULA), Mérida, Venezuela. Email: mvillas@ula.ve

 <https://orcid.org/0000-0002-7369-4707>

Study of the hair growth capacity of products derived from rosemary (*Rosmarinus officinalis*), in mice (*Mus musculus*) C57BL6//BIOU

Estudio de la capacidad de crecimiento capilar de productos derivados del romero (*Rosmarinus officinalis*), en ratones (*Mus musculus*) C57BL6//BIOU

Aljorna-Molero, Robert^{1*}; Amaro-Luis, Juan¹; García-Molina, Luis²

¹Laboratorio de Productos Naturales, Departamento de Química, Facultad de Ciencias, Universidad de Los Andes, Venezuela.

²Departamento de Materiales Avanzados, Centro de Investigación de Química Aplicada (CIQA), México.

*robertaljorna98@gmail.com

Abstract

In the present research work, the effect on hair growth of extracts derived from the rosemary plant (*Rosmarinus officinalis*) individually (essential oil, hydrolate and alcoholic extract) and together (in the form of a shampoo and hair tonic) was studied in male mice of the C57BL6//BIOU line, divided into 5 different groups: distilled water (AD), essential oil (AE), extract (ER), hydrolate (HR) and minoxidil 5% (MXD). Growth was evaluated for 5 weeks, using two methods: a growth scale with photographic record and the measurement of hairs taken by traction. The hair growth produced by these treatments was contrasted with a negative control group (distilled water) and positive control (minoxidil 5%). The growth scale used showed that the mice of the AE, ER and HR groups exhibited considerable hair growth; however, this scale proved to have serious limitations when evaluating mice with melanocytic nevus. On the other hand, the measurement of hair length showed that the AE, ER and HR groups presented a statistically superior growth than the control groups (p -value < 0.05). Finally, it was concluded that the extracts used in this research (essential oil, hydrolate and alcoholic extract) stimulate hair growth to a greater extent than the commercial drug minoxidil.

Keywords: *Rosmarinus officinalis*, alopecia, hair growth, C57BL/6 mice, extract.

Resumen

En el presente trabajo de investigación, se estudió el efecto sobre el crecimiento capilar de extractos derivados de la planta del romero (*Rosmarinus officinalis*) de manera individual (aceite esencial, hidrolato y extracto alcohólico) y en conjunto (en forma de un champú y tónico capilar) en ratones macho de la línea C57BL6//BIOU, repartidos en 7 grupos distintos: agua destilada (AD), aceite esencial (AE), extracto (ER), hidrolato (HR) y minoxidil al 5% (MXD). El crecimiento fue evaluado durante 5 semanas, mediante dos métodos: una escala de crecimiento con registro fotográfico y la medición de pelos tomados por tracción. El crecimiento capilar producido por estos tratamientos fue contrastado con un grupo control negativo (agua destilada) y control positivo (minoxidil al 5%). La escala de crecimiento empleada demostró que los ratones de los grupos AE, ER y HR; exhibían un crecimiento capilar considerable, sin embargo, esta escala demostró tener serias limitaciones a la hora de evaluar ratones con nevo melanocítico. Por su parte, la medición de longitud de los pelos, demostró que dichos grupos AE, ER y HR; presentan un crecimiento estadísticamente superior que el de los grupos control (p -valor $< 0,05$). Finalmente, se concluyó que los extractos empleados en esta investigación (aceite esencial, hidrolato y extracto alcohólico) estimulan el crecimiento capilar en mayor medida que el fármaco comercial minoxidil.

Palabra clave: *Rosmarinus officinalis*, alopecia, crecimiento capilar, ratones C57BL/6, extracto.

1 Introduction

For a long time, man has treated diseases with resources available to him, with the Plant Kingdom being the main source of therapeutic treatments. This has been documented in all ancient civilizations. With scientific advancements, the properties of medicinal plants have been proven, making treatments more effective and safer (Barquero, 2007; Caro Marquez et al., 2020; Marrelli, 2021).

The World Health Organization (WHO) recognizes many medicinal and toxic plants in its manual, "WHO Traditional Medicine Strategy 2014–2023." This manual outlines the uses of medicinal plants in natural, safe, effective, and low-cost treatments that are also accessible to the general population and widely accepted by them (Hosseinzadeh et al., 2015; World Health Organization, 2013; Salmerón-Manzano et al., 2020).

With the great therapeutic potential of medicinal plants, it is not surprising that from very early on, people were interested in using them for aesthetic purposes, such as hair care (Abelan et al., 2022; Patel et al., 2015). In the vast majority of ancient cultures, hair represents social status and personal attractiveness. The absence of hair often caused a great negative impact on both men and women (Barve & Dighe, 2016; Caro Marquez et al., 2020).

Many plants have been used on hair for various reasons. It is reasonable to assume that most plants known to man have been tried on hair at some point in history (Barve & Dighe, 2016).

One plant that has sparked the interest of researchers is *Rosmarinus officinalis*, commonly known as rosemary. This plant belongs to the Lamiaceae family (Andrade et al., 2018; de Macedo et al., 2020) and is native to countries on the Mediterranean Sea (Murata et al., 2013). Its use is widely linked to gastronomy (Moore et al., 2016; Nieto et al., 2018).

Several studies show that the extract of *Rosmarinus officinalis* has antiandrogenic properties, which prevent hair loss (de Macedo et al., 2020; Masoud et al., 2020; Murata et al., 2013). In this context, the objective of the present research is justified: to study the hair growth capacity of products derived from rosemary (*Rosmarinus officinalis*) in C57BL/6J mice (*Mus musculus*).

2 Theoretical Framework

2.1 Botanical Description of *Rosmarinus officinalis*

This is an aromatic, evergreen shrub of the Lamiaceae family, growing up to 1.2 m high. It has a straight stem, numerous branches, exfoliating bark, and is finely puberulent. The leaves are sessile, opposite, green, numerous, woolly, obtuse, and glandular. They are 1–3 cm long, nearly cylindrical, and folded inward. The flowers are fragrant, 10–12 mm long, and grow in small terminal clusters. It has a tubular calyx, a two-lipped violet corolla, an elongated sty-

le, and an oval fruit divided into four sections (González-Minero et al., 2020; Hammer & Junghanns, 2020).



Figure 1. *Rosmarinus officinalis* (rosemary).

2.2 Zoological Description of *Mus musculus*

Mus musculus, commonly known as the house mouse, is a small rodent belonging to the Muridae family. Adults typically measure between 6.5 to 9.5 centimeters in length, with tails that can be up to 10.5 centimeters long. They weigh from 12 to 30 grams. The fur color varies from light brown to black, often with a lighter or even white underside. Their long tails are either hairless or have very little fur and feature circular rows of annulations (scale-like skin cells) (Macholán et al., 2012).

This species is known for its high reproductive potential, which occurs year-round. However, wild mice may have reproductive seasons that last from April to September. The estrous cycle is 4 to 6 days long, with estrus (the period when the female is receptive to mating) lasting less than a day (Macholán et al., 2012).

Females usually have 5 to 10 litters per year if environmental and nutritional conditions are favorable. Gestation lasts approximately 21 days, and litters can consist of 3 to 12 pups, which are born hairless and blind. Pups are fully covered in fur at 10 days, open their eyes at 14 days, are weaned at 3 weeks, and reach sexual maturity at 5–6 weeks. Their average lifespan in captivity is 2 years, but some individuals have been recorded to live up to 6 years. In contrast, wild mice typically do not live longer than 18 months due to predation (Brust et al., 2015).



Figure 2. *Mus musculus* (common mouse)

3 Experimental Procedure

3.1 Preparation of ethanolic extract of rosemary (*Rosmarinus officinalis*)

Ten kilograms of plant material belonging to the *Rosmarinus officinalis* species were collected in the town of Mucuchíes, Rangel municipality, Mérida state, Venezuela. All material was washed with plenty of water to remove any dirt.

The leaves were then separated from the rest of the plant (stems, flowers, and seeds). The leaves were dried in an oven at 40°C for 24 hours, yielding 2,330 kilograms of dried leaves.

The dried leaves underwent continuous Soxhlet extraction, in a ratio of 250 g of plant material to 600 mL of ethanol (98% Merk) at 70°C for 4 continuous hours. A total of 15 extractions were performed, with a consumption of 10.36 L of 70% ethanol.

The resulting extract was concentrated to one-third of its initial volume (3,2 L) in a rotary evaporator at 70°C for 2 hours. The resulting liquid was a slightly thick, greenish-brown liquid with a pleasant odor and pH = 5. It was stored in an amber glass container until further use.

To determine the yield of the extract obtained, 6 flasks were weighed, then 10 mL of the extract was added to each flask (measured with a volumetric pipette) and reweighed. The extract was then dried in an oven at 40°C for 48 hours, and the flasks were reweighed.

3.2 Preparation of 4.8% rosemary essential oil

Six ml of rosemary essential oil (98% v/v, from Quimichouse) were mixed with 114 mL of mineral oil. The mixture was stored in a properly labeled amber glass container.

3.3 Preparation of 0.135% rosemary extract

Six ml of rosemary extract (2.7% w/v) were mixed with 114 mL of distilled water. The mixture was stored in a properly labeled amber glass container.

3.4 Test in C57BL6//BIOU mice

All animal procedures were evaluated and accepted by the Bioethics Committee of the Bioterium of the University of the Andes (CEBIOULA) under protocol identification "CEBIOULA/131."

Thirty male mice of the C57BL6//BIOU strain, approximately 8 weeks old and weighing an average of 25.7 g, were used. They were given a 1-week adaptation period and maintained under the following housing conditions:

- Individuals per Cage: 4.
- Ambient Temperature: (22 ± 1) °C.
- Adaptation Period: 1 week.
- Food and Water: ad libitum (on demand).
- Light/Dark Cycle: 12 hours.

After the adaptation period, the animals were anesthetized with a mixture of ketamine and xylazine, with a dose of 90 mg/kg of ketamine and 10 mg/kg of xylazine, intraperitoneally, obtaining an average anesthesia time of 7-10 minutes, then an area of 4 cm² (2 x 2 cm) was shaved from the dorsal region of its body (Figure 3), and each animal was identified by small cuts in its ears (Figure 4).

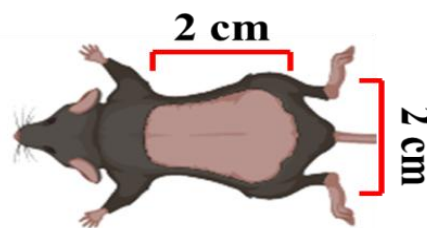


Figure 3. Representation of the shaved area on the dorsal region of the mice.

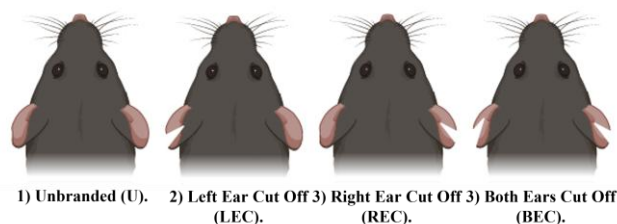


Figure 4. Representation of the marking of mice.

After the anesthesia time had passed, the mice were randomly distributed into 5 distinct groups, each made up of 4 individuals, based on the topical application they were given: distilled water (AD), 4.9% rosemary essential oil (AE), 0.135% rosemary extract (ER), rosemary hydrolat (HR) and 5% minoxidil (MDX).

The products were applied daily, with each individual receiving 0.1 mL (measured with a micropipette) of the corresponding product, which was adequately distributed with the help of fingers. In the case of the shampoo, after its application, it was removed with the help of a moist tissue.

3.4 Hair growth assessment

The evaluation of hair growth in mice was performed using two scales:

Method 1:

A photographic evaluation was conducted at the end of weeks 1, 2, 3, 4, and 5. An observation box was set up, con

- Cage Type: T1.

sisting of an uncovered box with the following dimensions: 15 cm high, 5 cm wide, and 7 cm deep.

This box had a small opening on its top, which allowed the animal's tail to pass through. The purpose of this box was to suspend the mouse in the air, limiting its movement, thus facilitating photographic capture without the need to anesthetize the individual (Figure 5).

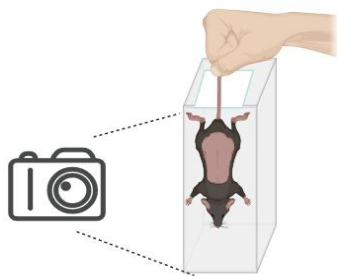


Figure 5. Representation of the manufactured observation box.

In this method, the following scoring scale was used:

Table 1: Hair growth scoring scale.

Score	% Growth
1	(0-20) %
2	(20-40) %
3	(40-60) %
4	(60-80) %
5	(80-100) %

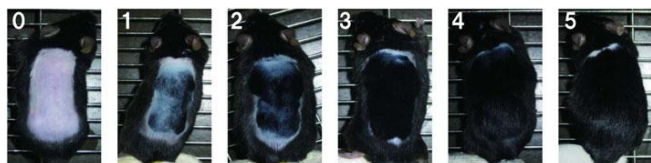


Figure 6. Scores for hair growth assessment: 0 = no growth; 1 = less than 20% growth; 2 = 20% to 40% growth; 3 = 40% to 60% growth; 4 = 60% to 80% growth; 5 = 80% to 100% growth (Murata et al., 2013).

Method 2:

At the end of weeks 2, 3, 4, and 5, a tuft of hair was pulled from within the shaved area, ensuring that the hairs were extracted with their respective follicles.

At week 5, a tuft of hair was pulled from within and outside the shaved area for comparison. This procedure was also performed on the control group mice.

The length of these hairs was measured using a 6-diopter magnifying glass (6x magnification) and a digital vernier caliper (DIGITAL CAPILPER brand) with an accuracy of 0.02 mm.

3.5 Statistical analysis

The data obtained in the study were processed using the statistical package GraphPrism version 8. The Shapiro-Wilk test was used to observe the normal distribution of the data.

The results of the quantitative variables were presented with measures of central tendency in frequencies, percentages, and absolute values using graphs. For differences in mean values, the Student t test was used, accepting significant values below $p < 0.050$.

In this sense, to observe the differences between the mean values among the different groups, a one-way ANOVA test was performed to obtain Fisher's F value.

To obtain the differences and comparative values between each group, a two-way ANOVA test was performed, considering the column factor as the treatment and the row factor as the values obtained between the study weeks.

This analysis was subjected to a post-hoc test using Tukey's method to verify the relationships between means, considering that each measurement was taken at different times. Significant F values above 1 were accepted, as were statistical differences with p values < 0.050 .

4 Results and Discussion

It is important to note that during the initial mouse shaving procedure, three individuals in the AD group (distilled water) were observed to have a melanocytic nevus (mole) covering the entire dorsal region of the animal (Figure 7). This trait was not present in any other mice in the other study groups (CC, AE, ER and MXD).

Initially, it was thought that this characteristic would not impact the hair evaluation of these individuals, and they were not discarded because no other mice of the same lineage and age were available. However, the moles were shown to have a negative effect on the hair growth scale and photographic records at the time of obtaining results. Furthermore, it did not appear to affect the methodology used to measure the length of the plucked hairs.

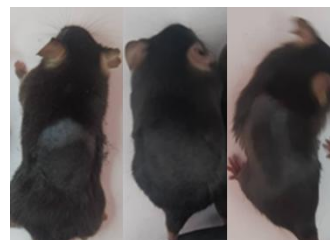


Figure 7. AD1, AD2 and AD3 mice presenting melanocytic nevus (mole) in the dorsal region of their body.

4.1 Photographic record and hair growth scale

The results shown in Figure 8 illustrate the progression of hair growth over time, from week 0 to week 5. After shaving (week 0), all C57BL6/BIOU mice displayed a pinkish coloration of their skin (with the exception of three individuals in the AD group).

Hair growth stimulation was assessed by observing the darkening of the skin color from bright pink to gray/black, indicative of the transition from the telogen (resting) phase to the anagen (active growth) phase of the hair follicles in the shaved area (Oh et al., 2014).

Throughout the study, no adverse effects due to topical application of the products were observed, such as irritation, scaling, or behavioral signs indicating discomfort in the mice (barbering, excessive grooming, or lack of appetite).

Starting at week 2, the skin of most individuals in the AD, AE, ER and HR groups changed from a pinkish color to a gray/black hue, reflecting significant hair growth in these groups. On the other hand, only half of the individuals in the MXD group exhibited this phenomenon.

At week 4, all mice in the AD, AE and HR groups showed significant hair growth (scoring between 3.5 and 5 on the scale), while the MXD group still had large areas of hairless skin (scoring 2), making this the group with the least hair growth.

At the end of week 5, it can be observed that all mice in the AD, AE and HR groups had recovered virtually all of their hair from the shaved region (scores between 4.75 and 5), while in the MXD group only two mice managed to recover all of their fur, resulting in an average score of 3.75.

Table 5 and Figure 8 show the group average hair growth scores for all groups over the 5 weeks of the trial.

Table 2: Group mean on the hair growth scale for the AD, AE, ER, HR and MXD groups, from week 1 to week 5.

Group	Week 1	Week 2	Week 3	Week 4	Week 5
AD	1	2,5	3,75	4,75	5
AE	0,5	2,25	3,75	5	5
ER	1	1,5	2,5	4,25	5
HR	1,25	1,5	3,25	3,75	4,75
MXD	0,25	1	2	2,75	3,75

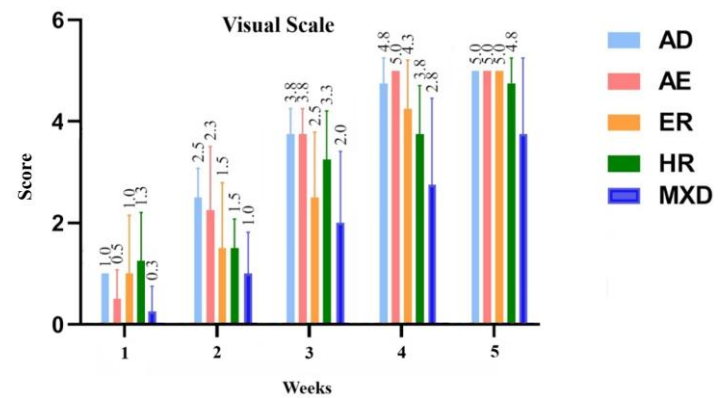


Figure 8: Comparison of the effect of hair growth, using the scoring scale, in C57BL6/BIOU mice after topical application of distilled water (AD), 5% essential oil (AE), 5% rosemary extract (ER), rosemary hydrolate (HR) and 5% minoxidil (MXD).

4.2 Measuring hair length

Below, Figure 9 shows a comparison of hair growth between weeks 2 and 5, in the form of column and box graphs.

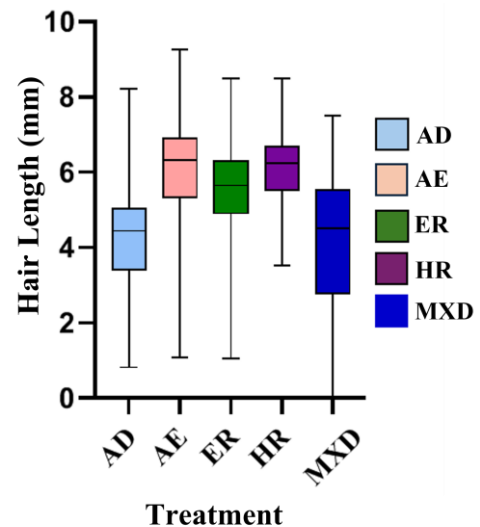


Figure 9: Comparison of hair growth (measured in mm) in the form of boxes, for the AD, AE, ER, HR and MXD groups between weeks 2 and 5.

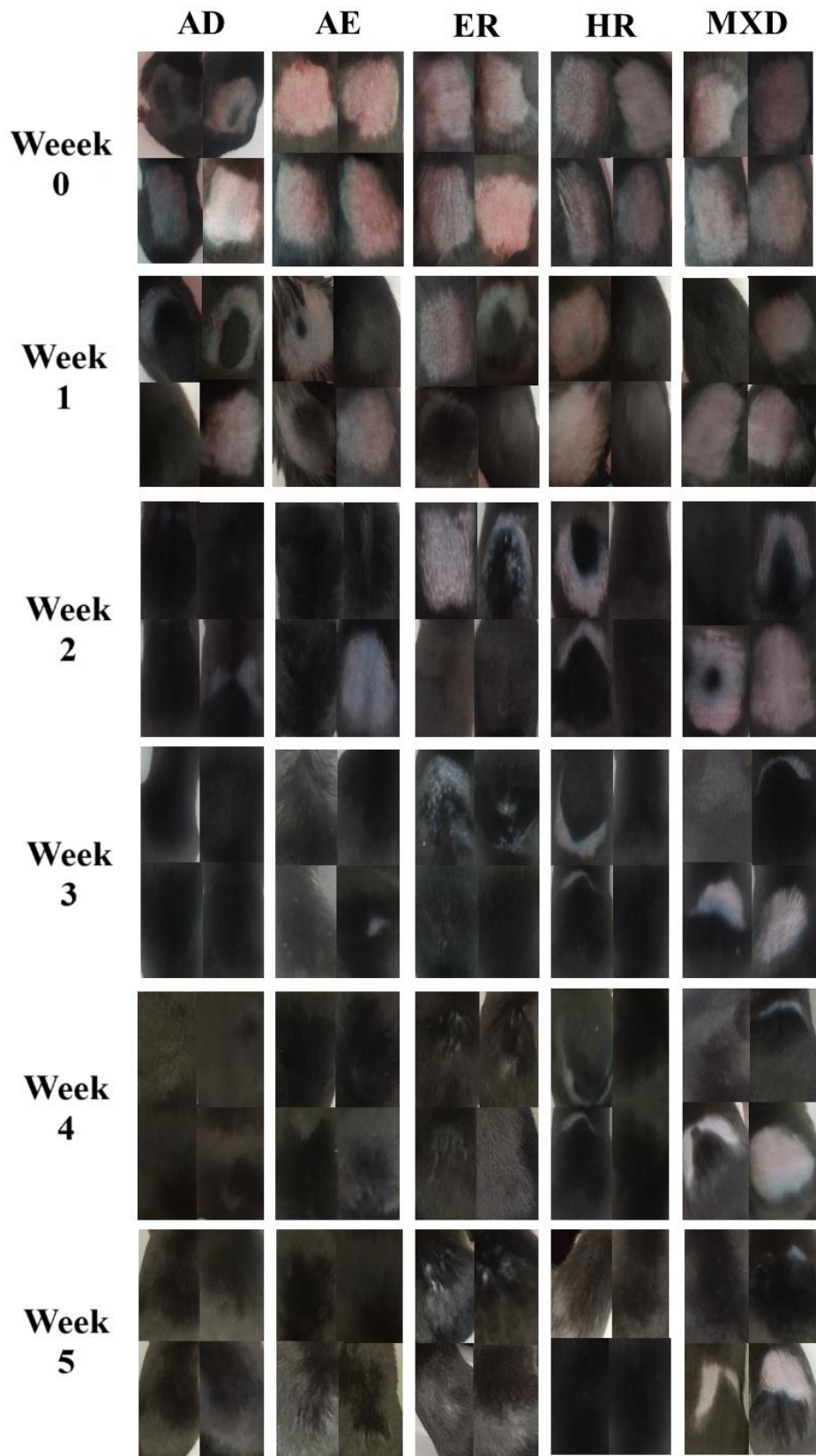


Figure 10. Macroscopic observation of the dorsal region of C57BL6/J mice. AD (distilled water), AE (rosemary essential oil), ER (rosemary extract), HR (rosemary hydrolate) and MXD (5% minoxidil).

The results of the p-value for the Shapiro-Wilk test (Table 3) demonstrate that the hair length values throughout the study fit the normality model in all study groups.

Table 3: Shapiro-Wilk normality test for data from the AD, AE and MXD groups between weeks 2 and 5.

	AD	AE	ER	HR	MXD
Shapiro-Wilk Test					
W	0,9893	0,8245	0,9304	0,8423	0,9561
p-value	0,9538	0,1539	0,5970	0,2022	0,7545
Normality	Yes	Yes	Yes	Yes	Yes

Note: Data normality is checked if p-value>0.05.

For its part, the results of the ANOVA test carried out considering all the study groups showed that there are statistically significant differences (p<0.05) in the hair growth of these (Table 4 and Figure 11).

Table 4: Results of the one-way ANOVA test, comparing the hair length of all study groups.

	SS	DF	MS	Value of F	Value of P
Between groups	642,3	4	160,5	71,7	0,006
Within the groups	1778,1	795	2,23		
Total	2420,4	779			

SS: sum of squares. **DF:** degrees of freedom. **MS:** mean squares. **Note:** There are statistically significant differences between group means if p<0.05.

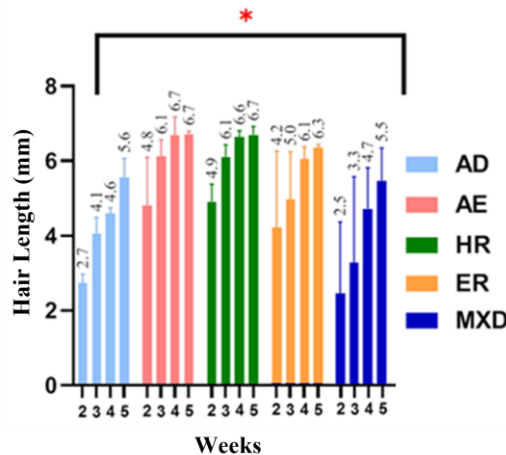


Figure 11: Results of the ANOVA test on hair length of the AD, AE, ER, HR and MXD groups, at weeks 2 and 5. The test result is indicated with (**), which expresses that p 0.05.

With this in mind, the means of each treatment group (AE, ER and HR) were compared with those of the AD and MXD groups using the Tukey test. This test determined that the hair length of the treatment groups was statistically different (longer) than that of the AD and MXD groups (Table 5 and Figure 12).

Table 5: ANOVA test with post-Hoc analysis under Tukey's test of the AE, ER and HR groups, assuming the AD and MXD groups as HDS.

Stimulus evaluated	p Value	
	Distilled water (AD)	5% Minoxidil (MXD)
AE	0,0039*	0,0079*
ER	0,0075*	0,0057*
HR	0,0044*	0,0086*

Note: The symbol (*) indicates that p < 0.05, and H1 is approved.

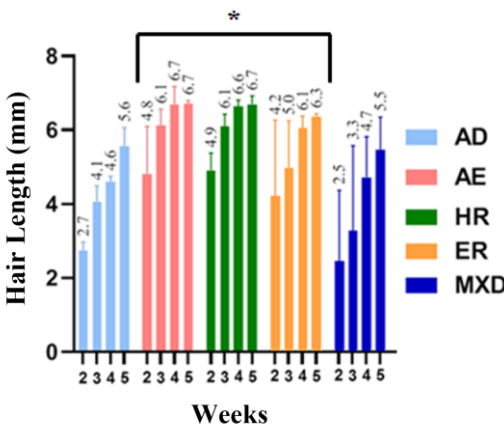


Figure 12: ANOVA with post-hoc analysis using Tukey's test for the AE, ER, HR, TC, and CH groups, assuming the AD and MXD groups as HDS. The symbol (*) indicates that the group mean presents statistically significant differences with the AD and MXD groups (p<0.05).

4 Conclusion

A hair growth study was conducted comparing the effect of rosemary-derived compounds, individually (oil, extract, and hydrolate) and in combination (hair tonic and shampoo). The results demonstrated that the hair scale method (method 1) has serious limitations when evaluating hair growth in mice with melanocytic nevus. On the other hand, method 2 demonstrated that the groups treated with rosemary-derived products (AE, HR, ER, CH, and TC) showed statistically superior hair growth (p-value 0.05) compared to the negative control group (distilled water) and the positive control group (5% minoxidil).

The results of this research demonstrate that the treatments used stimulate hair growth to a greater extent than the


commercial drug minoxidil, and that they could be a possible therapeutic alternative.


References


- R. A. Caro Marquez *et al.*, “Uso de plantas medicinales en la provincia de Sevilla,” *RESCIFAR Revista Española de Ciencias Farmacéuticas*, vol. 1, no. 2, pp. 138–147, 2020.
- A. A. Barquero, “Plantas sanadoras: pasado, presente y futuro,” Aug. 2007, Accessed: Nov. 19, 2024. [Online]. Available: <https://ri.conicet.gov.ar/handle/11336/98477>
- M. Marrelli, “Medicinal Plants,” *Plants*, vol. 10, no. 7, Art. no. 7, Jul. 2021, doi: 10.3390/plants10071355.
- Organización Mundial de la Salud, *Estrategia de la OMS sobre medicina tradicional 2014-2023*. Ginebra: Organización Mundial de la Salud, 2013. Accessed: Sep. 19, 2024. [Online]. Available: <https://iris.who.int/handle/10665/95008>
- E. Salmerón-Manzano, J. A. Garrido-Cardenas, and F. Manzano-Agugliaro, “Worldwide Research Trends on Medicinal Plants,” *International Journal of Environmental Research and Public Health*, vol. 17, no. 10, Art. no. 10, Jan. 2020, doi: 10.3390/ijerph17103376.
- S. Hosseinzadeh, A. Jafarikukhdan, A. Hosseini, and R. Armand, “The Application of Medicinal Plants in Traditional and Modern Medicine: A Review of *Thymus vulgaris*,” *International Journal of Clinical Medicine*, vol. 6, no. 9, Art. no. 9, Sep. 2015, doi: 10.4236/ijcm.2015.69084.
- S. Patel, V. Sharma, N. S. Chauhan, M. Thakur, and V. K. Dixit, “Hair Growth: Focus on Herbal Therapeutic Agent,” *Current Drug Discovery Technologies*, vol. 12, no. 1, pp. 21–42, Mar. 2015.
- U. S. Abelan *et al.*, “Potential use of essential oils in cosmetic and dermatological hair products: A review,” *Journal of Cosmetic Dermatology*, vol. 21, no. 4, pp. 1407–1418, 2022, doi: 10.1111/jocd.14286.
- K. Barve and A. Dighe, *The Chemistry and Applications of Sustainable Natural Hair Products*. in Springer-Briefs in Molecular Science. Cham: Springer International Publishing, 2016. doi: 10.1007/978-3-319-29419-3.
- J. M. Andrade, C. Faustino, C. Garcia, D. Ladeiras, C. P. Reis, and P. Rijo, “*Rosmarinus officinalis* L.: an update review of its phytochemistry and biological activity,” *Future Sci OA*, vol. 4, no. 4, p. FSO283, Apr. 2018, doi: 10.4155/fsoa-2017-0124.
- L. M. de Macedo *et al.*, “Rosemary (*Rosmarinus officinalis* L., syn *Salvia rosmarinus* Spenn.) and Its Topical Applications: A Review,” *Plants (Basel)*, vol. 9, no. 5, p. 651, May 2020, doi: 10.3390/plants9050651.
- K. Murata *et al.*, “Promotion of hair growth by *Rosmarinus officinalis* leaf extract,” *Phytother Res*, vol. 27, no. 2, pp. 212–217, Feb. 2013, doi: 10.1002/ptr.4712.
- J. Moore, M. Yousef, and E. Tsiani, “Anticancer Effects of Rosemary (*Rosmarinus officinalis* L.) Extract and Rosemary Extract Polyphenols,” *Nutrients*, vol. 8, no. 11, Art. no. 11, Nov. 2016, doi: 10.3390/nu8110731.
- G. Nieto, G. Ros, and J. Castillo, “Antioxidant and Antimicrobial Properties of Rosemary (*Rosmarinus officinalis*, L.): A Review,” *Medicines*, vol. 5, no. 3, Art. no. 3, Sep. 2018, doi: 10.3390/medicines5030098.
- F. Masoud, H. A. Alamdari, S. Asnaashari, J. Shokri, and Y. Javadzadeh, “Efficacy and safety of a novel herbal solution for the treatment of androgenetic alopecia and comparison with 5% minoxidil: A double-blind, randomized controlled trial study,” *Dermatol Ther*, vol. 33, no. 6, p. e14467, Nov. 2020, doi: 10.1111/dth.14467.
- F. J. González-Minero, L. Bravo-Díaz, and A. Ayala-Gómez, “*Rosmarinus officinalis* L. (Rosemary): An Ancient Plant with Uses in Personal Healthcare and Cosmetics,” *Cosmetics*, vol. 7, no. 4, Art. no. 4, Dec. 2020, doi: 10.3390/cosmetics7040077.
- M. Hammer and W. Junghanns, “*Rosmarinus officinalis* L.: Rosemary,” in *Medicinal, Aromatic and Stimulant Plants*, J. Novak and W.-D. Blüthner, Eds., Cham: Springer International Publishing, 2020, pp. 501–521. doi: 10.1007/978-3-030-38792-1_15.
- M. Macholán, S. J. E. Baird, P. Munclinger, and J. Piálek, *Evolution of the House Mouse*. Cambridge University Press, 2012.
- V. Brust, P. M. Schindler, and L. Lewejohann, “Lifetime development of behavioural phenotype in the house mouse (*Mus musculus*),” *Front Zool*, vol. 12, no. 1, p. S17, Aug. 2015, doi: 10.1186/1742-9994-12-S1-S17.
- J. Y. Oh, M. A. Park, and Y. C. Kim, “Peppermint Oil Promotes Hair Growth without Toxic Signs,” *Toxicol Res*, vol. 30, no. 4, pp. 297–304, Dec. 2014, doi: 10.5487/TR.2014.30.4.297.

Recibido: 9 de julio de 2025

Aceptado: 20 de octubre de 2025

Aljorna-Molero, Robert. J: Bachelor of Science in Chemistry 2024, Faculty of Sciences, ULA, Mérida, Venezuela.  <https://orcid.org/0000-0002-4769-6151>

Amaro-Luis Juan. M: Ph.D. in Science (Organic Chemistry) 1977, University of La Laguna, Canary Islands, Spain. Retired Professor, Natural Products Laboratory, Faculty of Sciences, ULA, Mérida, Venezuela.  <https://orcid.org/0000-0002-3297-6206>

García-Molina, Luis. O: Bachelor of Science in Chemistry 2016, Faculty of Sciences, ULA, Mérida, Venezuela. MSc. In Polymer Technology 2020, Center for Applied Chemistry Research (CIAQ). Saltillo, Mexico. Email: losvaldo.garcia.d21@ciqa.mx
 <https://orcid.org/0009-0001-7539-3676>

Optimización del flujo logístico mediante DMAIC ante el aumento del volumen diario de carga en PRModel-Logistic

Logistic flow optimization Using DMAIC under increased daily cargo volume at PRModel-Logistic

Sanz, Gabriela¹; Ledain, Mariangelie¹; González, Andrea¹; González, Carlos¹; Garcia, Maria¹; Rondón, Jairo^{1,2*}

¹Industrial Engineering Department, Universidad Politécnica de Puerto Rico, San Juan, PR 00918, USA

²Biomedical & Chemical Engineering Departments, Universidad Politécnica de Puerto Rico, San Juan, PR 00918, USA

* jrondon@upr.edu

Resumen

El incremento sostenido en la demanda global de transporte de paquetes ha intensificado los retos operativos en los centros de distribución aérea, particularmente en sistemas sometidos a ventanas temporales estrictas. Este estudio aplica la metodología DMAIC para optimizar el flujo logístico de PRModel-Logistic en Puerto Rico, expresando todas las métricas operativas en unidades de tiempo normalizado (T_n) donde 1.00 T_n corresponde al tiempo máximo permitido para completar el ciclo por vuelo y los indicadores económicos en unidades financieras normalizadas (U_n), con 1.00 U_n equivalente al costo fijo por vuelo. Los estudios de campo evidenciaron que el proceso presentaba un takt time normalizado de 0.19 T_n por tren de cinco contenedores, insuficiente para garantizar sistemáticamente el cumplimiento del límite temporal $T_{total} \leq 1.00 T_n$ bajo escenarios de alta demanda. La aplicación del ciclo DMAIC permitió identificar causas raíz asociadas a la asignación desigual de recursos, la secuenciación operativa y la disponibilidad de equipos, además de rediseñar la distribución de tareas para habilitar la paralelización de descarga en cabinas superiores e inferiores. La simulación del sistema validó que las mejoras implementadas aumentan la capacidad del proceso hasta 30 contenedores por vuelo, manteniéndose dentro del límite temporal establecido (0.95 T_n). A nivel financiero, el sistema mostró un desempeño robusto, con un ingreso relativo de 4.95 U_n por vuelo y una ganancia operativa de 3.95 U_n , valores que reflejan la eficiencia de un modelo logístico donde los costos por vuelo son esencialmente fijos. Los resultados demuestran que el uso integrado de métricas normalizadas, análisis estadístico y modelado de simulación bajo la estructura DMAIC constituye un enfoque eficaz para sostener la competitividad operativa y económica en sistemas de carga aérea sujetos a incrementos abruptos en la demanda.

Palabras clave: DMAIC, logística aérea, flujo de materiales, estudio de tiempos, eficiencia operativa.

Abstract

The sustained increase in global demand for parcel transportation has intensified operational challenges in air distribution centers, particularly in systems constrained by strict time windows. This study applies the DMAIC methodology to optimize the logistics flow of PRModel-Logistic in Puerto Rico, expressing all operational metrics in normalized time units (T_n), where 1.00 T_n corresponds to the maximum allowable time to complete the cycle per flight, and economic indicators in normalized financial units (U_n), with 1.00 U_n equivalent to the fixed cost per flight. Field studies showed that the process exhibited a normalized takt time of 0.19 T_n per train of five containers, which is insufficient to systematically ensure compliance with the temporal constraint $T_{total} \leq 1.00 T_n$ under high-demand scenarios. The application of the DMAIC cycle made it possible to identify root causes associated with unequal allocation of resources, operational sequencing, and equipment availability, as well as to redesign task distribution to enable parallel unloading in upper and lower cabins. System simulation validated that the implemented improvements increase process capacity to up to 30 containers per flight while remaining within the established time limit (0.95 T_n). At the financial level, the system exhibited robust performance, with a relative income of 4.95 U_n per flight and an operating profit of 3.95 U_n , values that reflect the efficiency of a logistics model in which per-flight costs are essentially fixed. The results demonstrate that the integrated use of normalized metrics, statistical analysis, and simulation modeling within the DMAIC structure constitutes an effective approach to sustaining operational and economic competitiveness in air-cargo systems facing abrupt increases in demand.

Keywords: DMAIC, air logistics, material flow, time study, operational efficiency.

1 Introducción

El crecimiento sostenido del comercio electrónico y de las operaciones logísticas globales ha impulsado una expansión sin precedentes en la industria del transporte de paquetes, imponiendo exigencias cada vez mayores sobre la eficiencia y flexibilidad de los sistemas de distribución (Christopher, 2016; Rushton *et al.*, 2022). En este contexto, los operadores de carga aérea enfrentan el desafío de mantener ventanas de entrega altamente estrictas, las cuales, para preservar la confidencialidad contractual, se expresan en unidades de tiempo normalizadas (T_u). Estas unidades permiten comparar el desempeño relativo sin exponer tiempos operativos reales.

En Puerto Rico, la logística aérea desempeña un papel estratégico dentro del comercio regional y la integración del Caribe, dada su localización geográfica y su conexión directa con los Estados Unidos continentales (Ruiz Moreno *et al.*, 2020). La empresa PRModel-Logistic constituye un nodo crítico para el flujo de mercancías de alto valor (especialmente farmacéutico, electrónico y agroindustrial). El incremento reciente en la frecuencia de vuelos ha generado un aumento significativo en el número de contenedores manejados por operación, elevando la presión sobre los sistemas asociados a dichas ventanas de tiempo normalizadas.

Dada esta situación, se propone aplicar la metodología DMAIC como herramienta estructurada para identificar, analizar y corregir ineficiencias en el flujo de carga, garantizando que las actividades de descarga, transporte y entrega se mantengan dentro del intervalo operativo expresado como $\leq 1.00 T_u$, donde T_u representa el límite temporal máximo permitido por vuelo. Este enfoque permite cuantificar pérdidas, estandarizar procedimientos y establecer métricas que aseguren la mejora continua (Snee, 2010; Psychogios & Tsironis, 2012).

La contribución principal de este trabajo radica en integrar estudios de tiempo, análisis estadístico de capacidad y simulación de flujos logísticos utilizando tiempos adimensionales, de forma que los resultados puedan extrapolarse a otros aeropuertos y sistemas de manipulación de carga sin comprometer datos operativos confidenciales. Este marco metodológico ofrece una referencia replicable para empresas logísticas que enfrentan incrementos súbitos en la demanda, contribuyendo a la productividad y sostenibilidad del sistema bajo principios contemporáneos de ingeniería industrial (Antony, 2014; De Felice, Petrillo & Monfreda, 2009).

2 Metodología

La metodología empleada en este estudio se fundamentó en la estructura sistemática del ciclo DMAIC

(Definir, Medir, Analizar, Mejorar y Controlar), ampliamente validada como un marco riguroso para optimizar procesos complejos bajo condiciones de variabilidad operacional (Pereira, 2024; George *et al.*, 2005). En concordancia con prácticas contemporáneas de ingeniería industrial y logística aeroportuaria, se incorporaron métricas adimensionales para preservar la confidencialidad operativa y financiera del sistema evaluado. En particular, todos los registros temporales se expresaron en unidades de tiempo normalizado (T_n) donde 1.00 T_n corresponde a la ventana operativa máxima permitida para completar la secuencia de descarga, formación de trenes y entrega al cliente, mientras que los análisis económicos se presentaron en unidades financieras normalizadas (U_n), con 1.00 U_n equivalente al costo fijo por vuelo.

Este planteamiento permite una interpretación técnica robusta, independiente de valores absolutos, garantizando al mismo tiempo la replicabilidad metodológica en otros entornos logísticos con restricciones temporales similares.

2.1 Fase definir

En esta fase se caracterizó el problema raíz asociado al incremento abrupto en la demanda operacional de PRModel-Logistic, provocado por la firma de un nuevo contrato que duplicó el volumen de vuelos diarios. Esta situación generó riesgos de incumplimiento del límite temporal operativo expresado como $T_{total} \leq 1.00 T_n$, coherente con los desafíos descritos en la literatura sobre sistemas logísticos sometidos a ventanas temporales estrictas (Christopher, 2016; Rushton *et al.*, 2022).

Se establecieron tres requisitos críticos:

1. Tiempo de entrega normalizado (T_n) como métrica principal del desempeño operativo.
2. Capacidad operativa instalada, dependiente de la disponibilidad de choferes, trenes y equipos (Gijo *et al.*, 2014; Lim, 2011).
3. Cumplimiento de normativas de la Federal Aviation Administration (FAA), necesarias para garantizar la integridad de la operación (Atlas Air, 2018).

El flujo completo, desde la recepción del manifiesto de vuelo hasta la entrega final al cliente, se definió como objeto del análisis DMAIC, siguiendo lineamientos metodológicos típicos de estudio de procesos aeroportuarios (Cohn, Root & Wang, 2007; Psychogios & Tsironis, 2012). Este flujo se representa en las Tablas 1 y 2.

2.2 Fase medir

La fase de medición se fundamentó en principios estadísticos de consistencia y representatividad (Montgomery, 2020; Joglekar, 2019). Se recopilieron 21 observaciones de vuelos consecutivos, capturando la va-

riabilidad real de:

- Número de contenedores,
- Distribución de peso,
- Tiempo de escaneo y descarga,
- Tiempo de formación de trenes,
- Tiempo de desplazamiento hacia el cliente.

Transformación a unidades normalizadas: cada tiempo medido t_i se transformó mediante:

$$T_i^{(norm)} = \frac{t_i}{T_{max}}$$

donde

$$T_{max} = 1.00T_n$$

Los tiempos originales en segundos o minutos fueron eliminados para preservar la confidencialidad operativa.

Tiempos normalizados por etapa: se realizó basado en estudios de campo y consistentes con operaciones

aeroportuarias comparables (Psychogios & Tsironis, 2012; Liker & Meier, 2021) (Tabla 3):

Para trenes de 5 contenedores:

- Escaneo total: 0.11–0.14 T_n
- Descarga total: 0.30–0.34 T_n
- Carga total: 0.12–0.15 T_n

Con estos valores se obtuvo un takt time normalizado de:

$$Takt^{(norm)} \approx 0.19T_n$$

Este valor fue alineado con reportes en sistemas de flujo continuo bajo restricciones temporales (Liker & Meier, 2021; Christopher, 2016).

Tabla 3. Actividad vs. Tiempo por contenedor.

Actividad	Tiempo por contenedor (T_n)
Escaneo	0.030 – 0.040 T_n
Descarga	0.065 – 0.075 T_n
Carga al tren	0.030 – 0.040 T_n

Tabla 1. Distribución de Contenedores por Avión (Valores Normalizados).

Métrica	Valor normalizado	Notas
Contenedores mínimos observados	0.36 (normalizado a 25 contenedores como referencia)	Valor adimensional
Contenedores máximos observados	1.04 (normalizado)	Define límite superior de variabilidad
Media por vuelo	0.80 (normalizado)	Consistencia operativa
Desviación estándar (σ)	0.27 (normalizado)	Variabilidad relativa
Rango operacional	0.36–1.04	Rango adimensional utilizado para simulación
Carga modal (ocupación contenedor)	Se mantiene como adimensional	No requiere normalización

Tabla 2. Distribución Normalizada del Peso por Contenedor (W_n).

Métrica	Valor normalizado (W_n)	Interpretación
Peso mínimo típico	0.714 W_n	Límite inferior esperado
Peso medio aproximado	0.857 W_n	Peso representativo del flujo
Peso máximo típico	1.000 W_n	Capacidad plena
Ocupación modal	0.950 W_n	Valor más frecuente

El peso “modal”, indicado como 95% de ocupación, también puede representarse así:

$$W_{modal} = 0.95 \times 1.000 = 0.950 W_n$$

2.3 Fase analizar

El análisis se realizó mediante un diagrama de Ishikawa estructurado según los seis factores clásicos en ingeniería industrial: ambiente, maquinaria, empleomanía, materiales, medidas y métodos (Gijo *et al.*, 2014). Este enfoque permitió identificar que la capacidad del sistema depende de la sincronización fina entre los recursos móviles (tren–chofer) y la secuencia de descarga, tal como señalan estudios de operaciones de paquetería (Cohn *et al.*, 2007; Lim, 2011).

La demanda temporal normalizada se definió co-

mo:

$$Demanda^{(norm)} = \frac{n}{5} \times Takt^{(norm)}$$

Donde n es el número de contenedores por vuelo. Los resultados indican:

- Operación estable para $n \approx 20$ contenedores ($\approx 0.76 T_n$)
 - Operación crítica para $n \approx 26$ ($\approx 0.99 T_n$)
 - Riesgo de incumplimiento para $n \geq 27$
- Se determinó que los factores de mayor impacto

sobre la eficiencia fueron el incremento de volumen no planificado, la disponibilidad de equipos, y la distribución ineficiente de operadores por turno (Minetti *et al.*, 2022). Estos hallazgos reflejan el comportamiento descrito típico de estudios de congestión y colas en sistemas logísticos con restricciones temporales fijas (Banks *et al.*, 2010; Gu *et al.*, 2010).

2.4 Fase mejorar

La fase de mejora se fundamentó en principios Lean Six Sigma, específicamente en la eliminación de tiempos de espera y la maximización del flujo continuo (George *et al.*, 2005; Snee, 2010).

Se implementaron dos acciones clave:

1. Paralelización operativa

Redistribución de los cinco choferes para atender simultáneamente las cabinas superior e inferior del avión, reduciendo tiempos no productivos y equilibrando el flujo de salida.

2. Priorización estructurada en SOP

Reordenamiento de los contenedores en el avión para reducir el tiempo de primera descarga (*first-out*), técnica alineada con estrategias de *priority slotting* (Psychogios & Tsironis, 2012).

La simulación demostró que:

$$\text{Demanda}_{30}^{(norm)} = 0.95T_n$$

Esto confirma la viabilidad de procesar hasta 30 contenedores por vuelo sin exceder $1.00 T_n$, coherente con recomendaciones de estudios previos de optimización logística (De Felice, Petrillo & Monfreda, 2009).

2.5 Fase controlar

Para garantizar la sostenibilidad de las mejoras implementadas, se definieron dos indicadores normalizados principales:

1. Cumplimiento temporal:

$$T_{total}^{(norm)} \leq 1.00T_n$$

2. Variabilidad de volumen:

$$\sigma_n \leq 6.8 \text{ contenedores}$$

Estos indicadores se integraron en un plan de monitoreo semanal y auditorías mensuales, siguiendo lineamientos de control estadístico del proceso (Montgomery, 2020; Desai & Shrivastava, 2008).

El uso de métricas adimensionales permite que las mejoras sean sostenibles, comparables entre vuelos y

replicables en otros escenarios operacionales, tal como recomiendan los marcos contemporáneos de ingeniería industrial aplicada a logística aérea (Antony, 2014; Proto *et al.*, 2020).

3 Discusión y Resultados

3.1 Desempeño operativo bajo tiempos normalizados

Los estudios de tiempo efectuados sobre el compartimiento superior del Boeing 767-300BCF permitieron caracterizar, con alto grado de consistencia, el comportamiento de cada etapa del proceso operativo: escaneo, descarga, carga al tren y transporte hacia el cliente. Para preservar la confidencialidad de la operación, todos los tiempos se expresaron en unidades de tiempo normalizado (T_n), donde $1.00 T_n$ representa la ventana máxima autorizada por vuelo.

Los valores normalizados obtenidos muestran una estructura de trabajo altamente estandarizada:

- Escaneo: $0.030\text{--}0.040 T_n$ por contenedor
- Descarga: $0.065\text{--}0.075 T_n$ por contenedor
- Carga al tren: $0.030\text{--}0.040 T_n$ por contenedor (Psychogios & Tsironis, 2012; Liker & Meier, 2021)

La consolidación de estas etapas para trenes de cinco contenedores arrojó:

- Escaneo total: $0.11\text{--}0.14 T_n$
- Descarga total: $0.30\text{--}0.34 T_n$
- Carga total: $0.12\text{--}0.15 T_n$

A partir de estas mediciones se determinó un *takt time* normalizado aproximado de:

$$\text{Takt}^{(norm)} = 0.19 T_n$$

Este indicador adquiere un peso central en el análisis, ya que permite evaluar la relación entre el ritmo operativo real y el ritmo requerido para cumplir consistentemente con el límite temporal $T_{total} \leq 1.00 T_n$. Tal como señalan Christopher (2016) y Cudney & Kestle (2018), la efectividad operacional en procesos logísticos bajo presión temporal depende de la alineación entre *takt time*, capacidad instalada y variabilidad de la demanda.

La inspección del flujo de demanda reveló una media de 20 contenedores por vuelo ($\sigma = 6.78$), con valores mínimos de 9 y máximos de 26 contenedores, concordando con los patrones de variabilidad típicos en redes de paquetería aérea (Lim, 2011; Proto *et al.*, 2020). Esta dispersión implica que el sistema opera de forma estable durante la mayor parte de las jornadas, pero presenta vulnerabilidad ante aumentos súbitos de volumen.

El análisis estadístico de la distribución de pesos, convertido a unidades normalizadas (Tabla 2), sugiere

además que los contenedores mantienen una ocupación en torno al 95%, lo cual incrementa la densidad del flujo logístico y acentúa la necesidad de procesos altamente coordinados (Montgomery, 2020; Rushton *et al.*, 2022).

3.2 Capacidad del sistema y determinación del cuello de botella

La evaluación de capacidad se desarrolló utilizando la ecuación de demanda temporal normalizada:

$$\text{Demanda}^{(norm)} = \frac{n}{5} \times \text{Takt}^{(norm)}$$

Donde n representa el número de contenedores por vuelo.

Los resultados muestran tres regiones críticas:

1. Región estable ($n \leq 20$):

$$\text{Demanda}^{(norm)} \approx 0.76 T_n$$

El proceso opera dentro del margen aceptable, sin acumulación de trenes (Montgomery, 2020).

2. Región de alerta ($n = 26$):

$$\text{Demanda}^{(norm)} \approx 0.99 T_n$$

Se observan tensiones en la coordinación de trenes, riesgo de saturación y mayor probabilidad de retrasos (Chopra & Meindl, 2023).

3. Región crítica ($n \geq 27$):

El sistema tiende al incumplimiento del límite temporal, incluso si no ocurren perturbaciones exógenas (demoras de vuelo, congestión, mantenimiento, clima).

Estos resultados coinciden con investigaciones en logística aeroportuaria que enfatizan la importancia de la sincronización entre recursos móviles (trenes, dollies, montacargas) como determinante del throughput efectivo (Cohn, Root & Wang, 2007; Lim, 2011).

La Figura 1 (diagrama de Ishikawa) confirma que las causas principales del cuello de botella se agrupan en torno a:

- Volumen incremental no planificado (Minetti *et al.*, 2022),
- Disponibilidad limitada de equipos,
- Secuenciación subóptima de operadores (Gijo *et al.*, 2014),
- Variabilidad en la ocupación de contenedores (Rushton *et al.*, 2022).

En conjunto, estos factores reducen la resiliencia temporal del sistema, especialmente bajo picos de demanda.

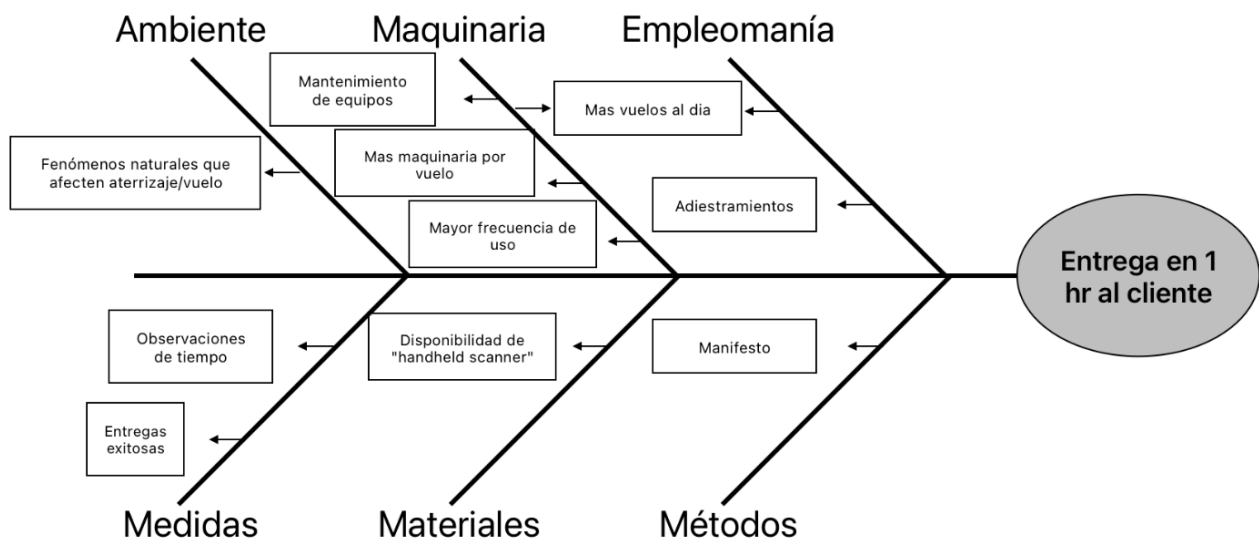


Figura 1. Causa y Efecto utilizando Ishikawa.

3.3 Intervención DMAIC: optimización mediante paralelización y secuenciación

La fase de mejora incorporó un rediseño operacional sustentado en principios Lean Six Sigma (George *et al.*, 2005; Snee, 2010). Dos intervenciones emergieron

como altamente efectivas:

1. Paralelización de la descarga en ambas cabinas:

Los cinco choferes pasaron a servir simultáneamente los compartimientos superior e inferior del avión. Esta modificación redujo tiempos ociosos y redistribuyó la carga de trabajo, generando un aumento inmediato de la capacidad efectiva.

2. Reordenamiento de contenedores en SOP (priority slotting):

Se optimizó la secuencia de salida priorizando contenedores del cliente principal, práctica altamente efectiva para minimizar *first-out time* en operaciones aeroportuarias (Tabla 4) (Psychogios & Tsironis, 2012; Christopher, 2016).

Los resultados de la simulación indicaron que, bajo la nueva configuración:

$$\text{Demanda}_{30}^{(norm)} = 0.95 T_n$$

Esto implica que el sistema puede procesar hasta 30 contenedores por vuelo sin violar el límite temporal de $1.00 T_n$, lo cual representa un incremento significativo de capacidad sin añadir personal ni equipos.

Estos hallazgos son coherentes con estudios previos que demuestran que pequeñas intervenciones, centradas en la reducción de tiempos de espera y en la optimización de la secuencia de tareas, pueden tener efectos multiplicadores sobre el flujo logístico global (Banks *et al.*, 2010; Gu *et al.*, 2010).

3.4 Desempeño financiero normalizado

El análisis económico se realizó utilizando unidades financieras adimensionales (U_n), donde $1.00 U_n$ equivale al costo fijo por vuelo (Tabla 4).

Dado que los costos del sistema son predominantemente fijos por vuelo, el margen operativo depende de:

- La densidad del contenedor,
- El número total de contenedores,
- La reducción de reprocesos.

Esto concuerda con modelos de sistemas logísticos donde la elasticidad del margen frente al volumen es positiva (Chopra & Meindl, 2023; Rushton *et al.*, 2022).

Asimismo, una disminución hipotética del 5% en el precio por libra reduciría el ingreso normalizado por vuelo a $4.70 U_n$, erosionando la ganancia aproximadamente un 6–7%, tal como anticipan los modelos de sensibilidad en logística aérea (Christopher, 2016).

Tabla 5. Indicadores financieros normalizados (U_n).

Métrica financiera	Valor normalizado (U_n)	Interpretación
Ingreso por vuelo (I_n)	$4.95 U_n$	Ingreso relativo por operación, basado en $1.00 U_n$ = costo fijo por vuelo
Ganancia por vuelo (G)	$3.95 U_n$	Margen operativo por vuelo después de cubrir costos fijos
Ingreso diario	$18.55 U_n$	Total relativo generado en la jornada completa
Ganancia diaria	$14.55 U_n$	Beneficio operativo neto diario

Tabla 4. Simulación itinerario de trenes.

Tren/Min	$0.21 T_n$	$0.41 T_n$	$0.47 T_n$	$0.60 T_n$	$0.66 T_n$	$0.81 T_n$	$0.86 T_n$	$1.07 T_n$
1	Salida		Llegada					
2		Salida			Llegada			
3				Salida			Llegada	
4	Salida		Llegada			Salida		Llegada
5		Salida			Llegada			
		Cabina Superior						Cabina Inferior

3.5 Implicaciones prácticas y generalización

Los resultados consolidan tres conclusiones esenciales:

1. El sistema posee una alta sensibilidad temporal: pequeñas variaciones en la carga total afectan la capacidad de cumplir la ventana operativa.
2. La paralelización y la secuenciación inteligente son de alto impacto: mejoras modestas, pero bien estructuradas, generan incrementos significativos de productividad sin inversiones adi-

cionales (Antony, 2014; Cudney & Kestle, 2018).

3. El uso de métricas normalizadas (T_n , U_n) mejora la transparencia metodológica y facilita la aplicación del modelo a otros aeropuertos con dinámica similar (Proto *et al.*, 2020).

En conjunto, la integración del análisis estadístico, las métricas adimensionales, el modelado mediante simulación y la estructura DMAIC aportan un marco metodológico replicable, robusto y de alta relevancia para la ingeniería logística contemporánea.

Finalmente, la consistencia entre simulación y me-

diciones de campo agrega solidez causal a las mejoras; no obstante, se sugiere en trabajos futuros incorporar modelos de filas (G/G/1, G/G/c) y simulación de eventos discretos para evaluar perturbaciones (clima, mantenimiento, no-shows de equipos) y políticas de priorización alternativas (Banks *et al.*, 2010; Gu *et al.*, 2010).

Tabla 6. Resultado financiero por vuelo (normalizado en U_n).

Concepto financiero	Valor normalizado (U_n)	Descripción
Costo fijo por vuelo (C_n)	1.00 U_n	Unidad base de referencia; representa el costo mínimo necesario por operación
Ingreso por vuelo (I_n)	4.95 U_n	Ingreso relativo total generado en cada vuelo
Ganancia por vuelo (G)	3.95 U_n	Margen operativo por vuelo después de cubrir C_n
Ingreso diario	18.55 U_n	Total ingresado por todas las operaciones del día
Ganancia diaria	14.55 U_n	Ganancia neta diaria tras múltiples vuelos

4 Conclusion y Recomendacion

Los resultados obtenidos permiten concluir que el proceso logístico de PRModel-Logistic presenta un desempeño operacional sólido, pero altamente sensible a fluctuaciones de volumen. La integración del enfoque DMAIC con métricas normalizadas (T_n y U_n) constituyó una herramienta metodológica eficaz para caracterizar con precisión los cuellos de botella, evaluar la capacidad instalada y proponer mejoras de alto impacto sin comprometer información confidencial.

El uso de tiempo normalizado (T_n) demostró que el sistema opera de manera estable cuando la demanda se ubica en torno a 20 contenedores por vuelo, con una demanda temporal equivalente a $\approx 0.76 T_n$. Sin embargo, al alcanzar 26 contenedores por vuelo, el proceso se aproxima al límite operativo ($\approx 0.99 T_n$), lo que evidencia la fragilidad del sistema ante aumentos repentinos de carga. Este comportamiento es consistente con estudios previos que destacan la importancia de la sincronización entre recursos móviles, la secuenciación operativa y la minimización de tiempos de espera en sistemas de flujo continuo.

La intervención desarrollada, basada en la paralelización de operaciones en ambas cabinas del avión y en la reorganización estratégica del SOP (*priority slotting*), permitió ampliar la capacidad efectiva del sistema hasta 30 contenedores por vuelo, manteniendo el tiempo total dentro del límite de $0.95 T_n$. Este resultado confirma la efectividad de las metodologías Lean Six Sigma en entornos aeroportuarios donde los ciclos operativos son estrechos y los recursos deben emplearse con precisión.

Desde la perspectiva económica, la normalización financiera (U_n) reveló un desempeño altamente favorable, con un ingreso relativo de 4.95 U_n por vuelo y una ganancia operativa de 3.95 U_n . Estos valores reflejan la

eficiencia de un modelo dominado por costos fijos, donde cada incremento marginal en volumen contribuye significativamente al margen operativo, en línea con los modelos de elasticidad en cadenas logísticas descritos en Chopra & Meindl (2023).

En conjunto, el estudio confirma que:

1. Las métricas normalizadas (T_n y U_n) constituyen un lenguaje robusto y replicable para evaluar procesos logísticos sin revelar información sensible.
2. La paralelización y secuenciación inteligente son estrategias de alto impacto, capaces de aumentar la capacidad hasta un 50% sin inversión adicional.
3. La metodología DMAIC garantiza una mejora continua estructurada, fortaleciendo la resiliencia operativa ante incrementos de demanda.
4. La simulación constituye un complemento crítico, permitiendo validar escenarios futuros sin interrumpir operaciones reales.

Como agenda de mejora continua, se proponen tres líneas de trabajo futuro:

Integración de sistemas digitales de trazabilidad y sensorización IoT, para medir en tiempo real el estado de los contenedores, la temperatura y la secuencia de despacho.

Simulación avanzada mediante modelos G/G/1 y algoritmos de optimización híbrida, a fin de evaluar estrategias de asignación dinámica de trenes y personal.

Evaluación de sostenibilidad operativa, incorporando métricas de eficiencia energética y huella de carbono asociadas al transporte terrestre y aéreo.

Finalmente, este estudio contribuye a la literatura sobre ingeniería industrial aplicada a la logística aérea, ofreciendo una base empírica para futuras investigaciones orientadas al diseño resiliente de cadenas de suministro insulares y a la consolidación de metodologías de mejora continua en el sector de transporte de carga.

Referencias

- Antony, J. (2014). Readiness factors for the Lean Six Sigma journey in the higher education sector. *International Journal of Productivity and Performance Management*, 63(2), 257-264.
- Atlas Air. (2018). *Dimensions and key data: 767-300BCF specifications*. Atlas Air Worldwide.
- Banks, J., Carson, J. S., Nelson, B. L., & Nicol, D. (2010). *Discrete-Event System Simulation* (5th ed.). Pearson.
- Chopra, S., & Meindl, P. (2023). *Supply Chain Management: Strategy, Planning, and Operation* (8th ed.). Pearson.
- Christopher, M. (2016). *Logistics & Supply Chain Management* (5th ed.). Pearson Education Limited.
- Cohn, A., Root, S., & Wang, A. (2007). *Integration of the*

- Load-Matching and Routing Problem with Equipment Balancing for Small Package Carriers. Transportation Science*, 41(2), 238–252.
- Cudney, E. A., & Kestle, R. (2018). *Implementing Lean Six Sigma throughout the supply chain: The comprehensive and transparent case study*. Crc Press.
- De Felice, F., Petrillo, A., & Monfreda, S. (2009). Improving Operations Performance with World Class Manufacturing Technique. *International Journal of Industrial and Engineering and Management*, 1(5).
- Desai, T. N., & Shrivastava, R. L. (2008). *Six Sigma—A new direction to quality and productivity management. Proceedings of the World Congress on Engineering and Computer Science*, 2, 22–24.
- George, M. L., Rowlands, D., Price, M., & Maxey, J. (2005). *The Lean Six Sigma Pocket Toolbook*. McGraw-Hill.
- Gijo, E. V., Bhat, S., & Inanesh, N. A. (2014). Application of Six Sigma methodology in a small-scale foundry industry. *International Journal of Lean Six Sigma*, 5(2), 193–211.
- Gu, J., Goetschalckx, M., & McGinnis, L. F. (2010). Research on warehouse operation: A comprehensive review. *European Journal of Operational Research*, 203(3), 539–549.
- Joglekar, A. M. (2019). *Statistical Methods for Six Sigma: In R and Minitab* (2nd ed.). Wiley.
- Lim, H. (2011). Modeling local service reliabilities for the parcel distribution system. *Journal of International Logistics and Trade*, 9(1), 71–87.
- Liker, J. K., & Meier, D. (2021). *The Toyota Way Fieldbook: A Practical Guide for Implementing Lean*. McGraw-Hill.
- Minetti, G. F., Salto, C., Alfonso, H., Bermúdez, C., Dielschneider Del Bono, M. J., & Vargas, J. (2022). Optimización de la logística de distribución utilizando técnicas de la Inteligencia Artificial. In *XXIV Workshop de Investigadores en Ciencias de la Computación (WICC 2022, Mendoza)*.
- Montgomery, D. C. (2020). *Introduction to Statistical Quality Control* (8th ed.). Wiley.
- Pereira, P. (Ed.). (2024). *Six Sigma and Quality Management*. BoD—Books on Demand.
- Proto, S., Di Corso, E., Apiletti, D., Cagliero, L., Cerquitelli, T., Malnati, G., & Mazzucchi, D. (2020). REDTag: a predictive maintenance framework for parcel delivery logistic. *IEEE Access*, 8, 14953–14964.
- Psychogios, A. G., & Tsironis, L. K. (2012). Towards an integrated framework for Lean Six Sigma application: Lessons from the airline industry. *Total Quality Management & Business Excellence*, 23(3-4), 397–415.
- Ruiz Moreno, S., Arango Serna, M. D., Serna Urán, C. A., & Zapata, J. A. (2020). *Modelo matemático para la optimización de la red de distribución de una empresa de transporte de paquetería y mensajería terrestre*. *Dyna*, 87(214), 127–134.
- Rushton, A., Croucher, P., & Baker, P. (2022). *The Handbook of Logistics and Distribution Management* (7th ed.). Kogan Page.
- Snee, R. D. (2010). *Lean Six Sigma - Getting better all the time*. *International Journal of Lean Six Sigma*, 1(1), 9–29.

Recibido: 1 de octubre de 2025

Aceptado: 25 de noviembre de 2025

Sanz, Gabriela: BSc. in Industrial Engineering, 2025, Universidad Politécnica de Puerto Rico, San Juan, PR, USA.

 <https://orcid.org/0009-0007-0992-7442>

Ledain, Mariangelie: BSc. in Industrial Engineering, 2025, Universidad Politécnica de Puerto Rico. San Juan, PR, USA. E-mail: ledain_146447@students.pup.edu


 <https://orcid.org/0009-0003-0976-7224>

González, Andrea: BSc. in Industrial Engineering, 2025, Universidad Politécnica de Puerto Rico. San Juan, PR, USA. E-mail: gonzalez_110507@students.pup.edu

 <https://orcid.org/0009-0006-0119-6318>

González, Carlos: Ph.D. in Industrial Engineering, 1995, North Carolina State University. Professor, VP of Academy Affairs and Dean of the School of Engineering and Surveying. Universidad Politécnica de Puerto Rico. San Juan, PR, USA. E-mail: gonzalez@pupr.edu

 <https://orcid.org/0009-0001-0255-1733>

Garcia, Maria: Ph.D. in Education, 2012, Ana G. Méndez University. Department Head, and Professor of Industrial Engineering Department, at the Universidad Politécnica de Puerto Rico. San Juan, PR, USA. E-mail: margaricia@pupr.edu  <https://orcid.org/0000-0002-7134-3057>

Rondón Contreras, Jairo: Ph.D. in Applied Chemistry, mention: Materials Study, 2015, Universidad de Los Andes. Professor of Biomedical & Chemical Engineering Departments, at the Polytechnic University of Puerto Rico. San Juan, PR-USA.

 <https://orcid.org/0000-0002-9738-966X>

A review on bioactive scaffolds in biomedical engineering: Functionalization with nanoparticles and biomolecules

Una revisión sobre andamios bioactivos en ingeniería biomédica: Funcionalización con nanopartículas y biomoléculas

Aponte, Nicole^{1*}; Rondón, Jairo^{1,2}; Gonzalez-Lizardo, Angel³; Lugo, Claudio⁴

¹ Biomedical Engineering Department, Universidad Politécnica de Puerto Rico, San Juan, PR 00918, USA

² Chemical Engineering Department, Universidad Politécnica de Puerto Rico, San Juan, PR 00918, USA

³ Department of Electrical and Computer Engineering & Computer Science, Universidad Politécnica de Puerto Rico, San Juan, PR 00918, USA

⁴ Laboratorio de Cinética y Catálisis, Universidad de Los Andes, Mérida, Venezuela.

*aponte_140892@students.pupr.edu

Abstract

Bioactive scaffolds functionalized with nanoparticles and biomolecules represent a fundamental strategy in tissue engineering, as they provide structural, biochemical, and mechanobiological cues that promote tissue regeneration. These systems emulate essential functions of the extracellular matrix (ECM), modulating cell adhesion, proliferation, differentiation, and new matrix formation. This review integrates the main categories of biomaterials and evaluates how functionalization strategies enhance their mechanical performance, bioactivity, and biological responsiveness. Nanoparticles offer unique advantages, such as antimicrobial properties, controlled release of therapeutic agents, mechanical reinforcement, and improved osteogenic or angiogenic potential. In contrast, biomolecules—including peptides, growth factors, and ECM proteins—strengthen cell-material interactions. Applications in bone, cartilage, and cardiovascular regeneration demonstrate the potential of these systems to overcome the limitations of conventional scaffolds. However, challenges remain regarding vascularization, immunomodulation, degradation control, reproducibility, and regulatory processes. Emerging trends such as 4D bioprinting, stimuli-responsive materials, gene-activated scaffolds, bioelectronic interfaces, and artificial intelligence-assisted design offer new opportunities to develop personalized and clinically viable regenerative platforms.

Keywords: scaffolds, bioactive scaffolds, biomolecules, bioactive nanoparticles, tissue engineering.

Resumen

Los andamios bioactivos funcionalizados con nanopartículas y biomoléculas representan una estrategia fundamental en la ingeniería de tejidos, al proporcionar señales estructurales, bioquímicas y mecanobiológicas que favorecen la regeneración tisular. Estos sistemas emulan funciones esenciales de la matriz extracelular (MEC), modulando la adhesión, proliferación, diferenciación y la formación de nueva matriz. Esta revisión integra las principales categorías de biomateriales y evalúa cómo las estrategias de funcionalización mejoran su desempeño mecánico, bioactividad y capacidad de respuesta biológica. Las nanopartículas aportan ventajas únicas, como propiedades antimicrobianas, liberación controlada de agentes terapéuticos, refuerzo mecánico y mayor potencial osteogénico o angiogénico; mientras que las biomoléculas, incluidas péptidos, factores de crecimiento y proteínas de la MEC, fortalecen las interacciones célula-material. Las aplicaciones en la regeneración ósea, cartilaginosa y cardiovascular demuestran el potencial de estos sistemas para superar las limitaciones de los andamios convencionales. No obstante, persisten retos relacionados con la vascularización, la modulación inmunológica, el control de la degradación, la reproducibilidad y los procesos regulatorios. Las tendencias emergentes, como la bioimpresión 4D, los materiales sensibles a estímulos, los andamios activados por genes, las interfaces bioelectrónicas y el diseño asistido por inteligencia artificial, ofrecen nuevas oportunidades para desarrollar plataformas regenerativas personalizadas y clínicamente viables.

Palabras clave: andamios, andamios bioactivos, biomoléculas, nanopartículas bioactivas, ingeniería de tejidos.

1 Introducción

The development of biomaterials and scaffolds for tissue engineering has transformed regenerative medicine by enabling the design of three-dimensional (3D) structures that partially reproduce the architecture, composition, and function of native tissues. In the classical tissue engineering paradigm, cells are harvested, expanded *in vitro*, and seeded onto a scaffold that acts as a temporary extracellular matrix (ECM), providing mechanical support, topographical cues, and biochemical signals to guide tissue repair after implantation (Krishani *et al.*, 2023; Lutzweiler *et al.*, 2020; Rondón *et al.*, 2025). To fulfill this role, scaffolds must exhibit interconnected porosity, adequate mechanical strength, controlled degradability, and a high degree of biocompatibility and bioactivity, while also minimizing immune rejection and toxicity (Eltom *et al.*, 2019; Williams, 2022).

Within this context, bioactive scaffolds represent an evolution from purely structural supports toward dynamically instructive biomaterials. Rather than acting as passive frameworks, bioactive scaffolds are engineered to modulate cell adhesion, proliferation, differentiation, and ECM deposition through tailored surface chemistry, nano-/micro-architecture, and controlled presentation of biochemical signals (Krishani *et al.*, 2023; Zielińska *et al.*, 2023).

Recent reviews have highlighted how such scaffolds can be designed from natural and synthetic polymers, ceramics, and composite systems, with increasing attention to the interplay between material composition, degradation behavior, and the host response (Eldeeb *et al.*, 2022; Kim *et al.*, 2024; Wong *et al.*, 2023). In this scenario, the work of Rondón, Vázquez, and Lugo has contributed to consolidating the conceptual and technological basis for scaffold design in tissue engineering, especially in Latin-American contexts (Rondón *et al.*, 2023).

A key strategy to enhance scaffold performance is functionalization, which involves the deliberate modification of the scaffold's bulk or surface to introduce specific physicochemical, biological, or topographical features that promote a desired cellular response (Zielińska *et al.*, 2023; Todd *et al.*, 2024). Functionalization can be achieved by incorporating nanoparticles (NPs) (metallic, ceramic, polymeric, or carbon-based) or by immobilizing biomolecules such as growth factors, peptides, polysaccharides, and proteins. Nanoparticles provide a high surface-to-volume ratio and tunable physicochemical properties, enabling controlled drug release, antimicrobial activity, imaging contrast, or mechanical reinforcement (Delfi *et al.*, 2020; Eker *et al.*, 2024; Anusiya & Jaiganesh, 2022). In parallel, biomolecules offer specific biological recognition motifs that can enhance cell adhesion, promote lineage-specific differentiation, and regulate angiogenesis and immunomodulation (Eldeeb *et al.*, 2022; Lutzweiler *et al.*, 2020).

The choice of biomaterial is equally critical. Natural polymers such as collagen, gelatin, chitosan, alginate, and

hyaluronic acid are attractive due to their structural similarity to native ECM, intrinsic bioactivity, and degradability (Chen *et al.*, 2022; Dovedytis *et al.*, 2020; Ressler, 2022; Lauritano *et al.*, 2024). However, they often suffer from batch-to-batch variability and limited mechanical strength, especially in load-bearing applications (Wong *et al.*, 2023; Ramos-Zúñiga *et al.*, 2022). Synthetic polymers (including polylactic acid (PLA), polycaprolactone (PCL), and polyethylene glycol (PEG)) as well as bioactive ceramics such as hydroxyapatite and zirconia, allow precise control over mechanical properties, degradation kinetics, and processing routes, but usually require surface modification or blending to reach an adequate level of bioactivity (Bolívar-Monsalve *et al.*, 2021; Bal *et al.*, 2020; Ma *et al.*, 2021; Ghosh & Webster, 2021). Hybrid scaffolds that combine natural and synthetic components, frequently processed by electrospinning, 3D printing, or foaming techniques, seek to integrate the biological advantages of natural matrices with the robustness and reproducibility of synthetic systems (Anusiya & Jaiganesh, 2022; Fermani *et al.*, 2021; Wulf *et al.*, 2022).

At the cellular level, cell-scaffold interactions (particularly adhesion, proliferation, and differentiation) mediate the success of any tissue engineering strategy (Wang *et al.*, 2023). Adhesion processes, governed by integrin-mediated recognition of ligands and ECM-mimetic motifs, regulate cytoskeletal organization, mechanotransduction, and downstream signaling pathways (Khalili & Ahmad, 2015; Shams *et al.*, 2025). Cell proliferation ensures adequate cell density and homogeneous colonization of the scaffold, while differentiation drives the acquisition of tissue-specific phenotypes, often controlled by tightly regulated gene networks and epigenetic mechanisms (Liu *et al.*, 2024; Wu & Yue, 2024). Functionalized scaffolds aspire to orchestrate these events by combining biochemical, mechanical, and topographical cues in a spatiotemporally controlled manner. From an application standpoint, bioactive and functionalized scaffolds have shown particular promise in bone and cartilage regeneration, where mechanical demands, vascularization constraints, and complex defect geometries remain challenging (Bal *et al.*, 2020; Xue *et al.*, 2022; Rawojć *et al.*, 2025; Trebunova *et al.*, 2025). Likewise, in cardiovascular tissue engineering, hybrid scaffolds integrating natural matrices, synthetic polymers, and conductive nanomaterials are being explored to restore contractile function, electrical conduction, and vascular integrity in damaged myocardium and vascular grafts (Razavi *et al.*, 2024; Rayat Pisheh *et al.*, 2024). Despite these advances, many systems remain at preclinical stages due to hurdles related to reproducibility, large-scale manufacturing, regulatory classification, and long-term safety (Jeraj & Zameer, 2025; Ramos-Zúñiga *et al.*, 2021).

In this framework, there is a need for integrative reviews that connect the chemical and structural design of functionalized bioactive scaffolds with their cellular mechanisms of action and their translation into specific biomed-

cal applications. Therefore, the objective of this work is to provide a critical and up-to-date overview of bioactive scaffolds functionalized with nanoparticles and biomolecules. The review analyzes their composition, functionalization strategies, and biological mechanisms. It discusses their applications in bone, cartilage, and cardiovascular tissue engineering, as well as the main challenges and future perspectives for their clinical translation.

2 Methodology

The methodology used in this research will be documentary-exploratory, based on:

a. Data search and compilation: Databases such as PubMed, ACS Publications, ScienceDirect, SCOPUS, IEEE, SCIELO, RedALyC, and Google Scholar will be used. Search keywords will include: "Functionalized bioactive scaffolds," "Nanoparticles in tissue engineering," "Biomolecules in tissue regeneration." The search will be limited to the period from 2011 to 2025.

b. Information selection and refinement: Mendeley will be used as a bibliographic manager to organize the information into five databases: composition, types, properties, mechanisms of action, and biomedical use. Relevant research articles and reviews will be prioritized.

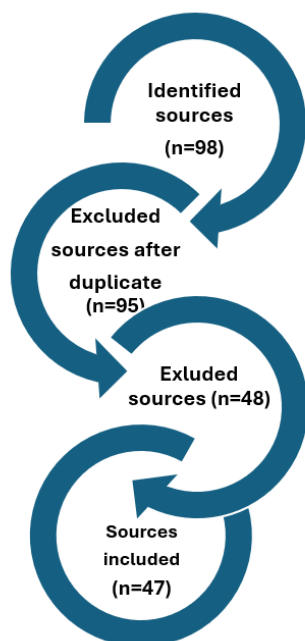


Figure 1. Study selection methodology flowchart for the research.

c. Subtopic selection: The collected information will be structured to identify recent trends and advances in the field.

d. Analysis of results: A critical analysis of the collected data will be performed, organizing the information into a structured review and discussing its implications for tissue engineering.

3 Results and Discussions

3.1 Bioactive scaffolds: concept and functional role

Bioactive scaffolds constitute a central pillar in contemporary tissue engineering because they provide a structural and biochemical microenvironment that emulates the natural extracellular matrix (ECM). From a regenerative perspective, the scaffold must support cell adhesion, proliferation, differentiation, and ECM deposition - functions tightly linked to its surface chemistry, mechanical properties, and architecture (Krishani *et al.*, 2023; Lutzweiler *et al.*, 2020). Traditional scaffolds were initially conceived as inert physical supports; however, their evolution into bioactive and instructive systems reflects a paradigm shift toward materials capable of modulating biological signaling pathways and influencing cellular phenotype.

Key properties such as porosity, pore interconnectivity, biodegradability, and mechanical stability determine the success of scaffold-mediated tissue regeneration (Satchanska *et al.*, 2024). Biocompatibility ensures the safe integration of materials without provoking cytotoxicity or inflammatory reactions (Sindhi *et al.*, 2025), while bioactivity enables active interactions with cells through ligand presentation, the release of chemical cues, or the direct modulation of cell behavior (Krishani *et al.*, 2023). The synergistic interplay between these variables ultimately dictates scaffold performance *in vivo*.

3.1.1 Types and properties of bioactive scaffolds

Bioactive scaffolds can be fabricated from natural polymers, synthetic polymers, ceramics, and hybrid composites, each offering distinct advantages and limitations, depending on the target tissue. Natural polymers (such as collagen, gelatin, chitosan, alginate, and hyaluronic acid) exhibit excellent biocompatibility and intrinsic bioactivity, features that replicate many ECM-like characteristics (Chen *et al.*, 2022; Eldeeb *et al.*, 2022). Their main limitations include batch-to-batch variability, rapid degradation, and insufficient mechanical strength for load-bearing tissues (Wong *et al.*, 2023; Ramos-Zúñiga *et al.*, 2022).

Synthetic polymers (PLA, PCL, PEG) allow precise control over mechanical properties and degradation kinetics and can be produced at scale with high reproducibility (Bolívar-Monsalve *et al.*, 2021). However, they typically require surface modification or blending with natural polymers to enhance bioactivity (Anusiya & Jaiganesh, 2022).

Ceramics such as hydroxyapatite (HAp) and tricalcium phosphate (TCP) exhibit osteoconductive properties and are widely used in bone tissue engineering (Ma *et al.*, 2021).

Hybrid composites that combine polymers and ceramics address mechanical limitations while improving cell response (Ghosh & Webster, 2021).

3.2 Functionalization strategies: nanoparticles and biomolecules

Functionalization refers to the intentional design of scaffold surfaces or bulk phases with chemical groups, nanomaterials, or biomolecules that elicit specific biological responses (Zielińska *et al.*, 2023; Todd *et al.*, 2024). This strategy transforms scaffolds from passive physical supports into biologically instructive systems.

3.2.1 Nanoparticle functionalization

Nanoparticles (NPs) (metallic, inorganic, carbon-based, polymeric, lipid-based) possess distinctive physico-chemical properties attributable to their nanoscale dimensions and high surface-area-to-volume ratio (Yameny *et al.*, 2024; Eker *et al.*, 2024). Their incorporation into scaffolds enables:

- Controlled release of growth factors and therapeutic agents
- Antimicrobial activity, especially with AgNPs, ZnO-NPs, and CuNPs (Khursheed *et al.*, 2022; Yang *et al.*, 2021)
- Mechanical reinforcement, improving rigidity or flexibility
- Enhanced osteoinduction or angiogenesis, as observed with TiO₂ and HAp nanoparticles (Delfi *et al.*, 2020)
- Diagnostic imaging enhancement, such as Fe₃O₄ NPs for MRI contrast

Metal nanoparticles such as AuNPs exhibit unique optical and surface plasmon resonance properties, enabling sensing, bioimaging, and targeted therapy. Ceramic nanoparticles enhance osteogenic potential, while carbon-based nanomaterials impart electrical conductivity useful for cardiac or neural tissue engineering.

3.2.2 Biomolecule functionalization

Biomolecules (including growth factors, short peptides, ECM proteins, and polysaccharides) provide biological recognition motifs that regulate cell adhesion, proliferation, and lineage commitment (Eldeeb *et al.*, 2022; Lutzweiler *et al.*, 2020).

Examples include:

- RGD peptides that promote integrin-mediated adhesion
- BMP-2 or VEGF for osteogenesis and angiogenesis
- Hyaluronic acid to enhance hydration and viscoelasticity

- Fibrin or collagen to promote ECM deposition and wound healing

The immobilization of biomolecules enables the spatial and temporal modulation of cell behavior, thereby mimicking tissue-specific microenvironments.

3.3 Biomaterials employed in functionalized scaffolds

3.3.1 Natural biomaterials

Natural biomaterials exhibit structural similarity to human ECM, facilitating cell-material interactions. Collagen and gelatin support osteogenesis and chondrogenesis; chitosan provides antibacterial and hemostatic properties; alginate allows gentle in situ gelation; hyaluronic acid improves tissue hydration and signals cellular migration (Kamatar *et al.*, 2020; Dovedytis *et al.*, 2020; Wu *et al.*, 2024; Lukin *et al.*, 2022). Their disadvantages (poor mechanical behavior and rapid degradation) require reinforcement through crosslinking or blending with synthetic materials (Ressler, 2022).

3.3.2 Synthetic biomaterials

Synthetic biomaterials such as PLA, PCL, and PEG offer predictability and tunability (Carbajal-De la Torre *et al.*, 2021). Ceramics and composites, including hydroxyapatite (HAp) and zirconia, provide stiffness suitable for bone regeneration but lack intrinsic bioactivity unless they are functionalized (Ma *et al.*, 2021). To overcome these limitations, polymers and ceramics are combined through electrospinning, 3D printing, and solvent casting to achieve improved mechanical and biological performance (Anusiya & Jaigamesh, 2022; Fermani *et al.*, 2021).

3.4 Cellular mechanisms: interaction between scaffolds and cells

The biological response to scaffolds is orchestrated by three core mechanisms: adhesion, proliferation, and differentiation.

3.4.1 Proliferation

Proliferation ensures adequate cell density and colonization throughout the scaffold. Its regulation depends on scaffold porosity, nutrient transport, stiffness, and biochemical signaling (Wang *et al.*, 2023).

3.4.2 Differentiation

Cell differentiation involves the transition of progenitor or stem cells into specialized lineages, regulated through gene expression programs, epigenetic signals, and scaffold-induced mechanotransduction (Liu *et al.*, 2024; Wu & Yue,

2024). Growth factor–functionalized scaffolds enhance lineage-specific outcomes such as osteogenesis or chondrogenesis.

3.4.3 Adhesion

Integrins and ECM-mimetic ligands mediate cell adhesion, controlling cytoskeletal organization, migration, and viability (Khalili & Ahmad, 2015). Scaffolds functionalized with peptides or proteins improve adhesion strength and stability (Shams *et al.*, 2025).

3.5 Biomedical applications

3.5.1 Bone and cartilage regeneration

Hydroxyapatite-based systems remain the gold standard for bone tissue engineering due to their chemical similarity to native bone (Bal *et al.*, 2020). However, their brittleness necessitates the use of composite reinforcement. Functionalized scaffolds incorporating nanoparticles or osteogenic biomolecules have demonstrated improved angiogenesis and mineralization (Xue *et al.*, 2022; Ye *et al.*, 2025). Clinical strategies such as bone grafting or PEMF therapies complement material-based interventions.

3.5.2 Cardiovascular tissue engineering

Cardiovascular scaffolds must emulate the anisotropic mechanical and electrical characteristics of myocardial tissue (Razavi *et al.*, 2024). Hybrid scaffolds combining collagen, fibrin, PLA, or PCL with conductive nanomaterials (graphene, carbon nanotubes) improve contractility and signal propagation (Rayat Pisheh *et al.*, 2024). Challenges include poor vascularization and an immature cardiomyocyte phenotype, which are partially addressed using induced pluripotent stem cells (iPSCs) and electrical stimulation (Hosseini *et al.*, 2021).

4 Challenges and Future Perspectives

The rapid evolution of bioactive scaffolds functionalized with nanoparticles and biomolecules has significantly advanced the field of tissue engineering; however, several scientific, technological, and regulatory challenges continue to limit their clinical translation. Understanding these limitations is crucial for guiding the development of the next generation of instructive, multifunctional, and patient-specific scaffolds.

4.1 Structural and material challenges

A central barrier lies in the difficulty of developing scaffolds that simultaneously satisfy mechanical robustness, biomimetic architecture, and biological performance. In

load-bearing tissues such as bone and cartilage, the need for high porosity to support vascularization conflicts with the mechanical stability required to withstand physiological loads (Rawojć *et al.*, 2025). For soft tissues, the challenge involves achieving elasticity, viscoelasticity, and degradation behaviors that recapitulate the native ECM without generating cytotoxic byproducts (Trebunova *et al.*, 2025).

Control over degradation kinetics remains a significant limitation. Many biodegradable polymers produce acidic or alkaline degradation products that perturb pH balance, negatively impacting cell viability and inflammatory responses (Ma *et al.*, 2021; Patel *et al.*, 2011). Similarly, natural polymers exhibit unpredictable degradation profiles due to batch variability, affecting reproducibility and long-term performance (Wong *et al.*, 2023).

Functionalization itself introduces complexity. While nanoparticles and biomolecules impart instructive cues, they may also alter mechanical behavior, influence degradation, or change hydrophilicity in unintended ways. Achieving precise, uniform, and reproducible incorporation of functional moieties (without compromising scaffold integrity) remains an unresolved challenge in engineering (Delfi *et al.*, 2020).

4.2 Biological and cellular barriers

The interaction between scaffolds and living tissues is intrinsically dynamic and highly dependent on the local biochemical and mechanical microenvironment. Significant biological challenges include:

4.2.1 Limited vascularization

A lack of prompt and robust vascularization is a primary cause of scaffold failure *in vivo*. Without an adequate blood supply, the inner regions of the scaffold become hypoxic, resulting in insufficient nutrient diffusion and compromised tissue formation (Xue *et al.*, 2022; Devillard & Marquette, 2021). This is especially critical in significant bone defects, engineered myocardium, and dense cartilage constructs.

4.2.2 Immune response and inflammation

Even biocompatible materials may elicit foreign body reactions, macrophage activation, or fibrous encapsulation. Nanoparticles, in particular, can modulate immune pathways in unpredictable ways depending on size, morphology, and surface chemistry (Yang *et al.*, 2021). Understanding and controlling immunomodulatory behavior is therefore essential.

4.2.3 Controlled release limitations

Biomolecule-functionalized scaffolds often struggle to maintain sustained, localized, and bioactive release of

growth factors or peptides. Uncontrolled release can lead to dosage inefficiency, off-target effects, or premature depletion of therapeutics (Zielińska *et al.*, 2023).

4.2.4 Cell source and maturation

Stem cell-based systems face inherent variability, risks of undesired differentiation, and difficulties in achieving full maturation. For example, cardiomyocytes derived from iPSCs often retain immature phenotypes that limit their functional integration (Hosseini *et al.*, 2021).

4.3 Manufacturing, standardization, and regulatory challenges

Translating scaffold systems from laboratory prototypes to clinically approved products requires overcoming formidable technological and regulatory hurdles.

4.3.1 Reproducibility and scale-up

Many laboratory-scale fabrication techniques, such as electrospinning, freeze-casting, and solvent-based printing, lack the precision and scalability required for industrial production. Variations in fabrication conditions can significantly modify pore size, mechanical strength, and functionalization efficiency (Rawojć *et al.*, 2025).

4.3.2 Quality control and standardized protocols

The absence of unified standards for mechanical testing, degradation evaluation, nanoparticle incorporation, and biomolecule immobilization limits comparability across studies and complicates the regulatory approval process.

4.3.3 Complex regulatory pathways

Functionalized scaffolds occupy a regulatory “grey zone” between medical devices, combination products, and advanced therapeutic medicinal products. Consequently, they often require extensive documentation, long-term safety data, and stringent biocompatibility testing under ISO 10993 guidelines (Ramos-Zúñiga *et al.*, 2021).

4.4 Emerging trends and strategic future directions

Despite these challenges, several technological innovations promise to redefine the field:

4.4.1 Smart and stimuli-responsive scaffolds

Advances in materials chemistry are enabling scaffolds that respond to pH, enzymes, mechanical load, or electrical signals, thereby enhancing control over drug release, cell behavior, and tissue integration (Trebunova *et al.*, 2025).

4.4.2 3D and 4D bioprinting

Hybrid bioprinting enables spatial control over scaffold architecture, cell placement, and biomolecular distribution. 4D bioprinting introduces time-dependent transformations triggered by environmental changes, providing dynamic control over tissue maturation (Aftab *et al.*, 2025).

4.4.3 Gene-activated and bioelectronic scaffolds

Gene-loaded constructs provide prolonged expression of therapeutic factors, while conductive polymers and nanomaterials enable the electrical stimulation of cardiac or neural tissues, thereby accelerating functional integration.

4.4.4 AI-assisted design and computational modeling

Artificial intelligence and machine learning can optimize scaffold architecture, predict degradation patterns, and reduce the need for animal experimentation. Data-driven platforms accelerate the discovery of novel biomaterial combinations and predict biological response based on physicochemical descriptors (Rawojć *et al.*, 2025).

4.4.5 Personalized and regenerative platforms

The integration of patient-specific imaging, iPSC-derived cells, and custom-printed scaffolds opens avenues toward personalized regenerative therapies. Tailoring scaffold geometry and biofunctionality to individual anatomical and biological needs may significantly enhance clinical outcomes.

4.5 Outlook

Overall, the future of bioactive, functionalized scaffolds rests on achieving a cohesive integration of material science, biology, engineering, and computational design. Overcoming current limitations will require interdisciplinary collaboration, advanced processing technologies, and rigorous preclinical and clinical validation. If these obstacles are addressed, functionalized scaffolds hold strong potential to transition from experimental constructs into reliable regenerative platforms capable of addressing complex clinical conditions in bone, cartilage, cardiovascular, and soft tissue repair.

5 Conclusion

Bioactive scaffolds functionalized with nanoparticles and biomolecules represent one of the most promising technological fronts in contemporary tissue engineering. Their ability to emulate key functions of the extracellular matrix, modulate cell behavior, and provide targeted therapeutic activity has significantly expanded the potential of regen-

erative medicine. As shown throughout this review, the structural design of scaffolds (whether derived from natural polymers, synthetic materials, ceramics, or hybrid composites) plays a critical role in determining their mechanical performance, degradation behavior, and biological compatibility. Functionalization further enhances these properties by enabling controlled release mechanisms, improving cell adhesion, and selectively stimulating proliferative and differentiation pathways.

Applications in bone, cartilage, and cardiovascular tissue engineering demonstrate that functionalized scaffolds can overcome several limitations of traditional biomaterials. Osteoconductive nanoparticle-reinforced composites improve mineralization; peptide-functionalized hydrogels enhance chondrogenesis; and hybrid, conductive scaffolds show potential in restoring cardiac electrical functionality. However, these advances remain constrained by challenges related to vascularization, immune response modulation, standardization of manufacturing processes, and long-term safety. Additionally, the integration of complex biochemical signals and nanostructured components requires precise control of scaffold architecture and physicochemical interactions, which often complicates reproducibility and regulatory approval.

Looking forward, next-generation regenerative platforms will increasingly rely on emerging technologies such as 4D bioprinting, gene-activated scaffolds, bioelectronic interfaces, and AI-guided material design. These innovations promise to deliver more dynamic, adaptive, and patient-specific constructs that can respond to physiological stimuli and promote robust functional tissue regeneration. To accelerate clinical translation, interdisciplinary efforts between materials scientists, biomedical engineers, clinicians, and regulatory experts will be critical.

Referencias

- Aftab, M., Ikram, S., Ullah, M., Khan, S. U., Wahab, A., & Naeem, M. (2025). Advancement of 3D Bioprinting Towards 4D Bioprinting for Sustained Drug Delivery and Tissue Engineering from Biopolymers. *Journal of Manufacturing and Materials Processing*, 9(8), 285. <https://doi.org/10.3390/jmmp9080285>
- Anusiya, G., & Jaiganesh, R. (2022). A review on fabrication methods of nanofibers and a special focus on the application of cellulose nanofibers. *Carbohydrate Polymer Technologies and Applications*, 4, 100262. <https://doi.org/10.1016/j.carpta.2022.100262>
- Bal, Z., Kaito, T., Korkusuz, F., & Yoshikawa, H. (2020). Bone regeneration with hydroxyapatite-based biomaterials. *Emergent Materials*, 3(4), 521-544. <https://doi.org/10.1007/s42247-019-00063-3>
- Bolívar-Monsalve, E. J., Alvarez, M. M., Hosseini, S., Espinosa-Hernandez, M. A., Ceballos-González, C. F., Sanchez-Dominguez, M., ... & Trujillo-de Santiago, G. (2021). Engineering bioactive synthetic polymers for biomedical applications: A review with emphasis on tissue engineering and controlled release. *Materials Advances*, 2(14), 4447-4478. <https://doi.org/10.1039/D1MA00092F>
- Carbajal-De la Torre, G., Zurita-Méndez, N. N., Ballesteros-Almanza, M. L., Mendoza, K., Espinosa-Medina, M. A., & Ortiz-Ortiz, J. (2021). Synthesis and characterization of polylactic/polycaprolactone/hydroxyapatite(PLA/PCL/HAp) scaffolds. *MRS Advances*, 6(39), 903-906. <https://doi.org/10.1557/s43580-021-00145-7>
- Chen, M., Jiang, R., Deng, N., Zhao, X., Li, X., & Guo, C. (2022). Natural polymer-based scaffolds for soft tissue repair. *Frontiers in Bioengineering and Biotechnology*, 10. <https://doi.org/10.3389/fbioe.2022.954699>
- Delfi, M., Ghomi, M., Zarrabi, A., Mohammadinejad, R., Taraghdari, Z. B., Ashrafizadeh, M., Zare, E. N., Agarwal, T., Padil, V. V., Mokhtari, B., Rossi, F., Perale, G., Sillanpaa, M., Borzacchiello, A., Kumar Maiti, T., & Makvandi, P. (2020). Functionalization of polymers and nanomaterials for biomedical applications: Antimicrobial platforms and drug carriers. *Prosthesis*, 2(2), 117-139. <https://doi.org/10.3390/prosthesis2020012>
- Dovedytis, M., Liu, Z. J., & Bartlett, S. (2020). Hyaluronic acid and its biomedical applications: A review. *Engineered Regeneration*, 1, 102-113. <https://doi.org/10.1016/j.engreg.2020.10.001>
- Devillard, C. D., & Marquette, C. A. (2021). Vascular tissue engineering: Challenges and requirements for an ideal large-scale blood vessel. *Frontiers in Bioengineering and Biotechnology*, 9. <https://doi.org/10.3389/fbioe.2021.721843>
- Eker, F., Duman, H., Akdaşçi, E., Bolat, E., Sarıtaş, S., Karav, S., & Witkowska, A. M. (2024). A comprehensive review of nanoparticles: from classification to application and toxicity. *Molecules*, 29(15), 3482. <https://doi.org/10.3390/molecules29153482>
- Eldeeb, A. E., Salah, S., & Elkasabgy, N. A. (2022). Biomaterials for tissue engineering applications and current updates in the field: A comprehensive review. *AAPS PharmSciTech*, 23(7). <https://doi.org/10.1208/s12249-022-02419-1>
- Eltom, A., Zhong, G., & Muhammad, A. (2019). Scaffold techniques and designs in tissue engineering functions and purposes: A review. *Advances in Materials Science and Engineering*, 2019, 1-13. <https://doi.org/10.1155/2019/3429527>
- Fermani, M., Platania, V., Kavasi, R.-M., Karavasili, C., Zgouro, P., Fatouros, D., Chatzinikolaidou, M., & Bouropoulos, N. (2021). 3D-printed scaffolds from alginate/methyl cellulose/trimethyl chitosan/silicate glasses for bone tissue engineering.

- Applied Sciences*, 11(18), 8677. <https://doi.org/10.3390/app11188677>
- Ghosh, S., & Webster, T. J. (2021). Metallic nanoscaffolds as osteogenic promoters: Advances, challenges and scope. *Metals*, 11(9), 1356. <https://doi.org/10.3390/met11091356>
- Hosseini, M., & Shafiee, A. (2021). Engineering bioactive scaffolds for skin regeneration. *Small*, 17(41). <https://doi.org/10.1002/sml.202101384>
- Jeraj, A. R., & Zameer, Z. (2025). AI-Enhanced Bioactive 3D-Printed Scaffolds for Tissue Regeneration: Innovations in Healing and Functional Additives. *Journal of Computing & Biomedical Informatics*, 8(02). <https://jcbi.org/index.php/Main/article/view/863>
- Kamatar, A., Gunay, G., & Acar, H. (2020). Natural and synthetic biomaterials for engineering multicellular tumor spheroids. *Polymers*, 12(11), 2506. <https://doi.org/10.3390/polym12112506>
- Khalili, A., & Ahmad, M. (2015). A review of cell adhesion studies for biomedical and biological applications. *International Journal of Molecular Sciences*, 16(8), 18149–18184. <https://doi.org/10.3390/ijms160818149>
- Khursheed, R., Dua, K., Vishwas, S., Gulati, M., Jha, N. K., Aldhfeeri, G. M., ... & Singh, S. K. (2022). Biomedical applications of metallic nanoparticles in cancer: Current status and future perspectives. *Biomedicine & pharmacotherapy*, 150, 112951. <https://doi.org/10.1016/j.biopha.2022.112951>
- Kim, Y. H., Vijayavenkataraman, S., & Cidonio, G. (2024). Biomaterials and scaffolds for tissue engineering and regenerative medicine. *BMC Methods*, 1(1), 2. <https://doi.org/10.1186/s44330-024-00002-7>
- Krishani, M., Shin, W. Y., Suhaimi, H., & Sambudi, N. S. (2023). Development of scaffolds from bio-based natural materials for tissue regeneration applications: a review. *Gels*, 9(2), 100. <https://doi.org/10.3390/gels9020100>
- Lauritano, D., Limongelli, L., Moreo, G., Favia, G., & Carinci, F. (2020). Nanomaterials for periodontal tissue engineering: Chitosan-based scaffolds. A systematic review. *Nanomaterials*, 10(4), 605. <https://doi.org/10.3390/nano10040605>
- Liu, J., Castillo-Hair, S. M., Du, L. Y., Wang, Y., Carte, A. N., Colomer-Rosell, M., ... & Schier, A. F. (2024). Dissecting the regulatory logic of specification and differentiation during vertebrate embryogenesis. *BioRxiv*. <https://doi.org/10.1101/2024.08.27.609971>
- Lukin, I., Erezuma, I., Maeso, L., Zarate, J., Desimone, M. F., Al-Tel, T. H., ... & Orive, G. (2022). Progress in gelatin as biomaterial for tissue engineering. *Pharmaceutics*, 14(6), 1177. <https://doi.org/10.3390/pharmaceutics14061177>
- Lutzweiler, G., Ndreu Halili, A., & Engin Vrana, N. (2020). The overview of porous, bioactive scaffolds as instructive biomaterials for tissue regeneration and their clinical translation. *Pharmaceutics*, 12(7), 602. <https://doi.org/10.3390/pharmaceutics12070602>
- Ma, Z., Wang, Q., Xie, W., Ye, W., Zhong, L., Hüge, J., & Wang, Y. (2021). Performance of 3D printed PCL/PLGA/HA biological bone tissue engineering scaffold. *Polymer Composites*, 42(7), 3593–3602. <https://doi.org/10.1002/pc.26061>
- Patel, H., Bonde, M., & Srinivasan, G. (2011). Biodegradable polymer scaffold for tissue engineering. *Trends in Biomaterials and Artificial Organs*, 25(1), 20–29.
- Ramos-Zúñiga, R., Segura-Duran, I., González-Castañeda, R. E., & Rios, J. G. (2022). The challenges of the bioactive scaffolds in nervous system: from their molecular conformation to their therapeutic efficiency. *Neurology Perspectives*, 2, S3–S18. <https://doi.org/10.1016/j.neurop.2021.07.007>
- Rawojć, K., Tadeusiewicz, R., & Zych-Stodolak, E. (2025). Advancements in Chitosan-Based Scaffolds for Chondrogenic Differentiation and Knee Cartilage Regeneration: Current Trends and Future Perspectives. *Bioengineering*, 12(7), 740. <https://doi.org/10.3390/bioengineering12070740>
- Rayat Pisheh, H., Nojabaei, F. S., Darvishi, A., Rayat Pisheh, A., & Sani, M. (2024). Cardiac tissue engineering: an emerging approach to the treatment of heart failure. *Frontiers in Bioengineering and Biotechnology*, 12, 1441933. <https://doi.org/10.3389/fbioe.2024.1441933>
- Razavi, Z. S., Soltani, M., Mahmoudvand, G., Farokhi, S., Karimi-Rouzbahani, A., Farasati-Far, B., ... & Afkhami, H. (2024). Advancements in tissue engineering for cardiovascular health: a biomedical engineering perspective. *Frontiers in Bioengineering and Biotechnology*, 12, 1385124. <https://doi.org/10.3389/fbioe.2024.1385124>
- Ressler, A. (2022). Chitosan-based biomaterials for bone tissue engineering applications: A short review. *Polymers*, 14(16), 3430. <https://doi.org/10.3390/polym14163430>
- Rondón, J.; Sánchez Martínez, V.; Lugo, C.; González-Lizardo, A. (2025). Tissue engineering: Advancements, challenges and future perspectives. *Ciencia e Ingeniería*, 46 (1), 19–28. <http://revistas.saber.ula.ve/index.php/cienciaingenieria/article/view/20607>
- Rondón, J., Vázquez, J., & Lugo, C. (2023). Biomaterials used in tissue engineering for the manufacture of scaffolds. *Ciencia e Ingeniería*, 44(3), 297–308. <http://revistas.saber.ula.ve/index.php/cienciaingenieria/article/view/20607>


- [niera/article/view/19221](https://doi.org/10.3390/polym16081159)
 Satchanska, G., Davidova, S., & Petrov, P. D. (2024). Natural and synthetic polymers for biomedical and environmental applications. *Polymers*, 16(8), 1159. <https://doi.org/10.3390/polym16081159>
- Shams, F., Jamshidian, M., Shaygani, H., Maleki, S., Soltani, M., & Shamloo, A. (2025). A study on the cellular adhesion properties of a hybrid scaffold for vascular tissue engineering through molecular dynamics simulation. *Scientific Reports*, 15(1), 16433. <https://doi.org/10.1038/s41598-025-01545-7>
- Sindhi, K., Pingili, R. B., Beldar, V., Bhattacharya, S., Rahaman, J., & Mukherjee, D. (2025). The role of biomaterials-based scaffolds in advancing skin tissue construct. *Journal of Tissue Viability*, 100858. <https://doi.org/10.1016/j.jtv.2025.100858>
- Todd, E. A., Mirsky, N. A., Silva, B. L. G., Shinde, A. R., Arakelians, A. R., Nayak, V. V., ... & Coelho, P. G. (2024). Functional scaffolds for bone tissue regeneration: a comprehensive review of materials, methods, and future directions. *Journal of Functional Biomaterials*, 15(10), 280. <https://doi.org/10.3390/jfb15100280>
- Trebunova, M., Cajkova, J., & Bacenkova, D. (2025). Hydrogels as bioactive scaffolds in biomedical engineering. *Acta Tecnológica*, 11(2), 75–79. <https://doi.org/10.22306/atec.v11i2.272>
- Wang, F., Cai, X., Shen, Y., & Meng, L. (2023). Cell-scaffold interactions in tissue engineering for oral and craniofacial reconstruction. *Bioactive Materials*, 23, 16–44. <https://doi.org/10.1016/j.bioactmat.2022.10.029>
- Williams, D. F. (2022). Biocompatibility pathways and mechanisms for bioactive materials: The bioactivity zone. *Bioactive Materials*, 10, 306–322. <https://doi.org/10.1016/j.bioactmat.2021.08.014>
- Wong, S. K., Yee, M. M., Chin, K.-Y., & Ima-Nirwana, S. (2023). A review of the application of natural and synthetic scaffolds in bone regeneration. *Journal of Functional Biomaterials*, 14(5), 286. <https://doi.org/10.3390/jfb14050286>
- Wu, E., Huang, L., Shen, Y., Wei, Z., Li, Y., Wang, J., & Chen, Z. (2024). Application of gelatin-based composites in bone tissue engineering. *Heliyon*, 10(16). <https://doi.org/10.1016/j.heliyon.2024.e36258>
- Wu, J., & Yue, B. (2024). Regulation of myogenic cell proliferation and differentiation during mammalian skeletal myogenesis. *Biomedicine & Pharmacotherapy*, 174, 116563. <https://doi.org/10.1016/j.biopha.2024.116563>
- Wulf, A., Mendgaziev, R. I., Fakhrullin, R., Vinokurov, V., Volodkin, D., & Vikulina, A. S. (2022). Porous alginate scaffolds designed by calcium carbonate leaching technique. *Advanced Functional Materials*, 32(14), 2109824. <https://doi.org/10.1002/adfm.202109824>
- Xue, N., Ding, X., Huang, R., Jiang, R., Huang, H., Pan, X., ... & Wang, Y. (2022). Bone tissue engineering in the treatment of bone defects. *Pharmaceuticals*, 15(7), 879. <https://doi.org/10.3390/ph15070879>
- Yameny, A. A. (2024). A Comprehensive Review on Nanoparticles: Definition, Preparation, Characterization, Types, and Medical Applications. *Journal of Medical and Life Science*, 6(4), 663–672. <https://doi.org/10.21608/jmals.2024.419629>
- Yang, X., Chung, E., Johnston, I., Ren, G., & Cheong, Y. K. (2021). Exploitation of antimicrobial nanoparticles and their applications in biomedical engineering. *Applied Sciences*, 11(10), 4520. <https://doi.org/10.3390/app11104520>
- Ye, J., Miao, B., Xiong, Y., Guan, Y., Lu, Y., Jia, Z., Wu, Y., Sun, X., Guan, C., He, R., Xiong, X., Jia, H., Jiang, H., Liu, Z., Zhang, Y., Wei, Y., Lin, W., Wang, A., Wang, Y., ... Peng, J. (2025). 3D printed porous magnesium metal scaffolds with bioactive coating for bone defect repair: enhancing angiogenesis and osteogenesis. *Journal of Nanobiotechnology*, 23(1). <https://doi.org/10.1186/s12951-025-03222-3>
- Zhang, G., Zhen, C., Yang, J., Wang, J., Wang, S., Fang, Y., & Shang, P. (2024). Recent advances of nanoparticles on bone tissue engineering and bone cells. *Nanoscale Advances*, 6(8), 1957–1973. <https://doi.org/10.1039/D3NA00851G>
- Zielińska, A., Karczewski, J., Eder, P., Kolanowski, T., Szalata, M., Wielgus, K., ... & Souto, E. B. (2023). Scaffolds for drug delivery and tissue engineering: The role of genetics. *Journal of Controlled Release*, 359, 207–223. <https://doi.org/10.1016/j.jconrel.2023.05.042>


Received: August 13th, 2025

Accepted: November 1st, 2025

Aponte Lopez, Nicole: BSc. in Biomedical Engineering, 2027, Polytechnic University of Puerto Rico. San Juan, PR-USA. <https://orcid.org/0009-0008-6182-9708>

Rondón Contreras, Jairo: Ph.D. in Applied Chemistry, mention: Materials Study, 2015, Universidad de Los Andes. Professor of Biomedical & Chemical Engineering Departments, at the Polytechnic University of Puerto Rico. San Juan, PR-USA. Email: jrondon@upr.edu <https://orcid.org/0000-0002-9738-966X>

Gonzalez-Lizardo, Angel: Ph.D. Engineering, 2003, University of Dayton, Dayton, OH. Professor; Director, Plasma Engineering Laboratory and Sponsored Research Office at the Polytechnic University of Puerto Rico, San Juan, Puerto Rico, USA. Email: agonzalez@pupr.edu
 <https://orcid.org/0000-0002-0722-1426>

Lugo Claudio, Doctor in Chemistry in Applied Chemistry, Materials Study, 2017. (ULA). Professor at the University of the Andes, Faculty of Sciences, Kinetics and Catalysis Laboratory. Email: claudiolugo@ula.ve
 <https://orcid.org/0000-0001-8003-0354>

Physicochemical and sensory evaluation of artisanal blackberry wines produced and marketed in Mérida state, Venezuela

Evaluación fisicoquímica y sensorial de vinos artesanales de mora producidos y comercializados en el estado Mérida, Venezuela

Moreno, Andrea^{1*}; Contreras, Ruvit, Carvajal, Martha, González, Aura¹, De Lima, Aida¹, Noboa, Glenda¹, Izaguirre, César¹, Celis, María -Teresa², Zoghbe, Yamil³

¹ Laboratory of Food Science, Engineering and Biotechnology, Faculty of Engineering, School of Chemical Engineering, Universidad de los Andes, Mérida, Venezuela.

² Laboratory of Polymers and Colloids, Faculty of Engineering, School of Chemical Engineering, Universidad de los Andes, Mérida, Venezuela.

³ Technical Laboratory for Quality Control in Construction, GH SpA, Cajón, Chile

*anmorenas@gmail.com

Abstract

This study aimed to conduct a comparative analysis of the physicochemical and sensory characteristics of three artisanal blackberry wines produced in the towns of Caño Zancudo (Wine 1), El Valle (Wine 2), and La Azulita (Wine 3), in the state of Mérida, Venezuela. The evaluation focused on determining their quality and compliance with Venezuelan national regulations. Key parameters such as alcohol content, total and volatile acidity, dry extract, tannin content, reducing and total sugars, and methanol concentration were measured. In addition, a panel of 41 semi-trained tasters performed a sensory evaluation of the samples. The results showed significant differences among the wines. Although all complied with the alcohol content range stipulated by COVENIN Standard 3042, all three wines presented dry extract levels far exceeding those permitted by COVENIN Standard 3287, indicating deficiencies in the standardization of production processes. Wine 2 presented a serious defect due to its high volatile acidity (3.03 g/L), exceeding the limit permitted by COVENIN Standard 3286 and resulting in rejection during the sensory evaluation. Wine 3 received the highest score, with 67.04 points and a preference of 75.61% of the panel, standing out for its sensory balance. The study highlights the need to improve and standardize artisanal production methods to ensure the quality and safety of these wines.

Keywords: blackberry wine, alcoholic fermentation, panelists, sensory analysis, standardization.

Resumen

El presente estudio tuvo como objetivo realizar un análisis comparativo de las características fisicoquímicas y sensoriales de tres vinos artesanales de mora elaborados en las localidades de Caño Zancudo (Vino 1), El Valle (Vino 2) y La Azulita (Vino 3), del estado Mérida, Venezuela. La evaluación se centró en determinar su calidad y conformidad con la normativa nacional venezolana. Se midieron parámetros clave como grado alcohólico, acidez total y volátil, extracto seco, contenido de taninos, azúcares reductores y totales, y concentración de metanol. Además, un panel de 41 catadores semientrenados realizó una evaluación sensorial de las muestras. Los resultados mostraron diferencias significativas entre los vinos. Aunque todos cumplieron con el rango de grado alcohólico estipulado por la Norma COVENIN 3042, los tres vinos presentaron niveles de extracto seco muy superiores a los permitidos por la Norma COVENIN 3287, lo que evidencia deficiencias en la estandarización de los procesos de producción. El Vino 2 presentó un defecto grave debido a su alta acidez volátil (3,03 g/L), superando el límite permitido por la Norma COVENIN 3286 y generando rechazo en la evaluación sensorial. El Vino 3 obtuvo la mejor aceptación, con 67,04 puntos y preferencia del 75,61% del panel, destacando por su equilibrio sensorial. El estudio resalta la necesidad de mejorar y uniformar los métodos de producción artesanal para asegurar la calidad y seguridad de estos vinos.

Palabras clave: vino de mora, fermentación alcohólica, panelistas, análisis sensorial, estandarización.

1. Introduction

Since ancient times, the discovery of fermentation has allowed humans to produce alcoholic beverages, the consumption of which was associated with feelings of pleasure and relaxation (García Zapateiro et al., 2016). Currently, wine production from fruit has gained relevance in various countries, especially those whose climatic conditions limit grape cultivation. This situation has driven the search for viable alternatives through the use of local fruits. To achieve proper alcoholic fermentation, it is necessary to adapt the environment to the available resources and establish technical parameters that guarantee the quality of the final product (Córdova et al., 2018).

Due to the abundant cultivation of blackberries in tropical countries, this fruit has been used as a viable alternative to grapes for the production of fermented wines, demonstrating remarkable oenological potential. The wine is produced from blackberry juice, which imparts distinctive organoleptic and sensory properties attributable to its chemical profile, characterized by the presence of compounds such as anthocyanins and carotenoids (Beltrán et al., 2023). These parameters were evaluated through physicochemical analyses and are reflected in the characteristic color of wines made with this fruit.

Despite the wide variety of artisanal blackberry wines in the region, a gap persists in their physicochemical and sensory characterization from a scientific perspective. This deficiency limits objective comparison between products, hinders the identification of factors that influence their quality, and impedes the design of effective strategies to improve production processes. Although some studies have addressed aspects such as fermentation and stabilization, significant variations in physicochemical parameters have been reported, influenced by both the properties of the fruit and the specific conditions of the process. These factors are crucial for ensuring the final product quality and its safety for the consumer.

The production of artisanal wines from fruits other than grapes has gained particular interest in various regions of Latin America as a way to diversify local production, add value to agricultural products, and preserve traditional knowledge. In the case of Mérida State, Venezuela, the use of blackberries (*Rubus glaucus*) as a raw material for wine production represents a sustainable alternative, given their widespread cultivation in Andean areas, their favorable organoleptic properties, and their richness in natural antioxidant compounds. Furthermore, it fosters the generation of direct and indirect employment and opens opportunities for the innovation of new products and expansion into new markets. (Torres Mejía & Torres Mejía, 2022).

The *Rubus* species cultivated in the Andean region of Venezuela is *Rubus glaucus* Benth., which is likely a hybrid of *Rubus* subgroup “*Idaeobatus*” (raspberry) and *Rubus*

subgroup “*Eubatus*” (blackberry). (Cedeño, L. and Carrero, C., 2000). The Andean blackberry (*Rubus glaucus*) is a fruit widely enjoyed for its exquisite flavor, aroma, and attractive color, both for fresh consumption and for its ease of processing as a raw material for preparing sweets, jams, juices, ice cream, syrups, and even wine. (Coronel, 2011).

Blackberries have demonstrated excellent adaptability to clay soils and tropical climates, which favors their use in the production of artisanal wines with a high antioxidant content. (Núñez, 2022). The production of artisanal blackberry wine has generated interest due to its economic and cultural value, as well as the potential health benefits it may offer. Research indicates that moderate wine consumption may reduce the incidence of certain age-related chronic diseases, such as heart disease, hypertension, metabolic diseases, and neurodegenerative diseases. (Johnson & De Mejia, 2011). Unlike grape wine, blackberry wine requires specific standardization in its production process, as the concentration of sugars, acidity, and phenolic compounds can vary significantly depending on the blackberry variety, the degree of ripeness at harvest, and the agroclimatic conditions of the region (Torres Mejía & Torres Mejía, 2022).

According to the Venezuelan Standard COVENIN 3342, the alcoholic strength of a wine should be between 7 and 14% ABV. This refers to the milliliters of ethanol and its homologues, such as methanol, higher alcohols, and 2,3-butanediol, present in a wine, which originate from the fruit or are formed during fermentation (Fernández et al., 2009). At a commercial level, this parameter is of great importance since wines and other alcoholic beverages are marketed and priced according to their alcohol content.

Among the compounds that make up wines are carbohydrates in the form of sugars. The best known are sucrose, glucose, and fructose, but there are others that, although found in lower concentrations in the products we consume daily, are very important due to their physical, chemical, and nutritional properties (Badui Dergal, 2006). Total sugars consider the overall concentration of all sugars, calculated after an acid hydrolysis process. To determine the sugar content in different samples of blackberry wine, the Fehling's and Lane-Eynon methods were combined. These methods are based on the reducing power of the carbonyl group of aldehydes. The Fehling's method is a qualitative method that indicates the reduction of copper by the sugar with the appearance of a red precipitate. While the Lane-Eynon method is a titration that allows quantifying the sugar present using tabulated values (Universidad Nacional de San Juan, 2018).

Wines must exhibit qualities such as color, fruity aroma, and distinctive flavor when evaluating their quality and consumer acceptance. These attributes are due to the presence of anthocyanins, tannins, and other phenolic compounds. Total acidity refers to the acids that make up wine, primarily tartaric and malic acids; other acids are

present in smaller amounts (lactic and acetic). The combined action of all these acids contributes to the development of aromas through the esterification of alcohols (Beltrán et al., 2023).

The food industry uses sensory evaluation as a tool to assess consumer perception of a product as a whole or of a specific aspect of it. In this type of testing, the information provided by a panel is perceived through the sensory organs of sight, smell, hearing, taste, and touch (Ávila de Hernández & González Torrivilla, 2011).

Furthermore, according to Ratti (2011), sensory analysis of wines allows for the evaluation of different attributes individually and/or globally, as well as the appreciation of their positive or negative characteristics. Among these, tannins stand out; these plant compounds give structure and body to the wine, as well as astringency. They influence the flavor and promote the aging process, as they tend to soften over time (Peña Neira, 2006).

In this context, the present study aims to conduct a comparative analysis of the physicochemical and sensory characteristics of three types of artisanal blackberry wines produced and marketed in Mérida, Venezuela. Various parameters were evaluated to identify the factors that influence the quality and safety of the product and to verify its compliance with the requirements established in the Venezuelan Standard COVENIN 3342 for wines and their derivatives. This research seeks to contribute scientific knowledge that will help in the development of high-quality functional beverages that are safe for consumers and have potential for increased value in the local market.

2. Experimental Procedure

To achieve the stated objectives, a sampling procedure was carried out, which included the acquisition of three samples of artisanal wine from the state of Mérida. This approach allows for the evaluation of the quality and characteristics of the products available to the consumer. The methodology was structured in two fundamental areas: physicochemical analysis and sensory evaluation. For the physicochemical analysis, the procedures and methodologies established in Venezuelan regulations were followed, primarily using COVENIN 3342 as the reference standard. Within this framework, the following key parameters were determined: alcoholic strength, volatile acidity and total acidity, dry extract, tannin content, sugar concentration, and the presence of methanol, the latter determined by a spectrophotometric colorimetric method.

Additionally, a sensory evaluation was conducted with a panel of semi-trained tasters to assess the organoleptic properties of the wines. This analysis focused on attributes such as color, aroma, flavor, and texture, in order to obtain a complete profile of the quality and acceptance of the products studied.

2.1 Alcohol Content

The method is based on the distillation of an aliquot of the wine sample, separating the ethanol from the non-volatile components, following the COVENIN 3042-1993 standard, with some variations. The ethanol content in the distillate is determined using a hydrometer alcoholmeter and expressed in degrees Gay-Lussac (GL) using a scale calibrated directly in units of alcohol concentration.

2.2 Volatile Acidity

The method is based on the separation of volatile acids (mainly acetic acid) from the wine by steam distillation. The distilled volatile acids are collected in a container and titrated with a standardized sodium hydroxide (NaOH) solution until an endpoint is reached, indicated by a visual indicator (phenolphthalein) or by potentiometric detection at a specific pH according to COVENIN 3286:1997. Volatile acidity is conventionally expressed as grams of acetic acid per liter (g/L).

2.3 Total Acidity

The method is based on the volumetric titration of the acids present in the wine with a standardized sodium hydroxide solution, until an endpoint is reached, indicated by a visual indicator (phenolphthalein) or by potentiometric detection (SPER SCIENTIFIC 860033 digital potentiometer) at a specific pH according to COVENIN 3286:1997. Total acidity is conventionally expressed as grams of tartaric acid per liter (g/L).

2.4 Dry Extract

The determination of tartaric acid, malic acid, sugars, and other crystals is carried out by evaporating volatile substances at atmospheric pressure and the boiling point of water, following the methodology of COVENIN standard 3287:1997.

2.5 Tannins

The method consists of the hot acid hydrolysis of tannins in the presence of butanol and an iron salt as a catalyst. This process transforms proanthocyanidins into anthocyanidins (cyanidin and delphinidin), which are quantified by visible light spectrophotometry at 550 nm. The final concentration is obtained by subtracting the pre-existing anthocyanidins in the sample and is calculated in mg/L of wine using a cyanidin calibration curve. This method is based on the manual of analytical techniques for musts and wines (Nazralla et al., 2009).

2.6 Sugars

The methodology employed was based on the procedures established in COVENIN Standard 3285:1987. Initially, Fehling's solution (A and B) was prepared and standardized with a 5% glucose solution. The blackberry wine was diluted in two steps to reach a final concentration of 10% for analysis. In the determination of reducing sugars, the diluted blackberry wine sample was used to titrate Fehling's solution under hot conditions. The amount of blackberry wine required for the color change allows for the quantification of reducing sugars. To measure total sugars (including non-reducing sugars such as sucrose), a portion of the diluted wine sample was subjected to acid hydrolysis (with hydrochloric acid and heat) to convert non-reducing sugars (such as sucrose) into reducing sugars. After neutralization, it was titrated in the same way as in the previous step. The concentration of total and reducing sugars is expressed in grams of sugar per liter (g/L). Total sugars were also determined using a digital refractometer that measures Brix degrees (°Brix).

2.7 Methanol

A colorimetric method, based on standard NTC 5159, was used to quantify methanol. The methanol in the sample was oxidized to formaldehyde using potassium permanganate. The formaldehyde then reacted with chromotropic acid to form a colored compound. The intensity of this color, which is directly proportional to the original amount of methanol, was measured with a spectrophotometer at 575 nm (Instituto Colombiano de Normas Técnicas y Certificación, 2003).

2.8 Sensory Analysis

For the sensory analysis of the blackberry wines, a total of 41 semi-trained panelists were used to evaluate the following variables: color, aroma, flavor, texture, and overall experience. This experiment consisted of three phases. In the visual phase, color intensity and turbidity were evaluated; in the olfactory phase, odor intensity and fruity character were assessed; and in the gustatory phase, flavor intensity, sweetness, acidity, persistence in the mouth, and the drying effect of the retronasal passage were evaluated. These variables were assessed according to a modified Robert and Parker scale, totaling 100 points (Torres Mejía & Torres Mejía, 2022).

2.9 Statistical Analysis

For the statistical treatment of the experimental data, an analysis of variance (ANOVA) was applied to determine if

there were significant differences between the treatments evaluated. This method allows for the comparison of the means of several groups and establishes whether the variations observed in the response variable are attributable to the factors studied or to chance. The assumptions of normality and homogeneity of variances were verified beforehand. When significant differences were detected ($\alpha < 0.05$), multiple comparison tests were performed to identify the treatments that differed from each other.

3. Results and discussion

3.1 Physicochemical Characterization

Table 1 presents a comparative analysis of three samples of artisanal blackberry wine produced in the state of Mérida, identified as Wine 1, Wine 2, and Wine 3, based on their main physicochemical parameters. The interpretation is based on the values obtained and the statistical significance analysis (α is less than or equal to 0.05), indicated by the superscripts (a, b, c), where different letters imply statistically significant differences.

Regarding alcohol content, all three wines have an alcohol content within the typical range for table wines and corresponds to the value shown on the commercial label. Wine 1 (14 °GL) is the most alcoholic, followed by Wine 2 (13 °GL) and Wine 3 (12 °GL). This variation is due to the different fermentation methods and the sugar content of the blackberry must. It is important to note that the alcohol content of the three wines complies with the range established by COVENIN Standard 3342, between 7 and 14% ABV, and with the MERCOSUR Wine Regulations, which establish a minimum limit of 7% ABV for wines.

Regarding volatile acidity, the Venezuelan Standard COVENIN 3342 establishes a limit of 1.20 g/L for this variable. The volatile acidity analyses applied to blackberry wines 1, 2, and 3 recorded values of 0.22 g/L, 3.03 g/L, and 2.17 g/L, respectively. According to these results, blackberry wine 1 is below the established limit, suggesting acceptable sensory quality in this respect. However, the results obtained indicate that blackberry wines 2 and 3 have volatile acidity levels significantly higher than the limit established by Venezuelan regulations (1.20 g/L), suggesting excessive exposure to oxygen during winemaking or storage. According to Causes Of Wine Spoilage And How To Prevent Them - Grapeworks - Taniun Machinery (2023), high acidity can inhibit bacterial growth, negatively affecting the taste and quality of the wine.

Total acidity is a key parameter for evaluating wine quality, as it affects both microbiological stability and sensory characteristics. In this regard, Beltran et al. (2023) indicate that maintaining adequate total acidity in blackberry wine is necessary to balance its natural sweetness, providing a freshness that prevents the wine from being too heavy or cloying.

Table 1. Physicochemical analysis of blackberry wine.

Parameter	Wine_1	Wine_2	Wine_3	Method
Alcohol content (°GL)	14	13	12	COVENIN 3042-1993
Volatile acidity (g/L)	0,22 ^a	3,03 ^b	2,17 ^c	COVENIN 3286:1997
Total acidity (g/L)	8,75 ^a	11,95 ^b	7,20 ^b	COVENIN 3286:1997
Dry extract (g/L)	262,49 ^a	245,53 ^a	173,53 ^b	COVENIN 3287:1997
Tannins (g/L)	198,45 ^a	77,18 ^a	132,30 ^a	(Nazralla et al., 2009)
Reducing sugars (g/L)	13,82 ^a	13,05 ^b	11,16 ^c	COVENIN 3285:1987
Total sugars (g/L)	14,01 ^a	13,91 ^a	11,24 ^b	COVENIN 3285:1987
°Brix	14,4	14,2	11,7	Refractómetro digital
Methanol (mg/L)	39,6	39,6	39,6	NTC 5159

^{a,b,c}: The mean values of the parameters for each sample with different superscripts are significantly different ($\alpha \leq 0,05$)

The results summarized in Table 1 show that blackberry wine 1 had an average acidity of 8.75 g/L, considered suitable for artisanal fruit wines. Blackberry wine 2 registered a higher acidity of 11.95 g/L, while wine 3 had an acidity of 7.20 g/L. It is worth noting that all three wine samples exhibited tartaric acid values between 5 and 12 g/L, which comply with the range established by the MERCOSUR Wine Regulations. However, blackberry wine 2 stands out as the most acidic in the group, and according to the study by González Hernández (2016), this high acidity could be due to a higher concentration of natural organic acids in the fruit or specific conditions during fermentation, which could result in a more pronounced acidic taste. The variations observed in total acidity among the wines could be explained by the characteristic acidity of blackberries. According to CataTú (2022), factors such as temperature, fermentation duration, or inoculum characteristics could favor an increase in acid production in the fermented must.

In the dry extract measurements of the blackberry wines, wine 1 had a value of 262.5 g/L, the highest in the group, followed by blackberry wine 2, which had a concentration of 245.5 g/L, and finally wine 3 with a result of 173.5 g/L, which is notably the lightest. In all cases, the results obtained exceed the limits established in the COVENIN 3342 standard, whose maximum value is 28 g/L of dry extract. According to the study by Vega et al. (1971), high dry extract values suggest non-standardized production, which hinders the proper conversion of sugars into alcohol.

A drastic difference is observed in the tannin results obtained in this trial. Blackberry wine 1 has a very high tannin content of 198.45 mg/L, predicting a strong sensation of astringency and structure in the mouth. Blackberry wine 3, with a value of 132.3 mg/L, has a moderate level, while

blackberry wine 2 presented the lowest tannin value at 77.18 mg/L. According to the study by Peña Neira (2006), a low tannin value can make blackberry wine appear softer in texture.

The values obtained in the determination of reducing sugars in the blackberry wines show a hierarchy. First, blackberry wine 1 has a value of 13.82 g/L, followed by blackberry wine 2 with 13.04 g/L, and finally blackberry wine 3, the driest of the group with 11.16 g/L. The differences, especially between blackberry wines 1 and 2 and blackberry wine 3 (a difference of 2.69 g/L), suggest variations in the winemaking process or the raw materials used, ranging from fruit ripeness and the fermentation process to the yeast strain employed. These results allow us to classify all three wines as semi-dry. According to Vidaurre Rojas (2004), in a dry wine, the reducing sugar content is less than 5 g/L. A semi-dry or off-dry wine contains between 5 and 60 grams per liter of reducing sugars, while sweet wines have a reducing sugar content greater than 60 g/L.

The values for reducing and total sugars are very similar in each blackberry wine, indicating a predominance of simple sugars (glucose and fructose). Blackberry wine 1 and blackberry wine 2 are the sweetest, with total sugar values of 14 and 13.89 g/L and Brix values of 14.4 and 14.2 °Brix, respectively, while blackberry wine 3 is slightly drier with a total sugar concentration of 11.2 g/L and Brix value of 11.7 °Brix. According to Vidaurre Rojas (2004), the alcohol content of wines is proportional to their tannin content, since a higher sugar content implies a higher alcohol content.

Methanol in wines is a natural byproduct formed during fermentation from the enzymatic demethylation of pectins present in the raw material. The methanol concentration in each of the wine samples was 39.6 mg/L. This quantification was performed following the standardized procedure described in Colombian Technical Standard NTC 5159. Blackberries (*Rubus glaucus*), like other berries and fruits, are characterized by a high pectin content in their cell walls and skin, which are rich in methyl esters. According to the study by Hodson et al. (2017), the result obtained indicates that there was normal extraction of compounds from the blackberry skin during maceration, releasing pectins into the must.

3.2 Sensory Evaluation

The true quality of a wine is revealed by connecting chemical data with consumer perception. According to the study by Torres Mejía & Torres Mejía (2022), these attributes are the pillars of oenological quality. Tables 2 and 3 report the sensory evaluation performed on three blackberry wine samples, which reveal significant differences in their organoleptic profiles and in the overall acceptance by the tasting panel. The results obtained by the panel of semi-trained tasters allow us to establish a clear hierarchy of preference, where blackberry wine 3 stands out as having the

highest perceived quality, followed by blackberry wine 1, and finally blackberry wine 2 as having the lowest acceptance, as shown in Figure 1.

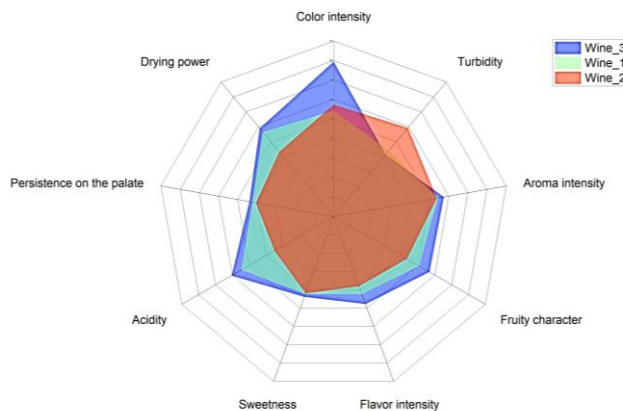


Figure 1. Sensory Characterization.

According to the results shown in Tables 2 and 3, Blackberry Wine 3 obtained the highest total score (67.04 points), which directly correlates with the most favorable overall experience: 75.61% of the tasters rated it positively (31.71% "I liked it very much" and 43.9% "I liked it"), while only 9.76% expressed a neutral opinion ("I neither liked it nor disliked it"). Based on the values obtained in the physicochemical analysis and sensory evaluation, Blackberry Wine 3 presents several key attributes that, together, create a balanced and appealing wine.

Table 2. Sensory Analysis Score.

Characteristic	Wine_1	Wine_2	Wine_3
Color intensity	7,80	7,62	9,94
Turbidity	6,40	7,93	6,16
Aroma intensity	7,44	7,38	7,74
Fruity character	7,07	6,34	7,68
Flavor intensity	6,24	5,80	6,78
Sweetness	6,24	6,20	6,39
Acidity	7,46	5,51	8,05
Persistence on the palate	6,24	6,05	6,39
Drying power	7,66	6,34	7,90
Total	62,57	59,17	67,04

Wine 3 stands out notably for its color intensity (9.94), although with a slight turbidity (6.16). Its aroma intensity (7.74) is subtly superior to the others, and its fruit character (7.68) is the highest. According to CataTú (2024), fruit character is one of the main drivers of consumer preference. Furthermore, the most defining aspect of Blackberry Wine 3 is its flavor balance. It presents the highest flavor intensity (6.78) and, crucially, the highest acidity (8.05). High acidity in a wine, along with a drying effect (7.90), creates a

complex, structured mouthfeel with good persistence (6.39). According to Fernández et al. (2009), acidity enhances the characteristic aromas of blackberries, contributing to a more complex and appealing sensory profile, with a clean and refreshing finish.

Table 3. Overall wine experience.

Overall Experience	Wine_1(%)	Wine_2(%)	Wine_3(%)
I liked it a lot	24,39	7,32	31,71
I liked it	39,02	29,27	43,90
I didn't like it	24,39	12,20	9,76
I liked it a little	9,76	26,83	12,20
I didn't like it	2,44	24,39	2,44

Wine 1 is positioned as an intermediate option, with a total score of 62.47 points. Its reception was mostly positive (63.41% combining "I liked it a lot" and "I liked it"), but a significant 24.39% of the tasters were indifferent, suggesting that it is a decent wine but not as exciting as Wine 3. Furthermore, Blackberry Wine 1 has a balanced sensory profile; its acidity (7.46) and drying power (7.66) are good, giving it a correct and pleasant structure on the palate. Its aroma intensity (7.44) and fruity character (7.07) are adequate, surpassing Blackberry Wine 2 but without reaching the expressiveness of Blackberry Wine 3. However, Blackberry Wine 1 obtained a lower flavor intensity (6.24) and fruity character (7.07) compared to Blackberry Wine 3, according to the tasting panel. Therefore, it is a well-made wine, without obvious defects, but lacking the complexity and intensity that characterize a superior quality wine. This aligns with «Vino de Calidad: Factores y Características» (2020).

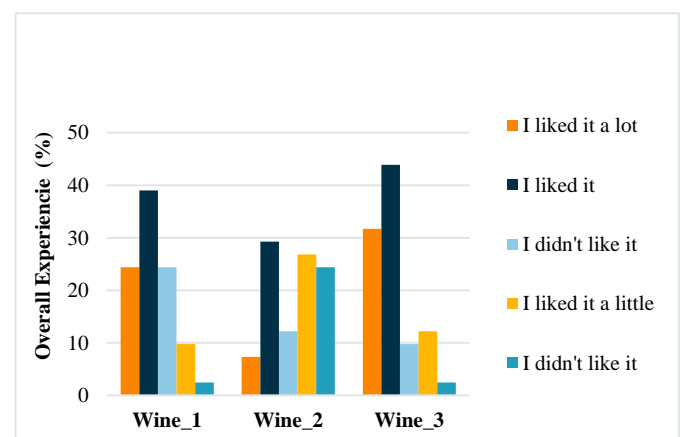


Figure 2. Overall sensory analysis experience.

Regarding Blackberry Wine 2, it received the lowest rating (59.17 points) and the lowest overall acceptance from the tasting panel, with 53.66% of panelists expressing a

negative opinion ("I didn't like it much") or indifference ("I neither like it nor dislike it"). The most notable deficiency of Blackberry Wine 2 was its acidity, which resulted in a low score for this attribute, making it seem lacking in freshness and unbalanced. This may have contributed to the low scores for flavor intensity (5.80) and persistence on the palate (6.05), since acidity is a flavor enhancer. Similarly, it also obtained the lowest scores for fruit character (6.34) and aroma intensity (7.38). The lack of a clear fruit expression and limited aromatic intensity make the wine less appealing and memorable to the taster. Although its color intensity was not as badly rated (7.62), its turbidity score (7.93) was the highest of the three wines, suggesting a potential lack of clarity that may be penalized by consumers. Furthermore, its low drying power (6.34) indicates a weak tannic structure, which, combined with low acidity, results in a wine with little body and character, according to «Vino de Calidad: Factores y Características» (2020). Therefore, Blackberry Wine 2 was perceived as an unbalanced wine, negatively impacting its intensity, persistence, and overall freshness, making it the least preferred by the panel.

4. Conclusions and recommendations

The three blackberry wines analyzed meet the alcohol content requirement (between 7 and 14 °GL) stipulated by Venezuelan Standard COVENIN 3342. However, all significantly exceed the maximum dry extract limit (28 g/L), suggesting a lack of control in the concentration and clarification processes during their artisanal production.

The quality of artisanal blackberry wines is heterogeneous. It was identified that the balance between total acidity, sweetness, and a pronounced fruity character are the determining factors for high sensory acceptance, as demonstrated in wine 3. On the other hand, high volatile acidity is a critical indicator of deterioration that directly impacts the product's low quality and rejection, as occurred with wine 2.

All three wines are safe for consumption, as their methanol levels (39.6 mg/L) are well below the maximum limit of 300 mg/L permitted by the COVENIN 3042 standard, ruling out any risk of toxicity from this compound.

This study highlights the need to implement standardized protocols in the production of artisanal blackberry wines in the region. Greater control over fermentation variables and physicochemical parameters is essential to avoid serious defects, improve consistency, and develop high-quality products that meet consumer preferences.

References

Ávila de Hernández, Rita M, & González-Torrivilla, César C. (2011). La evaluación sensorial de bebidas a base de

fruta: Una aproximación difusa. Universidad, Ciencia y Tecnología, 15(60), 171-182. Recuperado en 07 de junio de 2025, de http://ve.scielo.org/scielo.php?script=sci_arttext&pid=S1316-48212011000300007&lng=es&tlng=es.

Badui Dergal, S. (2006). Química de los Alimentos (Cuarta ed.). (E. Quintanar Duarte, Ed.) México, México: PEARSON.

Beltrán Balarezo, C., Yáñez Romero, M. E., Flores Acosta, A. R., Carchi Tandazo, T. A., & Lam, A. M. (2023). Influencia de las propiedades fisicoquímicas del vino de mora, determinadas mediante análisis sensorial. *Ciencia Latina Revista Científica Multidisciplinar*, 7(4). https://doi.org/10.37811/cl_rcm.v7i4.7125

CataTú. (2021, 16 julio). *El Color del Vino según distintos Tipos de Vinos. Factores que influyen*. Blog. <https://catatu.es/blog/color-vino/>

CataTú. (2024, 8 mayo). *Los aromas del vino. Primarios, secundarios y terciarios*. Blog. <https://catatu.es/blog/aromas-vino/>

Causes of Wine Spoilage and How to Prevent Them - Grapeworks - Tanium Machinery. (2023, 20 abril). Grapeworks - Tanium Machinery. <https://grapeworks.com.au/news/winemaking/causes-of-wine-spoilage-and-how-to-prevent-them/#:~:text=Deterioro%20bacteriano%20del%20vino,minimizar%20la%20presencia%20de%20bacterias>.

Cedeño, L., & Carrero, C. (2000). Coniothyrium fuckelii causando quema en cañas de mora de Castilla. *Revista Científica de la Facultad de Ciencias Agropecuarias*, 13(2), 38.

Córdova Guambo, I. V., Tituaña Pulluquitin, G. I., Tobar Jácome, M. C., & Lascano Sumbana, A. V. (2018). Comparación del comportamiento fermentativo de levadura de panificación y levaduras vínicas (uvaferm cm, lalvin ec1118, lalvin qa23) y sus efectos sobre la calidad de vinos de mora (rubus glaucus benth). *Revista Caribeña de Ciencias Sociales*. <https://www.eumed.net/rev/caribe/2018/05/calidad-vinos-mora.html>

Cómo apreciar el sabor del vino. (2023, 14 diciembre). El Blog de Vinoselección. https://www.vinoseleccion.com/blog/vinos/apreciar-sabor-vino/?srsltid=AfmBOoq91BlftZH0V7JUfG7JDmmbIB_ouAZgbpyimif7doE01i58VutK

Coronel Feijó, M. A. (2011). Estandarización y optimización de procesos de vino de mora de Castilla (Rubus glaucus Benth). Tsafiqui - Revista de Investigación Científica UTE, (2), 20.

Cruz de Aquino, Mario A. de la, Martínez-Peniche, Ramón A., Becerril-Román, A. Enrique, & Chávaro-Ortiz, Ma. del Socorro. (2012). Caracterización física y química de vinos tintos producidos en Querétaro. *Revista fitotecnia mexicana*, 35(spe5), 61-67. Recuperado en 07 de junio

- de 2025, de http://www.scielo.org.mx/scielo.php?script=sci_arttext&pid=S0187-73802012000500013&lng=es&tlng=es.
- Fernández, V., Berradre, M., Sulbarán, B., Ojeda de Rodríguez, G., & Peña, J. (2009). Caracterización química y contenido mineral en vinos comerciales venezolanos. *Revista de La Facultad de Agronomía*, 26(3), 382–397. http://ve.scielo.org/scielo.php?script=sci_arttext&pid=S0378-78182009000300005&lng=es&nrm=iso&tlng=es
- García Zapateiro, Luis Alberto, Florez Mendoza, Cielo Inés, & Marrugo Ligardo, Yesid. (2016). Elaboración y caracterización fisicoquímica de un vino joven de fruta de borjón (B patinoi Cuatrec). Ciencia, docencia y tecnología, (52), 507-519. Recuperado en 06 de junio de 2025, de https://www.scielo.org.ar/scielo.php?script=sci_arttext&pid=S1851-17162016000100020&lng=es&tlng=es.
- González Hernández, M. (2016). Características sensoriales y composición no volátil de vinos tintos: avances en la exploración de la calidad. Dialnet. <https://dialnet.unirioja.es/servlet/tesis?codigo=46984>
- González Seguí, H. o. G., Hernández López, J., & Hendrik Giersiepen, J. H. (2019). *Metanol: tolerancias y exigencias en las normas para mezcal y bebidas de agave*. *Revista RIVAR*, 7(19), 1-21. <https://doi.org/10.35588/rivar.v7i19.4246>
- Hodson, G., Wilkes, E., Azevedo, S., & Battaglene, T. (2017). Methanol in wine. *BIO Web Of Conferences*, 9, 02028. <https://doi.org/10.1051/bioconf/20170902028>
- Instituto Colombiano de Normas Técnicas y Certificación. (2003, 26 febrero). NTC 5159 DETERMINACION CONTENIDO DE METANOL.pdf. Scribd. <https://es.scribd.com/document/144965156/NTC-5159-DETERMINACION-CONTENIDO-DE-METANOL-pdf>
- Johnson, M. H., & Gonzalez de Mejia, E. (2011). Comparison of chemical composition and antioxidant capacity of commercially available blueberry and blackberry wines in Illinois. *Journal of Food Science*, 77(1), C141–C148. <https://doi.org/10.1111/j.1750-3841.2011.02505.x>
- Los taninos del vino | Tannins.org. (2022, 30 diciembre). Tannins.org. <https://www.tannins.org/es/los-taninos-del-vino/>
- Nazralla, J. J. B., Paladino, S. C., Vila, H. F., & Lucero, C. C. (2009). Manual de técnicas analíticas para mostos y vinos. Instituto Nacional de Tecnología Agropecuaria. <https://repositorio.inta.gob.ar/handle/20.500.12123/6664>
- Norma Venezolana COVENIN: 3042 (1997). Bebidas alcohólicas. Determinación del grado alcohólico.
- Norma Venezolana COVENIN: 3285 (1997). Vinos y sus Derivados. Determinación de azúcares.
- Norma Venezolana COVENIN: 3286 (1997). Vinos y sus Derivados. Determinación de acidez total y acidez volátil.
- Norma Venezolana COVENIN: 3287 (1997). Vinos y sus Derivados. Determinación de extracto seco libre.
- Norma Venezolana COVENIN: 3342 (1997). Vinos y sus Derivados.
- Núñez Cárdenas, L. (2022). Identificación y caracterización de los productos bioactivos presentes en los vinos cubanos de alta gama (Tesis doctoral, Universidad de Córdoba, UCOPress). <http://hdl.handle.net/10396/23354>
- Peña Neira, A. (2006). En la calidad de uvas y vino Los taninos y su importancia. VENDIMIA. <http://www.gie.uchile.cl/pdf/Alvaro%20Pe%F1a/taninos.pdf>
- Ratti, R. (2011). Cómo degustar los vinos. Manual del catador. Ed. Mundi-Prensa, Madrid (España).
- Reglamento Vitivinícola del MERCOSUR. (1997). WIPO. <https://www.wipo.int/wipolex/en/legislation/details/10477>
- Rua Joao, L. f. (s.f.). TECNAL. doi:13.413-102
- Shen, J., Huang, W., You, Y., & Zhan, J. (2024). Controlling strategies of methanol generation in fermented fruit wine: Pathways, advances, and applications. *Comprehensive Reviews In Food Science And Food Safety*, 23(6). <https://doi.org/10.1111/1541-4337.70048>
- Torres Mejía, J. A., & Torres Mejía, F. (2022). Evaluación fisicoquímica del vino de mora (*Rubus glaucus*), elaborado en Santa Rosa de Copán, Honduras. *Nexo Revista Científica*, 35(01), 60–71. <https://doi.org/10.5377/nexo.v35i01.13916>
- Universidad Nacional De San Juan. (2018). *Glúcidos*. Recuperado el 13 de Marzo de 2022, de <http://dea.unsj.edu.ar/quimica2/LABORATORIO%202%20GLUCIDOS.pdf>
- Vega, R., Flores, E., & Ofrías, H. (1971). Determinación rápida del extracto seco en vinos por densimetría. Facultad de Ciencias Agrarias. https://bdigital.uncu.edu.ar/objetos_digitales/19602/2-roberto-vega-eduardo-o.-flores-y-humberto-v.-ofria-p.-7-18
- Vidaurre Rojas, P. (2004). Evaluacion De La Temperatura Y La Concentración De Azucar Durante La Elaboracion De Vino Utilizando Levaduras Seleccionadas (*Saccharomyces cerevisiae* R.f. *cerevisiae*). [UNIVERSIDAD NACIONAL DE SAN MARTIN]. <https://core.ac.uk/download/pdf/287328309.pdf>
- Vino de calidad: factores y características. (2020, 29 octubre). Bodegas Bianchi. <https://www.bodegasbianchi.com.ar/blogs/blog/que-factores-inciden-en-la-calidad-de-un-vino?srsltid=AfmBOoqwt1nW-NLIQv760JKMyYUJ6wufMUDmbvDT1QEmaxsUbV2xCUy>

Received: July 17th, 2025

Accepted: November 5th, 2025

Moreno Acosta, Andrea Carolina: Chemical Engineer ULA. MSc. in Chemical Engineering ULA. Asistent Professor attached to the Department of Unit Operations and Projects of the Faculty of Engineering ULA. Researcher at the Food Science, Engineering and Biotechnology Laboratory. Email: anmorenas@gmail.com.

🔗 <https://orcid.org/0009-0005-3174-5552>

Contreras Guerrero, Ruvit Isoley: Chemical Engineer. ULA. Email: ruvitcontreras@gmail.com.

🔗 <https://orcid.org/0009-0004-9242-8772>

Carvajal Peña, Martha Gabriela: Chemical Engineer. ULA. Email: marthagcarvajal18@gmail.com.

🔗 <https://orcid.org/0009-0007-1789-2809>

González, Aura Marina, Chemical Engineer, MSc Applied Chemistry ULA Faculty of Sciences, Doctorate in Applied Sciences ULA Engineering Faculty, Full Professor, Researcher in Science and Technology of Applied Chemistry. Email: auragonza274@gmail.com.

🔗 <https://orcid.org/0009-0003-4147-1044>

De Lima, Aída Josefina, Chemical Engineer ULA, MSc Chemical Engineering ULA. Assistant Professor, attached to the Department of Industrial and Applied Chemistr. School of Chemical Engineering. ULA Engineering Faculty, researcher in food science and technology. Email: aidajdl@gmail.com

🔗 <https://orcid.org/0009-0003-3850-0019>

Noboa, Glenda. MSc in Chemical Engineering (ULA). Associate Professor. Department of Industrial and Applied Chemistry, School of Chemical Engineering, Faculty of Engineering. Head of the Food Science, Engineering, and Biotechnology Laboratory. Email: glenda.noboa@gmail.com

🔗 <https://orcid.org/0009-0008-4585-8437>

Izaguirre, César. Bachelor of Science in Chemistry, ULA. Interfaculty Postgraduate Course in Food Science and Technology, CIENCIAS-UCV. Master's Level. Researcher, School of Chemical Engineering, Food Science, Engineering, and Biotechnology Laboratory, ULA. Email: cmizag@gmail.com 🔗 <https://orcid.org/0009-0004-0351-8515>

Celis, María-Teresa, Chemical Engineer, University of Los Andes (ULA), Mérida, Venezuela, 1981; Master's in Chemical Engineering, 1997, University of South Florida (USF), USA; Ph.D. in Chemical Engineering, 2000, USF, USA; Post-Doctoral Fellow (Water-based, Natural Polymer

Surfactants: Implications for Deep-water Horizon Oil Spill Dispersions and Cleanup Operations), 2012, USF, USA; Director of the Polymers and Colloids Laboratory, Faculty of Engineering (ULA); Full Professor, Faculty of Engineering, ULA. Researcher and expert in the area of polymers, emulsions, and characterization of dispersed systems using spectroscopy. Email: celismt@ula.ve

🔗 <https://orcid.org/0000-0003-3618-3569>

Zoghbe Nuñez, Yamil Abdallah: Chemical Engineer with 3 years of experience in the "Design and Implementation of Sugarcane Derivative Agro-industrial Complexes" Project for PDVSA Agrícola. Responsibilities included: reviewing drawings (PFD and PI&D) and basic and detailed engineering documents, and executing conceptual engineering, 2015. Instructor with over 5 years of experience in Reactor Calculation, over 1 year of experience in Industrial Plant Design, and over 3 years of experience in the Unit Operations Laboratory, 2022. Currently, a soil chemical analyst at the GH SpA Construction Quality Control Technical Laboratory in Cajón, Chile, 2025. Email: yamil.zoghbe@ghlab.cl

🔗 <https://orcid.org/0009-0006-8219-177X>

Valorization of gamelote (*Megathyrsus maximus*) as lignocellulosic biomass for a biorefinery

Valorización del gamelote (*Megathyrsus maximus*) como biomasa lignocelulósica para una biorrefinería

Villanueva, Iván^{1*}; Pereira, Juan Carlos¹

¹Laboratory of Petroleum, Hydrocarbons and Derivatives, University of Carabobo, Valencia, Venezuela.
**ivillanu@uc.edu.ve*

Abstract

The growing interest in generating and/or consuming products obtained with environmentally friendly technologies, using raw materials from renewable resources, is leading to a focus on residual and untapped biomass sources in the production of lignocellulosic materials. Megathyrsus maximus, an abundant and underutilized biomass widely distributed in our country, is the central focus of this research, which aims to establish its potential for large-scale lignocellulosic material production. To this end, the biomass was subjected to various physical and chemical stages, including cutting, drying, grinding, sieving, delipidation, delignification, and bleaching, to ultimately obtain cellulose. It was found that the drying process at 60°C for 4 hours is equivalent to one month of air drying under ambient conditions. After the refining process, 13.8% cellulose was obtained on a wet basis from the fed biomass. The cellulose obtained was characterized by infrared spectroscopy in comparison with commercial cellulose, demonstrating the quality of the treatment carried out. Furthermore, it was characterized by thermogravimetric analysis and polarized light optical microscopy, which revealed the crystalline nature of the cellulose fibers obtained. In the studied area, between 13.9 tons/ha and 26.9 tons/ha of fresh Megathyrsus maximus (MM) can be harvested, from which it is projected to obtain between 1.7 tons/ha and 3.3 tons/ha of cellulose from the planted MM, demonstrating the potential of Megathyrsus maximus for processing into lignocellulosic substrates.

Keywords: *Megathyrsus maximus, cellulose, lignocellulosic biomass, biorefinery.*

Resumen

El creciente interés en generar y/o consumir productos obtenidos con tecnologías respetuosas con el medio ambiente, utilizando materias primas procedentes de recursos renovables, está impulsando la concentración de biomasa residual y sin explotar en la producción de materiales lignocelulósicos. Megathyrsus maximus, una biomasa abundante y subutilizada, ampliamente distribuida en nuestro país, es el foco central de esta investigación, cuyo objetivo es establecer su potencial para la producción de materiales lignocelulósicos a gran escala. Para ello, la biomasa se sometió a diversas etapas físicas y químicas, incluyendo corte, secado, molienda, tamizado, deslipidización, deslignificación y blanqueo, para obtener finalmente celulosa. Se observó que el proceso de secado a 60 °C durante 4 horas equivale a un mes de secado al aire en condiciones ambientales. Tras el proceso de refinación, se obtuvo un 13,8 % de celulosa en base húmeda a partir de la biomasa alimentada. La celulosa obtenida se caracterizó mediante espectroscopia infrarroja en comparación con la celulosa comercial, lo que demuestra la calidad del tratamiento realizado. Además, se caracterizó mediante análisis termogravimétrico y microscopía óptica de luz polarizada, lo que reveló la naturaleza cristalina de las fibras de celulosa obtenidas. En el área de estudio, se pueden cosechar entre 13,9 y 26,9 toneladas/ha de Megathyrsus maximus (MM) fresco, de lo cual se proyecta obtener entre 1,7 y 3,3 toneladas/ha de celulosa a partir del MM plantado, lo que demuestra el potencial de Megathyrsus maximus para su procesamiento en sustratos lignocelulósicos.

Palabras clave: *Megathyrsus maximus, celulosa, biomasa lignocelulósica, biorrefinería.*

1 Introduction

Grasses are primarily composed of cellulose and hemicellulose, which constitute approximately 70% of the total biomass (dry basis), and lignin, which comprises between 10-30% (Heinze et al, 2018). This chemical composition varies according to the species, tissue type, growth stage, and growing conditions, and also includes lipids and other polysaccharides to a lesser extent (Ríos et al., 2021). The grass *Megathyrsus maximus* (MM), also known as Guinea grass, native to Africa, has spread to many other regions of the world (Bryan et al, 2003). It forms isolated clumps with thin, green leaves are shown in Figure 1. It is a fast-growing grass that can reach a height of up to 3 m. It can withstand strong winds and rain thanks to its thick, resistant stem (Álvarez et al, 2016).

It produces seed year-round, with peak production occurring during the dry season. Annually, gambeteen 2-6 tona/ha of dry biomass can be produced in relatively fertile soils, and this can be increased with optimized agricultural strategies (Aristega et al., 2021). MM has been used to prevent soil erosion and as a livestock feed crop, but it has already been replaced by other species. If not managed properly, it can become an invasive grass and have a negative impact on native plant communities, given its rapid ability to establish itself over other plants (Cabrera et al., 2015). In Venezuela, this species is widespread, with a national distribution of approximately 16%, being more concentrated in the state of Zulia and the central region of the country (Guevara et al., 2012).

Of the three main constituents of MM, cellulose represents the most abundant renewable polymeric resource available worldwide, and in the plant, it is located in the cell walls, primarily bound to hemicelluloses, lignin, and pectins (Figueiredo et al., 2010). Globally, most plant-based cellulose is derived from wood; however, in recent years, other non-timber plant species, industrial waste, and agricultural byproducts have been used. In this regard, cellulose has been obtained from paper mill sludge (He et al., 2009), cereal crop waste (Sun et al, 2004), Musaceae (Zuluaga et al, 2007), pineapple bagasse (Antonio et al., 2014), among others. It is also possible to obtain cellulose from algae such as *Valonia* (Baker et al., 1997) or through the extracellular activity of microorganisms such as *Acetobacter*, *Agrobacterium*, *Rhizobia*, or *Sarcina* (Jung et al., 2005). The type of source used influences the physical, morphological, and mechanical characteristics of the cellulose. It is worth noting that the composition of lignocellulosic substrates also varies depending on the source used (Gonzalez et al, 2022).

Cellulose, chemically, is a polysaccharide, a linear natural polymer whose monomers are primarily β -(1 \rightarrow 4)-D-glucopyranose (glucose) structures. Each β -anhydroglucose (UAG) unit has three exposed hydroxyl groups, which are capable of forming inter- and intramolecular hydrogen bonds.¹⁶ This allows the polymer units to assemble into a hierarchical system. First, they form fibrillar units approximately 1.5–3.5 nm in diameter, which then assemble into microfibrils (nanofibers) with diameters ranging from tens to hundreds of nanometers. Finally, somewhat more

randomly, they form interconnected microfibrillar networks (microfibers) with diameters on the micrometer scale or larger. These structures contain alternating sequences of crystalline and amorphous zones and represent the basic units of the plant cell wall in familiar cellulosic materials such as wood and cotton (Perez, 2005; Klemm et al, 2005; Heinze et al, 2012; Morales, 2015).

Throughout this system, hydrogen bonds play a fundamental role, as they are primarily responsible for the intramolecular interactions between the hydroxyl groups of adjacent anhydroglucose units and the intermolecular interactions that form between one cellulose chain and an adjacent one (León-Fernández et al, 2014). This has a strong influence on its mechanical, physical, and chemical properties, such as solubility, OH group reactivity, and crystallinity, among others. Furthermore, there are axial interactions between the C-OH sheets and Van der Waals interactions that stack these sheets (Nishiyama et al., 2002; Nishiyama et al., 2003; Tashiro et al., 2005).

Although cellulose is a highly hydrophilic polymer, it is insoluble in water. The intensity of the aforementioned interaction forces confers high stability to the crystalline structure. Cellulose solubilization is achieved by promoting the appearance of amorphous regions, with the weakening of intermolecular hydrogen bonds and the achievement of a positive interaction of the solubilizing agent with the cellulose (Carreño et al., 2005).

2 Experimental procedure

Megathyrsus maximus was collected fresh from an area of approximately 1 hectare located near the Faculty of Experimental Sciences and Technology at University of Carabobo, with geographic coordinates latitude: 10.2797° N and longitude: -68.0069° W. Within this area, a 1 m² square was delimited, and all the *Megathyrsus maximus* clumps contained therein were collected. The ears of each clump were counted and cut approximately 10 cm from the root, which was not evaluated in this study.

2.1 Obtaining Cellulose from *Megathyrsus maximus*

The methodology for obtaining cellulose was based on previous studies (Canche, 2005; Moreno, 2007; Rodríguez et al., 2007; Castillo, 2008; Carrero, 2013; Minmunin et al., 2015) carried out using plant biomass (see Figure 1). The leaves were manually cut into small pieces and then dried, some at room temperature and others in an oven at 60°C, in order to comparatively evaluate mass loss. Grinding was carried out in a helical mill. The material was then pulverized in a blade processor and subsequently fractionated using sieves of different pore sizes [ASTM80 (0.177mm); ASTM60 (0.250mm); ASTM20 (0.833mm) and ASTM18 (1mm)].

Delipidation was carried out using solid-liquid extraction with hexane in a Soxhlet extractor and in a glass reactor under total reflux. Different particle sizes of the dried plant material and total reflux times of 2 and 4 h were evaluated in this process. The extracted fat content was determined using Equation 1.

$$\text{Extracted fat content} = \frac{\text{mo} - \text{mf}}{\text{mMM}} * 100 \quad (\text{Eq. 01})$$

mo: sample mass before extraction (g)

mf: sample mass after extraction (g)

mMM: net mass of *Megathyrsus maximus* sample (g)

The delignification stage was carried out using the alkaline peroxide method at 70°C, in two stages, where the lignins and hemicelluloses present in the biomass were removed. The dried biomass was subjected to a reaction with 25% w/v hydrogen peroxide and 12% w/v sodium hydroxide at a mass/volume ratio of 1:30 (biomass: volume of aqueous phase) with stirring at 250 rpm or higher. Subsequently, the sample was filtered through a cloth, the filtrate was reserved, and the lignocellulosic residue was washed and then bleached with alkaline peroxide. A 25% w/v H₂O₂ solution was added progressively to achieve a 30:1 liquor/biomass ratio. Finally, the resulting material was filtered and dried to quantify the cellulose obtained for use in subsequent stages. Each batch of black liquor was stored for later analysis.

The characterization of the obtained cellulose consisted of ash determination, thermogravimetric analysis, FT-IR spectroscopy, polarized light optical microscopy, and scanning electron microscopy. Commercial cellulose and all chemicals were analytical grade, purchased from Sigma-Aldrich.

2.2 Thermogravimetric Analysis (TGA)

Thermogravimetric analysis allows for the study of the thermal stability of the materials under study and was performed on a NETZSCH STA 409 PC thermobalance. These analyses were carried out under an argon atmosphere with a flow rate of 50 mL/min. A heating ramp of 10 °C/minute was used, from 30 °C to 450 °C.

2.3 Infrared Spectra Determination

The cellulose obtained was analyzed by Fourier Transform Infrared (FT-IR) spectroscopy and compared with the spectra obtained for cotton (the natural material with the highest cellulose content) and commercially available cellulose. For this purpose, the sample was placed on the dish designed for direct Fourier Transform Infrared Spectroscopy analysis in a Perkin Elmer Frontier FT-IR Spectrometer, in the spectral range between 400 and 4,000 cm⁻¹.

2.4 Analysis by Polarized Light Microscopy

A MOTIC BA310 POL trinocular Siedentopf-type microscope, inclined at 30° and rotatable 360°, was used. A 360° rotating analyzer was used to take polarized light images of the cellulose obtained from *Megathyrsus maximus* and of the commercially available cellulose. This was done to compare the morphology of both materials at the scales used.

2.5 Scanning Electron Microscopy Determination

The cellulose obtained was analyzed by Scanning Electron Microscopy using a JEOL JCM-6000 instrument. The voltage used was 15 kV, and the samples were placed in the holder covered with a thin film of gold.

3. Results and discussion

3.1 Collection of *Megathyrsus maximus*

In the collection of the tillers, 2073.2 g/m² and 2693.4 g/m² of fresh biomass of *Megathyrsus maximus* were obtained. The number of clumps and the number of ears present in the samples taken are reported in Table 1, according to the methodology described.

Table 1. Collection of fresh *Megathyrsus maximus* in an area of 1 m²

Clumb	Number of ears of corn	High ears of corn ± 0,2 (m)	Clumb Mass ± 0,1 (g)
1	6	1,7	231,5
2	14	1,7	525,4
3	10	2,2	360,7
4	11	2,0	435,1
5	9	1,8	310,6
6	21	2,0	830,2
Averages	12	1,9	448,9

As can be seen in Table 1, 6 clumb were obtained in the demarcated area, with a variable number of ears per clumb, as well as variable ear length. It is worth noting that the mass of *Megathyrsus maximus* per area is not uniform, but rather falls within a range of values. On average, the number of ears per tiller per m² was 12 ± 4, and their length was 1.9 ± 0.2 m.

To estimate the availability of MM per area, the smallest clump mass (as an unfavorable scenario) and the average mass of the clumps (as a favorable scenario) were considered. This indicates that between 13.9 tons/ha and 26.9 tons/ha of fresh MM can be harvested. If the mass obtained in the other sampled area (20.7 tons/ha) is included in the estimate, it can be observed that it falls within the proposed range. Other studies of fresh MM harvesting reported yields between 14 and 25 tons/ha, and some achieved up to 40 tons/ha (Aristega et al., 2021). Gomez et al. (2021) reported between 20.3 and 28.0 tons/ha of fresh MM after 40 and 60 days of growth, respectively (Gómez et al., 2021). The observed differences can be attributed to soil quality, climatic conditions, and the agricultural strategies employed when applying nutrients during planting (Cerdas, 2011). This result demonstrates the potential of the land adjacent to the laboratory where the research was conducted, where more than 6 hectares of *Megathyrsus maximus* (MM) are planted but not currently being utilized.

3.2 Drying of the Cut *Megathyrsus maximus*

The drying process was performed on the smallest clump. The root was removed, and the rest of the plant was cut into small pieces. This was divided into three (3) parts, and the final appearance can be seen in Figure 1. The mass

loss during the drying process under ambient conditions was determined.

Table 2 shows the mass variation of the MM during storage at ambient temperature over the study period.

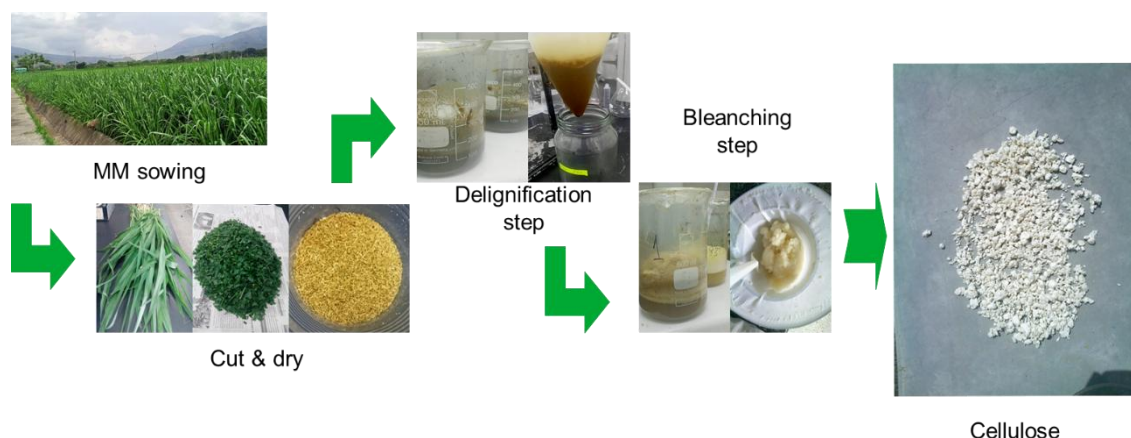


Figure 1. Production of cellulose from MM

It began with a total initial mass of 230.9 g, divided among the three samples. Additionally, the total mass loss of the evaluated clump was observed, reaching a net loss of 155 g in 180 days. On average, over a period of 6 months, the fresh MM sample had a percentage mass loss of $67 \pm 1\%$. This percentage is mainly due to the water content in the plant material.

Table 2. Drying of fresh *Megathyrsus maximus* at room temperature

Sample	Percentage mass loss per day (%)				
	0	3	30	63	180
1	0,0	31,2	68,1	71,5	68,9
2	0,0	28,3	64,5	68,1	65,3
3	0,0	35,8	66,3	69,8	67,2
Average	0,0	32 ± 3	66 ± 1	70 ± 1	67 ± 1

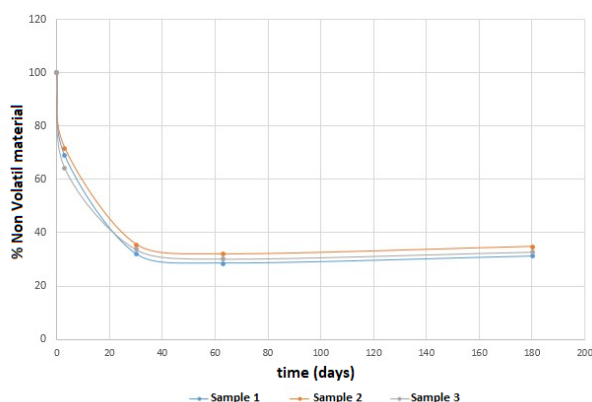


Figure 2. Variation of the non-volatile content of the plant material at ambient temperature

For comparison, the mass loss during the drying of *Megathyrsus maximus* ranged from 78.6% to 81.2%, measured after 40 and 60 days of drying, respectively

(Gómez et al., 2021).

Similarly, the behavior of the non-volatile compounds present in the plant material is shown in Figure 2, as a function of the number of days exposed to ambient temperature.

It is worth noting that after 30 days, the change was minimal. At 6 months, a slight increase in mass was observed. Considering that plant material loses mass until it reaches equilibrium with its environment, this slight increase in mass at 6 months could be attributed to higher relative humidity at the time of weighing.

Furthermore, drying the fresh MM samples in an oven at 60 °C resulted in a mass loss of $65 \pm 2\%$. That is, under the established conditions, the amount of mass obtained in 4 hours was equivalent to what would have taken approximately one (1) month at ambient temperature. This is very important when considering shortening the drying time, given the additional energy required for drying at a temperature higher than ambient. It is noteworthy that fresh MM has a high water content (Gonzalez et al., 2022; Dominguez, 2017) reported at 67.6% and 71.0%, respectively. This corresponds to the fact that water content can vary depending on the time of year and the climatic conditions present at the time of harvest. It is projected, then, that between 650 and 710 kg of water will evaporate for every ton of fresh MM processed, or, equivalently, between 9.1 and 17.6 tons of water per hectare of harvested land. Therefore, in large-scale processes, it would be an opportunity to consider studying the feasibility of condensing this water for use in subsequent processes.

Regarding the projected dry biomass of *Megathyrsus maximus*, it is projected to be between 4.8 and 9.3 tons/Ha. These levels are consistent with several studies that report ranges of 4.8 to 8.7 tons/Ha (Fortes et al., 2016); 2.0 to 3.9 ton/Ha (Milera et al., 2017); 5.8 to 8.7 ton/Ha (Pilco, 2017) and 1.3 to 6.2 ton/Ha (Homen et al., 2010), the latter in Venezuela (Edo. Miranda) in periods of 40 to 60 days of growth.

The values obtained are close to those reported for *Megathyrsus maximus* species in Colombia, where an average lipid content of 1.64% on a dry basis was obtained,

and for species from Mexico with a lipid content of 1.6% on a dry basis.⁴¹ A range of hexane extractables between 0.51 and 1.72% has also been reported (Milera et al., 2017).

Table 3. Sieving of the dried, ground, and crushed plant material

Sample	Percentage mass distribution of the sieved plant material (%m/m ± 1)				
	$\varnothing < 177$ μm	$177 < \varnothing < 833$ μm	$833 < \varnothing < 1000$ μm	$1000 < \varnothing < 1400$ μm	$\varnothing > 1400$ μm
Dry MM	14	51	15	14	6

3.3 Grinding, crushing, and sieving of *Megathyrsus maximus*

The purpose of crushing the dried *Megathyrsus maximus* was to reduce the particle size to increase the exposed surface area, thus facilitating subsequent treatments. The mass distribution obtained after crushing and sieving, by particle size, is shown in Table 3. The most prevalent particle size range was between 177 and 833 μm .

In any case, the resulting mass distribution is associated with the time spent during crushing, the number of times it is repeated, the equipment used, and the energy applied. This distribution can be controlled by varying the time and frequency.

It is known that the energy required to reduce a plant source to a specific particle size is mainly influenced by the starting biomass (wood or grasses) (Cadoche, 1989) and the type of equipment used. Depending on the type of grinding employed and the type of material to be pretreated, the reduction in the final particle size desired is inversely proportional to the energy consumption required to achieve it, and its variation is not linear (Cadoche, 1989). As expected, the energy consumption to achieve a specific particle size is much higher when using wood as the starting source compared to when using grasses, such as *Megathyrsus maximus*. Similarly, greater energy or shear will be required to increase the proportion of particle sizes from larger to smaller.

3.4 Extraction of fatty components (delipidation)

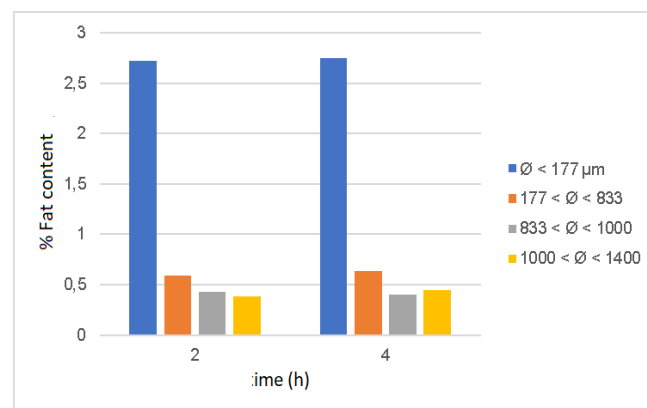
It is known that fatty components are contained in the cells and cell walls of leaves, where they fulfill various roles in plants, such as hydrophobicity (waterproofing), energy storage, and signal transport, among others (Marcano, 2002). The lipid fraction obtained from grasses is mainly composed of galactolipids and phospholipids (86% molar) and, to a lesser extent, free fatty acids (3.1%), triglycerides (8.4%), and sterols (2.5%). The reported fatty acid composition was mostly unsaturated with 18 carbon atoms (75.3%) Carvajal-Tapia et al., 2023).

In this research, the removal of fat aimed to quantify the amount of its lipid content on a dry basis. Figure 3 shows the fat content extracted at different particle sizes from the plant material after 2 and 4 hours of extraction. It can be observed that the delipidation process with total reflux was favored when the particle size was smaller. The lipid content was extracted in the first two hours of reflux.

The highest fat content was obtained for a particle size of

$\varnothing < 177 \mu\text{m}$, which can be attributed to the increased contact between the solvent and the solid due to greater disruption of the plant's epidermal tissue, resulting in greater solubility of the fats present in the plant matter (Kumoro et al, 2021). In the Soxhlet extraction process, 1.90% was obtained in 4 h. After this stage, the solvent was recovered by vacuum distillation with a rotary evaporator, achieving a recovery percentage of 88%.

Figure 3. Fat content extracted from MM samples according to their size.



3.5 Delignification using the alkaline peroxide method

The final stage in obtaining cellulose consisted of removing hemicelluloses and lignins through the solid-liquid process already described, where the reaction raw material consisted of a dark brown liquor and a brown solid fraction that followed the bleaching process with H_2O_2 . This liquid (black liquor) has an intense dark color, attributable to the activation of chromophoric groups present in the lignin. The reactions that occur are based on condensation and oxidation processes of phenolic groups, in which phenolates are obtained that promote its dissolution (Huang et al., 2019).

During the addition of H_2O_2 , a large amount of foam was produced, promoted by the formation of oxygen from the reaction; therefore, the addition of H_2O_2 to the reaction medium had to be gradual to control the foam. During gravity filtration through a cloth filter, turbidity and sedimentation were observed in the filtered liquid fraction due to the passage of very fine cellulose particles. The filter cake was subjected to a second reaction with alkaline peroxide, decreasing the NaOH concentration to 6% and maintaining the H_2O_2 concentration at 25% w/w to improve the bleaching of the resulting cellulose.

After this stage, the mixture was filtered through a cloth. The filter cake (cellulose) was washed with distilled water until the wash water reached a neutral pH.

The percentage yield (dry basis) of cellulose, according to the particle size of the starting dry plant material, was higher for the largest particle size (43.00%) and 35.00% for the smallest size studied, values close to those reported (Gonzalez et al., 2022). This reduction in the efficiency of the cellulose production process is attributable to the particle size of the initial cellulose fibers, which turned out to be very fine particles that were not retained by the filtration mesh, as evidenced by sedimentation in the collection container of the reaction liquor. The cellulose obtained appears as agglomerated particles with a paper-like appearance as shown in Figure 1. This agglomeration occurs during the filtration process.

It is worth noting that the biomass characterization of dry *Megathyrsus maximus* is summarized as follows: 13.2% moisture, 9.4% ash, 2.8% hexane extractables, 23% lignin, and 39.3% cellulose. Protein content was not determined; however, crude protein levels for *Megathyrsus maximus* have been reported in several countries, ranging from 13.95% to 16.53% in Colombia (Barragán-Hernández et al., 2019), 10.20% in Costa Rica (López-Herrera et al., 2019),

11.03% to 16.92% in Ecuador (Gomez et al., 2021), and from 19.76% to 16.43% in Venezuela (Homen et al., 2010), during a growth period of 21 to 35 days. Finally, based on the results obtained, the projected cellulose yield is between 1.7 and 3.3 tons/Ha planted with *Megathyrsus maximus*.

3.6 Thermogravimetric Analysis (TGA)

Thermogravimetric analysis allowed us to determine the stability of the cellulose samples as a function of temperature increase under an inert atmosphere. Figure 4 shows the thermogravimetric curves (TGA) and their corresponding derived thermogram (DTGA). These curves illustrate the variation of the percentage of residual mass with respect to the temperature increase up to 450°C.

It has been reported that the variation in the mass of lignocellulosic materials (cellulose, hemicellulose, and lignin) in a range of approximately 80 to 120°C is attributable to mass loss due to moisture (Reddy et al., 2018). This is observable in the DTGA curve in Figure 5, and Table 4 shows the mass loss values up to 120°C.

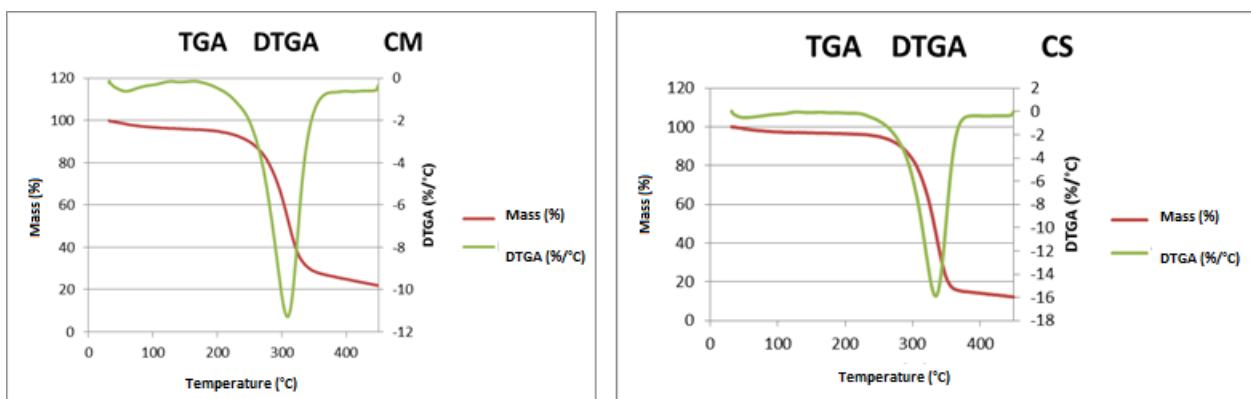


Figure 4. TGA and DTGA thermograms of cellulose from MM (left) and commercial cellulose (right)

Table 4. Thermogravimetric analysis of the celluloses

Cellulose	T _{initial} (°C)	T _{final} (°C)	T _{pico} (°C)	Percentage of mass lost to 120°C (%)	Percentage of mass lost to the T _{pico} (%)
MM	280	334	311	3,60	48,1
CS	305	355	336	2,85	57,5

Subsequently, the decomposition process of any hemicellulose present in the samples begins (above 190°C). This is followed by the decomposition of the cellulose, which overlaps with the decomposition of lignin (Yang et al., 2007).

The peak or average decomposition temperature (T_{peak}) is represented by the inflection point in the thermogram and by the minimum reached in the DTGA curve. It should be noted that this material is composed of a distribution of molecules with different degrees of polymerization and under different crystalline arrangements; therefore, an average value will be obtained. These values are shown in Table 4.

Table 4 shows that at 120 °C, the percentage of mass loss was slightly higher for MM cellulose compared to commercial cellulose. In the former case, the mass loss was 3.60%, while for commercial cellulose it was 2.85%. This reduction is attributable to the elimination of moisture contained in the cellulose (Reddy et al., 2018). The mass loss at the average decomposition temperature was greater for commercial cellulose, at 57.5%, compared to MM cellulose, at 48.1%. Additionally, the initial decomposition temperature ($T_{initial}$) of MM cellulose began earlier than that of commercial cellulose. This greater decomposition was reached at a higher temperature in commercial cellulose compared to MM, indicating that commercial cellulose, comparatively, showed greater thermal stability. This may be associated with differences in the degrees of polymerization and crystallinity.

3.7 Characterization of Cellulose by FT-IR

Samples of the obtained cellulose and commercially available cellulose were analyzed by Fourier transform infrared spectroscopy (FTIR) and are shown in Figure 5. In each of the spectra obtained, the characteristic absorption bands of the analyzed samples are observed. The absorption band at 3328 cm^{-1} is attributed to the stretching vibration of the inter- and intramolecular H-O hydrogen bonds, characteristic of those present in cellulose (Oh SY et al., 2005a; Moran, 2008; Fan et al., 2012). The band at 2896 cm^{-1} corresponds to the stretching of the sp^3 -hybridized carbons corresponding to the methylene (CH_2) groups of cellulose (Fan et al., 2012). The absorption band at 1638 cm^{-1} indicates a certain amount of water adsorbed on the fiber, seen through the bending vibration of the OH group (Oh SY et al., 2005b). The band corresponding to the bending vibration of CH_2 (Oh SY et al., 2005b) is observed at 1423-1429 cm^{-1} . The band at 1315 cm^{-1} is attributed to the rocking vibration of the CH_2 group of carbon C_6 (Poletto, 2014). The band at 1159 cm^{-1} is attributed to the vibration of the β -glycosidic bond COC (Oh SY et al., 2005b).

The stretching vibrations of the C-O bond of ether groups appear in the range of 1050 to 1150 cm^{-1} , which are characteristic of the polymeric structure of cellulose (Coates, 2000). The intense band at 1026-1031 cm^{-1} is attributed to the stretching vibrations of the C-O bonds of primary alcohols Cichosz et al., 2022). At 896 cm^{-1} , the band is attributed to the stretching vibrations of the COC,

CCO, and CCH bonds (Fan et al., 2012). Bands are observed at 1200 and 1500 cm^{-1} in the *Megathyrus maximus* biomass, which disappear in the obtained cellulose and are also absent in commercial cellulose. These bands are attributable to the C-O stretching of aromatic alcohols characteristic of the lignin contained in the biomass (Coates, 2000).

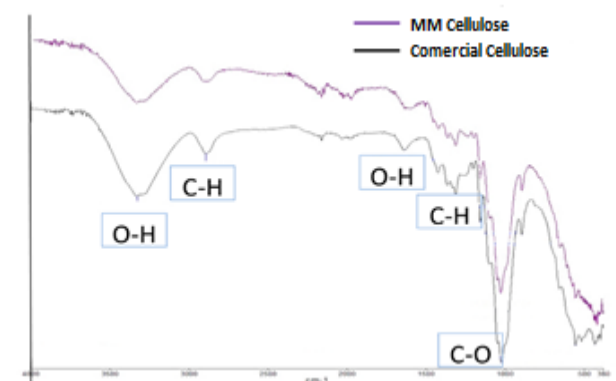


Figure 5. Comparison of functional groups present in cellulose obtained from *Megathyrus maximus* with respect to commercial cellulose

Figure 5 shows a comparative analysis of the infrared spectra of MM cellulose, highlighting its similarity to the bands obtained from commercial cellulose, which was used for comparison. These results demonstrate the efficiency of the refining process used to obtain cellulose from MM biomass.

3.8 Polarized light optical microscopy

The commercial cellulose samples and the cellulose obtained from MM were analyzed by polarized light optical microscopy at magnifications of 40x and 100x (Figures 6 and 7). The commercial cellulose samples and the one obtained from MM were analyzed by polarized light optical microscopy, with a magnification of 40x and 100x (Figures 6 and 7).

It is worth noting that the observations made using this methodology reveal structures exhibiting birefringence, which is associated with the anisotropic crystalline structures present in cellulose. In the cellulose obtained from MM (Figure 6), aggregates of fibers of varying sizes are observed, structured longitudinally in parallel. The fibers of commercial cellulose have a uniform size distribution and shorter lengths than those obtained in the cellulose sample (Figure 7).

It is known that cellulose fibers form hierarchical structures, composed of cellulose chains distributed in crystalline and amorphous domains (Heinze, 2012). The crystalline structure confers high strength in mechanical properties, while the amorphous region contributes to elasticity. Furthermore, the amorphous region enhances the reactivity of cellulose.

3.9 Scanning Electron Microscopy

Figure 8 shows the microstructures formed by the cellulose fibers obtained from MM. They are arranged as loose filaments stacked on top of each other in three-dimensional space. They exhibit a linear conformation characteristic of cellulose microfibrils, with variable thicknesses, mostly between 5 and 10 μm . Additionally, some show fibrillar aggregates with longitudinal channels on their surface. The cellulose is organized hierarchically, with each fiber composed of other, thinner fibers stabilized

by hydrogen bond interactions present in the cellulose (Heinze, 2012).

The morphology observed in commercial cellulose shows fibers with greater thicknesses than those observed in cellulose from MM. The greater thickness and crystallinity observed in commercial cellulose fibers may confer greater thermal stability than those obtained from MM, which is consistent with the results obtained in the thermograms. This arrangement is composed of microfibrils stabilized by numerous hydrogen bonding forces.

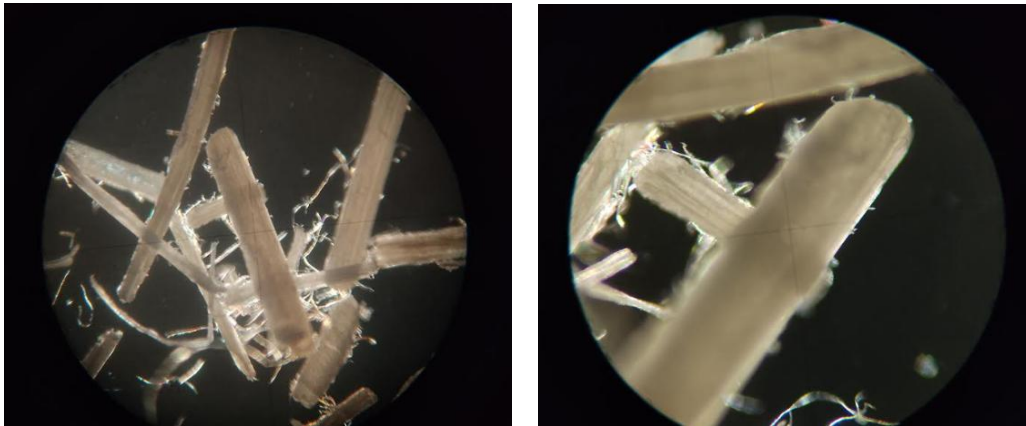


Figure 6. Polarized light microscopy image of cellulose obtained from *Megathyrus maximus*. Left (40x), Right (100x)

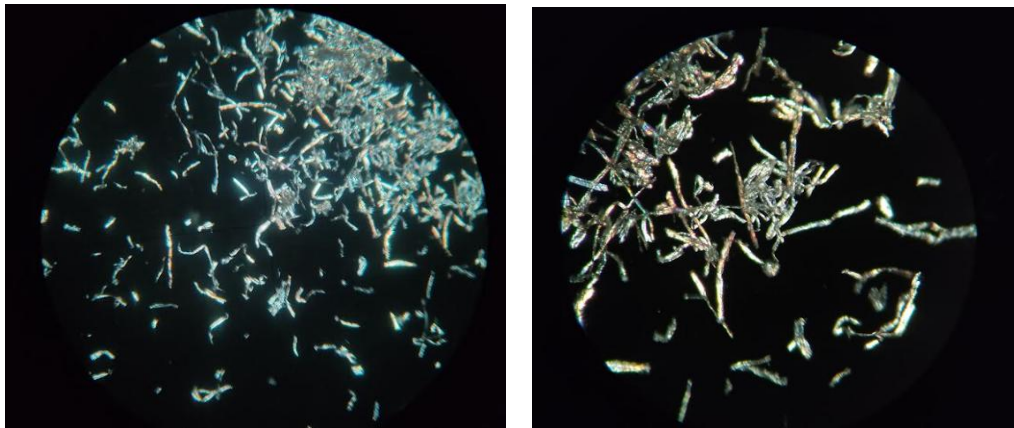


Figure 7. Polarized light microscopy image of commercial cellulose. Left (40x), Right (100x)

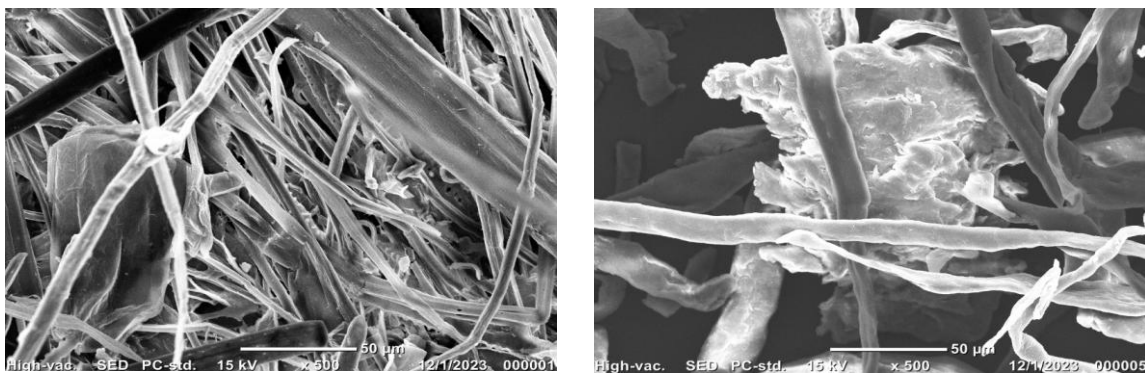


Figure 8. Scanning electron microscopy of *Megathyrus maximus* cellulose from commercial cellulose (500x)

4 Conclusions

The production of cellulose from *Megathyrsus maximus* biomass was effective using physical processes such as cutting, drying, grinding, sieving, and solvent extraction of lipids, under chemical refining processes such as delipidization and delignification (bleaching) using 25% w/w H₂O₂ and 12% w/w NaOH.

Drying the pre-treated *Megathyrsus maximus* material at 60 °C for 4 h was equivalent to drying it in 30 days at room temperature.

The crystallinity and hierarchical structure of the cellulose fibers were evident by polarized light microscopy, and the refinement was demonstrated by visualizing disaggregated fibrillar structures using scanning electron microscopy, both in commercial cellulose and in that obtained from *Megathyrsus maximus*. FTIR spectroscopy confirmed the presence of the main characteristic bands in the cellulose obtained from *Megathyrsus maximus*, equivalent to those present in cotton cellulose and commercial cellulose.

The estimated availability of fresh *Megathyrsus maximus* per unit area (area adjacent to FACYT) is between 13.9 tons/ha and 26.9 tons/ha. The drying process (if the evaporated water is condensed) is estimated to yield between 9.1 and 16.5 tons/ha of water per unit area of planted land. Finally, the projected cellulose yield is between 1.7 and 3.3 tons/ha of planted *Megathyrsus maximus*.

References

- Álvarez, G. R.; Vargas, J. C.; Franco, F. J.; Álvarez, P. E.; Samaniego, M. C.; Moreno, P. A.; Chacón, E.; García, A. R.; Arana, R. S. y Ramírez de la Ribera, J. L. (2016). Rendimiento y calidad del pasto *Megathyrsus maximus* fertilizado con residuos líquidos de cerdo. REDVET. Revista Electrónica de Veterinaria, Vol. 17 (6), pp. 1-9.
- Antonio R., Ramos C., García R., Sandoval G. y Arellano L. (2014). Gel de carboximetilcelulosa (CMC) a partir del bagazo de piña. Ciencias de la Ingeniería y Tecnología, Handbook. ECORFAN., Valle de Santiago, Guanajuato. ISBN 978-607-8324-24-8.
- Aristega, M. J. C., Murillo, R. A. L., Coronel, A. L. E., & Garaicoa, D. A. R. (2021). Producción y composición química de *Megathyrsus maximus* cultivares Tanzania y Mombasa bajo condiciones del subtrópico ecuatorial. Ciencia Latina Revista Científica Multidisciplinar, Vol. 5 (4), pp. 6427-6443.
- Baker, A., Helbert, W., Sugiyama, J. y M. Miles (1997). High-Resolution Atomic Force Microscopy of Native Valonia Cellulose I Microcrystals. J. Struct. Biol., Vol. 119, pp. 129-138.
- Barragán-Hernández, W. A., y Cajas-Girón PhD, Y. S. (2019). Cambios bromatológicos y estructurales en *Megathyrsus maximus* bajo cuatro arreglos silvopastoriles. Ciencia y Tecnología Agropecuaria, Vol. 20 (2), pp. 231-258.
- Bryan, K., y Surrey, W. (2003). *Megathyrsus*, a new generic name for panicum subgenus megathyrsus. Austrobaileya, Vol. 6, pp. 571-5743.
- Cadoche L. y López G. D. (1989) Assessment of size reduction as a preliminary step in the production of ethanol from lignocellulosic wastes. Biological Wastes. Vol. 30, pp. 153-157.
- Canche G., De los Santos J., y col. (2005). Obtención de Celulosa a Partir de los Desechos Agrícolas del Banano. TEG. Universidad Juárez Autónoma de Tabasco. México.
- Carreño, S., y Murcia, L. (2005). Obtención de acetato de celulosa a partir de residuos celulósicos postconsumo. Universidad Industrial de Santander. Bucaramanga, Colombia, pp. 8-205.
- Carrero, M. (2013). Factores que afectan la transformación de biomasa en bioetanol. Ingeniería y Sociedad UC. Vol. 8 (1), pp. 53-60.
- Carvajal-Tapia J.L., Barahona-Rosales R., Castro-Montoya J., Arango J. y Vivas-Quila N.J. (2023). Nutritional and biomass evaluation of a *Megathyrsus maximus* collection in a dry tropical climate in Colombia Tropical Grasslands-Forrajeros Tropicales, Vol. 11 (1), pp. 11-21.
- Castillo, V. y Núñez, M. (2008). Evaluación de la factibilidad técnico-económica de una planta para producir celulosa a partir de la masa foliar del MM y del Jacinto de agua. TEG. Universidad de Carabobo. Venezuela.
- Cerdas R. y Vallejos E. (2011). Disponibilidad de biomasa del pasto Guinea (*Megathyrsus maximus*) Tanzania con varias fuentes y dosis de nitrógeno en Guanacaste, Costa Rica. InterSedes: Revista de las Sedes Regionales, Vol. 12 (23), pp. 32-44. Consultado en <https://revistas.ucr.ac.cr/index.php/intersedes/article/view/975>
- Cichosz S., Masek A. Dems-Rudnicka K. (2022) Original study on mathematical models for analysis of cellulose water content from absorbance/wavenumber shifts in ATR FT-IR spectrum. Scientific Reports, Vol.12 (1), pp.19739.
- Coates J. (2000). Interpretation of Infrared Spectra, A Practical Approach. In Encyclopedia of Analytical Chemistry R.A. Meyers (Ed.). pp. 10815-10837
- Dominguez, A. (2017). Síntesis de una molécula con actividad interfacial partiendo de la celulosa extraída de la masa foliar del *Megathyrsus maximus* (MM). Estudio en diferentes medios de solventes. Obtenido de (Tesis pregrado) Universidad de Carabobo, Venezuela.
- Fan, M., Dai, D., y Huang, B. (2012). Fourier transform infrared spectroscopy for natural fibres. Fourier transform: materials analysis, Vol. 3, pp. 45-68.
- Figueiredo, J., Ismael, M., Anjo, C., & Duarte, A. (2010). Cellulose and derivatives from wood and fibers as renewable sources of raw materials. Topics in Current Chemistry, Vo. 294, pp. 117-128.
- Fortes, D., Valenciaga, D., García, C. R., García, M., Cruz, A. M., & Romero, A. (2016). Evaluación de tres


- variedades de *Megathyrsus maximus* en el período poco lluvioso. *Cuban Journal of Agricultural Science*, Vol. 50 (1), pp. 131-137.
- Gómez V., J., Galarza, G., Pérez, J., y Moran, C. (2021). Rendimiento de biomasa del pasto Saboya (*Megathyrsus maximus*) con relación a dos frecuencias de corte. *Magazine de las ciencias. Revista de investigación e innovación*. Vol. 6 (2), pp. 55-63.
- González, M., Pereira-Rojas, J., Villanueva, I., Agüero, B., Silva, I., Velasquez, I., Delgado B., Hernández J., Rodríguez G., Labrador H., Barros H., Pereira, J. (2022). Preparation and characterization of cellulose fibers from *Megathyrsus maximus*: Applications in its chemical derivatives. *Carbohydrate Polymers*, Vol. 296, pp. 119918.
- Guevara E. y Espinoza F. (2012). Nuevos materiales forrajeros para la producción de leche y carne en las sabanas de Venezuela. Instituto Nacional de Investigaciones Agrícolas (INIA) Anzoátegui-Centro Nacional de Investigaciones Agropecuarias (CENIAP), Maracay. pp. 57-144. Consultado en: http://www.avpa.ula.ve/eventos/ii_simposio_pastca2006/13.pdf
- He, X., Wu, S., Fu, D., & Ni, J. (2009). Preparation of sodium carboxymethyl cellulose from paper sludge. *Journal of Chemical Technology & Biotechnology: International Research in Process, Environmental & Clean Technology*, Vol. 84 (3), pp. 427-434.
- Heinze T. y Liebert T. (2012). Celluloses and Polyoses/Hemicelluloses. In: *Polymer Science: A Comprehensive Reference*. Matyjaszewski K and Möller M (eds.) Vol. 10, pp. 83-152. Amsterdam: Elsevier BV. ISBN 9780080878621
- Heinze T., El Seoud O.A. y Koschella A. (2018). Production and Characteristics of Cellulose from Different Sources. In: *Cellulose Derivatives*. Springer Series on Polymer and Composite Materials. Springer, Cham. pp. 1-18.
- Homen, M., Entrena, I., Arriojas, L., & Ramia, M. (2010). Biomasa y valor nutritivo del pasto Guinea *Megathyrsus maximus* (Jacq.) BK Simon & SWL Jacobs. Gamelote en diferentes períodos del año en la zona de bosque húmedo tropical, Barlovento, estado Miranda. *Zootecnia Tropical*, Vol. 28 (2), pp. 255-266.
- Huang, J., Fu, S., y Gan, L. (2019). *Lignin Chemistry and Applications*. Amsterdam, Netherlands: Elsevier. ISBN 0128139633
- Jung, J., Park, J. y H. Chang (2005). Bacterial cellulose production by *Glyconacetobacter hansenii* in an agitated culture without living non-cellulose producing cells. *Enzyme Microb. Tech.*, Vol. 37, pp. 347-354.
- Klemm D., Heublein B., Fink H-P. y Bohn A. (2005). Cellulose: fascinating biopolymer and sustainable raw material. *Angew Chem Int Ed*, Vol. 44 (22), pp.3358-3393.
- Angelo, R., Meléndez, H., Villarroel, M., Rodríguez, P., Imbert, F. y Del Castillo, H., (2017). Study of the reaction of dry reforming of methane using mixed oxide perovskites type $\text{La}_x\text{Sr}_{1-x}\text{Ni}_y\text{Al}_{1-y}\text{O}_3$. *Revista Ciencia e Ingeniería*, Vol. 38 (1), pp. 17-30.
- Kumoro, A. C., Wardhani, D. H., Retnowati, D. S., Haryani, K., Yustika, S., & Fajar, T. A. (2021). Extraction of essential oil from ultrasound pre-treated citronella grass (*cymbopogon Nardus*) leaves by hydro-distillation method. *Chemical Engineering Transactions*, Vol. 87, pp. 643-648.
- León-Fernández, V., Rieumont-Briones, J., Bordallo-López, E., López-Hernández, O. D., y García-Peña, C. M. (2014). Mecanismo de liberación de diclofenaco a partir de un copolímero entérico base celulosa. *Revista CENIC Ciencias Químicas*, Vol. 45 (1), pp. 096-0101.
- López-Herrera, M., Rojas-Bourrillon, A., & Briceño-Arguedas, E. (2019). Substitution of *Megathyrsus maximus* grass by square guineo and urea in silage mixtures. *Agronomía Mesoamericana*, Vol. 30 (1), pp. 179-194.
- Marcano D. y Hasegawa M. (2002). *Fitoquímica Orgánica*. Consejo de Desarrollo Científico y Humanístico. 2da Ed. Venezuela.
- Milera Rodríguez, M., Alonso Amaro, O., Machado Martínez, H. C., & Machado Castro, R. L. (2017). *Megathyrsus maximus*. Resultados científicos y potencialidades ante el cambio climático en el trópico. *Avances en Investigación Agropecuaria*, Vol. 21 (3), pp. 41.
- Minmunin, J., Limpitpanich, P., y Promwungkwa, A. (2015). Delignification of elephant grass for production of cellulosic intermediate. *Energy Procedia*, Vol. 79, pp. 220-225.
- Morales S. (2015). Hidrólisis ácida de celulosa y biomasa lignocelulósica asistida con líquidos iónicos. Tesis Doctoral. Universidad Autónoma de Madrid. España. Consultado en <http://hdl.handle.net/10261/132717>
- Morán JI, Alvarez VA, Cyrus VP, Vázquez A (2008) Extraction of cellulose and preparation of nanocellulose from sisal fibers. *Cellulose* Vol. 15, pp. 149-159.
- Moreno, N. (2007). Obtención de acetato de celulosa a partir de la masa foliar del Jacinto de agua (*Eichornia crassipes*) proveniente del Lago de Valencia. TEG. Facultad de Ingeniería. Universidad de Carabobo. Venezuela.
- Nishiyama Y., Langan P. y Chanzy H. (2002). Crystal Structure and Hydrogen-Bonding System in Cellulose I β from Synchrotron X-ray and Neutron Fiber Diffraction. *J. Am. Chem. Soc.*, Vol. 124, pp. 9074-9082.
- Nishiyama Y., Sugiyama J., Chanzy H. y Langan P. (2003). Crystal Structure and Hydrogen Bonding System in Cellulose I α from Synchrotron X-ray and Neutron Fiber Diffraction. *J. Am. Chem. Soc.*, Vol. 125, pp. 14300-14306.
- Oh SY, Yoo D I., Shin Y, Kim H. C., Kim H. Y., Chung Y. S., Park W. H., Youk J. H. (2005a). Crystalline structure analysis of cellulose treated with sodium hydroxide and

- carbon dioxide by means of X-ray diffraction and FTIR spectroscopy. *Carbohydr Res*, Vol. 340, pp. 2376–2391.
- Oh SY, Yoo D I., Shin Y, Seo G (2005b) FTIR analysis of cellulose treated with sodium hydroxide and carbon dioxide. *Carbohydr Res*, Vol. 340, pp. 417–428.
- Pérez, S. y Mazeau, K. (2005). Conformations, structures and morphologies of celluloses. In *Polysaccharides: Structural Diversity and Functional Versatility*; Dumitriu, S. Ed.; Marcel Dekker: New York, Vol. 1, pp. 41. ISBN 1420030825
- Pilco Herrera, L. J. (2017). Comportamiento agronómico y composición química de variedades de Bruchiarias y Megathyrus maximus" (Bachelor's thesis, Ecuador: La Maná: Universidad Técnica de Cotopaxi; Facultad de Ciencias Agropecuarias y Recursos Naturales; Carrera de Ingeniería Agronómica).
- Poletto M, Ornaghi Júnior HL, Zattera AJ (2014) Native cellulose: Structure, characterization and thermal properties. *Materials (Basel)* Vol. 7, pp. 105–119.
- Reddy, K., Maheswari, C., Dhlamini, M., Mothudi, B., Kommula, V., Zhang, J., Zhang, J., y Rajulu, A. (2018). Extraction and characterization of cellulose single fibers from native african Napier grass. *Carbohydrate Polymers*, Vol. 188, pp. 85–91.
- Ríos J. V., Santiago O. M. A., Barrera-Martínez I., Álvarez V. P., Carrillo L. P., JoséAmadorHonorato S. J. A. (2021). Characterization of mombaza grass as raw material to produce bioethanol. *Revista Mexicana Ciencias Agrícolas*, Vol. 12, 2.
- Rodríguez O. Luis M. (2007). Estudio del proceso de obtención de celulosa a partir del MM (panicum virgatum), a nivel de planta piloto, utilizando un extractor Soxhlet. TEG. FACYT. Universidad de Carabobo. Venezuela.
- Sun, X., Sun, R., Su, Y. y J. Sun. y M. Wada (2004). Comparative study of crude and purified cellulose from wheat straw. *J. Agric. Food Chem.*, 52: 839-847.
- Tashiro, K. y Kobayashi, M. (1991). Theoretical evaluation of three-dimensional elastic constants of native and regenerated celluloses: role of hydrogen bonds. *Polymer*. Vol. 32, pp. 1516-1526.
- Yang, H., Yan, R., Chen, H., Lee, D.H., y Zheng, C. (2007). Characteristics of hemicellulose, cellulose and lignin pyrolysis. *Fuel*, Vol. 86, pp. 1781-1788.
- Yang, U. M. y Fujita, H. (1997). Changes in grass lipid fractions and fatty acid composition attributed to hay making. *Japanese Journal of Grassland Science*, Vol. 42 (4), pp. 289-293.
- Zuluaga, R.; Putaux, J. L.; Restrepo, A.; Mondragon, I. y Gañán, P. (2007). Cellulose microfibrils from banana farming residues: isolation and characterization. *Cellulose*. Vol. 14 (6), pp. 585–592.

Received: Aug 09th, 2025

Accepted: Nov 04th, 2025

Villanueva Sequera, Iván José: Bachelor's Degree in Chemistry, 2001, Full Professor, Chemistry Department at Faculty of Engineering, University of Carabobo, Carabobo, Venezuela.

 <https://orcid.org/0000-0003-4527-2280>

Pereira Antique, Juan Carlos: PhD in Applied Sciences (ULA). Director at Laboratory of Petroleum, Hydrocarbons and Derivatives (PHD). Full Professor, Department of Chemistry at Faculty of Experimental Sciences and Technology, University of Carabobo, Carabobo, Venezuela. Industrial Consultant in Interfacial Phenomena.

Email: jcpereir@uc.edu.ve

 <https://orcid.org/0000-0003-4600-726X>

